TOWARDS AN UNDERSTANDING OF THE ROLE OF CONNEXIN26 IN BREATHING

JOSEPH VAN DE WIEL

DOCTOR OF PHILOSOPHY IN

INTERDISCIPLINARY BIOMEDICAL SCIENCE

THE UNIVERSITY OF WARWICK,

WARWICK MEDICAL SCHOOL

FEBRUARY 2019

TABLE OF CONTENTS

FIGURES AND TABLES

ACKNOWLEDGEMENTS

Thank you to my supervisor, Professor Nicholas Dale, for proving me with the fantastic opportunity to take on this PhD project, and for his continual support, guidance, and encouragement in all aspects of my work and professional development these past 3 years. I would also like to thank my secondary supervisor, Dr Mark Wall.

Thank you to my advisory committee – Dr Robert Dallmann and Dr Robert Durafford-Huckstepp – for their corrections, suggestions, and genuine enthusiasm to see me succeed. Additional thanks to Dr Robert Durafford-Huckstepp, for his exceptional teaching and continued mentorship concerning the *in vivo* aspects of my project, and for all his advice and explanations concerning research techniques and the respiratory field.

Thank you to all members of C116 and C117, past and present, for the teaching and support – with special mention to Greta, JC, Liz, Eric, Louise, and Amol, without whom I would have got nowhere.

Thank you to all members of the BSU facility, for their teaching and the diligent work they do for the animals in the facility.

Thank you to the MRC for my funding, and to The Univeristy of Warwick and the IBR-DTP for providing me with abundant opportunities. Thank you to Nick and Gokhan, who traversed the DTP years with me and brought me endless laughter.

To those named above: I did not deserve to be so lucky to have met and worked with even one of you and I am very glad that I got to share my PhD with you.

Thank you to my parents and family for their unconditional love, and the blind faith that they have always had in me.

Most of all thank you to my fiancée Kathryn, words cannot express my gratitude for all you have done for me during my PhD, and I only hope that I can repay you over the rest of our life together.

DECLARATION

This thesis is submitted to the University of Warwick in support of my application for the degree of Doctor of Philosophy. It has been composed by myself and has not been submitted in any previous application for any degree.

The work presented (including data generated and data analysis) was carried out by the author except in the cases outlined below:

- Patching of cells for $[Ca^{2+}]_i$ experiments in chapter 2 was done by Nicholas Dale, all other parts of the experiments and analysis were performed by Joseph van de Wiel
- A subset of dye loading experiments in chapter 2 were performed in conjunction with Elizabeth de Wolf and Jonathan Cook
- Time course dye loading experiments in chapter 3 (Figure 3.9) were performed by Louise Meigh
- Connexin26-KO data shown in chapter 4 (Supplement figure 4.1 and Supplement figure 4.2) was performed by Xintao Zhang

Parts of this thesis have been published by the author:

- de Wolf, E., van de Wiel, J., Cook, J., & Dale, N. (2016). Altered CO 2 sensitivity of connexin26 mutant hemichannels in vitro. Physiological reports, 4(22), e13038.

All figures or images not originally produced by the author were reproduced with permission.

SUMMARY

Connexin26 (Cx26) hemichannels expressed in glia at the ventral medullary surface (VMS) have been proposed to play a role in respiratory chemoreception, although this is disputed. At the VMS Cx26 hemichannels open in response to CO_2 directly, causing ATP release that is capable of increasing respiratory drive. The main aim of this work was to establish a genetic strategy that can be used *in vivo* to elegantly remove Cx26 CO_2-sensitivity from chemosensitive areas of the VMS, and to thereby investigate the role that Cx26 CO_2 sensitivity plays in the chemoreception of awake mice.

Using Förster resonance energy transfer and dye loading studies a Cx26 mutant ($Cx26^{DN}$) was found to coassemble with $Cx26^{WT}$ subunits (forming heteromeric connexon hemichannels) and to remove CO_2-induced hemichannel opening from cells stably expressing $Cx26^{WT}$.

In mice aged 12-18 weeks, bilateral lentivirus injections were used to express $Cx26^{DN}$ in $GFAP^{+}$ cells at the VMS, as a means of removing CO_2-induced Cx26 hemichannel opening and subsequent ATP release. As determined by whole-body plethysmography, expression of $Cx26^{DN}$ in the retrotrapezoid nucleus (RTN) had no effect on the hypercapnic ventilatory response in mice. Accidental $Cx26^{DN}$ expression in the caudal chemosensitive area resulted in reduced tidal volume 3 weeks post-transduction, however this was not well supported statistically. Such an auspicious result from sub-optimal caudal expression warrants this to be repeated in order to validate these results.

The work performed in this thesis outlines the first use of a highly novel genetic tool to remove the CO_2-sensitivity property of Cx26 from specific cells, without removing the protein from the system. The results shed light on our understanding of central respiratory chemoreception, suggesting that Cx26 plays no role in chemoreception in the RTN but is likely to play a role in caudal areas of the VMS. Such a tool could aid research into the virtually unexplored role that Cx26 CO_2 gating has in the body.

ABBREVIATIONS

Standard single and 3-letter amino acid codes and notations are used. E.g. K125, lysine residue at amino acid position 125 of the peptide; K125R, lysine residue at position 125 has been mutated to an arginine.	
3WXA	3-way mixed ANOVA
2WXA	2-way mixed ANOVA
7N	7th nerve – not to be confused with the 7th nucleus (VII)
$[Ca2^+]_i$	Intracellular Calcium ion concentration
$[Ca2^+]_e$	Extracellular Calcium ion concentration
%E	FRET efficiency as a percentage
^0C	Degrees Celsius
µg	Microgram
µm	Micrometer
µM	Micromole
Å	Angstrom
A	Acceptor abundance relative to total fluorophore flourescence
A level	Relative acceptor quantity
AAV	Adeno-associated virus
aCSF	Artificial cerebrospinal fluid
adFRET	Acceptor depletion Förster Resonance Energy Transfer
AFM	Atomic force microscopy
AM	acetoxymethyl
Amb	Ambiguous
ASIC	Acid-sensing ion channel
ATP	Adenosine triphosphate
ANOVA	Analysis of variance
B	Bleaching efficiency
BGHpA	Bovine growth hormone polyadenylation signal
BötC	Bötzinger Complex
C-terminus	End of an amino acid chain that terminates in a free carboxyl group
CA	Carbonic anhydrase

cAMP	Cyclic AMP
CAN	Calcium-activated non-selective
Ca^{2+}	Calcium ions
$CaCl_2$	Calcium chloride
CCHS	Congenital central hypoventilation syndrome
ChAT	Choline acetyltransferase
CT	C-terminus
CL	Cytoplasmic loop
cm^2	Centimetre cubed
CNS	Central nervous system
cNTS	Caudal nucleus tractus solitarious
CO_2	Carbon dioxide
CPG	Central pattern generator
CsCl	Caesium chloride
CSF	Cerebrospinal fluid
cVLM	Caudal ventrolateral medulla
cVRG	Caudal ventral respiratory group
Cx	Connexin
D	Donor abundance relative to total fluorophore flourescence
DA	Relative donor-acceptor ratio
DREADD	Designer receptors exclusively activated by designer drugs
DMEM	Dulbecco's modified eagle medium
DMSO	Dimethyl sulfoxide
DN	Dominant Negative
DNA	Deoxyribonucleic acid
E	FRET efficiency
e-pF	Embryonic parafacial region
EGTA	Ethylene glycol tetraacetic acid
ELISA	Enzyme-linked immunosorbent assay
EMCCD	Electron-multiplying charge-coupled device
ER	Endoplasmic reticulum
ERGIC	Endoplasmic reticulum-Golgi intermediate compartment

FCS	Fetal calf serum
fps	Frames per second
Fr	Frequency
FRET	Förster Resonance Energy Transfer
g	grams
GFAP	Glial fibrillary acidic protein
GFP	Green fluorescent protein
GPCR	G protein-coupled receptor
GPR	G protein-coupled receptor
hr	Hour
H^+	Hydrogen ion/proton
H_2O	Water
HCl	Hydrochloric acid
HeLa	Henrietta Lacks
HCO_3^-	Bicarbonate ions
HCVR	Hypercapnic ventilatory response
I	Current
IRES	Internal ribosome entry site
K^+	Potassium ion
K-F	Kölliker-Fuse nucleus
Kb	Kilobase
KCl	Potassium chloride
K_d	Dissociation constant
KDa	Kilodalton
KID	Keratitis-Ichthyosis Deafness
Kir	Inwardly rectifying K^+ channel
KO	Knock-out
KOH	Potassium hydroxide
L	Litre
LacZ	β-galactosidase
LC	Locus coeruleus
LSO	Lateral Superior Olive

LV	Lentivirus
mCherry	Monomer form of the cherry fluorescent protein
mCMV	Mini-cytomegalovirus
$MgCl_2$	Magnesium Chloride
$MgSO_4$	Magnesium sulphate
mL	Millilitre
ms	Millisecond
MSO	Medial Superior Olive
nm	Nanometer
mM	Millimolar
mmHg	Millimetres of mercury
Mo5	Motor trigeminal nucleus
mV	Millivolts
Mol	Mole
N_2	Nitrogen
N-terminus	Start of an amino acid chain that has a free amine group
NA	Numerical aperture
Na^+	Sodium ion
NaCl	Sodium chloride
$NaHCO_3$	Sodium bicarbonate
$NaHPO_4$	Sodium phosphate
$NaNO_3$	Sodium nitrite
NBC	Na^+/HCO_3^- cotransport
NBCe1	Electrogenic Na^+/HCO_3^- cotransporter 1
NCCs	Neural crest cells
NCX	Na^+/Ca^{2+} exchange
nL	Nanolitre
nM	Nano mole
NO	Nitric oxide
NP-EGTA	Nitrophenyl ethylene glycol tetraacetic acid
NPPB	5-nitro-2-(3-phenylpropylamino)benzoic acid
NSHL	Non-syndromic sensorineural hearing loss

NT	N-terminus
NTS	Nucleus tractus solitarious
nS	nanosiemens
O_2	Oxygen
P12	Postnatal 12 (i.e. 12 days after birth)
P2YR	Puringergic receptor
PB	Parabrachial nucleus
PBS	Phosphate buffer solution
PBS-T	PBS containing 0.1% triton X-100
pCO_2	Partial pressure of CO_2
PCR	Polymerase chain reaction
PFA	Paraformaldehyde
pF_L	Lateral parafacial region
pFRG	Parafacial respiratory group
pF_V	Ventral parafacial region
PGE_2	Prostaglandin E_2
pH	Negative base 10 logarithm of hydrogen ion molar concentration
pH_e	Extracellular pH
pH_i	Intracellular pH
pO_2	Partial pressure of O_2
preBötC	pre-Bötzinger Complex
pXII	Parahypoglossal region
qPCR	Quantitative polymerase chain reaction
R	Donor-acceptor distance
R_0	Effective FRET distance
RM	Raphé Magnus
ROb	Raphé Obscurus
ROI	Region of interest
RPa	Raphé pallidus
RTN	Retrotrapezoid nucleus
rVRG	Rostral ventral respiratory group
SIDS	Sudden infant death syndrome

SNO	S-Nitrosothiol
SO	Superior olive
TASK	TWIK-related acid sensitive potassium channel
TEACL	Tetraethylammonium Chloride
TM	Transmembrane region
TU	Transfection units
TWIK	Two pore domain potassium channel
u-adFRE	adFRET with spectral unmixing
UV	Ultraviolet
V	Voltage
VII	Facial motor nucleus/7th nucleus
VMS	Ventral medullary surface
WPRE	Woodchuck hepatitis virus posttranscriptional regulatory element
VRG	Ventral respiratory group
V_T	Tidal volume
WT	Wild type
XII	Hypoglossal region

"Our breath… ever renewed it was always forthcoming, destined to be the last adjunct that shall leave the body, and the only one to remain when all is gone beside; it drew, in fine, its origin from heaven"

- Pliny the Elder (approx. 50 AD)

1 INTRODUCTION

1.1 Taking a breath

Breathing is essential for human life – this has been recognised for millennia. In approximately 400 BC, Democritus theorised that breathing exists to bring mind and soul atoms into the body as a means to counteract pressure from internal soul atoms – thus preventing expulsion of the soul that resides in the animal (Aristotle approx. 350 BC). Our understanding of how and why we breathe has progressed somewhat since then, although certain parts of this process still remain a mystery.

1.1.1 How do we breathe?

A breath consists of the flow of air from the external environment into the lungs (inspiration), followed by the flow of air within the lungs out into the external environment (expiration). Air flows in through the mouth or nose, down the trachea, through the bronchi and bronchioles, and into alveolar sacks. Alveoli are richly supplied with capillaries and therefore provide a perfect environment for the exchange of gases between the outside air and the blood.

Inspiration occurs due to contraction of the diaphragm and external intercostal muscles, which expands the chest cavity and subsequently the lungs. This deceases the pressure within the lungs (Boyle's law) below the atmospheric pressure in the outside environment, resulting in air to flow into the lungs (i.e. from higher to lower pressure). Expiration occurs due to compression of the chest cavity and lungs, which increases the pressure within the lungs above that of atmospheric pressure and subsequently expels air out of the lungs. At rest expiration usually occurs simply through the relaxation of the diaphragm and external intercostal muscles and subsequent elastic recoil of the lungs. However, when the body is in demand of greater gaseous exchange forced expiration can be employed, during which internal intercostal muscles and abdominal muscles contract (in addition to diaphragm and external intercostal relaxation) in order to help drive a quicker and more forceful breathing (Evans, Hartridge, and Starling 1956, Pocock et al. 2013).

1.1.2 Why do we bother breathing?

Every cell in the body undergoes (cellular) respiration in order to produce energy for performing various tasks. This requires the use of O_2 and yields CO_2 as a waste product. As cells are rarely dormant, there needs to be both a continuous supply of O_2, for metabolic processes, and continual removal of CO_2, which will otherwise build up and disrupt the acid-base balance (potentially leading to respiratory acidosis) (Engelking 2015). In vertebrates this is achieved via breathing.

Breathing facilitates the exchange of gas at the alveoli-capillary interface, thereby enabling the partial pressure of blood O_2 (pO_2) and CO_2 (pCO_2) to be maintained at the levels required for cellular processes to continue. In humans pO_2 is adjusted from ~40 mmHg to 100 mmHg, and pCO_2 is adjusted from 45 mmHg to 35 mmHg; although pCO_2 levels may range as far as 20 mmHg and 70 mmHg (West 2012).

1.1.3 What keeps us breathing?

In order to maintain pO_2 and pCO_2 homeostasis we have to breathe all the time, even at rest. The two mechanical respiratory phases (inspiration and expiration) are controlled by three neural phases: i) inspiratory, ii) post-inspiratory, and iii) expiratory (when active expiration is required) (Richter 1996). Therefore, it is logical for a central pattern generator (CPG) to set up rhythmic breathing, which can then be adapted to meet our dynamic metabolic needs (Hooper 2000). Accordingly, this is what has been found for breathing, although emerging evidence suggests that separate CPGs might exist for the three neural phases of respiration.

The pre-Bötzinger Complex (preBötC) was the first of these CPGs to be proposed. It is found close to the ventral medullary surface (VMS) in the ventrolateral respiratory column (VLRC) (**Figure 1.1c,d**). The preBötC has a wealth of evidence (and support from the respiratory community) showing that it is the microcircuit responsible for the rhythmogenesis of inspiratory neurons (Feldman et al. 1990, Smith et al. 1991, Feldman and Kam 2015, Schwarzacher, Rüb, and Deller 2010, Tan et al. 2008, Johnson, Koshiya, and Smith 2001, Dobbins and Feldman 1994, Koizumi et al. 2008, Heywood et al. 1996, Feldman, Del Negro, and Gray 2013, Moore et al. 2013, Moore, Kleinfeld, and Wang 2014). It has been proposed that the preBötC consists of pre-inspiratory neurons that produce 'burstlets', thus providing rhythmogenic properties of the CPG, as well as

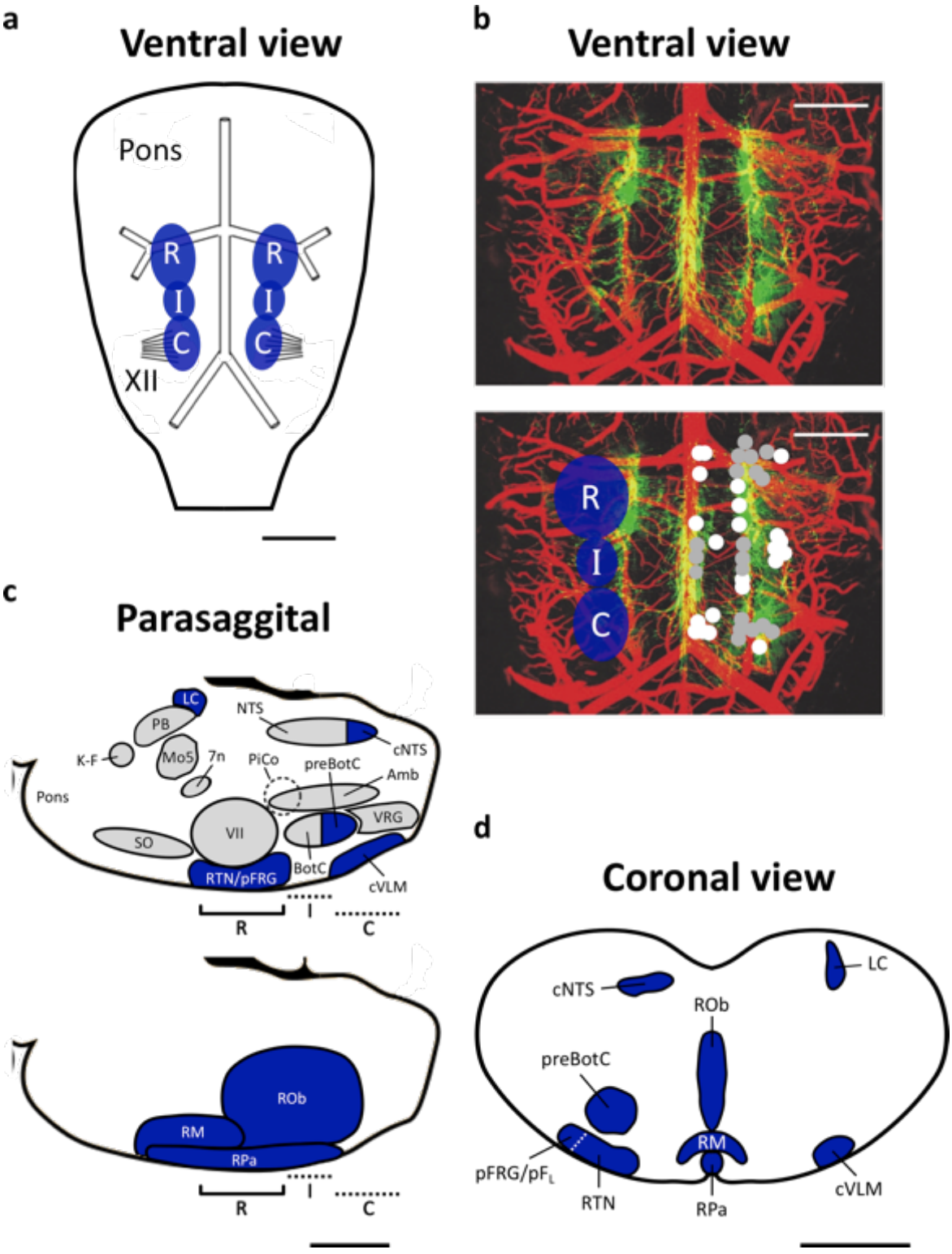

Figure 1.1 **Neuroanatomy of central respiratory chemoreceptors in the medulla oblongata**. **a)** Ventral view of the mouse medulla showing the classic chemosensitive sites that were first identified - Rostral, Intermediate, and Caudal (blue ovals). **b)** Top: Confocal image (ventral view) showing serotonergic neurons of the rat medulla stained with anti-TpOH antibody (green), and blood vessels filled with fluorescein-tagged albumin (red). (*image reproduced from Bradley, S. R., et al., 2002*). Bottom: same image as the top panel but overlaid is the classical chemosensitive sites (blue ovals), and sites that exhibit an ATP release in response to CO_2 (black circles), along with sites that do not exhibit such ATP release (white circles). These serotonergic neurons, and the sites of ATP release are chemosensitive. **c)** Parasagittal view of the mouse medulla,

representing the entire mediolateral axis, showing regions with evidence supporting their role in central respiratory chemoreception (blue), and landmarks in grey. For the visual purposes of distinguishing between the chemosensitive regions two diagrams are shown, with the bottom only showing chemosensitive raphé nuclei. Below each diagram show how the classical chemosensitive sites correlate to the rostrocaudal axis: unlike the rostral area, the true position of the intermediate and caudal areas are poorly characterised, as such they are represented by dashed lines. **d)** Coronal view of the mouse medulla, representing the entire rostrocaudal axis, showing regions with evidence supporting their role in central respiratory chemoreception (blue). R, rostral; I, Intermediate; C, caudal; LC, locus ceruleus; 7N, facial nerve; NTS, nucleus tractus solitarious; cNTS, caudal nucleus tractus solitarious; Amb, ambiguous; VII, facial nucleus; SO, superior olive; preBotC, pre-Bötzinger Complex; BotC, Bötzinger Complex; VRG, ventral respiratory group; cVLM, caudal ventrolateral medulla; RTN/pFRG, retrotrapezoid nucleus/parafacial respiratory group; PB, parabrachial nucleus; K-F, Kölliker-Fuse nucleus; Mo5, motor trigeminal nucleus; RM, raphé magnus; ROb, raphé obscurus; RPa, raphé pallidus. Scale bars; 1 mm in (**a, c, d**), 1.5 mm in (**b**).

inspiratory neurons that pattern the respiratory output (Feldman and Kam 2015, Kam et al. 2013, Cui et al. 2016).

It has been hypothesised that different rhythm generators exist for inspiration and active expiration (Janczewski and Feldman 2006), and this notion has since been supported with the discovery of silent neurons that, during active expiration, can be transformed into rhythmically active cells with a firing pattern correlating with late-phase active expiration (Pagliardini et al. 2011, Huckstepp et al. 2015). The location of this conditional expiratory oscillator has been defined, by injection site, as the lateral parafacial region (pF_L) (Huckstepp et al. 2015). The pF_L is located within the VLRC (**Figure 1.1c,d**) and develops from the embryonic parafacial region (e-pF) (Huckstepp et al. 2016) – the region responsible for early rhythmic and patterned respiratory activity in the embryo (Oku, Masumiya, and Okada 2007).

The most recently proposed CPG is the post-inspiratory complex (PiCo). This is a region containing neurons with autonomous rhythmogenic properties that are sufficient for post-inspiratory activity (Anderson et al. 2016). The PiCo is also found within the VLRC, medial to the rostral section of the nucleus ambiguous (NA) (**Figure 1.1c,d**). The status of the PiCo as a CPG has been strongly contested (Poon and Song 2017), and other studies would suggest that much of the post-inspiratory drive is derived from pontine structures such as the Kollicker Fuse nucleus (K-F) (Mörschel and Dutschmann 2009).

Rational interactions between these respiratory CPGs have been proposed, with evidence being provided for the influence that the preBötC (inspiratory) and pF_L (expiratory) have on one other in a hypothetical coupled oscillator system (Mellen et al.

2003, Feldman and Del Negro 2006, Huckstepp et al. 2015, Huckstepp et al. 2016, Anderson and Ramirez 2017). However, given how recent the discovery of the PiCo (post-inspiratory) CPG is, further work is required in order to affirm the precise interactions between all three. Nevertheless, these findings show great promise for our fundamental understanding of central respiratory networks.

The respiratory output that determines breathing pattern does not depend solely on signals from CPGs, but also upon signals relayed from other, non-CPG, nucle. Often nuclei involved in orchestrating respiration are divided into one of three respiratory groups. The ventrolateral respiratory column (VLRC) is the major group with which this thesis is concerned and contains the CPGs mentioned above as well as many putative central respiratory chemoreceptors (CRCs) (see *1.2 Central respiratory chemoreception*), **Figure 1.1**. It also contains inspiratory neurons that signal to premotor and motoneurons, and expiratory neurons that signal to control upper airway resistance. *Note that the VLRC is also referred to as the ventral respiratory group (or VRG), however in this thesis the name "VRG" is reserved for the nuclei found at the caudal region of the VLRC.*

The other two respiratory groups are the pontine respiratory group (PRG) and the dorsal respiratory group (DRG). Since the discovery of the nuclei that make up the VLRC research concerning the DRG and PRG has declined massively, owing to the great promise that the VLRC shows for controlling respiration. That being said, the PRG and DRG do play some role in contributing to breathing pattern. The PRG is situated within the dorsolateral pons and is responsible for receiving afferents from vagal reflexes associated with lung volume. Notably it contains the K-F. Although the PRG is capable of producing respiratory activities, including generating respiratory rhythm (St John and Bledsoe 1985, St John 1998), its neurons are largely inhibited in conscious animals and so it is considered to play more of a redundant role to back up, rather than contribute to, respiratory control (Feldman and Gautier 1976a, Feldman, Cohen, and Wolotsky 1976b, Cohen and Feldman 1977, Mörschel and Dutschmann 2009). The DRG is situated within the nucleus tractus solitarious (NTS) of the dorsal medulla and is believed to be relay for peripheral inputs – receiving primary afferents from both mechanical and chemical peripheral signals and sending efferent neurons to respiratory premotor neurons in the medulla, motoneurons in the spinal cord, and down to nuclei of the VLRC. The DRG is also responsible for cardiovascular reflexes (Nattie 1999, Kubin 1994, Stornetta et al. 2006, Takakura et al. 2006, Huckstepp and Dale 2011).

1.1.4 Why should we study central breathing networks?

As it is so important, evolution has ensured that our ability to breath is robust and has the redundancy to compensate in the face of defects. In testimony to this, the respiratory problems that are most prevalent in the population (e.g. chronic obstructive pulmonary disease and asthma) are mechanical in nature, reducing airflow into or out of the lungs. Nevertheless, certain diseases states have been linked to the central components, and others may yet be linked as our understanding increases.

Sleep apnoea (respiratory pauses) affects 3-7% of males and 2-5% of adult females (Punjabi 2008) and whilst many cases are mechanical in nature there are those that result from central dysfunctions (Fairchild et al. 2016), such as congenital central hypoventilation syndromes (CCHS). As it stands we poorly understand the mechanisms behind central sleep apnoeas, even in the case of CCHS for which a causative gene has been identified (PHOX2B).

Sudden infant death syndrome (SIDS) effects around 1 in 5,000 births (Kinney and Thach 2009) and although it is defined as the death of an infant by unknown cause, it has been attributed to an inability to counteract rises in blood CO2 during sleep (Harper et al. 2000). As it stands we are yet to make a definitive link between central respiratory dysfunction and SIDS, although there are ideas that warrant investigating further. Recent studies suggesting that inflammatory-induced release of prostaglandin E_2 (PGE_2), in the retrotrapezoid nucleus (RTN), can modify the hypercapnic ventilatory response (HCVR) and could have far-reaching implications in this event (Forsberg et al. 2016, Forsberg, Ringstedt, and Herlenius 2017). Additionally, there have been reported cases of SIDS infants that showed signs of medullary serotonin dysfunction (Paterson, Hilaire, and Weese-Mayer 2009). Serotonin is a neurotransmitter and is released from medullary raphé neurons that have been proposed to play a role in chemoreception (Hodges and Richerson 2010) (see *1.2.6 Serotonergic neurons*). It is likely that there are multiple defects that give rise to the diagnosis of SIDS, and therefore the more respiratory pathways we can connect/dismiss the closer we become to developing prevention measures and treatments.

Rett syndrome affects around 1 in 10,000 female births (Neul et al. 2010) and results in mental and physical disability. Patients with Rett syndrome also experience severe breathing disturbances characterised by abnormal breathing patterns and

reduced CO_2 sensitivity (Ramirez, Ward, and Neul 2013). This reduced CO_2 chemosensitivity has been linked to a deficiency in the expression of methyl-CpG-binding protein 2 (MeCP2) in glial, which is believed to be important in sensing CO_2 (Garg et al. 2015, Turovsky et al. 2015). With increased understanding we may be able to uncover targets to help develop therapies that could rectify or compensate for this deficiency.

The need to study respiratory networks extends beyond disease. Opiate intoxication depresses respiratory activity (Stuth, Stucke, and Zuperku 2012), which can become dangerous and limits the safe use of opiate analgesics. With a better understanding of respiratory network mechanisms, we may be able to provide new targets to counteract these effects, thus opening the doors to new methods of pain relief.

Another forward-looking reason to study central respiratory circuits is because it represents one of the least complex rhythmic behaviours that is common across animals (Feldman and Kam 2015, Feldman and Grillner 1983) and can be measured in well-defined manner. The relationship between neural microcircuits and behaviour is subject to numerous confounding variables, which makes it difficult when trying to ascertain what components are relevant and why (Carandini 2012). Therefore, comprehension of the circuitry responsible for a simpler operation, like breathing, might uncover processes that are common to many rhythmic circuits and is likely to inspire progressive approaches and attitudes to further dissect the role of behavioural circuits.

1.2 Central respiratory chemoreception

It is important that the body has a way to sense and process chemical inputs (chemoreception) such as pO_2 and pCO_2 so that respiratory patterns can be regulated in order to adjust breathing to meet metabolic needs. pO_2 sensing occurs centrally and peripherally, with ~80% of the hypoxic ventilatory response being attributed to peripheral sensing of pO_2 (Acker 1989, Prabhakar 2006), and ~20% attributed to central O_2 chemoreception (Powell et al. 2009, Neubauer and Sunderram 2004). Sensing of pCO_2 also occurs peripherally and centrally, however unlike pO_2 it is central CO_2 chemoreception that takes precedence, being responsible for ~60-70% of the hypercapnic respiratory reflex, while peripheral CO_2 chemoreception attributes ~30-40% (Carpenter, Hatton, and Peers 2000). Although it is important to monitor pO_2, it appears

that pCO_2 chemoreception is more important, and that hypercapnia (not hypoxia) is in fact the bigger threat to air-breathing animals (Phillipson, Duffin, and Cooper 1981, Spyer and Gourine 2009, Haldane and Priestley 1905). The focus of this thesis is on central respiratory chemoreception.

Central chemoreception was first hypothesised over a hundred years ago when Winterstein suggested that CO_2-stimulated breathing might be brought about through acidification of extracellular fluid near respiratory centres (Winterstein 1911). Central chemoreception was first demonstrated in 1953 when increased breathing was observed in response to the application of acidic solutions to the cerebral ventricles (Leusen 1953a, 1953b). The studies that followed confirmed central chemoreception and identified particular areas of the VMS that are responsible; with focal acidification (to pH 7.0) of either a caudal site (a.k.a. Loeschcke's area) or a rostral site (a.k.a. Mitchell's area) increasing respiratory activity, and acidification of a third, intermediate, region (a.k.a. Schlaefke's site) reducing respiratory activity (Mitchell et al. 1963a, Mitchell et al. 1963b, Loeschcke et al. 1970, Schlaefke, See, and Loeschcke 1970, Trouth et al. 1973, Schlaefke, Kille, and Loeschcke 1979), **Figure 1.1a**.

The original focal acidification experiments were performed on anaesthetised animals and used very high changes in pH to bring about a respiratory reflex, suggesting that there may be chemosensitive cells deeper within the medulla that are serviced by blood vessels that penetrate into the parenchyma from the surface. Since the 21st century our understanding of chemoreception has begun to accelerate, and there are now defined cell populations that have been identified as having chemosensitive properties. Cells with chemosensitivity that influences respiratory pattern are referred to as central respiratory chemoreceptors (CRCs) and some do indeed reside deeper within the medulla (Nattie and Li 2012, Huckstepp and Dale 2011), **Figure 1.1c,d**. The use of anaesthetised animal preparations is still a confounding problem in many of the experiments undertaken in the 21st century, and should be considered when interpreting their results.

The chemosensitive sites that were originally defined are often still referred to, however the current consensus is that the rostral site lies ventral to the facial motor nucleus (VII), comprising of the RTN/pFRG. The caudal and intermediate sites on the other hand are still poorly defined. Roughly, the intermediate site lies ventral to the Bötzinger complex (BötC) and rostral part of the preBötC, whilst the caudal site lies

ventral to the ventral respiratory group (VRG) and the caudal part of the preBötC, in the vicinity adjacent to the hypoglossal nerve (XII) rootlets, **Figure 1.1a,c**.

Currently proposed chemosensitive sites in the brainstem are usually found close to the brain surface, in regions richly supplied with blood vessels that have neuronal cell bodies or axon terminals juxtaposed (Okada, Chen, and Kuwana 2001, Okada et al. 2002). Below we discuss putative central respiratory chemoreceptors (CRCs):

1.2.1 Locus Coeruleus (LC)

The Locus Coeruleus (LC) is in the PRG and contains catecholaminergic neurons. It acts as a fear relay for the Amygdala and is involved in hypoxia-induced hyperventilation. The LC has been proposed as a CRC based on hypercapnia-evoked c-fos immunoreactivity, preservation of chemosensitivity in cultured neurons even when subjected to synaptic blockade (suggesting intrinsic chemosensitivity), and ablation and focal acidification studies in anaesthetised animals (Huckstepp and Dale 2011, Berquin et al. 2000, Stunden et al. 2001, Filosa, Dean, and Putnam 2002, Fabris et al. 2000, Ferreira, de Paula, and Branco 2004).

This evidence does not necessarily show that the LC is a site of primary chemoreception, although a potential chemosensory transducer has been identified (see *1.3 Central respiratory chemosensory transducers for pCO_2*). Therefore, in an intact animal under physiological conditions, the CRC properties reported in the literature might be secondary, responding instead to signals received from a primary CRC. Whatever the role that the LC plays in chemoreception it would appear to change depending on the stage of development – the percentage of chemosensitive neurons in the LC is highest in neonates, however in rodents this number drops dramatically (Nichols et al. 2008, Gargaglioni, Hartzler, and Putnam 2010).

1.2.2 Nucleus tractus solitarious (NTS)

The nucleus tractus solitarious (NTS) is more-or-less synonymous with the DRG – a relay for peripheral respiratory and cardiovascular stimuli, with neuronal connections to many respiratory-related nuclei. The evidence for NTS chemosensitivity is similar to that of the LC. The NTS shows hypercapnia-evoked immunoreactivity for c-fos, and cultured NTS slices preserved almost-all chemosensitivity upon synaptic blockade (Berquin et al. 2000,

Sato, Severinghaus, and Basbaum 1992). Additionally, in unanaesthetised rats acidification of the NTS, especially the caudal NTS (cNTS), resulted in increased breathing (Nattie and Li 2002). Interestingly, bilateral lesions of the cNTS in rats increased, not decreased, the HCVR (Sinclair, John, and Battlett 1985). The cNTS is also the region that is most responsible for coordinating the effect that peripheral chemoreceptors have on circulation and breathing (Boscan, Pickering, and Paton 2002).

As with the LC, this is not definitive evidence for any part of the NTS to be considered a primary CRC, although potential chemosensory transducers in the NTS have been postulated (see *1.3 Central respiratory chemosensory transducers for pCO_2*). Regardless of its role in primary chemoreception, the NTS seems to be an important node for integrating cardiovascular and respiratory signals during hypercapnia. Furthermore, because NTS properties and coupling change during early development (Nichols et al. 2008, Vincent and Tell 1997), like the LC its precise role in the respiratory network is likely to differ throughout an animal's development.

1.2.3 preBötzinger complex (preBötC)

The preBötC is part of the VLRC. We have discussed its (confirmed) role in respiratory rhythmogenesis and potential role in mediating pattern (see *1.1.3 What keeps us breathing*). Given its importance in respiratory activity it might stand to reason that the preBötC is itself intrinsically chemosensitive and acts as a primary site of chemoreception. In neonatal rat brainstem-spinal cord preparations, preBötC neurons showed activity in response to hypercapnic conditions, which was maintained during synaptic blockade (Koizumi et al. 2010, Kawai et al. 1996, Kawai, Onimaru, and Homma 2006). Also focal acidification in anaesthetised animals increases respiratory drive (Solomon, Edelman, and O'Neal III 2000, Solomon, Chon, and Rodriguez 2003) and in awake goats caused mild tachypnoea (Krause et al. 2009). As of yet no chemosensory transducer molecule has been proposed for this CRC, although there is evidence of ATP release in the preBötC in response to hypercapnia (Thomas and Spyer 2000) and therefore presumably such a molecule does exist.

1.2.4 Retrotrapezoid nucleus (RTN)

The retrotrapezoid nucleus (RTN) is part of the VLRC and is found rostral and ventral to the preBötC (**Figure 1.1c,d**). The RTN is widely believed to be more or less synonymous with the classical rostral chemosentive region. There has been confusion as to which region encompasses the RTN and which encompasses the parafacial group (PFG) – and because of this some previous studies combine them together as the RTN/PFG. The PFG is now believed to be synonymous with the newly determined lateral parafacial region (pF_L), which was defined in an unbiased manner based on location. In the same manner the ventral parafacial region (pF_V), which provides generic excitatory drive to breath, was coined and defined to lie within the RTN (Huckstepp et al. 2015, Huckstepp et al. 2016, Korsak et al. 2018).

The RTN clearly plays a large role in relaying or integrating respiratory information. Selective inhibition of the RTN reduces the HCVR by 60% in conscious rats (Marina et al. 2010). Also, the RTN has recently been shown to be critical in the respiratory response during exercise, demonstrating its importance during periods of hypercapnia (Korsak et al. 2018). Its role as a node for integration is supported by the numerous connections it is has with key breathing nuclei. The RTN has neurons projecting to the preBötC, rostral ventral respiratory group (rVRG), caudal ventral respiratory group (cVRG), BötC, K-F, and to a parahypoglossal region (pXII) that likely relays inspiratory drive to the XII (Chamberlin et al. 2007, Rosin, Chang, and Guyenet 2006, Huckstepp et al. 2015, Feldman, Del Negro, and Gray 2013, Takakura et al. 2006, Moreira et al. 2013, Takakura and Moreira 2016, Núñez-Abades, Morillo, and Pásaro 1993, Gerrits and Holstege 1996). The RTN also receives information from various CNS nuclei, peripheral chemoreceptors, and local astrocytes (Huckstepp et al. 2010a, Gourine et al. 2010, Turovsky, Theparambil, Kasymov, Deitmer, del Arroyo, et al. 2016, Takakura et al. 2006).

Given its connections and location (very close to the ventral surface and coinciding with the classical rostral chemosensitive site) the RTN is a strong candidate for a CRC with much evidence in its support. The RTN shows hypercapnia-induced c-fos immunoreactivity (Berquin et al. 2000) and its neurons are sensitive to CO_2 both *in vitro* and *in vivo* (anaesthetised rats), even in the presence of synaptic blockade (Mulkey et al. 2004). Also focal acidification of the RTN increases ventilation in conscious rats (Hewitt et al. 2004) and optogenetic stimulation has shown that glutamate released from $Phox2b^+$

RTN neurons is capable of stimulating breathing in conscious mice (Holloway et al. 2015). Furthermore, when the *Phox2b* gene was altered to include mutations responsible for causing CCHS in humans, neonatal mice completely lacked CO_2 sensitivity (Ramanantsoa et al. 2011, Dauger et al. 2003, Dubreuil et al. 2009).

This nucleus shows much promise as a primary site of chemoreception, although it is not yet clear whether the importance of RTN chemosensitivity varies over development. Multiple chemosensory transducers have been put forwards for RTN neurons, the evidence for which is discussed in the next section (see *1.3 Central respiratory chemosensory transducers for pCO_2*).

1.2.5 Caudal chemosensitive site/caudal ventrolateral medullar (cVLM)

The originally-identified caudal chemosensitive site is sometimes referred to as the caudal ventrolateral medulla (cVLM), as this new term reflects the importance of the later-found VLRC. However, calling this area the 'cVLM' would imply that this region is confined to the lateral portion of the medulla, when in truth the precise area is poorly defined and has been largely ignored since its discovery. In this thesis this area is referred to as the caudal chemosensitive site.

In addition to early experiments (Mitchell et al. 1963a, Mitchell et al. 1963b, Loeschcke et al. 1970, Schlaefke, See, and Loeschcke 1970, Trouth et al. 1973, Schlaefke, Kille, and Loeschcke 1979) neurons in this area have since been shown to have c-fos immunoreactivity in response to acidic stimulation (Ohtake et al. 1996), and to be stimulated by infusion of hypercapnic saline (Arita et al. 1989) and focal acidification (Nattie and Li 2012). In unanaesthetised rats focal acidification of this area also increases ventilation whilst awake (but not asleep) (da Silva, Li, and Nattie 2010). The cell type/s and mechanisms behind chemosensitivity in this area may be attributed to serotonergic neurons that (see *1.2.6 Serotonergic neurons*) or glia (see *1.2.7 Glia and ATP release*).

1.2.6 Serotonergic neurons

It has been suggested that chemosensitive serotonergic neurons in the ventral medulla are involved in chemoreception. These neurons are found closely associated with arteries, along the midline (the raphé nuclei) and also in more lateral regions that correlate fairly well with the classical rostral and caudal chemosensitive sites (Bradley et

al. 2002), **Figure 1.1**. The chemosensitivity shown from raphé neurons may not have been picked up in original studies because they are found in the midline region, which was often avoided during *in vivo* experimentation in order to prevent bleeding from the basilar artery (Bradley et al. 2002).

There has been dispute over the chemosensitivity of medullary serotonergic neurons, however this discrepancy appears to have arisen due to differing experimental conditions and the effects of anaesthesia on these neurons (Teran, Massey, and Richerson 2014, Massey et al. 2015). Upon review of the data, these neurons would appear both intrinsically chemosensitive and greatly important in respiratory chemoreception. Firstly, serotonergic neurons in the medulla have connections to respiratory nuclei including the RTN and preBötC (Teran, Massey, and Richerson 2014, Li, Zhou, and Nattie 2006, Hodges et al. 2008, Pace et al. 2007, Li and Nattie 2008, Ptak et al. 2009), and so a role in chemoreception is plausible. *In vitro* they maintain chemosensitivity during synaptic blockade (Wang and Richerson 1999) and have been shown to respond to pH changes from 7.4-7.2, which falls within a realistic physiological range (Wang, Pizzonia, and Richerson 1998). *In vivo* they show hypercapnia-induced c-fos immunoreactivity (Larnicol et al. 1994) and increased ventilation during focal acidification in anaesthetised rats (Bernard, Li, and Nattie 1996). In unanaesthetised animals hypercapnia has been shown to increase serotonin levels in the caudal medulla (~2.5 fold) (Kanamaru and Homma 2007) and serotonergic neuronal activity throughout (Veasey et al. 1995, 1997, Richerson et al. 2005). Furthermore, genetic silencing of theses neurons in adult mice by either preventing their differentiation (Teran, Massey, and Richerson 2014, Hodges et al. 2008) or activating DREADD receptors (Ray et al. 2011) both reduced the HCVR by 50%. Serotonergic neurons appear less important in neonates, suggesting that their importance in chemosensitivity matures with development (Teran, Massey, and Richerson 2014).

As has been mentioned before, to be a primary site of chemoreception a chemosensory transducer must be identified and shown to play a role in the HCVR of conscious animals. A role for TASK channels was suggested but has since been dismissed (see *1.3.2 TASK channels*) and the current proposition is that these neurons mediate a response via a pH sensitive calcium-activated non-selective cation (CAN) current (Teran, Massey, and Richerson 2014). The chemosensory transducer that mediates this current might prove to be GPR4 (see *1.3.3 GPR4*).

1.2.7 Glia and ATP release

Glial are electrically non-excitable cells found in amongst neurons throughout the brain. They were first described in the mid 19th century (Somjen 1988, Virchow 1858) and many different sub-types have been characterised; including microglia, astrocytes, and oligodendrocytes. However, it is only in recent years that there has been significant interest in glia, and exciting new functions and roles for these cells are starting to come to light (Jäkel and Dimou 2017, Kettenmann and Verkhratsky 2016).

In 2005 an important role for ATP in CNS sensory transduction was uncovered. Using biosensors it was observed that ATP is released from sites in the VMS in response to an increase in inspired CO_2, and that blocking ATP receptors at these regions attenuated the respiratory reflex to CO_2 (Gourine et al. 2005). In a subsequent study (Gourine et al. 2010) Ca^{2+}-imaging and biosensors were used to show that astrocytes in the RTN of young adult rats respond to small changes in pH (7.4 to 7.2) with an increase in $[Ca^{2+}]_i$, which propagates to other astrocytes, and that in brain slices this is accompanied by a release of ATP that activated nearby RTN neurons. Astrocytic Ca^{2+} activity was maintained in the presence of synaptic blockade but was diminished upon ATP blockade (suggesting $Ca2^{+}$ propagation is ATP-dependent). Patch clamp data from neonatal brain slices confirmed the chemosensitivity of astrocytes, and that their effect on RTN neuronal firing was purinergic in manner (Wenker et al. 2010). Furthermore, alteration of chemosensitivity-related astrocytic activity within the RTN directly affects respiratory activity. For example, although a non-physiological stimulus, optogenetic stimulation to mimic astrocytic $[Ca^{2+}]_i$ responses increases respiratory drive in anaesthetised animals and is inhibited by blocking ATP receptors (Gourine et al. 2010). Also, when the chemosensitivity of RTN astrocytes is compromised in mice models for Rett syndrome (characterised by reduced ventilatory CO_2 sensitivity) animals show an inappropriate HCVR (Garg et al. 2015, Turovsky et al. 2015). This data demonstrates that the pH chemosensitivity of astrocytes may be responsible for release of a signal (i.e. ATP) that is capable of modulating the activity of nearby respiratory neurons *in vitro*, and respiratory drive *in vivo*. ATP release in this pH-mediated manner is believed to take place via vesicular release (Kasymov et al. 2013).

In addition to this pH-mediated ATP release, glia of the VMS were found to release ATP in response to molecular CO_2 directly, in a connexin-dependent manner thought to be mediated by Connexin26 (Cx26) (Huckstepp et al. 2010a) (see *1.3.6*

Connexin26). This Cx26-mediated ATP release occurs through open Cx26 hemichannels, although additional vesicular release has not been discounted (Huckstepp et al. 2010b).

In the original study of ATP release (Gourine et al. 2005) many of the sites at which ATP release was observed lie close to the classical chemosensitive areas of the VMS (**Figure 1.1b**), and in subsequent studies hypercapnia-induced ATP release has been shown within the classical chemosensitive areas (Huckstepp et al. 2010a, Gourine et al. 2010, Huckstepp, Llaudet, and Gourine 2016). Since glia are found across the VMS they could hypothetically act at any site, providing a primary chemosensory role and generating a stimulus for local respiratory-related neurons. For this reason, focal acidification studies that support the status of aforementioned CRCs also support a role for the glia within the area.

The role of glia-dependent ATP release in chemoreception is becoming increasingly accepted, be it an alternative or supportive role to other proposed CRCs. There have been multiple chemosensory transducers that have been proposed to give rise to hypercapnia-evoked glial ATP release (see *1.3 Central respiratory chemosensory transducers for pCO_2*), however their relevance in the intact animal are not fully accepted.

ATP release from glia may contribute to chemoreception in ways additional to activating P2X/P2Y receptors. For example, breakdown of released ATP into adenosine has been suggested to provide end-product inhibition in order to limit the chemoreceptive response that ATP produces (Falquetto et al. 2018). Furthermore, hypercapnia-evoked ATP release has been shown to mediate the release of acetylcholine (ACh) (Huckstepp, Llaudet, and Gourine 2016), which has been suggested to play a role in controlling changes in breathing (Dev and Loeschcke 1979, Fukuda and Loeschcke 1979).

Recently another role of glia in chemoreception, which is ATP-independent, has been proposed. In organotypic cultures of RTN slices PGE_2-ELISA revealed CO_2-evoked release of PGE_2 from a subpopulation of glia. Using Ca^{2+} imaging, bath application of PGE_2 was shown to stimulated RTN neurons. In organotypic cultures from Ptger-KO mice (which encodes for the main PGE_2 receptor, EP3R) stimulation of RTN neurons was reduced (Forsberg et al. 2016, Forsberg, Ringstedt, and Herlenius 2017). This data identifies the potential of a PGE_2 signalling pathway in chemoreception.

However, the plethysmography data from these studies is inconclusive with their current interpretation. For example, mice with global Ptger-KO showed a blunted change

in tidal volume (V_T) under hypercapnia, compared to wild-type mice, suggesting that PGE_2 signalling might be involved in chemoreception. However, this change was normalised to normocapnia and does not identify the ~1.5 times higher baseline V_T exhibited by Ptger-KO mice (which is higher than even the wild-type V_T during hypercapnia). This would instead suggest that defective PGE_2 signalling has resulted in the development of a defective respiratory system. Also, in wild-type mice under normocapnia intracerebroventricular injection of PGE_2 showed increased tidal volume compared to sham injections, however these recordings were performed some time >10 mins after PGE_2 injections which, along with variation in the speed of injections, casts doubt on its reproducibility as a technique.

In vitro data shows a clear potential for a role of PGE_2 in chemoreception, which would be exciting given the links between PGE_2 and inflammation, however more elegant *in vivo* experiments are required to investigate the precise effect of any PGE_2 release in the RTN, and to discern its physiological relevance to breathing.

1.3 Central respiratory chemosensory transducers for pCO_2

For a region of the brain to be a primary source of chemoreception the cells within it should be intrinsically chemosensitive, containing a molecule that converts a chemical stimulus (e.g. changes in pO_2 or pCO_2) into a signal that acts on the respiratory network in order to cause an adaptive change in breathing. Such a molecule is known as a chemosensory transducer. Identifying a putative chemosensory transducer, which is expressed in a particular chemosensitive region, is the first step towards clarifying whether a CRC is involved in primary chemoreception, or whether it merely responds to signals from primary CRCs. After a chemosensory transducer is proposed genetic studies can be designed in order to test the specific role of that transducer *in vivo*, with the aspiration of showing whether or not it is responsible for chemoreception under physiological conditions in an intact, conscious, animal. Only in this way can we be truly certain that a given transducer, and the corresponding CRC, plays a relevant role in respiratory chemoreception, and only with such confirmation will we be able to rationally design and develop strategies to manipulate a biological system.

Here we discuss central respiratory chemosensory transducers that may be involved in responding to increased blood pCO_2. Much of the past work on respiratory

chemoreception has focused on "reaction theory", which proposes that changes in blood pCO_2 are detecting via the sensing of pH rather than CO_2 directly (Loeschcke 1982, Winterstein 1949). This might have led to alternative mechanisms of pCO_2 sensing being overlooked. Owing to the presence of carbonic anhydrase in mammalian tissue, any of CO_2, H^+ (pH), or HCO_3^- could theoretically act as signals to detect the level pCO_2 (**Figure 1.2**). Following from this, there is clear evidence that CO_2 regulates breathing via the direct detection of CO_2 itself; with the effect being independent of that which is evoked from pH detection, (Shams 1985, Harada, Kuno, and Wang 1985, Huckstepp et al. 2010a).

Below we discuss putative central respiratory chemosensory transducers for pCO_2 and comment on the strength of their relevance to wild-type animals based on their current evidence.

1.3.1 ASIC1 and ASIC2

ASIC Acid-sensing ion channels (ASICs) have been shown to be important in sensing CO_2 and electing a fear response in the amygdala (Ziemann et al. 2009) – cultured neurons lack chemosensitivity and KO mice have blunted fear responses. ASIC channels are also expressed in the NTS and broadly in the VLRC (levels higher in neonates than adults) and have been suggested to play a role in chemoreception (Huda et al. 2012, Song et al. 2016). However, although these studies linked neuronal chemosensitivity to ASIC channels, a physiologically unrealistic pH value was required to activate these channels (pH <6.5). At the VMS only very small changes in pH occur in response to physiological changes in pCO_2 (Shams 1985), with pH maintained between 7.4 and 7.25

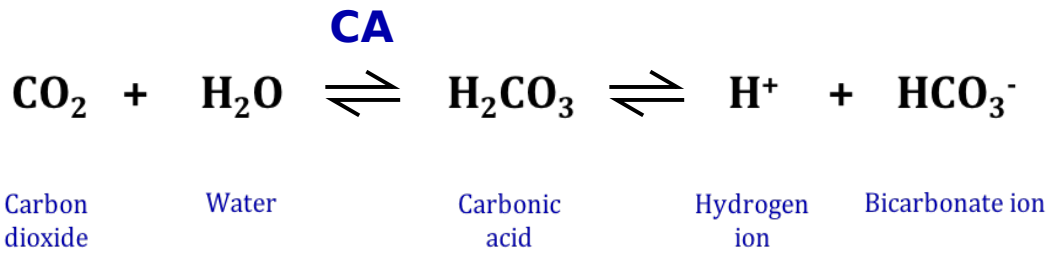

Figure 1.2 Equation of the reaction driven by carbonic anhydrase. Carbonic anhydrase (CA) converts carbon dioxide and water into carbonic acid, which dissociates into hydrogen ions and bicarbonate ions. Because of this, any one of CO_2, H^+ or HCO_3^- could theoretically be a signal for increased levels of CO_2

(Fencl 1971, 1986) and a pCO_2 >100 mmHg required for pH to drop below pH 7.1 (Katsura et al. 1992b, Katsura, Ekholm, and Siesjö 1992a). Furthermore, no evidence has been provided for the effect ASICS channels have on breathing (in either anaesthetised or conscious animals). Consequently, the current evidence linking ASIC channels to respiratory chemoreception is weak, and the proposed mechanism is not likely to occur under healthy physiological conditions.

1.3.2 TASK channels

The Tandem-pore acid sensing potassium (TASK) channels TASK-1 and TASK-3 had been implicated to be the chemosensory transducer for serotonergic neurons, which were then concluded to play no role in central chemoreception in the conscious animal as KO of TASK-1, TASK-3, or TASK-1/TASK-3 in mice resulted in a normal HCVR (Mulkey et al. 2007). However, these studies targeted dorsal raphé neurons that have not actually been implicated in chemoreception and only showed a pH dependent response to a pH decrease from pH 7.5 to 6.9. Therefore, the serotonergic neurons in the ventral medulla (which respond to pH change of 7.4 to 7.2) might still play a role in chemoreception via another chemosensory transducer such as GPR4 (Teran, Massey, and Richerson 2014). TASK1 channels have been shown to play a role in peripheral chemoreception, contributing to the carotid body discharge that occurs in response to hypoxia or hypercapnia (Trapp et al. 2008). This supports the role of TASK1 as a chemosensory transducer for *peripheral* chemoreception.

TASK-2 has been suggested to mediate RTN chemosensitivity (Wang et al. 2014, Kumar et al. 2015) although whether or not this should be thought of as a chemosensory transducer is still to be clarified. Although patch clamp data found that a subpopulation of RTN neurons from TASK-2-KO mice brain slices lost their pH sensitivity (Wang et al. 2014), the pH change used was from pH 7.8 to 7.0 (not a physiologically realistic decrease). Furthermore, using working heart-brainstem preparations this study did not find any difference between the respiratory drive of global TASK-2-KO and wild-type mice preps in response to hypercapnia, although they did find higher baseline respiratory drive in TASK-2-KO mice at resting CO_2 levels. Consistent with this, global TASK-2-KO mice showed a dysregulated HCVR in the form of hypersensitivity to low CO_2 levels, and failure to reach appropriate levels at higher CO_2 (Gestreau et al. 2010, Kumar et al. 2015). Taken together the current evidence might suggest that TASK-2 is indeed important for CO_2

chemoreception, however it may not be a chemosensory transducer but rather a channel that is required to stabilise cellular conditions in order for a transducer molecule (e.g. GPR4) to function properly (Wang et al. 2014).

1.3.3 GPR4

G-protein coupled receptor 4 (GPR4) is highly sensitive to pH over the range of 6.8-7.8 (Ludwig et al. 2003) and expression can be found in cerebrovascular endothelium and neurones of raphé, RTN, LC, and lateral septum (Hosford et al. 2018, Kumar et al. 2015). GPR4 has been suggested to be responsible for chemoreception, acting as a chemosensory transducer in RTN neurons. In global GPR4-KO mice hypercapnia-induced c-fos immunoreactivity in the RTN was significantly reduced, and *in vitro* neuronal chemosensitivity under hypercapnic conditions was reduced – although chemosensitivity was defined as a >30% decrease in activity from pH 7.0 to 7.8 (i.e. a big change in pH for a relatively small change). Nevertheless, these mice also showed a severely reduced HCRV, and reintroduction of GPR4 specifically into the RTN rescued the aforementioned phenotypes. This suggests that GPR4 is sufficient to provide adequate chemoreception in this global KO system, although GPR4 was never introduced into WT mice and so the apparent rescue could be a result of GPR4 over-expression causing hypersensitivity that compensates for the defects rather than rescuing them (Kumar et al. 2015).

Interestingly the effect of global GPR4-KO presents predominantly as a diminished elevation in breathing frequency, with the effect on tidal volume being much weaker (and only significantly different once the level of CO_2 was raised to 8%) (Kumar et al. 2015). This contradicts reports that pH acidification of the RTN elicits a HCVR that is almost entirely a change in tidal volume (Li, Randall, and Nattie 1999) and questions whether or not GPR4 is indeed acting as a primary site of chemoreception (in which case it would be expect to yield the same, tidal volume only, phenotype), or whether it is instead a component of the RTN involved in integrating signals that give rise to a HCVR.

Although KO studies are necessary to support the role of a protein they must be interpreted with caution, especially when the KO has no cell-specificity (i.e. global KO's). It is very difficult to understand what developmental roles a protein has, and therefore how the resulting mutated system differs from wild type. The drastic effect that these confounding factors can have was made apparent in a recent study that used *in vivo* pharmacological manipulation of GPR4 (Hosford et al. 2018). Although this study

confirmed that GPR4 is intrinsically chemosensitive – showing GPR4-dependent increases in cyclic AMP (cAMP) in cultured RTN neurons within a somewhat more physiological range (pH decrease from 7.4 to 7.0) – IP injection of a GPR4 antagonist presented as a minor reduction in both tidal volume and frequency, as opposed to the large reduction in tidal volume only that was previously reported. Like the GPR4-KO studies, theses pharmacological studies will have also affected GPR4 activity globally (i.e. not just the RTN) and so it is interesting to see such a different response when GPR4 activity is ablated after development.

Given the differences in breathing phenotype observed between the genetic and pharmacological studies there are questions concerning the true contribution of GPR4. On the other hand, GPR4 is also expressed in ventral raphé neurons (Kumar et al. 2015). If GPR4 proves to be the chemosensory transducer responsible for serotonergic chemosensitivity then this might explain some of these discrepancies. As it stands, there is sufficient evidence of some role for GPR4 in central respiratory chemoreception, which would support its status as a chemosensory transducer, however more refined experiments are required in order to confirm this.

1.3.4 Inwardly rectifying potassium (Kir) channels

The Inwardly rectifying potassium (Kir) channels Kir4.1 and Kir5.1 are found in neurons and glia, including astrocytes in the RTN where they have been suggested to play a role in chemoreception. Global Kir5.1-KO mice, and inducible conditional GFAP:Kir4.1-KO mice, show a reduced HCVR (Trapp, Tucker, and Gourine 2011, Hawkins et al. 2014, Hawkins and Mulkey 2015, Hawkins et al. 2016). However, expression of Kir5.1 alone is unable to produce a functional channel (Bond et al. 1994, Pessia et al. 1996), and the central chemosensitive response in global Kir5.1-KO mice was found to be intact (Trapp, Tucker, and Gourine 2011). Also Kir4.1 channels are not sensitive to pH in a physiological range (pK_a 6.1) (Xu et al. 2000). Therefore, the effect seen in these KO mice cannot be because these channels alone acts as chemosensory transducers, as there is no rational mechanism as to how either would be able to respond to physiological changes in pCO_2.

As Kir4.1 is believed to be key in establishing resting membrane potential in astrocytes (Olsen and Sontheimer 2008) and Kir5.1-KO mice were found to have chronic metabolic acidosis (Trapp, Tucker, and Gourine 2011), it is likely that these KO's affects cells in other ways. For example, the GFAP:Kir4.1-KO could disrupt glial conditions that

are required for effective ATP release from chemosensitive mechanisms, and global Kir5.1-KO could alter the environment such that chemosensitive mechanisms that function in wild-type animals no longer operate properly.

Although Kir4.1 and Kir5.1 channels may not have suitable properties, their coexpression yields a Kir5.1/4.1 heteromer which is sensitive to physiological changes in pH (pK_a 7.45) (Xu et al. 2000). As Kir4.1 and Kir5.1 are expressed in proposed CRC – NTS, LC, and VII (immediately dorsal to the RTN) (Wu et al. 2004) – this heteromer could act as a chemosensory transducer and the effect that the individual KO's had on HCVR could be explained by ablation of this heteromer. Consistent with this, *in vitro* patch clamp data has suggested that pH-driven inhibition of Kir4.1/Kir5.1-like currents in sub-pial astrocytes contribute to astrocytic ATP release in the RTN (Wenker et al. 2010). This being said, the extent to which changes in astrocytic membrane potential influence the chemosensitivity of these non-electrically excitable cells is debated, and it has been argued that Ca^{2+} signalling, rather than membrane potential, plays the key role in pH-mediated astrocytic chemoreception (Gourine et al. 2010, Trapp, Tucker, and Gourine 2011). For the time being the status of the Kir4.1/Kir5.1 heteromer as a chemosensory transducer, relevant in conscious animals, is uncertain.

1.3.5 Electrogenic sodium bicarbonate cotransporter (NBCe1)

Electrogenic sodium bicarbonate cotransporter (NBCe1) is a high-affinity HCO_3^- carrier responsible for fast HCO_3^- transport and pH buffering in glia, and is expressed in most cell types of the brain, including prominent expression in glia of the brainstem (Turovsky, Theparambil, Kasymov, Deitmer, Del Arroyo, et al. 2016, Theparambil et al. 2014). Na^+/HCO_3^- cotransport (NBC) was proposed to play a role in RTN chemoreception after patch clamp data showed that the pH-sensitive current of RTN astrocytes had different properties in HCO_3^--free buffer (Wenker et al. 2010).

In vitro data has now identified a mechanism by which NBCe1 expression could contribute to the chemosensitivity of these glia (Turovsky, Theparambil, Kasymov, Deitmer, Del Arroyo, et al. 2016). This data showed that pH-induced $[Ca^{2+}]_i$ responses (comparing pH 7.4 to 7.0) from RTN astrocytes were preceded by Na^+ entry and were reduced by blocking either NBC or Na^+/Ca^{2+} exchange (NCX) – with complete abolishment upon blocking both NBC and NCX. These $[Ca^{2+}]_i$ responses were significantly reduced in brain slices form global NBCe1-KO mice. The suggestion has been made that, under

hypercapnic conditions, CO_2 entry into astrocytes leads to a decrease in pH, which activates NBCe1 causing Na^+ influx. Increasing $[Na^+]_i$ in turn activates NCX to operate in reverse mode and bring Ca^{2+} into the cell, which triggers a signalling pathway that results in ATP release.

The proposed mechanisms would advocate NBCe1 as a chemosensory transducer, translating pH_i into a Na^+ current that (via NCX) gives rise to pathway responsible for ATP release. As of yet no *in vivo* genetic data has been acquired for NBCe1 mice (constitutive KO of NBCe1 is lethal) and therefore the relevant role of this mechanisms in the animal is yet to be determined. As NBCe1-KO is likely to disrupt the resting conditions of cells, even inducible KO systems might prove difficult to interpret correctly.

1.3.6 Connexin26

Connexin 26 (Cx26) is a member of the connexin family and forms hemichannels in the plasma membrane that are capable of allowing the transporting of small molecules. Cx26 is expressed in tissues throughout the body, and expression in the medulla is restricted the ventral surface, in sub-pial glia (and the leptomeninges) (Huckstepp et al. 2010a, Nagy et al. 2001, Solomon et al. 2001, Mercier and Hatton 2001). Cx26 has been proposed to be a respiratory chemosensory transducer, playing a role in chemosensitive regions to mediate glia-dependent ATP release (see *1.2.7 Glia and ATP release*).

Cx26 hemichannels were revealed to be gated by CO_2, and not pH, via whole-cell patch clamp recordings from HeLa cells with heterologous Cx26 expression. When pH was maintained (at 7.5) Cx26 hemichannels partially opened at physiological pCO_2 (~40 mmHg), and there was increased hemichannel closing at lower pCO_2 (20 mmHg) and increased opening at higher pCO_2 (55 mmHg and 70 mmHg). In fact, acidification appeared to reduce this CO_2-dependent opening. Dye-loading under similar conditions confirmed this CO_2-depenent opening profile of Cx26 hemichannels. As inside-out and outside-out patches showed that Cx26 chemosensitivity to pCO_2 was maintained during constant pH, local pH changes were ruled out as a stimulus (Huckstepp et al. 2010b). Furthermore, biosensor recordings showed that (if pre-loaded with ATP) HeLa cells release ATP upon a pH-independent stimulus. (Huckstepp et al. 2010b, Meigh et al. 2013, Meigh et al. 2014, de Wolf et al. 2016, de Wolf, Cook, and Dale 2017). This data confirms that Cx26 hemichannels can open in response to physiological levels of pCO_2 and are sufficient to bestow upon cells the ability to release ATP in response to CO_2 directly.

In vitro biosensor recordings from rat brain slices showed the same CO_2-dependent ATP release at chemosensitive sites of the VMS. This ATP release was maintained when other potential stimuli (pH_i, HCO_3^-, adenylate cyclase) were maintained/blocked (Huckstepp et al. 2010a). ATP release was shown to occur independent of exocytosis as profound ATP release was recorded in the absence of Ca^{2+} – an ion vital for exocytosis. As hemichannels open in in the absence of Ca^{2+} (Müller et al. 2002) this supports hemichannel involvement. Pharmacological blockade of pannexin-1, known to form hemichannels and release ATP (Bao, Locovei, and Dahl 2004, Huang et al. 2007), did not affect ATP release however blockade of connexin channels did (Bruzzone et al. 2005, Huckstepp et al. 2010a).

CO_2-dependent dye loading in VMS brain slices colocalised with $GFAP^+$ cells, with a distribution profile that matches Cx26 immunohistochemical- and Cx26:LacZ-labelling (Huckstepp et al. 2010a) – thereby suggesting that VMS glia might respond to CO_2 by opening Cx26 hemichannels. Furthermore, *In vivo* recordings from anaesthetised rats showed the same CO_2-mediated ATP release along with increased respiratory drive, both of which were diminished upon connexin blockade (Huckstepp et al. 2010a).

Subsequent patch clamp and Ca^{2+} imaging studies from RTN slices have supported the involvement of glial connexins in chemoreception, reporting that RTN neuronal stimulation is inhibited by connexin blockade and reversed by its washout (Wenker et al. 2012, Moreira et al. 2015, Forsberg et al. 2016).

Cx26 is the only connexin present at the VMS that has a CO_2-dependent opening profile that matches the CO_2-dependent ATP release at the VMS chemosensitive sites (Huckstepp et al. 2010b). Given the location of Cx26 at the VMS, and that it is closed upon acidification, this protein may have finally shed light on the intermediate (Schlaefke) region, which was identified back in 1970 to cause a decrease in ventillatory response when acidified (Schlaefke, See, and Loeschcke 1970). It could be that acidification causes closure of Cx26 hemichannels in this region, thereby decreasing ATP basal tone – as has shown to occur upon connexin blockade in VMS slices (Huckstepp et al. 2010a).

It has been suggested that connexins are only involved in chemoreception in neonates (Hewitt et al. 2004), however this conclusion was drawn from data during which the RTN was focally perfused with very unrealistic hypercapnic conditions (50%

CO_2, pH 6.5) and so these results should not be considered relevant to the usual working mechanics of chemoreception.

In addition to ATP release, it has been suggested that Cx26 acts as a chemosensory transducer for the release of PGE_2 (Forsberg et al. 2016, Forsberg, Ringstedt, and Herlenius 2017). The hypothesis is that CO_2-mediated opening of Cx26 hemichannels in RTN glia allows for the release of PGE_2 through the hemichannel, which stimulates RTN neurons to alter respiratory drive. However, as has been discussed (see *1.2.7 Glia and ATP release*), the precise role of PGE_2 in chemoreception still needs to be clarified.

Cx26 has the properties expected of chemosensory transducer and we have a strong understanding of the molecular mechanisms behind its CO_2-sensitivity (see *1.4.4 Connexin26 CO_2-sensitivity*). However, as the current evidence stands the role of Cx26 in chemoreception is disputed and further genetic data is required to build a certain case for this hypothesis. Considering constitutive KO of Cx26 is lethal, and even conditional KO studies have their drawbacks, ideally we require a genetic data from a technique capable of investigating Cx26 CO_2-sensitivity in an inducible manner. To provide such genetic data was one of the aims of this thesis.

1.4 Connexin26

The protein Connexin26 (Cx26) is encoded by the *GJB2* (Gap junction beta 2) gene and is one of 21 connexins found in humans. Connexin proteins can be found in all tissues and form hexameric channels (connexons) in the plasma membrane that can open and close in response to various stimuli in order to allow molecules into and out of a cell (Stout, Goodenough, and Paul 2004, Wang, De Bock, et al. 2013). Expression of Cx26 can be found in many tissues including the liver, uterus, skin, eyes, ears, and brain (Nicholson et al. 1987, Nagy et al. 2011, Dalamón et al. 2016).

1.4.1 Connexin26 trafficking and assembly

As with all connexins, Cx26 is translated as a peptide subunit that goes on to assemble into a hexameric connexon. Assembly into connexons is known to occur before delivery to the plasma membrane (Kumar and Gilula 1996, Goodenough, Goliger, and Paul 1996, Willecke et al. 2002), although not all connexons will be trafficked straight to the plasma

membrane; instead they may be added to intracellular stores for later use in connexon turnover from the plasma membrane (George, Kendall, and Evans 1999). The precise assembly and the trafficking pathway varies depending on the connexin (George, Kendall, and Evans 1999, Martin et al. 2001).

Details of Cx26's trafficking pathway have remained elusive, and we have little further understanding than that from fifteen years ago: Cx26 shows co-translational and post-translational insertion into membranes of intracellular compartments, its targeting from the ER to the plasma membrane can be via the Golgi pathway or a yet uncharacterised microtubule-dependent pathway, and assembly of Cx26 connexons starts in the ER – with significant assembly detectable within the Endoplasmic reticulum-Golgi intermediate compartment (ERGIC) (Martin et al. 2001, Zhang et al. 1996, George, Kendall, and Evans 1999).

1.4.2 Connexin26 structure

All connexin proteins have the same general structure; an intracellular N- and C-terminus (NT and CT, respectively), four α-helical transmembrane domains (TM1-4), two flexible extracellular linker loops (EL1-2), and one flexible cytoplasmic linker loop (CL), **Figure 1.3a**.

As has been mentioned, six individual connexin subunits assemble to form a connexon with a central pore. Individual connexon channels are known as hemichannels and two hemichannels from apposing membranes are capable of docking and fusing with each other, creating gap junctions (**Figure 1.3b**). Crystal structure data (at 3.5 Å resolution) has shown Cx26 gap junctions to be 9.1 nm at its widest point and 15.4 nm in length (Maeda et al. 2009). Although hemichannel docking is very likely to induce a conformational change, Cx26 hemichannels can be assumed to have a similar maximum width, and a length of ~7.7 nm (half that of a gap junction).

One of the most interesting properties of connexins is their ability to coassemble with other members of the connexin family, forming heteromeric connexon hemichannels. On top of this, connexons with different compositions to one another are able to dock to form heterotypic gap junctions. Heteromeric compatibility depends upon a specificity motif between CL and TM3, whilst heterotypic compatibility depends upon a specificity motif in EL2. Cx26 is known to have heteromeric compatibility with Cx30, Cx30.3, Cx31 and Cx32. Cx26 is known to have heterotypic compatibility with Cx30, Cx32,

Cx46 and Cx50, and there is conflicting data as to its compatibility with Cx31 (which does not contain the same specificity motif as the others listed). The functional versatility that heteromeric/heterotypic interactions could provide for connexins is vast, and probably accounts for their widespread expression and evolution (Koval, Molina, and Burt 2014).

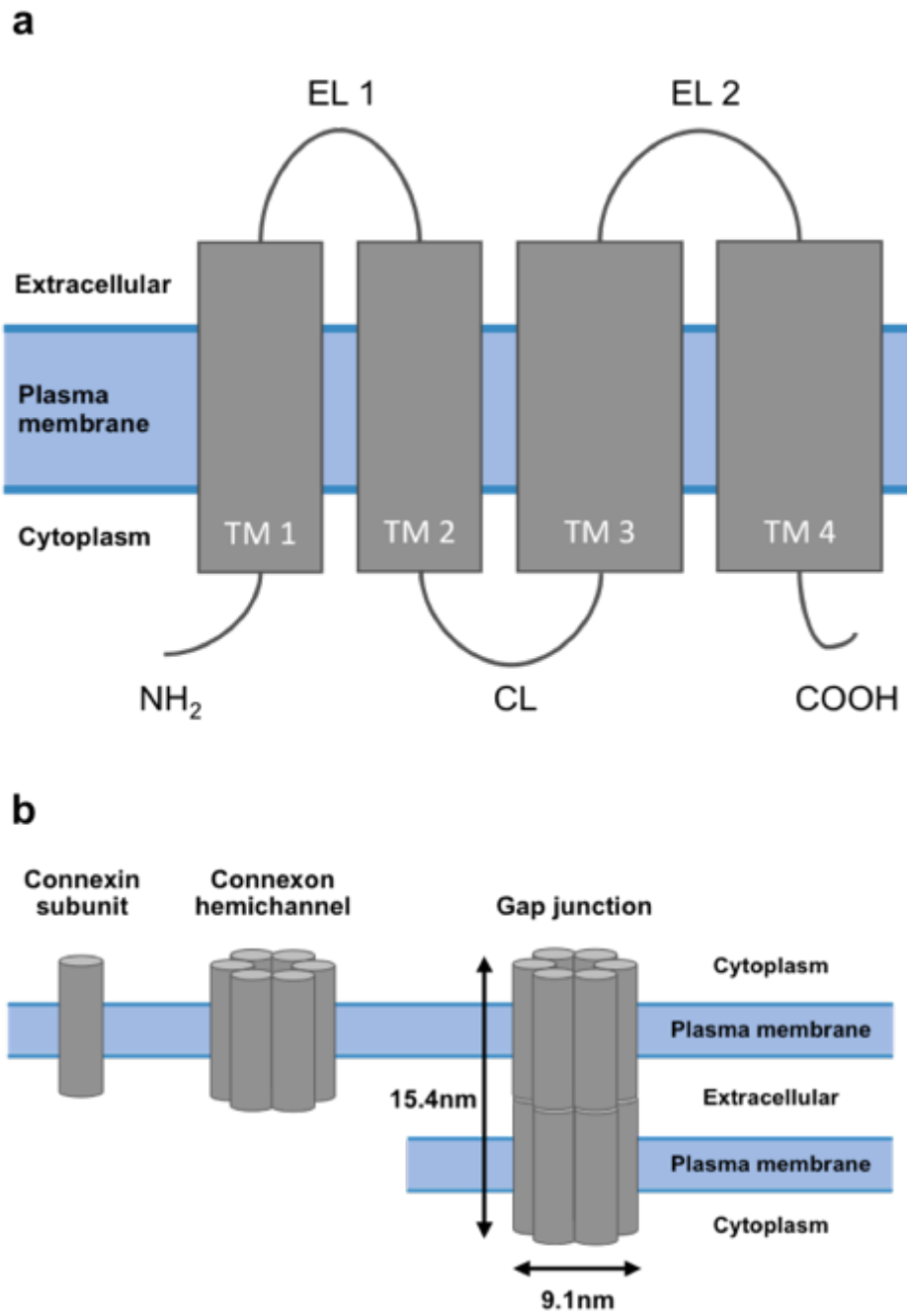

Figure 1.3 **Connexin26 structure a)** Cartoon structure of the connexin protein expressed in the plasma membrane. **b)** Cartoon showing the arrangement of connexin subunits when arranged as connexon hemichannels, and when connexons from apposing membranes fuse to form gap junctions. TM, transmembrane region; EL, extracellular loop; CL, cytoplasmic loop.

1.4.3 Connexin26 gating

Connexin hemichannels and gap junctions, including Connexin26 (Cx26), have widespread functions in many different cell types. Connexin channels provide their function by opening or closing in response to various stimuli, thus controlling the movement of small molecules into and out of the cell. Permeability varies between connexins but is based on size (<1 KDa) and charge (although precise properties are uncertain) (Kanaporis, Brink, and Valiunas 2010). Sweeping statements are often made about the properties of Connexins; grouping together results from vastly different family members (e.g. Cx26 and Cx43). Although these statements are correct and demonstrate the physiological importance of connexins, for studies trying to dissect the key players in a particular pathway, or those focusing on the function of one particular connexin (such as this thesis), it is important to make the reader aware of the evidence that links specifically to the connexin of interest.

The same is true for the comparison between hemichannels and gap junctions. Connexin hemichannels are often thought of as half a gap junction, a belief that can lead to assumptions and studies that do not provide the true story. Another confounding factor is the myriad of heteromeric connexon hemichannels and heterotypic gap junction channels that can form across the connexin family of proteins, e.g. Cx26/Cx32 heteromeric hemichannels are sensitive to pH-dependent taurine gating, whereas Cx32 homomeric hemichannels are not (Locke et al. 2011). Here, the various stimuli that are capable of controlling homomeric/homotypic Cx26 gating are discussed; with distinctions made between hemichannel and gap junction gating

Extracellular Ca^{2+} $[Ca^{2+}]_e$ decreases connexin hemichannel and gap junction activity at physiological levels (Müller et al. 2002, Bennett et al. 2016, Gómez-Hernández et al. 2003, Chen et al. 2005, Kamermans et al. 2001, Unwin and Zampighi 1980, Unwin and Ennis 1984, Burra and Jiang 2011). On the other hand, $[Ca^{2+}]_e$ activation of connexin channels can occur under millimolar $[Ca^{2+}]_e$, which occurs in the cochlear and under various conditions such as inflammation, ischemia, extracellular alkalinisation (Bao, Altenberg, and Reuss 2004, Orellana et al. 2012, Schalper et al. 2010, Scheckenbach et al. 2011). The mechanism behind connexin $[Ca^{2+}]_e$ is debated, however one explanation is that electrostatic interactions between residues D50 and E47 physically block hemichannel pores (Müller et al. 2002, Lopez et al. 2016), and that the residues E42, G45, and E47 play a role in forming an electrostatic barrier in gap junctions (Bennett et al.

2016). No intracellular Ca^{2+} $[Ca^{2+}]_i$ effect on gating has been reported.

Cx26 gap junctions and hemichannels have been shown to exhibit voltage-gating opening, with voltage sensitivity varying from cell to cell. It used to be thought that gap junctions had a single, transjunctional, voltage gating mechanism however it is now understood that a given connexon hemichannel, and each of the two connexons that make up a gap junction, have two distinct voltage gating mechanisms – fast and slow (loop) gating. (Bargiello et al. 2012, Bukauskas and Verselis 2004, González, Gómez-Hernández, and Barrio 2006, Kojima et al. 2001).

Perhaps the most confusing Cx26 gating property that is reported in the literature is gating via pH changes. Cx26 gap junctions were shown to undergo pH-sensitive gating in response to changes in intracellular pH (pH_i), with a lower pH resulting in lower conductance (no conductance at pH < 6.5 and max conductance at values > 7.4) (Stergiopoulos et al. 1999). However, there is now evidence suggesting that the story may be more complicated. A pH dependent interaction has been shown to occur between the C-terminus (CT) and cytoplasmic loop (CL), however it is only upon the disruption of this interaction by aminosulphonates, such as taurine, that Cx26 channels close. In other words, at higher pH values aminosulphonates are not able to disrupt any part of Cx26, however once pH drops the interaction can be disrupted, potentially leaving the CT free to physically occlude the channel pore. This finding has been shown to be comparable between both gap junctions and hemichannels (Locke et al. 2011, Yu et al. 2007).

Cx26 has also been shown to have temperature-sensitive gating, with small molecule conductivity increasing upon exceeding a temperature of 23^0C. This gating is thought to involve the TM1/EL1 3_{10} helix (parahelix) and TM4 helix, with indications of additional involvement from the plug domain (Steffens et al. 2008, Kniggendorf et al. 2014). It is assumed, but not confirmed, that this gating property is relevant to both Cx26 hemichannels and gap junctions.

Interestingly, pathogen-induced opening of Cx26 hemichannels has also been reported. In epithelial cells expressing Shigella, actin- and phospholipase C-dependent opening of Cx26 hemichannels caused the release of ATP into the medium (which increased bacterial spreading). Any such effects on gap junctions could not be discerned, however blocking of all gap junctions did reduce Shigella spread (Van Nhieu et al. 2003).

The most recent stimuli found to gate Cx26 (amongst other connexins) is CO_2.

Dye-loading and molecular simulations show that, at hypercapnic conditions (55mmHg CO_2), K125 is carbamylated and forms a salt bridge with the R104 residue of the closest adjacent subunit. Formation of all 6 possible bridges fully stabilise the connexon hemichannel in an open state (Huckstepp et al. 2010b, Meigh et al. 2013, Meigh et al. 2015b, Meigh 2015a). Additionally, acidification has been shown to reduce the opening sensitivity of Cx26 hemichannels in response to a CO_2 stimulus (with alkalisation increasing this CO_2-sensitivity) (Huckstepp et al. 2010b). Excitingly, patch clamp and dye-transfer studies have revealed that CO_2 has the opposite effect on Connexin26 gap junctions – closing them as pCO_2 increases (personal communication with Nicholas Dale). The benefit of CO_2 opening hemichannels but closing gap junctions is yet to be understood.

Other gating properties that have been documented in other members of the connexin family (but not in Cx26) include sensitivity to mechanical stimulation, metabolic stimulation, phosphorylation, and $[Ca^{2+}]_i$ (De Vuyst et al. 2006, Bao, Sachs, and Dahl 2004, Gomes et al. 2005, Li et al. 1996, Bruzzone et al. 2001, Bao, Altenberg, and Reuss 2004).

As stated at the beginning of this section, it is important to make the reader aware of which results are relevant to the study at hand. For many of the stimuli discussed above their physiological relevance for many *in vivo* systems is debatable. For example, although Cx26 is found in many different environments throughout the body, only in the cochlear of the ear does $[Ca^{2+}]_e$ reach a level at which $[Ca^{2+}]_e$-mediated activity can occur. This thesis seeks to investigate the role of Cx26 hemichannel-mediated ATP release in response to hypercapnia, and it seeks to do so by specifically manipulating Cx26 within glial cells of a restricted area of the VMS. Glial cells are non-excitable and within the VMS pH and temperature are tightly regulated (Shams 1985, Fencl 1971, Katsura et al. 1992b), therefore these stimuli are unlikely to have any gating influence on the Cx26 hemichannels under study.

1.4.4 Connexin26 CO_2-sensitivity

Given the significance that Cx26 CO_2 gating has to this thesis, this section outlines the discovery of this property and the evidence that provides the basis of our understanding for the mechanisms behind CO_2 gating.

Cx26 was first found to be sensitive to CO_2 (along with Cx30 and Cx32) less than a decade ago, when Huckstepp *et al.* found that Cx26 hemichannels open in response to molecular CO_2 directly, which results in ATP release at chemosensitive sites of the VMS (Huckstepp et al. 2010a, Huckstepp et al. 2010b) (see *1.3.6 Connexin26*)

To uncover the mechanisms underlying Cx26 CO_2-sensitivity Meigh *et al.* performed a number of molecular and structural studies investigating the interaction between CO_2 and Cx26. Cx26, Cx30, and Cx32 (all CO_2-sensitive) contain a carbamylation motif (KVREI) that is absent from Cx31, which is CO_2-insensitive (Meigh et al. 2013, Huckstepp et al. 2010b). Carbamylation involves the nucleophilic attack of CO_2 to an amine, which can occur at lysine side chains, or the N-terminus, and introduces a novel negative charge (Meigh 2015a). The lysine residue (K125) of the carbamylation motif is orientated towards an arginine (R104) of a neighbouring subunit (both on which are found on the cytoplasmic loop), and the distance between them is only 6.5Å (Maeda et al. 2009) - **Figure 1.4**. Coarse-grained model simulations showed that carbamylation of K125, and subsequent inter-subunit bridging with R104, stabilises the hemichannel and biases it towards an open state (Meigh et al. 2013).

There is much evidence from dye-loading and patch clamp experiments that supports carbamylation bridge formation between K125 and R104:

- Insertion of the carbamylation motif into the Cx31 gene (CO_2-insensitive) generated a CO_2-sensitive mutant and when an additional mutation was introduced, exchanging K125 for A125, the resulting hemichannel was CO_2-insensitive; as the higher pK_a of arginine prevents its carbamylation and thus formation of a bridge at residue number 125 (Meigh et al. 2013)
- Point mutations to disrupt the ability of K125 or R104 to form carbamate bridges in Cx26 (yielding $Cx26^{K125R}$ and $Cx26^{R104A}$, respectively) were enough to remove

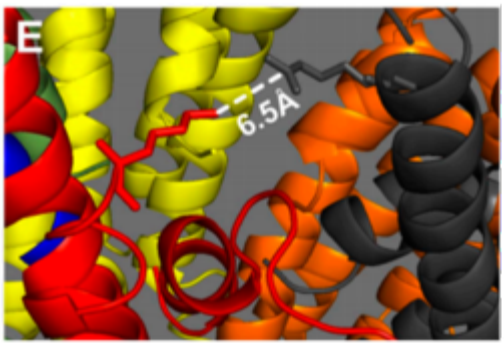

Figure 1.4 **Amino acid residues vital for Connexin26 CO_2-sensitivity**. The orientation of R104 (dark grey) and K125 (red) towards each other, and their proximity to one another, suggests that carbamylation of K125 would result in the formation of a salt bridge between them. Cytoplasmic loops are orientated towards the top of the image. Protein structure from (Maeda et al. 2009). *Image reprodcued from: Meigh et al. (2013)*

CO_2 sensitivity from Cx26 (Meigh et al. 2013)

- By utilising the analogy that glutamate has to carbamylated lysine, substitution of either K125 or R104 with glutamate yielded constitutively open hemichannels – rationalised to be a result of glutamate (in either position) being sufficient to form a salt bridge under normocapnia, in the same way that carbamylated K125 does under hypercapnia (Meigh et al. 2013)
- The K125C mutation provided for the formation of inter-subunit S-Nitrosothiol (SNO) bridges (between C125 and R104 residues), and the additional R104C mutation provide for disulphide bridges (between C125 and C104 residues), both of which triggered channel opening – implying that the formation of any inter-subunit bridge at these residues is what causes hemichannel opening (Meigh 2015a)

The CO_2-sensing property of Cx26 explains and supports the role of Cx26 as a chemosensory transducer (see *1.3.6 Connexin26*); during hypercapnia Cx26 expressed at the VMS undergoes carbamylation, resulting in inter-subunit bridge formation that stabilise hemichannels in the open state, and subsequently increases ATP release (which goes on to stimulate respiratory drive).

1.4.5 Connexin26 in disease

Cx26 is responsible for ~50% of non-syndromic sensorineural hearing loss (NSHL) (Petersen and Willems 2006), with over 70 different mutations reported (Mishra et al. 2018). Deafness-linked Cx26 mutations resulting in a premature STOP codon give rise to profound hearing loss and have been reported to have a pathophysiology related to a lack of gap junctions. Deafness-linked Cx26 mutations resulting in missense mutations tend to be associated with less sever hearing loss and have been suggested to reduce channel permeability (Petersen and Willems 2006, Beltramello et al. 2005). We have not yet identified the underlying cause for all of the Cx26 mutations involved in hearing loss, and with the fairly recent discovery of Cx26 CO_2-sensitivty it will be interesting to see if consideration of this property leads to novel links being made between hearing loss and CO_2 gating.

Another human pathology linked to Cx26 is Keratitis-Ichthyosis Deafness (KID) syndrome. KID syndrome is a rare disorder characterised by a combination of deafness,

visual impairment, and dermatological defects (Caceres-Rios et al. 1996). There are nine known missense mutations that that cause KID syndrome (Xu and Nicholson 2013, Yotsumoto et al. 2003). Mutations predominantly arise through *de novo* mutations and act in a dominant negative manner (Sbidian et al. 2010).

As of yet we are not clear of the mechanisms underlying KID syndrome pathology and given the complexity of this syndrome it is likely to be a result of multiple dysfunctions. Theories have been made suggesting that some of the pathophysiology arises due to '"leaky" hemichannels (Mhaske et al. 2013, Gerido et al. 2007). Another hypothesis, and one of relevance to this thesis, is that aberrant CO_2 gating plays a role in KID syndrome pathology.

The KID syndrome mutation A88V renders the Cx26 hemichannel insensitive to CO_2, and furthermore $Cx26^{A88V}$ subunits act in a dominant negative manner to remove CO_2 sensitivity (just as KID mutations act in a dominant manner in patients) (Meigh et al. 2014, Sbidian et al. 2010). Furthermore, in one case study a patient with A88V-linked KID syndrome exhibited a respiratory pattern that suggests a diminished central respiratory drive (Meigh et al. 2014). Whilst it has not been proven if the lack of CO_2 sensitivity is to blame for this deficiency in respiratory drive, such an explanation is consistent with current evidence for Cx26 in central CO_2 chemoreception (see *1.3.6 Connexin26*) and brings to light a possible connection between Cx26 CO_2 sensitivity and human pathology. In fact, there are multiple cases in which KID syndrome patients have been reported to suffer from severe breathing problems (Meigh et al. 2014, Koppelhus et al. 2011, Janecke et al. 2005, Sbidian et al. 2010), however given that KID syndrome is a rare disorder with severe skin, eye and hearing afflictions, the effect that this disorder has on breathing may be overshadowed, resulting in failure to report/test the respiratory system.

A recent study (part of which is included in this thesis) has further investigated whether there might be an undiscovered a role for Cx26 CO_2 sensitivity in human pathophysiology. In this study the CO_2 sensitivity of a range of pathological Cx26 mutants were tested *in vitro*. From the results two more KID syndrome mutants, N14K and N14Y, were shown to be insensitive to CO_2 whereas two recessive deafness mutants, M34T and V84L, had lesser effects on CO_2-sensitivity of cells. It was suggested that the severity of the effect a mutant has on CO_2 sensitivity could correlate with the severity of the pathological effect the mutant has in humans (de Wolf et al. 2016).

More research into Cx26 is required in order to ascertain the precise nature of the pathophysiology that presents in patients expressing certain Cx26 mutants, and to identify new targets or therapies that could be of benefit to patients.

1.4.6 Connexin26 as a conduit for evolutionary adaptions of air breathing animals

Given the proposed role for Cx26 in central respiratory chemoreception (see *1.3.6 Connexin26*) the CO_2-sensing properties have been tested and compared across the Cx26 homologs in human, rat, mole rat, and chicken. In human and rat the pCO_2 is maintained ~40mmHg and Cx26 hemichannels show significant opening at 55mmHg, which is expected if Cx26 hemichannel opening acts to signal an excess of CO_2. In contrast, mole rat Cx26 CO_2-sensitivty was shifted towards a higher pCO_2 (not showing significant opening until 70mmHg) and chicken Cx26 CO_2 sensitivity was shifted to lower pCO_2 (showing significant opening at 35mmHg) (de Wolf, Cook, and Dale 2017).

Evolutionarily this contrast across different species, based upon the environments their ancestors were accustomed to, supports the role for Cx26 in respiratory chemoreception. The pCO_2 underground, where mole rats reside, is greater than above it and so sensitivity to CO_2 would need to be lower so that the animal is not receiving constant signals that they are under hypercapnic conditions. On the other hand, birds have a lower resting pCO_2 compared to mammals (~30 mmHg compared to ~40 mmHg). When birds (including flying ancestors of the chicken) fly at high altitudes they breathe more frequently thereby lowing their pCO_2. Therefore, sensitivity to CO_2 would need to be higher in order to correctly regulate breathing and cerebral blood flow (which might also be controlled by Cx26).

1.5 Experimental aims

The hypothesis of this thesis is that the Cx26 hemichannel CO_2 sensitivity, in $GFAP^+$ cells of the VMS, plays a role in central respiratory chemoreception.

The three main aims of this thesis are to:

1. Further our understanding of the CO_2-mediated Cx26 hemichannel opening that might take place within physiological systems or be altered in disease states.
2. Characterise an artificially engineered Cx26 mutant ($Cx26^{DN}$) to determine if it is appropriate for *in vivo* use to investigate Cx26 CO_2-sensitivity.
3. Develop a strategy for using the $Cx26^{DN}$ mutant in mice to determine the role that Cx26 CO_2-sensitivity plays in central respiratory chemoreception.

2 GATING DETERMINANTS OF CONNEXIN26 HEMICHANNELS: INTRACELLULAR CALCIUM AND CO_2 SENSITIVITY OF A PATHOLOGICAL MUTATION

2.1 Introduction

The gating of Connexin26 (Cx26) hemichannels and gap junctions is multifaceted, being regulated by Ca^{2+}, pH, temperature, membrane potential, and CO_2. Additional complexity arises when considering the gating of heteromeric connexon hemichannels or heterotypic gap junctions (see *1.4.3 Connexin26 gating*). Perhaps understandably characterisation of Cx26 gating is far from complete; with many gating mechanisms remaining elusive, antagonism/synergism between stimuli being almost unmentioned, and the physiological relevance of many stimuli being uncertain.

The finding that CO_2 opens Cx26 hemichannels is a fairly recent discovery (Huckstepp et al. 2010a, Meigh et al. 2013), and shows that CO_2 must be thought of as more than a waste product. Interestingly, CO_2 also closes Cx26 gap junctions by acting at the same residues that open the hemichannel (personal communication from Nicholas Dale). As Cx26 expression is widespread throughout the body – being found in the liver, uterus, skin, eyes, ears, and brain (Nicholson et al. 1987, Nagy et al. 2011, Dalamón et al. 2016) – this finding may have widespread signalling implications throughout the body. Such a novel and exciting finding demands further study of this new found characteristic, in order to fully document its physiological importance in animals and to investigate any possible involvement in pathologies. Currently, Cx26 CO_2 sensitivity has been implicated in respiratory chemoreception at the ventral medullary surface (VMS), where Cx26 hemichannel opening, in glia, results in the release of ATP that acts to increase respiratory activity (Huckstepp et al. 2010a, Huckstepp et al. 2010b). Also, all currently tested Cx26 mutations that are linked to Keratitis, Ichthyosis, and Deafness (KID) syndrome lack CO_2 sensitivity – and a novel link may be made to reduced respiratory drive experienced in some KID syndrome patients (Meigh et al. 2014, de Wolf et al. 2016).

Intracellular Ca^{2+} concentration ($[Ca^{2+}]_i$) has the potential to be another Cx26 gating stimulus, however it has not yet been investigated. It is well documented that

connexin hemichannels and gap junctions are involved in Ca^{2+} wave signalling through a combination of gap-junction coupling and hemichannel-mediated ATP release (Pearson et al. 2005, Anselmi et al. 2008, Cotrina et al. 1998, Ceriani, Pozzan, and Mammano 2016); however the role of Cx26 in such signalling is unclear. As Cx26 expression is so widespread and Ca^{2+} signalling is all-but universal (Clapham 2007, Bootman et al. 2001, Bootman and Berridge 1995, Lodish et al. 2008, Berg, Tymoczko, and Gatto Jr 2002), this alone provides reason to investigate $[Ca^{2+}]_i$ gating of Cx26. However, of particular interest to this thesis, changes in $[Ca^{2+}]_i$ have been shown to occur in chemosensitive glia of the VMS when they respond to hypercapnic conditions (Gourine et al. 2010). VMS glia have also shown CO_2-mediated ATP release that acts to increases respiratory drive (Huckstepp et al. 2010a). If $[Ca^{2+}]_i$ opens Cx26 hemichannels then it could serve as a mechanism to augment their CO_2-mediated opening, thereby increasing Cx26-mediated ATP release in the VMS. If Cx26 is gated by $[Ca^{2+}]_i$ we hypothesise that an initial influx of Ca^{2+} via CO_2-induced opening of Cx26 hemichannels, or alternative mechanisms, will enhance Cx26 opening (**Figure 2.1**).

In this chapter we aimed to further understand Cx26 hemichannel properties that might influence Cx26-mediated release at the VMS. To investigate the role that $[Ca^{2+}]_i$

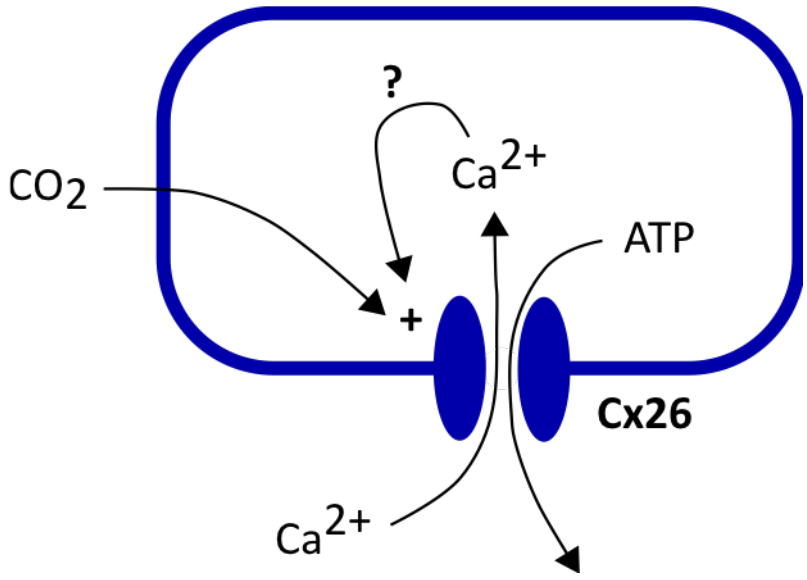

Figure 2.1 Hypothesis for enhanced CO_2-mediated ATP release via $[Ca^{2+}]_i$. It is possible that connexin26 (Cx26) hemichannels are opened by increases in $[Ca^{2+}]_i$. If so, then opening of Cx26 hemichannels by CO_2 could cause an influx of Ca^{2+} that acts to enhance this opening and the subsequent ATP release.

might have in CO_2-mediated Cx26 hemichannel opening (and in Cx26 channel gating more generally) this chapter also investigates whether or not, in the absence of extracellular messengers, $[Ca^{2+}]_i$ is sufficient for Cx26 channel opening. Following on from this, to help characterise the link between Cx26 CO_2 gating and pathology (including respiratory defects) this chapter investigates the CO_2 sensitivity of the Cx26 N14K mutant – a KID syndrome mutant.

The $Cx26^{N14K}$ data presented in this chapter has been published as part of de Wolf, E., van de Wiel, J., Cook, J., & Dale, N., 2016.

2.2 Materials and methods

2.2.1 HeLa cell culture and sample preparation

HeLa DH cells were maintained in Dulbecco's modified Eagle's medium (DMEM) supplemented with 10% fetal calf serum (FCS), 50µg/mL Penicillin Streptomycin, and 3mM $CaCl_2$. Cells were grown at 37^0C in a 5% CO_2 humidified incubator.

HeLa cells stably expressing *Mus musculus* Cx26 (Cx26-HeLa cells) were obtained from the laboratory of Dr Klaus Willecke, Bonn, and were maintained in Dulbecco's modified Eagle's medium (DMEM) supplemented with 10% fetal calf serum (FCS), 50µg/mL Penicillin Streptomycin, 3mM $CaCl_2$. Cx26-HeLa cells were also grown in 1µg/mL Puromycin to maintain selection pressure. Cells were grown at 37^0C in a 5% CO_2 humidified incubator.

All cells were plated onto coverslips at densities such that cells were not too confluent by the time of experiments. For whole-cell patch clamp (intracellular Ca^{2+}) experiments cells were plated at 1 x 10^4 per well (9cm^2) and experiments carried out 3 days later. For dye loading experiments involving single expression of a Cx26 constructs in parental HeLa cells, plating was at 1 x 10^4 per well and experiments carried out 4 days later (3 days post transfection). For dye loading experiments involving coexpression into Cx26-HeLa cells, plating was at 1 x 10^4 per well and experiments carried out 7 days later (6 days post transfection). When appropriate, transfection of cells occurred 24hrs after plating. Cells were transiently transfected with 1µg of appropriate DNA using the GeneJuice transfection agent protocol (Merck Millipore).

2.2.2 Photoactivation of intracellular Ca^{2+}

NP-EGTA (Thermo Fisher, UK) loading was achieved by incubating glass coverslips containing Cx26-HeLa cells in 15 µM NP-EGTA AM for 20 mins, followed by 10 µM Rhod-2 loading for 20mins, followed by a 20 min de-esterification in 35 mmHg CO_2 aCSF (see *2.2.6 – Experimental aCSF solutions*) – during which intracellular esterases remove the acetoxymethyl ester allowing NP-EGTA direct contact with the cytosol). All loading steps were performed at room temperature. Suspension and dilution of NP-EGTA AM was achieved via dissolving in DMSO containing 20% Pluronic F-127 solution (Life Technologies, UK) to a concentration of 6 mM, and then diluted in 35 mmHg CO_2 aCSF to a final concentration of 15 µM.

UV field illumination (375 nm) during 2 s (alternating 50 ms exposure, 50 ms closed shutter) was used to photolyse NP-EGTA and release Ca^{2+} across a filed of view of NP-EGTA-loaded cells on glass coverslips. NP-EGTA exhibits a high affinity for Ca^{2+} (Kd = 80 nM), however upon illumination with UV light the NP-EGTA chelator is cleaved, and the resulting iminodiacetic acid photoproducts have a very low affinity for Ca^{2+} (Kd > 1 mM) – thus releasing sequestered Ca^{2+} (Ellis-Davies and Kaplan 1994). In this way changes in $[Ca^{2+}]_i$, and its effect on Cx26 gating, can be assessed.

2.2.3 Ca^{2+} imaging data capture and analysis

Rhod-2 (Thermo Fisher, UK) loading was achieved in the same manner as NP-EGTA loading: incubation of glass coverslips containing Cx26-HeLa cells in 15 µM NP-EGTA AM for 20 mins, followed by 10 µM Rhod-2 loading for 20mins, followed by a 20 min de-esterification in 35 mmHg CO_2 aCSF, all performed at room temperature. Suspension and dilution of Rhod-2 AM was achieved via dissolving in DMSO containing 20% Pluronic F-127 solution (Life Technologies, UK) to a concentration of 4 mM, and then diluted in 35 mmHg CO_2 aCSF to a final concentration of 10 µM.

Cells were imaged using epifluorescence (Scientifica Slice Scope, Cairn Research OptiLED illumination, 60x water Olympus immersion objective, NA 1.0, Hamamatsu ImageEM EMCCD camera, Metafluor software). Rhod-2 was excited with a 535nm LED, and its emission recorded between 570-640 nm (0.25 fps). Rhod-2 undergoes > 100 fold increase in fluorescence intensity upon binding Ca^{2+} – thus allowing the detections of even small changes in $[Ca^{2+}]_i$ (Minta, Kao, and Tsien 1989). In these experiments Rhod-2 was used to assess the increase in $[Ca^{2+}]_i$.

2.2.4 Patch clamping data capture and analysis

Patching of cells was performed by Nicholas Dale, all other parts of the experiments and analysis were performed by Joseph van de Wiel.

HeLa cells stably expressing Cx26 and loaded with NP-EGTA and Rhod-2, were subjected to whole-cell patch clamping, with a change in whole cell conductance interpreted as channel opening. Whole-cell patching records channel opening throughout the entire cell, as opposed to other forms of patch clamping that only record channel activity from a small section of membrane.

Glass coverslips containing Cx26-HeLa cells were perfused in a bath chamber with 35mmHg CO_2 aCSF (see *2.2.6 – Experimental aCSF solutions*), to keep cells oxygenated and viable. For whole cell patching a glass electrode, filled with a buffer solution mimicking cytosolic conditions and a platinum wire to register electrical currents, makes a seal with the plasma membrane of a selected cell. Suction is then applied to rupture the membrane and cause it to form a seal around the electrode. Electrode buffer solution (sterile filtered and pH adjusted to 7.2 with KOH): 120 mM K-gluconate, 10 mM TEACl, 10 mM EGTA, 10 mM CsCl, 3 mM ATP, 1 mM $CaCl_2$, 1 Mm $MgCl_2$.

Analysis was performed on an application purposely written for patch clamp analysis (MacAnalysis, Nicholas Dale), with the step change in current being measured before, at the peak of, and after a stimulus (Ca^{2+} release, or hypercapnia). Measurements before and after were averaged to provide a value used for baseline, which was subtracted from measurements obtained at peak response and converted to conductance (nS). Conductance was calculated as: ΔI/V were ΔI is the current change in Amps and V is the voltage step applied (10 mV). Calculation of conductance change is summarised in **Figure 2.2**. A one-way ANOVA with post hoc testing was carried out in the statistical package SPSS.

2.2.5 Construction of connexin gene constructs

Connexin26 DNA sequence from *Rattus norvegicus* (accession number NM_001004099.1) was synthesised by Genscript USA (omitting the STOP codon) and subcloned into a Puc19 vector such that the transcript would form a fusion protein with the mCherry fluorophore we engineered to be 3' (downstream) of Cx26. For subsequent experiments, this vector was cloned to yield different Connexin-fluorophore fusion protein constructs, using a combination of Kpn1, Xho1, Age1, and Nde1 restriction site digests.

Whenever mutations were required the Agilent Quikchange method protocol was followed. Guided by the Quikchange manual, the PCR reaction was performed over 16 cycles to achieve a single amino acid change. The extension time was 6 minutes, allowing for 1 minute per Kb of DNA; with the vector, mCherry and Cx26 gene accounting for ~5.1

$$Conductance\ (G) = \frac{\Delta I}{\Delta V}\ ;where\ \Delta V\ is\ a\ constant = 10\ mV$$

$$Conductance\ change\ (\Delta G) = G_{Stim} - \frac{G_{B_1} - G_{B_2}}{2}$$

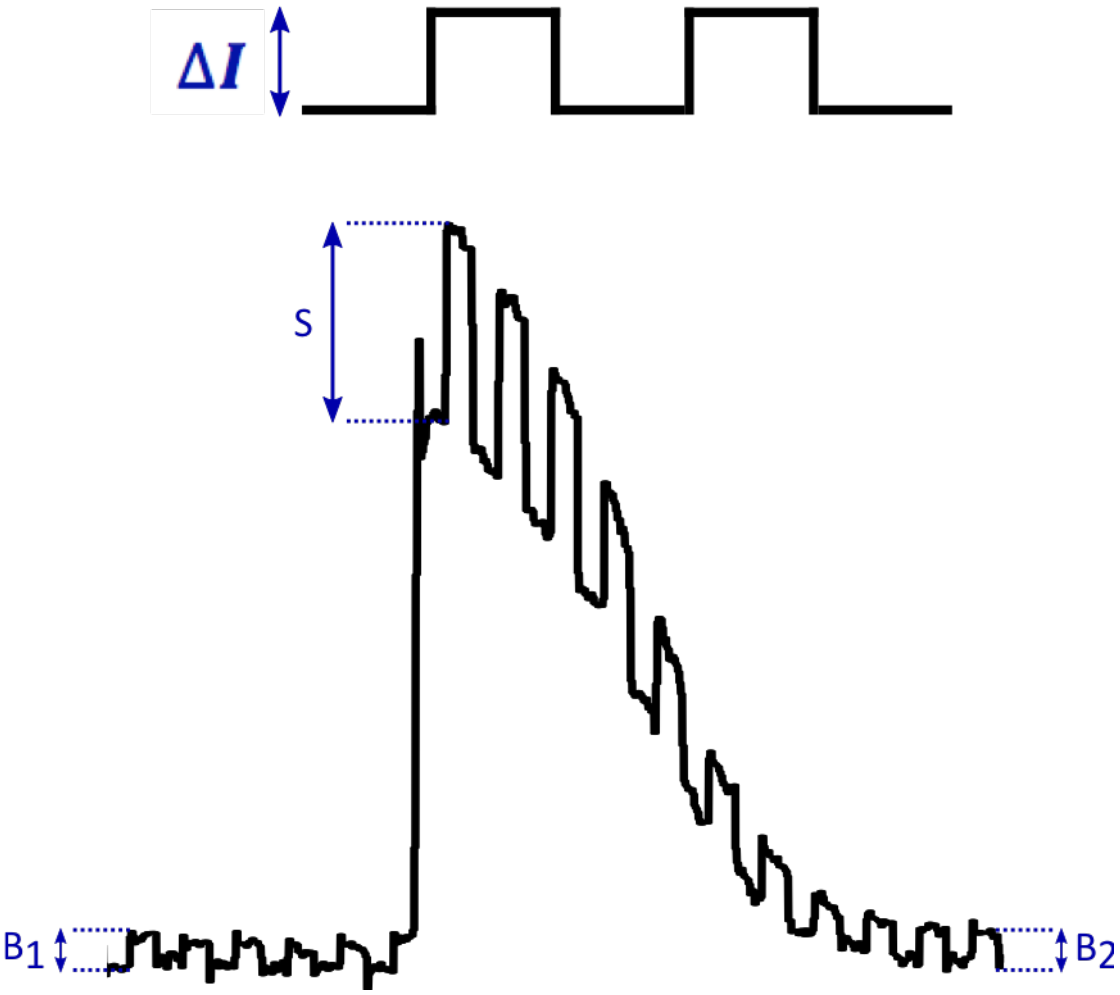

Figure 2.2 **Measurements and calculation for conductance change.** Whole-cell patch recordings were taken by voltage clamping with a 10 mV step (ΔV). Baseline measurements of conductance were averaged from measurements made before (B_1) and after (B_2) the response to a stimulus. Peak conductance in response to a stimulus was taken at point showing largest current change (S). Conductance change was calculated by subtracteing baseline conductance from conductance at S.

Kb. The PCR reaction was then digested for 1 hr at 37^0C with 1 µl Dpn1. This enzyme digests methylated DNA and thus removes the template, leaving only the newly synthesised, mutated DNA. Agarose gel electrophoresis confirmed that synthesised DNA was present – showing that the PCR reaction had been successful. For $Cx26^{N14K}$ mutation the following primers were used: forward, 5' ATC CTC GGG GGT GTC AAG AAG CAC TCC ACC AGC 3'; reverse, 5' GCT GGT GGA GTG CTT CTT GAC ACC CCC GAG GAT 3'.

All subcloning steps were confirmed by DNA sequencing (GATC Biotech). To amplify DNA, plasmids were (heat shock) transfected into Top 10 E.Coli cells, which were grown up overnight before harvesting and purifying transfected DNA via a miniprep kit (Thermo Fisher). For mammalian cell expression, all constructs were subcloned into the pCAG-GS vector (which contains the CAG mammalian promoter).

2.2.6 Experimental aCSF solutions

Artificial cerebrospinal fluid (aCSF) was made and used to imitate fluid environments in the brain. Listed below are the aCSF solutions used during dye loading, ester loading, and patch clamping (writing in brackets refer to the solution's purpose in dye loading experiments):

<u>35 mM HCO_3^- aCSF without dye (Wash aCSF)</u>

124 mM NaCl, 26 mM $NaHCO_3$, 1.25 mM NaH_2PO_4, 3 mM KCl, 10 mM D-glucose, 1 mM $MgSO_4$, 1 mM $CaCl_2$.

This solution was saturated with 95% O_2/5% CO_2 in order to provide the cells with oxygen throughout experimentation. This solution had a final pH of 7.4 and a pCO_2 of 35 mmHg.

<u>35 mM HCO_3^- aCSF with dye (Control aCSF)</u>

124 mM NaCl, 26 mM $NaHCO_3$, 1.25 mM NaH_2PO_4, 3 mM KCl, 10 mM D-glucose, 1 mM $MgSO_4$, 1 mM $CaCl_2$, *and 200 µM 5(6)-Carboxyfluorescein (dye)*.

This solution was saturated with 95% O_2/5% CO_2 in order to provide the cells with oxygen throughout experimentation. This solution had a final pH of 7.4 and a pCO_2 of 35 mmHg.

<u>50 mM HCO_3^- Isohydric aCSF with dye (Hypercapnic aCSF)</u>

100 mM NaCl, 50 mM $NaHCO_3$, 1.25 mM NaH_2PO_4, 3 mM KCl, 10 mM D-glucose, 1 mM $MgSO_4$, 1 mM $CaCl_2$, *and 200 µM 5(6)-Carboxyfluorescein (dye)*.

This solution was saturated with ~91%O_2/9% CO_2 to provide the cells with oxygen and match the final pH to that of the control aCSF (pH 7.4). This removes any potential effects of changes in extracellular pH. The final pCO_2 of this solution is 55 mmHg.

Zero Ca^{2+} aCSF with dye (Positive Control aCSF)

124 mM NaCl, 26 mM $NaHCO_3$, 1.25 mM NaH_2PO_4, 3 mM KCl, 10 mM D-glucose, 2 mM $MgSO_4$, 1 mM $MgCl_2$ 1 mM EGTA, *and 200 µM 5(6)-Carboxyfluoroscein (dye)*.
This solution was saturated with 95% O_2/5% CO_2 in order to provide the cells with oxygen throughout experimentation. This solution had a final pH of 7.4 and a pCO_2 of 35 mmHg. The absence of Ca^{2+} opens hemichannels.

2.2.7 Dye loading assay

The dye loading assay used in this study is based off that used in published literature (Huckstepp et al. 2010a, Meigh et al. 2013, Meigh et al. 2014, Meigh 2015a, de Wolf et al. 2016, de Wolf, Cook, and Dale 2017). Coverslips of HeLa cells, at sub-confluent levels, were placed in a flow chamber for dye loading analysis and exposed to carboxyfluorescein dye - a membrane impermeable dye (molecular mass, 380 Da). In this assay, carboxyfluorescein can only enter HeLa cells when connexin hemichannels are expressed in the membrane and open to some stimulus (in this case CO_2). When the stimulus is removed the connexin channels close, trapping molecules of carboxyfluorescein inside the cells. Carboxyfluorescein is then visualised using epifluorescence microscopy.

Dye loading was performed 3 days post transfection for transfections into parental HeLa cells, and 6 days post transfection for transfections into Cx26-HeLa cells. Dye loading was tested under 35mmHg CO_2 (control), 55mmHg CO_2 (hypercapnic), and zero Ca^{2+} conditions. To investigate the CO_2 sensitivity of homomeric hemichannels dye loading was performed on parental HeLa DH cells transfected with either $Cx26^{WT}$-mCherry or $Cx26^{N14K}$-mCherry. To investigate the effect that $Cx26^{N14K}$ has when coexpressed with $Cx26^{WT}$, dye loading was performed on Cx26-HeLa cells that had either been transfected with $Cx26^{N14K}$-mCherry or untreated.

During control experiments cells were exposed to control aCSF (35 mM HCO_3^- aCSF with dye – 200 µM carboxyfluorescein) for 15 minutes before being washed with wash aCSF (35 mM HCO_3- aCSF without dye) for 30 minutes to remove external

carboxyfluorescein, which would increase background fluorescence.

To investigate CO_2 sensitivity, cells were exposed to the hypercapnic aCSF (50 mM HCO_3^- Isohydric aCSF with dye) for 10 minutes, followed by 5 minutes of control aCSF. The 5 minute step gives time for any open hemichannels to close, ensuring that any loaded dye is not washed away as the channels are closing. After hemichannels are given the chance to close, cells are washed with control aCSF for 30 minutes (as with control experiments).

To confirm functional expression of hemichannels in the membrane, a positive control was performed; exposing cells to zero Ca^{2+} aCSF for 10 minutes, followed by 5 minutes of control aCSF and then 30 minutes of wash aCSF (as with CO_2 experiments). As low extracellular calcium is known to fully open Cx26 hemichannels (see *1.4.3 Gating of Connexin26*), we used the zero Ca^{2+} aCSF as a measure of maximum dye loading. The zero Ca^{2+} aCSF was supplemented with $MgCl_2$, rather than Ca^{2+}, and contains 1 mM EGTA for Ca^{2+} chelation.

Each experiment involved testing these three conditions on cells that resulted from the same transfection. The experiment was repeated 5 times, with each repeat performed on cells resulting from a different transient transfection.

The dye loading protocol is summarised in **Figure 2.3**.

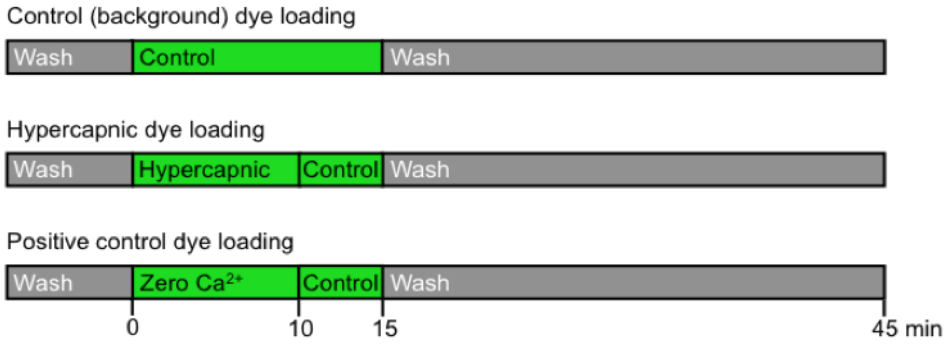

Figure 2.3 **Dye loading protocol**. The control-background loading protocol accounts for any fluorescence that is brought about through anything other than CO_2-dependent dye loading through hemichannels. Hypercapnic dye loading tests carboxyfluorescein loading brought about through the presence of 55mmHg CO_2. The positive control uses zero Ca^{2+} conditions as a test to confirm the presence of functional hemichannels. Grey boxes represent time periods during which cells are exposed to wash aCSF (not containing carboxyfluorescein. Green boxes represent time periods during which cells are exposed to aCSF solutions containing carboxyfluorescein.

2.2.8 Dye loading data capture and analysis

Dye loading experiments in this chapter were performed in conjunction with Elizabeth de Wolf and Jonathan Cook.

Cells were imaged using epifluorescence (Scientifica Slice Scope, Cairn Research OptiLED illumination, 60x water Olympus immersion objective, NA 1.0, Hamamatsu ImageEM EMCCD camera, Metafluor software). Carboxyfluorescein was excited with a 470 nm LED, and its fluorescence emission was recorded between 507-543nm. The Cx26-mCherry constructs used in these experiments (and experiments in future chapters, unless otherwise stated) yields a fusion protein of $Cx26^{XX}$ with a C-terminal mCherry tag. mCherry was excited with a 535 nm LED, and its emission recorded between 570-640 nm.

After cells had been exposed to one of the three conditions (control, hypercapnic, or Zero Ca^{2+}), multiple images of carboxyfluorescein loading were acquired to obtain many fields of view, each containing a different set of cells. To check for connexin expression in the cells selected for analysis, mCherry images were taken for each field of view that was selected.

Images were analysed using Image J. Fluorescence intensity from background-subtracted cells were obtained by drawing regions of interest (ROIs) around individual cells and measuring the mean pixel intensity for individual cells. For each experimental repeat at least 40 cells for each condition were measured. The mean pixel intensities across all repeats were plotted as cumulative probability distributions for each condition. Also, the Mann Whitney test was used to compare the median differences in pixel intensity across selected groups.

2.3 Results

2.3.1 Increased intracellular Ca^{2+} can be evoked through photolysis of NP-EGTA

Although it is established that even low levels of extracellular Ca^{2+} (0.05 mM) closes Cx26 channels (Unwin and Ennis 1984), the effects of intracellular Ca^{2+} have not been reported. To investigate the effect that increasing $[Ca^{2+}]_i$ has on Cx26 channels, HeLa cells stably expressing Cx26 (Cx26-HeLa cells) were loaded with NP-EGTA – a Ca^{2+} chelator that can be photolysed upon demand in order to release sequestered Ca^{2+} – and Rhod-2 – a calcium indicator that exhibits an increase in fluorescence upon Ca^{2+} binding (**Figure 2.4**).

Using Rhod-2 fluorescence intensity as a measure, UV-photolysis of NP-EGTA produced robust increases in $[Ca^{2+}]_i$ during our experiments – mean increase over baseline, 79.5%±33.7 (n = 25), **Figure 2.4b**.

Initial experimental attempts to investigate the effect that $[Ca^{2+}]_i$ involved loading cells with a fluorescent dye, in addition to NP-EGTA and Rhod-2, and then to observe dye efflux. Both calcein and carboxyfluorescein were tried as the dye, but due to a combination of bleaching, and unusual fluorescence changes (in both the florescent dye and Rhod-2) no valid data could be collected. Instead, patch clamp recordings were used to measure the opening of Cx26 channels in response to increased $[Ca^{2+}]_i$.

2.3.2 CO_2-dependent opening of Connexin26 hemichannels causes an influx of Ca^{2+}

Cx26 hemichannel permeability to Ca^{2+} has been demonstrated in preps of purified Cx26 hemichannels reconstituted in liposomes (Fiori et al. 2012), however it has not been witnessed in living cells. During our patch-clamp experiments, Rhod-2 recordings revealed a rise in intracellular Ca^{2+} upon opening of Cx26 hemichannels by CO_2. (**Figure 2.5d**, **Figure 2.6b**). This suggests Ca^{2+} influx through the expressed Cx26 hemichannels, which is consistent with our hypothesis that similar influx *in vivo* could occur and result in augmented Cx26 hemichannel opening.

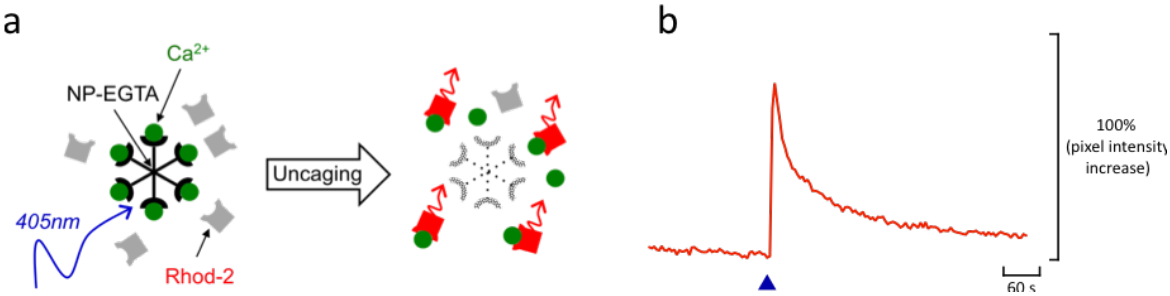

Figure 2.4 Experimental rationale: Increased $[Ca^{2+}]_i$ can be evoked through photolysis of NP-EGTA. Cells loaded with NP-EGTA and Rhod-2 show normal $[Ca^{2+}]_i$ until exposure to UV light. **a)** Photolysis of NP-EGTA releases caged-Ca^{2+} which is then available to act as a signalling molecule and interact with cytoplasmic proteins. The increase in $[Ca^{2+}]_i$ is detected via the calcium indicator Rhod-2, which increases fluorescence upon Ca^{2+} binding. **b)** Average Rhod-2 intensity upon flashing with 405nm light (blue triangular arrow). Photolysis of NP-EGTA results in a rapid increase in $[Ca^{2+}]_i$ followed by an exponential decay back towards baseline. Trace was averaged from experimental cells; n = 25 (from 11 preparations).

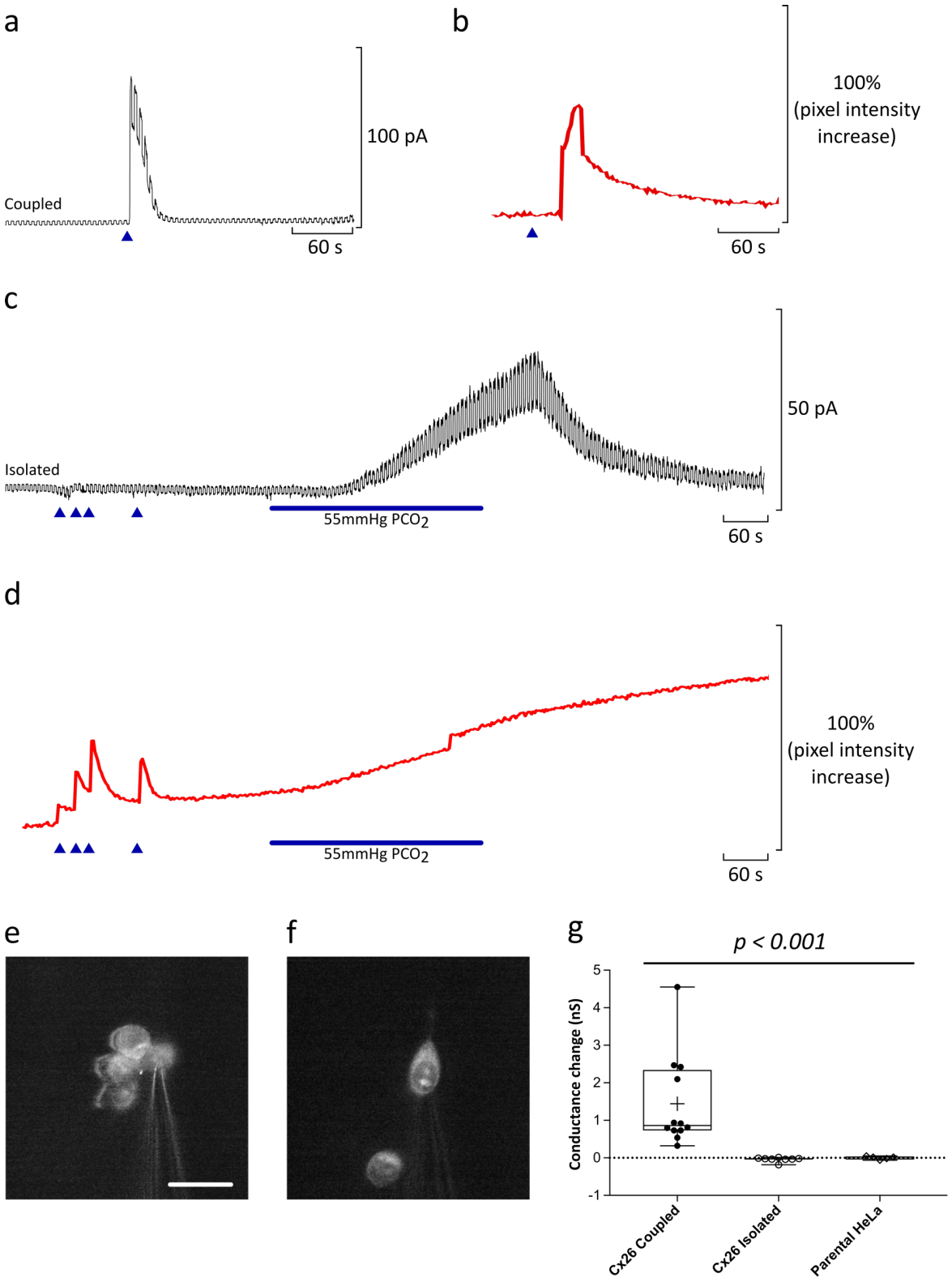

Figure 2.5 **Connexin26 gap junctions but not hemichannels open in response to $[Ca^{2+}]_i$.** HeLa cells stably expressing Cx26 were loaded with NP-EGTA and Rhod-2 before whole-cell patch recordings were taken. Patched cells were voltage clamped, being held at a potential of -50mV, with 10mV step. **a)** Representative trace from a coupled cell showing a robust change in whole-cell current upon release of $[Ca^{2+}]_i$ (blue triangular arrows). **b)** corresponding Rhod-2 trace for experiment shown in (**a**). **c)** Representative trace from an isolated cell showing no change in whole-cell current upon release of $[Ca^{2+}]_i$ (blue triangular arrows), despite functional Cx26

hemichannels being present – as seen by an increase in current upon bath perfusion with hypercapnic aCSF. **d)** corresponding Rhod-2 trace for experiment shown in (**c**). **e)** Example brightfield image showing a patched cell that was considered to be coupled due to apposing membranes with another cell. **f)** Example images (from the Rhod-2 channel) showing a patched cell that was considered to be isolated due to no apposing membranes from neighbours. **g)** Box and whisker plot showing conductance change upon release of $[Ca^{2+}]_i$. Almost no change in conductance is seen in isolated cells or parental cells, however cells that were coupled showed a clear conductance change. Coupled, n = 12; isolated, n = 8; parental; n = 5. One-way ANOVA (represented by the top bar) was carried out in the statistical package SPSS. Post-hoc testing revealed the coupled dataset to be significantly different ($p < 0.001$) from the isolated and parental datasets. Conductance change (S) was calculated as: ΔI/V were ΔI is the current change in Amps and V is the voltage step (10 mV). Boxes show the interquartile range. The median is indicated as a horizontal line within the box, and the mean is represented by a cross within the box. Range bars show minimum and maximum values. Scale bar 40μM, Cx, Connexin; aCSF, artificial cerebrospinal fluid

2.3.3 Connexin26 gap junctions, but not hemichannels, exhibit a whole cell conductance change in response to $[Ca^{2+}]_i$

Changes in the whole-cell conductance of Cx26-HeLa cells was used to measure Cx26 channel opening in response to increased $[Ca^{2+}]_i$. Upon photolysis of cytosolic NP-EGTA, transient conductance changes were only recorded in Cx26-HeLa cells that had membranes apposed to other cells (termed coupled) – mean conductance change, 1.44±1.23 nS (n = 12), **Figure 2.5a,e,g**. The time taken from the start of UV illumination to the onset of a conductance change was ~3.5 s, however the time at which Rhod-2 intensity increased and conductance change increased were all-but indistinguishable, **Figure 2.5a,b**. Cx26-HeLa cells that were clearly isolated from others showed no such change – mean conductance change = 0.04±0.06 nS (n = 8), **Figure 2.5c,f,g** – despite their expression of functional Cx26 hemichannels; shown by a prolonged conductance change in response to hypercapnic conditions (**Figure 2.5c**). Parental HeLa cells (not expressing Cx26) were also tested and showed no such response to increased $[Ca^{2+}]_i$ – , mean conductance change, 0.00±0.04 nS (n = 5), **Figure 2.5g**. Mean conductance change was compared by a one-way ANOVA ($p < 0.001$), with post hoc testing revealing a significant difference between coupled and both isolated and parental cells.

Patch clamp recordings record current flow across the membrane and the result (on transmembrane current flow) of opening hemichannels or gap junctions is almost indistinguishable from the point of view of the recorded cell. If either gap junctions or hemichannels open, more current will flow across the membrane in response to a given

voltage step (because the membrane conductance has increased). Given that large conductance changes in response to intracellular Ca^{2+} were never seen in the parental HeLa cells, any large conductance changes seen in the transfected cells must be due to the presence of Cx26. The only difference between "coupled" and "isolated" cells is the presence/absence (respectively) of gap junctions. This makes it most likely that the conductance change observed in coupled cells is due to the presence of gap junctions. Similarly, the lack of conductance change in isolated cells must be due to the absence of gap junctions. Therefore, the simplest interpretation of this data is that intracellular Ca^{2+} opens Cx26 gap junctions, but does not open Cx26 hemichannels.

2.3.4 Whole cell conductance change evoked by $[Ca^{2+}]_i$ does not occur after exposure to hypercapnia

Lack of Cx26 hemichannel opening by $[Ca^{2+}]_i$ disproves our hypothesis and rules out the potential for synergistic CO_2/$[Ca^{2+}]_i$ hemichannel opening. However, it is possible that during these experiments we witnessed an interaction between Cx26 gap junction opening by $[Ca^{2+}]_i$ and closing by CO_2.

In the protocol used, coupled Cx26-HeLa cells usually contained sufficient NP-EGTA for at least two robust Ca^{2+} releases, and subsequent changes in conductance – mean conductance change, 1.36±1.48 nS (n = 7), **Figure 2.6c-e**. However, a second conductance change was not observed when NP-EGTA was photolysed after perfusion of the chamber bath with aCSF containing 55 mmHg CO_2 – mean conductance change, 0.08±0.12 nS (n = 5), **Figure 2.6a,b,e**. The timing of photolysis was at the point cell conductance returned to baseline (**Figure 2.6a, second blue triangular arrow**), and Rhod2 intensity values showed that a substantial rise in intracellular $[Ca^{2+}]_i$ still occurred upon this second uncaging on Ca^{2+} (**Figure 2.6b**). Mean conductance changes in response to a second release of intracellular Ca^{2+} were compared between coupled Cx26-HeLa cells before or after perfusion with 55mmHg (**Figure 2.6e**). Comparisons were made using an independent t-test and showed a significantly lower change in whole-cell conductance when the second Ca^{2+} release occurred after hypercapnic conditions. This hints at a possible Cx26 gating hierarchy/antagonism between $[Ca^{2+}]_i$ and the CO_2 stimulus, in which gap junction closing in response to CO_2 prevents opening by Ca^{2+}.

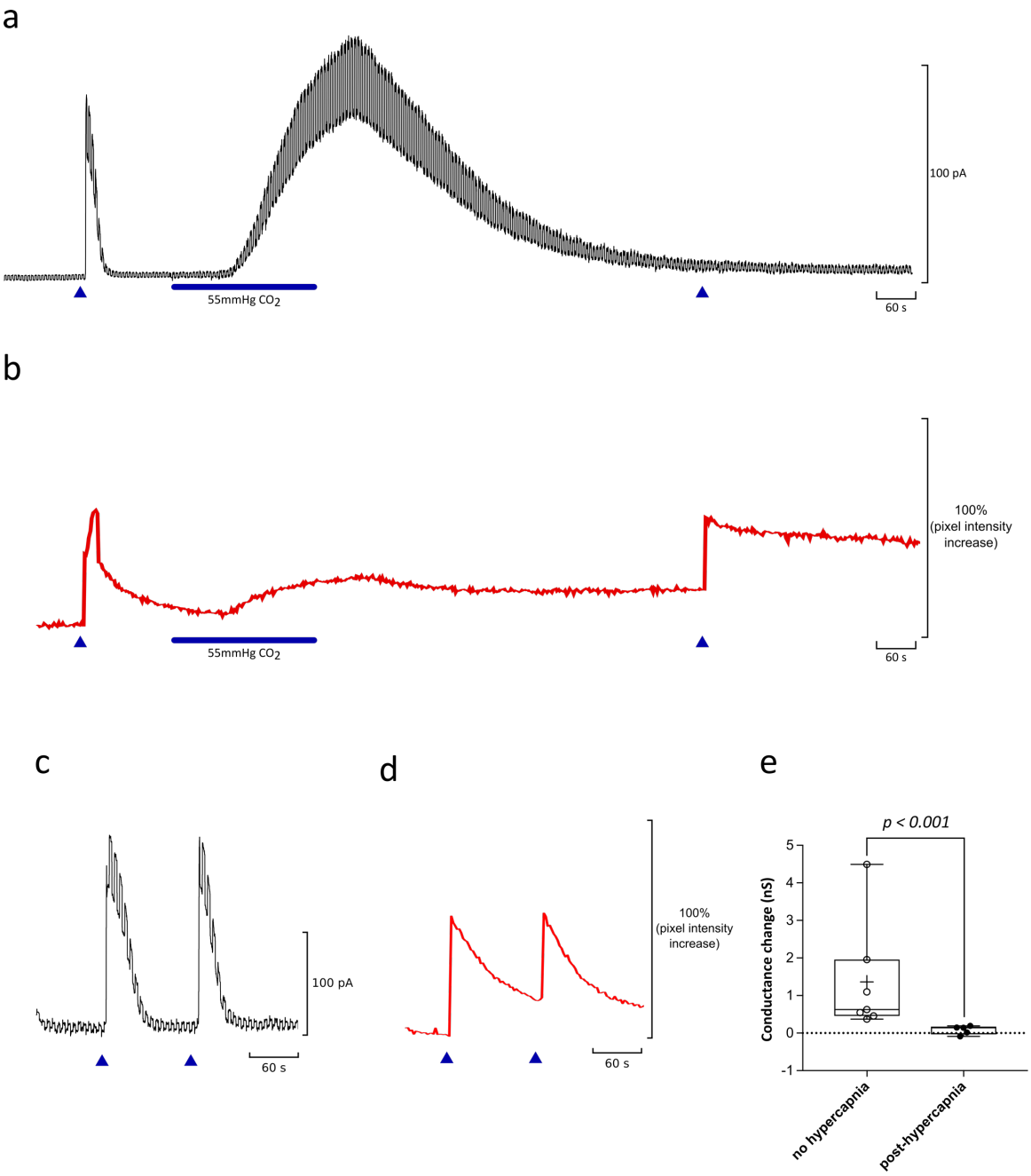

Figure 2.6 **Connexin26 gap junction opening via $[Ca^{2+}]_i$ may be blocked by CO_2-dependent closing of Connexin26**. HeLa cells stably expressing Cx26 were loaded with NP-EGTA and Rhod-2 before whole-cell patch recordings were taken. Coupled cells were were voltage clamped, being held at a potential of -50mV, with 10mV step. **a)** Representative trace from a coupled cell showing a robust change in whole-cell current upon first release of $[Ca^{2+}]_i$ (first blue triangular arrow) but not upon a second release that occurs after perfusion with hypercapnic aCSF (second blue triangular arrow). **b)** corresponding Rhod-2 trace for experiment shown in (**a**). **c)** Representative trace showing that, in the absence of hypercapnia, a second release of $[Ca^{2+}]_i$ is sufficient to cause a second change in whole-cell conductance. **d)** corresponding Rhod-2 trace for experiment shown in (**c**). **e)** Box and whisker plot showing conductance change in coupled cells upon a second release of $[Ca^{2+}]_i$. Almost no change in conductance is seen when the second release occurs after perfusion with hypercapnic aCSF, however if cells were not subjected to

hypercapnia a clear conductance change was seen. No hypercapnia, n = 7; post-hypercapnia, n = 5. Independent t-test was carried out in the statistical package SPSS, revealing a significant different ($p < 0.001$) between cells exposed to hypercapnic aCSF and those exposed to standard aCSF (35 mmHg CO_2). Conductance change (S) was calculated as: ΔI/V were ΔI is the current change in Amps and V is the voltage step (10 mV). Boxes show the interquartile range. The median is indicated as a horizontal line within the box, and the mean is represented by a cross within the box. Range bars show minimum and maximum values. Release of $[Ca^{2+}]_i$ (blue triangular arrows) was brought about via photolysis of NP-EGTA upon UV excitation. Scale bar 40 µm, Cx, Connexin; aCSF, artificial cerebrospinal fluid.

2.3.5 Connexin26 N14K hemichannels do not open in response to CO_2

Upon finding that intracellular Ca^{2+} does not open Cx26 hemichannels, and therefore does not contribute to their CO_2-dependent gating, our attention turned to the pathological implications of Cx26 hemichannel CO_2 gating. This thesis aims to investigate the role that Cx26 hemichannels play in producing a breathing response. As an extension from this, any pathological roles for the CO_2 gating of Cx26 hemichannels are of interest as they may have the respiratory implications.

Of specific interest to this thesis is the lack of CO_2 sensitivity that has been reported in all KID syndrome mutations that have been tested (Meigh et al. 2014, de Wolf et al. 2016). KID syndrome is a complex disorder affecting the skin, eyes, and ears, however several patients present with respiratory problems, which for some was the reported cause of death (Meigh et al. 2014, Koppelhus et al. 2011, Janecke et al. 2005, Sbidian et al. 2010). This suggests that KID mutations might affect the hypercapnia-induced release of ATP that occurs at the VMS via Cx26 hemichannels. Such a finding could help further characterise this syndrome, and might identify more focused treatments for patients. It would also help consolidate the importance of Cx26 in chemoreception. In light of this, it is prudent to characterise the effect KID mutations have on the CO_2 gating of Cx26 hemichannels and to see how they affect a cells response to hypercapnia.

One KID syndrome mutation is N14K. To test the CO_2 sensitivity of $Cx26^{N14K}$ hemichannels, parental HeLa cells were transient transfected with either $Cx26^{WT}$ or $Cx26^{N14K}$ constructs (each tagged with a C terminal mCherry fusion). 3 days post-transfection, cells were loaded with dye under 35mmHg CO_2 aCSF (control), 55mmHg CO_2 aCSF (hypercapnic), or zero Ca^{2+} conditions. Consistent with previous studies, cells expressing $Cx26^{WT}$ showed greater dye loading in response to hypercapnic conditions (p

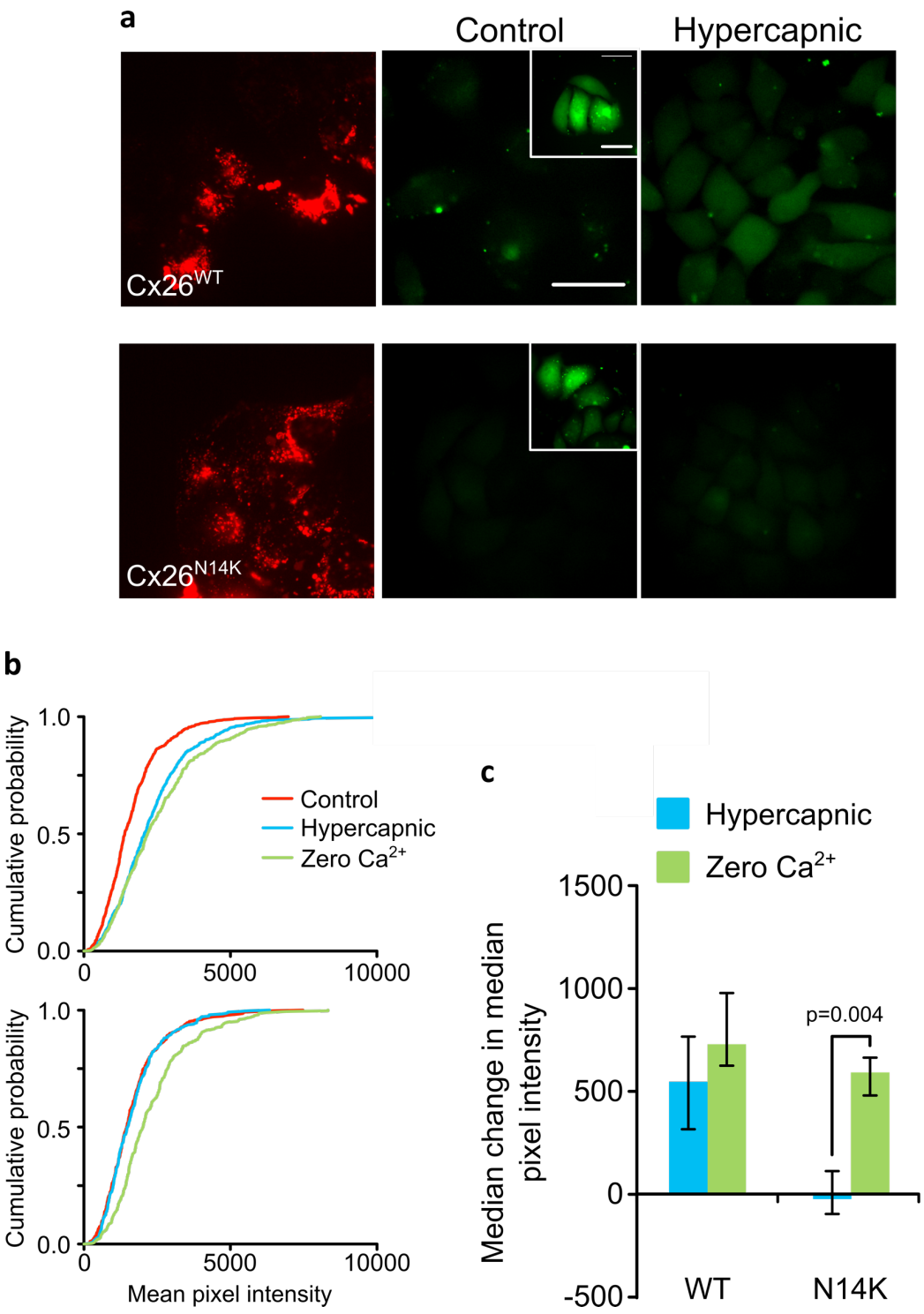

Figure 2.7 **Connexin26 N14K hemichannels do not open in response to CO_2.** HeLa cells were transfected with either $Cx26^{WT}$ or $Cx26^{N14K}$, and dye-loading experiments were carried out 3 days post-transfection. **a)** Representative images showing expression of mCherry tagged to Cx26 protein (left), and dye loading under 35mmHg PCO_2 (control, middle) and 55mmHg PCO_2 (hypercapnic, right) conditions – insert shows dye loading under zero Ca^{2+} conditions; a positive control showing functional Cx26 hemichannels. HeLa cells expressing $Cx26^{WT}$ show an increase in dye loading under hypercapnic conditions (top panels), however cells expressing $Cx26^{N14K}$ do not (bottom panels). **b)** Cumulative probability distributions comparing mean pixel intensity for each

condition ($Cx26^{WT}$, top; $Cx26^{N14K}$; bottom). **c)** Median change between 35mmHg and 55mmHg, and 35mmHg and Zero Ca^{2+}, median pixel intensities. Cells expressing $Cx26^{N14K}$ hemichannels do not to respond to CO_2, whilst cells expressing $Cx26^{WT}$ hemichannels do. n > 50 cells per treatment repeat, with 5 independent repeats for each treatment. Error bars show the first and third quartiles. Median pixel intensities (from independent repeats) were compared using the Mann-Whitney U test. Scale bars, 40µm. *Figures reproduced from de Wolf, E., van de Wiel, J., Cook, J., & Dale, N., 2016.*

= 0.003, compared to $Cx26^{WT}$ control). In contrast to this, cells expressing $Cx26^{N14K}$ showed no such increase in dye loading in response to hypercapnia conditions, **Figure 2.7a,b**. Protein-tagged mCherry confirmed expression of the connexin variants (**Figure 2.7a, left panels**). To confirm that this expression included functional hemichannels in the plasma membrane, we used extracellular zero Ca^{2+} conditions as a means of measuring dye loading when hemichannels are fully open (Sánchez et al. 2010). Dye loading above control conditions was no different when comparing hypercapnic and zero Ca^{2+} conditions in cells expressing $Cx26^{WT}$, however there was a difference in those cells expressing $Cx26^{N14K}$ (p = 0.004), **Figure 2.7c**. These results suggest that, whilst $Cx26^{WT}$ hemichannels open in response to CO_2, the N14K mutation results in hemichannels that do not.

2.3.6 The Connexin26 N14K mutant acts to drastically reduce CO_2 sensitivity from cells expressing wild-type Connexin26

Cx26 mutants that cause KID syndrome are dominant in nature (Yotsumoto et al. 2003, Janecke et al. 2005, Kelly et al. 2008, Koppelhus et al. 2011, Sbidian et al. 2010, Terrinoni et al. 2010, Terrinoni et al. 2010a, Terrinoni et al. 2010b, Van Geel et al. 2002, Sonoda et al. 2004, Mazereeuw‐Hautier et al. 2007, Lazic et al. 2008, de Zwart‐Storm et al. 2011). It has previously been demonstrated that another KID mutant, A88V, is not sensitive to CO_2 (like the N14K mutant). Furthermore, A88V was shown to have a dominant negative action on CO_2 sensitivity (Meigh et al. 2014). $Cx26^{A88V}$ took 6 days from transfection (into Cx26-HeLa cells) to impose its dominant negative action and remove CO_2 sensitivity from the Cx26-HeLa cells. Using the same assay, we transfected Cx26-HeLa cells with the $Cx26^{N14K}$ construct (containing an mCherry-tag) and the CO_2 sensitivity was assessed 6 days post-transfection. mCherry fluorescence shows abundant $Cx26^{N14K}$ expression at 6 days (**Figure 2.8a, bottom left**), and extracellular zero Ca^{2+}

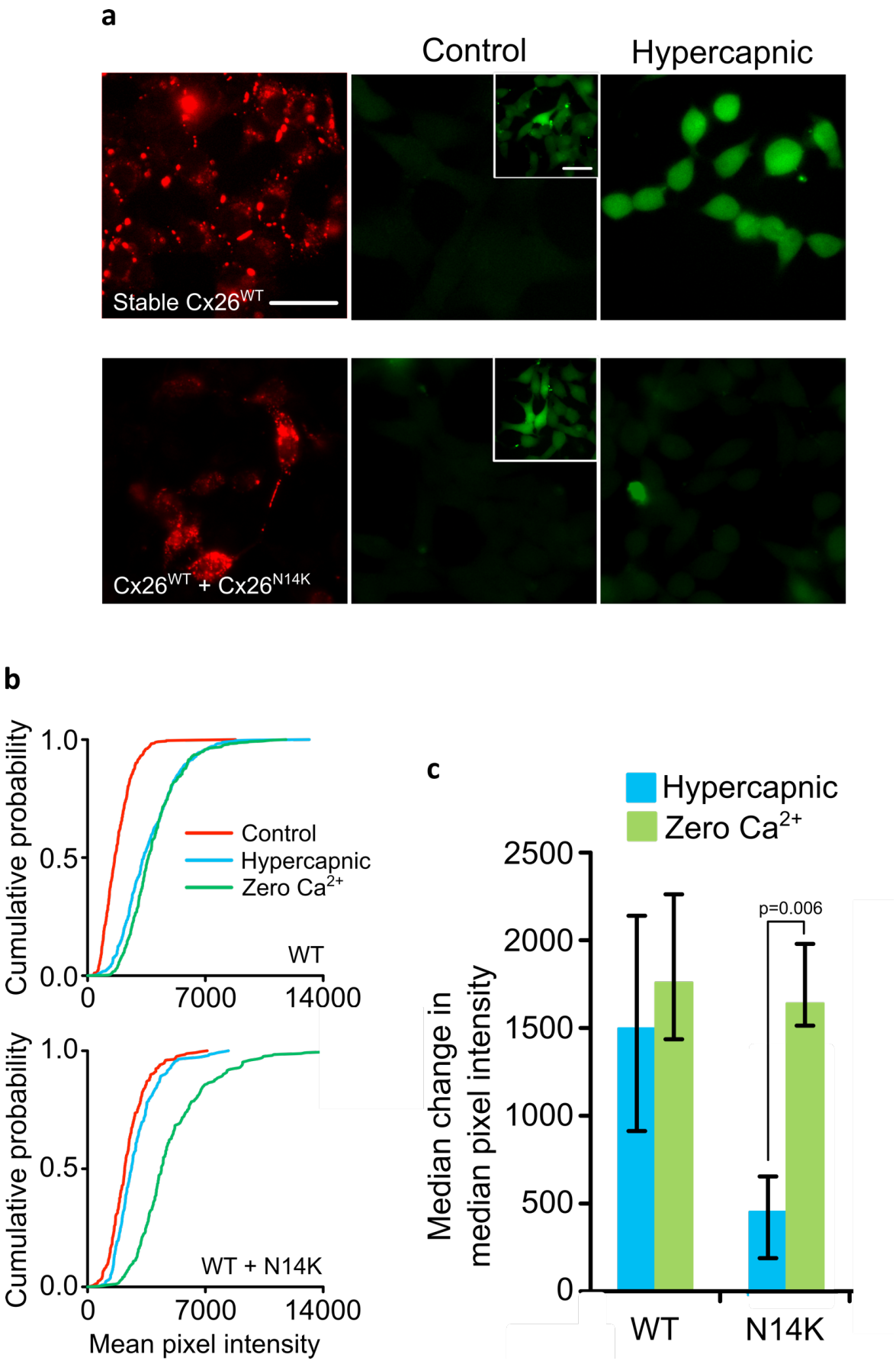

Figure 2.8 **The Connexin26 N14K mutant acts in a dominant negative manner to remove CO_2 sensitivity from cells expressing wild type Connexin26**. HeLa cells stably expressing $Cx26^{WT}$ (Cx26-HeLa cells) were either untreated or transfected with $Cx26^{N14K}$, and dye-loading

experiments were carried out 6 days post-transfection. **a)** Representative images showing expression of Cx26 variants (left: immunostaining shows stable expression of Cx26 in Cx26-HeLa cells, top; mCherry tagged to $Cx26^{N14K}$ shows expression of $Cx26^{N14K}$ at 6 days post-transfection, bottom), and dye loading under 35mmHg PCO_2 (control, middle) and 55mmHg PCO_2 (hypercapnic, right) conditions – insert shows dye loading under zero Ca^{2+} conditions; a positive control showing functional Cx26 hemichannels. Untreated Cx26-HeLa cells show an increase in dye loading under hypercapnic conditions (top panels), however cells also expressing $Cx26^{N14K}$ do not (bottom panels). **b)** Cumulative probability distributions comparing mean pixel intensity for each condition (untreated Cx26-HeLa cells, top; $Cx26^{N14K}$-transfected, bottom). n > 50 cells per treatment repeat, with 5 independent repeats for each treatment. **c)** Median change between 35mmHg and 55mmHg, and 35mmHg and Zero Ca^{2+}, median pixel intensities. Cells expressing $Cx26^{N14K}$ hemichannels loose their ability to respond to CO_2, whilst cells stably expressing $Cx26^{WT}$ hemichannels maintain CO_2 sensitivity throughout the time course. Error bars show the first and third quartiles. Median pixel intensities (from independent repeats) were compared using the Mann-Whitney U test. Scale bars, 40µm. *Figures reproduced from de Wolf, E., van de Wiel, J., Cook, J., & Dale, N., 2016*

controls showed that this expression included functional hemichannels in the plasma membrane.

Consistent with previous work, Cx26-HeLa cells were still sensitive to CO_2 at 6 days, however coexpression of $Cx26^{N14K}$ subunits (with the stably expressed $Cx26^{WT}$) was found to profoundly reduce the CO_2-sensitivity of these cells, **Figure 2.8a,b**. Dye loading above control conditions was no different when comparing hypercapnic and zero Ca^{2+} conditions in non-transfected Cx26-HeLa cells, however there was a difference in cells expressing $Cx26^{N14K}$ ($p = 0.006$), **Figure 2.8c**. These results suggest that $Cx26^{N14K}$ acts in a dominant negative manner to remove CO_2 sensitivity from Cx26-HeLa cells. However, unlike coexpression of $Cx26^{A88V}$ and $Cx26^{N14Y}$ (Meigh et al. 2014, de Wolf et al. 2016), complete removal of hypercapnia-evoked dye loading was not seen, with ~20% remaining (**Figure 2.8c**).

2.4 Discussion

2.4.1 Differential opening of Connexin26 hemichannels and gap junction

Although the absence of extracellular Ca^{2+} is well known to open Cx26 hemichannels, the effects of intracellular Ca^{2+} have not been reported. By comparing coupled and isolated Cx26-HeLa cells (HeLa cells stably expressing $Cx26^{WT}$), it was demonstrated that Cx26 gap junctions, but not hemichannels, open in response to increased $[Ca^{2+}]_i$ (**Figure 2.5**). This

contrasts the response shown by Cx32 hemichannels, which open in response to an $[Ca^{2+}]_i$ of ~500nM (De Vuyst et al. 2006). It would be interesting to test the response of Cx26/Cx32 heteromeric hemichannels to $[Ca^{2+}]_i$.

It must be noted that cells assigned to the "coupled" group did not have coupling confirmed (e.g. via dual patch clamping), however patching was performed on cells stably expressing $Cx26^{WT}$, which readily form gap junctions with neighbouring cells (**Figure 2.8a, top left panel**), and cells for the "coupled" group were only selected if they had apposing membranes with their neighbours.

The observed conductance change was transient in nature. Ca^{2+} released from NP-EGTA photolysis cannot re-associated with the photolysed NP-EGTA and so will be pumped out of the cell through efflux pumps, or taken up into intracellular stores. For this reason there was usually only sufficient NP-EGTA within cells for two clear NP-EGTA-mediated responses.

Owing to the design of the experiment, and the knowledge that extracellular Ca^{2+} closes hemichannels and gap junctions, it can be assumed that there is a cytoplasmic domain on Cx26 gap junction connexons that is responsible for this $[Ca^{2+}]_i$ gating. As photolysis was applied across the field of view, we cannot ascertain whether an increase in $[Ca^{2+}]_i$ is required in both cells that share a gap junction, or just in one. As the change in conductance was very rapid in response to increased $[Ca^{2+}]_i$, it is likely that Ca^{2+} modulate gating directly, rather than causing the release of another messenger molecule that acts on Cx26 gap junctions.

Given the extensive use of Ca^{2+} signalling throughout the body, and widespread expression of Cx26, this result has far-reaching implications. Our result that Cx26 gap junctions open in response to $[Ca^{2+}]_i$ may help explain, in part, the well-established roll of connexin gap junctions in the propagation of Ca^{2+} waves (Cotrina et al. 1998, Hassinger et al. 1996, Leinonen et al. 2007, Sáez et al. 2003). It remains to be confirmed whether or not the magnitude of $[Ca^{2+}]_i$ release that was achieved in these experiments is of physiological relevance – however similar NP-EGTA studies in Cx32-expressing cells increases $[Ca^{2+}]_i$ to ~500nM (within physiological range) (De Vuyst et al. 2006), and it is likely we achieved comparable concentrations. It might be that the opening of Cx26 gap junctions by $[Ca^{2+}]_i$ only occurs at very high concentrations of $[Ca^{2+}]_i$ that don't often occur in cells, or that only occur after initial stimulation (e.g. from extracellular ATP) – thus being capable of augmenting Ca^{2+} signalling but rarely initiating it. Whether opening

only occurs at very high $[Ca^{2+}]_i$ or not, it is interesting that this gating mechanism exists, as it suggests that cells prioritise $[Ca^{2+}]_i$-mediated Cx26 gap junction opening over uncoupling from cells with high $[Ca^{2+}]_i$ – which can cause cell death (Neher and Sakaba 2008, Clapham 2007, Hajnóczky et al. 2006).

Of importance to this thesis, a large part of the Ca^{2+} wave cell-to-cell signalling in glia, amongst other cells, is contributed by ATP release rather than intercellular coupling (Cotrina et al. 1998, Anselmi et al. 2008, Gourine et al. 2010, Cotrina, Lin, and Nedergaard 1998, Hassinger et al. 1996). The mechanisms behind hemichannel ATP release are still being elucidated (see *1.3 Central respiratory chemosensory transducers for pCO_2*), however the data presented in this chapter rules out a $[Ca^{2+}]_i$ stimulus in the opening of Cx26 hemichannels. Subsequently, this disproves our initial hypothesis that $[Ca^{2+}]_i$ could act to augment the Cx26-mediated ATP release that is known to mount a respiratory response. However, our finding that Ca^{2+} influx occurs through CO_2-opened Cx26 hemichannels might prove important for other ATP release mechanisms in glial, which have been shown to be reliant on $[Ca^{2+}]_i$ signalling (Gourine et al. 2010).

2.4.2 Blocking of $[Ca^{2+}]_i$-mediated Connexin26 gap junction gating by CO_2: possible stimuli interactions

Although speculative, the lack of a second conductance change after perfusion with 55 mmHg CO_2 hints that there could be some interaction occurring between the Cx26 gating modulated by $[Ca^{2+}]_i$ and CO_2 (or pH, owing to the carbonic anhydrase-driven reaction). If this is true, one explanation would be that each stimuli competes to exert its action on the gap junctions, and that in our experiments the CO_2 stimulus outcompeted that of intracellular calcium. However, the timing of the second Ca^{2+} release (i.e. when the hypercapnic aCSF had been washed out) might suggest that it is not a straight forward competitive interaction. Given that the opening of Cx26 hemichannels by CO_2 is quickly reversible (Meigh et al. 2013, Huckstepp et al. 2010b) but the closing of Cx26 gap junctions by CO_2 has a longer lasting effect (personal communication from Nicholas Dale), it could be that until the effects of CO_2-mediated gap junction closing wear off, the channels are insensitive to the mechanism by which intracellular calcium opens them. With this explanation, I propose the CO_2-mediated closing of gap junctions was not reversed at the point of a second Ca^{2+} release, and thus no response was seen.

2.4.3 A hemichannel is not half of a gap junction

For a long while connexin hemichannels were largely ignored with focus being given to gap junctions, and hemichannels simply thought of as half a gap junction. In the last couple of decades hemichannels have received much more attention and now, with the recent development of peptides that suppress hemichannel but not gap junction activity (by binding connexon cytosolic loop regions), we are starting to be able to explore the roles of endogenously expressed hemichannels (Sáez and Leybaert 2014, Vinken 2015, Iyyathurai et al. 2013, Abudara et al. 2014, Wang, De Vuyst, et al. 2013). However, there is still an underlying impression that hemichannels, although now accepted to play a variety of roles themselves, act in a mechanistically comparable manner to gap junctions. However, it is becoming apparent that this is not always the case.

Our finding that $[Ca^{2+}]_i$ likely mediates opening of Cx26 gap junctions, but has no effect on hemichannels, further illustrates the difference between these two channel conformations. The docking of two connexon hemichannels forces a conformational change as the channels fuse, and regions that were previously exposed to a soluble environment are instead exposed to peptide or lipid environments, which could consist of a vastly different hydrophobicity or charge. Considering this, it can be assumed that the formation of a gap junction does more than simple connect two cells; it might significantly change the tertiary and quaternary structure of the involved connexins. This difference between hemichannels and gap junctions could be expected to play an integral role in why the body is able to use the same protein within the same cell, and in many different tissues, for completely different processes/signalling pathways. Careful structural studies are required to discern what motifs are important for the difference seen between hemichannel and gap junction responses to $[Ca^{2+}]_i$.

Another stimulus that has different gating properties on Cx26 hemichannels and gap junctions is CO_2. The recently discovered modulator of Cx26 opens Cx26 hemichannels (Huckstepp et al. 2010b) but closes Cx26 gap junctions (personal communication with Nicholas Dale). Such complex gating characteristics could be considered of great evolutionary advantage, enabling one protein to have many different functions within and across different tissues. The differential gating of hemichannels and gap junctions may further contribute to the multifunctionality of Cx26 when taking into consideration the heteromeric connexons and heterotypic gap junctions that it forms with other members of the connexin family, and when considering potential interactions

between gating stimuli (such as the dominance of CO_2 over intracellular Ca^{2+} that we have proposed). Studying heteromeric and heterotypic channels is difficult, and little is known about their characteristics. However, many inter-connexin interactions are known to form in native tissue (Koval, Molina, and Burt 2014), and as such the true power of connexin gating is yet to be revealed.

This discussion highlights the importance for continued characterisation of Cx26 in order to help us better understand its function in the body and its role in pathologies; including those that are well-established to be linked to Cx26, such as non-syndrome hearing loss (Kelsell et al. 1997) and KID syndrome (Kelly et al. 2008), and those that Cx26 might yet prove play a key role in, such as SIDS (Harper et al. 2000) and central sleep apnoea's.

2.4.4 Possible mechanisms by which the N14K loss of function mutant prevents Connexin26 hemichannel gating by CO_2

In order to better understand the role that Cx26 CO_2-sensitivty plays in KID syndrome pathologies, we used a published assay to analyse the CO_2-dependent channel opening of $Cx26^{N14K}$, one of the 9 known KID syndrome mutations. This assay is suitable for investigating hemichannels, but not gap junctions, and as such caution should be taken when extrapolating results in the context of gap junctions. In this chapter, it is shown that, unlike $Cx26^{WT}$, homomeric $C26^{N14K}$ hemichannels did not open in response to hypercapnic conditions, showing it to be a loss of function mutant (for CO_2 sensitivity). Furthermore, this mutant drastically reduced opening of channels in cells coexpressing $Cx26^{WT}$ and $Cx26^{N14K}$.

The N14 residue is located within the cytoplasmic linker region, between the N-terminus and TM1 and in close proximity to the site where K125 is carbamylated; which subsequently forms a salt bridge with R104 from an adjacent subunit, stabilising the hemichannel in an open state. The N14K mutation is 6.6 Å from R104 and 9.3 Å from K125 (**Figure 2.9**) and as such it could interfere with the formation of a carbamate bridge – possibly via a change in environment resulting from the introduction of a novel positive charge and larger sidechain where there once was a polar residue (Asparagine → Lysine). Alternatively, this mutation could hinder the conformational change that usually occurs upon carbamate bridge formation.

Interestingly, the N14Y mutation also causes KID syndrome, and has also been shown to lack CO_2 sensitivity (de Wolf et al. 2016). It is tempting to stipulate that either mutation at the N14 locus prevents CO_2 sensitivity via disruption of the same mechanism, although if these mutations acted through different mechanisms it might help to better explain why complete abolishment of CO_2 sensitivity is seen from $Cx26^{N14Y}/Cx26^{WT}$ coexpression, but not $Cx26^{N14K}/Cx26^{WT}$ coexpression. Tyrosine is bulky and may be expected to hinder conformational changes more than the N14K mutation (thus having less of an effect on the carbamylation event). Furthermore, it is known that the N14Y mutation changes the local structural flexibility of the cytoplasmic N-terminal

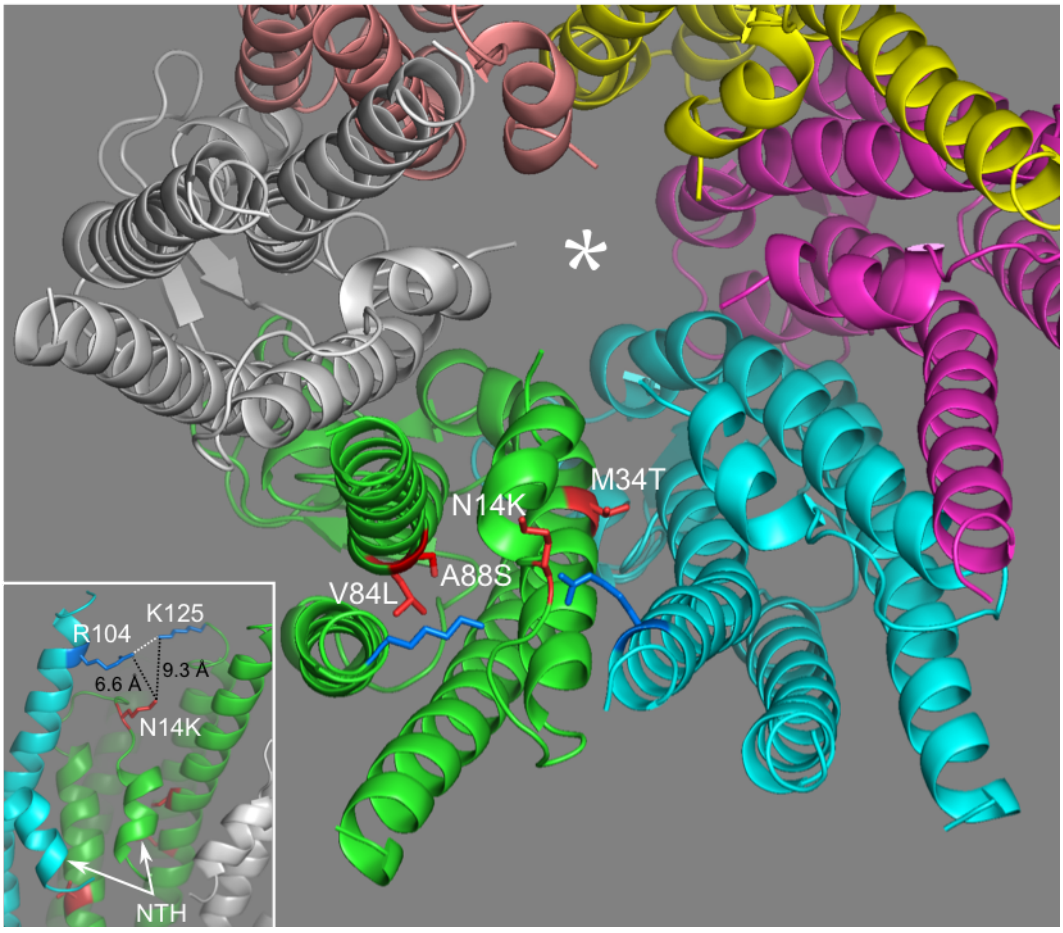

Figure 2.9 Location of the N14K Keratitis, Ichthyosis, and Deafness (KID) syndrome mutation. Molecular cartoon structure of a connein26 hemichannel (central pore, *) viewed from the cytoplasmic side. The N14K, A88S, M34T, and V84L KID syndrome mutations (red) on the green subunit. Shown also are the R104 and K125 residues that are involved in CO_2-binding and carbamate bridge formation (blue). Insert shows an alternative view, highlighting the close proximity of the N14K mutation to the K125 and R104 residues (carbamate bridge is represented by dotted white line). Molecular model drawn from the PDB structure 2zw3. NTH, N terminal; *, hemichannel pore. *Figures reproduced from de Wolf, E., van de Wiel, J., Cook, J., & Dale, N., 2016*

domain, subsequently interfering with $Cx26^{N14Y}$ gap junction channel function (Arita et al. 2006). This mechanism could be extrapolated to explain the CO_2 insensitivity reported in homomeric and heteromeric $Cx26^{N14Y}$ hemichannels – i.e. steric hindrance of the conformational change that results from carbamylation.

A recent study has suggested that hemichannel voltage-dependent loop gating is shifted towards higher opening probabilities in $Cx26^{N14K}$, due to altered electrostatic interactions between the N-terminus and the cytoplasmic end of TM2 from the adjacent subunit, but is shifted to lower opening probabilities in $Cx26^{N14Y}$ hemichannels, due to different electrostatic interactions (Sanchez et al. 2016). This may seem to contrast our suggestion that both N14K and N14Y mutants exhibit a loss-of-function however the truth may lie somewhere in-between, with a tendency for higher opening probabilities explaining why $Cx26^{N14K}$/$Cx26^{WT}$ coexpression did not completely remove dye loading from cells.

As it stands, there is no robust rationale as to why the N14K or N14Y mutants render Cx26 hemichannels insensitive to CO_2. The other KID mutant reported to lack CO_2 sensitivity, A88V, has no evidence-based suggestions for its CO_2-insensitive aetiology. This residue is not particularly close to either K125 or R104, and so it seems more likely to cause steric hindrance than affect CO_2 binding. Clearly, better structural understanding is required to fully elucidate the mechanism by which these mutations prevent gating via CO_2.

As it is highly likely that Cx26 KID mutants coassemble with $Cx26^{WT}$ subunits, it is also highly likely that whatever mechanisms prevent mutant hemichannel opening in response to CO_2 is also capable of disrupting opening in coassembled (heteromeric) connexons. This hypothesis would explain the dominant effect seen when $Cx26^{WT}$ is coexpressed with $Cx26^{N14K}$, $Cx26^{N14Y}$, or $Cx26^{A88V}$.

2.4.5 Implications for KID syndrome

In this chapter it is shown that the $Cx26^{N14K}$ mutant lacks any CO_2 sensitivity when expressed as homomeric hemichannels and has a severe negative action on CO_2 sensitivity when coexpressed with $Cx26^{WT}$. This parallels that of the severe pathology shown in patients with the N14K mutation; whereas the N14K mutation is dominant in causing KID syndrome (Lazic et al. 2008), two other Cx26 mutations (M34T and V84L), that are only linked to hearing loss, were found to have much less of an affect on CO_2

sensitivity – with $Cx26^{V84L}$ retaining CO_2 sensitivity when expressed alone and $Cx26^{M34T}$ showing reduced CO_2 sensitivity when expressed alone, but no affect on CO_2 sensitivity when coexpressed with $Cx26^{WT}$ (de Wolf et al. 2016). Furthermore, $Cx26^{N14K}$ did not show complete removal of CO_2 sensitivity when coexpressed with $Cx26^{WT}$. This also parallels pathology when comparing it to other KID mutations. The A88V and N14Y mutants do show complete removal of sensitivity when coexpressed with $Cx26^{WT}$ (Meigh et al. 2014, de Wolf et al. 2016), and both of these mutations result in more severe forms of KID syndrome than $Cx26^{N14K}$ – $Cx26^{A88V}$ is fatal at infancy (Koppelhus et al. 2011, Haruna et al. 2010) and $Cx26^{N14Y}$ presents with a complete array of symptoms (Arita et al. 2006). On the other hand, $Cx26^{N14K}$ has been suggested to cause a modified version of the disease (Lazic et al. 2008, Steijlen, Bladergroen, and Hoefsloot 2004). The CO_2 sensitivity of the other 6 KID mutations is yet to be investigated.

The leading hypothesis for why dominant missense Cx26 mutations cause syndromes is a gain of function increase in hemichannel activity (Sanchez and Verselis 2014, Sanchez et al. 2014, Levit et al. 2015, Levit and White 2015, Lilly et al. 2016). The emerging data on KID mutant CO_2-sensitivity (discussed here) provides another hypothesis – that losing CO_2-mediated Cx26 hemichannel gating plays a part in KID pathology.

Cx26 mutations that remove CO_2 sensitivity from cells (such as the N14K, N14Y, and A88V KID mutants) are also likely to affect respiratory chemoreception. Cx26 is involved in the respiratory response to increases pCO_2 (Huckstepp et al. 2010a, Huckstepp et al. 2010b) breathing. Furthermore, KID syndrome patients have been reported to suffer respiratory problems (Janecke et al. 2005, Sbidian et al. 2010, Koppelhus et al. 2011, Meigh et al. 2014), and in some cases it was the cause of death. One such patient presenting with deceased respiratory drive carried the A88V mutation, which has subsequently been shown to lack CO_2-sensitivity thereby making the first connection between Cx26 CO_2 sensitivity and human pathology (Meigh et al. 2014). It is possible that many KID syndrome patients present with respiratory problems that are overshadowed by other characteristics of the disease and have thus not been reported in the literature.

2.4.6 A gateway to studying Connexin26 CO_2 sensitivity *in vivo*

The identification of Cx26 variants that are not only CO_2-insensitive when expressed alone, but also act in a dominant negative manner to remove the CO_2 sensitivity from cells stably expressing $Cx26^{WT}$, inspires a theoretical application in which this characteristic could be used to elegantly investigate the role of Cx26 CO_2 sensitivity in different cells *in vivo*.

The experimental design of an *in vivo* study to specifically remove Cx26 CO_2 sensitivity raises the question of which mutant Cx26 variant to use. Although we have shown that the N14K, N14Y, and A88V KID syndrome mutations are capable of removing CO_2-insensitivity (de Wolf et al. 2016, Meigh et al. 2014), there is no solid rationale as to why these mutants do not respond to CO_2, nor why they remove CO_2-sensitivity from $Cx26^{WT}$ expressing cells. Furthermore, we also had problems expressing these mutants and as such consistent viable expression was not possible, making their use for continued investigations undesirable. Reconcilable with this, other groups have reported cell death as a result of the expression of KID mutants (Gerido et al. 2007, Mhaske et al. 2013, Lee, DeRosa, and White 2009, Montgomery et al. 2004, Stong et al. 2006, Terrinoni et al. 2010, Sánchez et al. 2010). For these reasons, currently characterised KID mutants are unsuitable to use in the proposed *in vivo* experiments. Instead, we required a mutant for which there was a robust rationale explaining its dominant negative CO_2-insensitivity, and that could be viably expressed for characterisation (and other experimentation) purposes. An intelligently designed and engineered Cx26 variant – referred to as the Dominant Negative mutant, or $Cx26^{DN}$ – could provide such a tool. This mutant has two mutations, K125R and R104A. The rationale is that these mutations will prevent the K125 carbamylation, and subsequent K125-R104 carbamate bridge formation, which is required for hemichannel opening in response to CO_2 (Meigh et al. 2013). This mutant needs to be characterised, and the rationale confirmed, before advancing it to *in vivo* experimentations.

3 CHARACTERISATION OF CO-ASSEMBLY AND CO_2-INSENSITIVITY OF A CONNEXIN26 DOMINANT NEGATIVE MUTANT

3.1 Introduction

The recently discovered gating of Connexin26 (Cx26) hemichannels by molecular CO_2 may have implications in any cells expressing Cx26 – including the liver, uterus, skin, eyes, ears, and brain (Nicholson et al. 1987, Nagy et al. 2011, Dalamón et al. 2016). The next step in assessing the physiological importance of this property is to develop a technique that inhibits or removes Cx26 CO_2 gating, whilst maintaining the expression of functional Cx26 hemichannels. One solution may come from Cx26 mutants that are dominant negatively CO_2-insensitive, such as the A88V, N14Y, and N14K mutants that are linked to KID syndrome (Meigh et al. 2014, de Wolf et al. 2016). These mutants remove CO_2-mediated Cx26 hemichannel opening in cells expressing wild type Cx26, despite the expression of functional hemichannels being retained. As we do not fully understand the mechanisms by which these mutants remove CO_2 sensitivity (see *2.4.4 - Possible mechanisms by which the N14K loss of function mutant prevents Connexin26 hemichannel gating by CO_2*), their direct use *in vivo* would leave questions as to what is really going on to bring about a hypothetical phenotype. Furthermore, viably expressing any KID mutant *in vitro* is difficult (Gerido et al. 2007, Mhaske et al. 2013, Lee, DeRosa, and White 2009, Montgomery et al. 2004, Stong et al. 2006, Terrinoni et al. 2010, Sánchez et al. 2010, de Wolf et al. 2016), and made any further studies involving $Cx26^{A88V}$, $Cx26^{N14Y}$, or $Cx26^{N14K}$ unfeasible.

This chapter presents the investigation of a Cx26 mutant that has been rationally designed and engineered for the purpose of removing CO_2 sensitivity in a dominant negative fashion. The mutant – dubbed "Dominant Negative" (DN) – has the mutations K125R, and R104A (**Figure 3.1a**). These two residues are vital components for CO_2 gating, and both the K125R or R104A mutations individually yield homomeric hemichannels that are insensitive to CO_2 (the effect of the mutants when coexpressed with $Cx26^{WT}$ has not been tested) (Meigh et al. 2013).

Within a connexon hemichannel, CO_2 acts on the lysine at position 125 of a given subunit, forcing a carbamylation event, which results in a carbamate bridge forming between the K125 residue and the R104 residue of the adjacent subunit. Such bridge

formation across all six subunits fully stabilises the hemichannel in an open state (Meigh et al. 2013). We hypothesise that the DN alterations will yield a mutant that is unable to

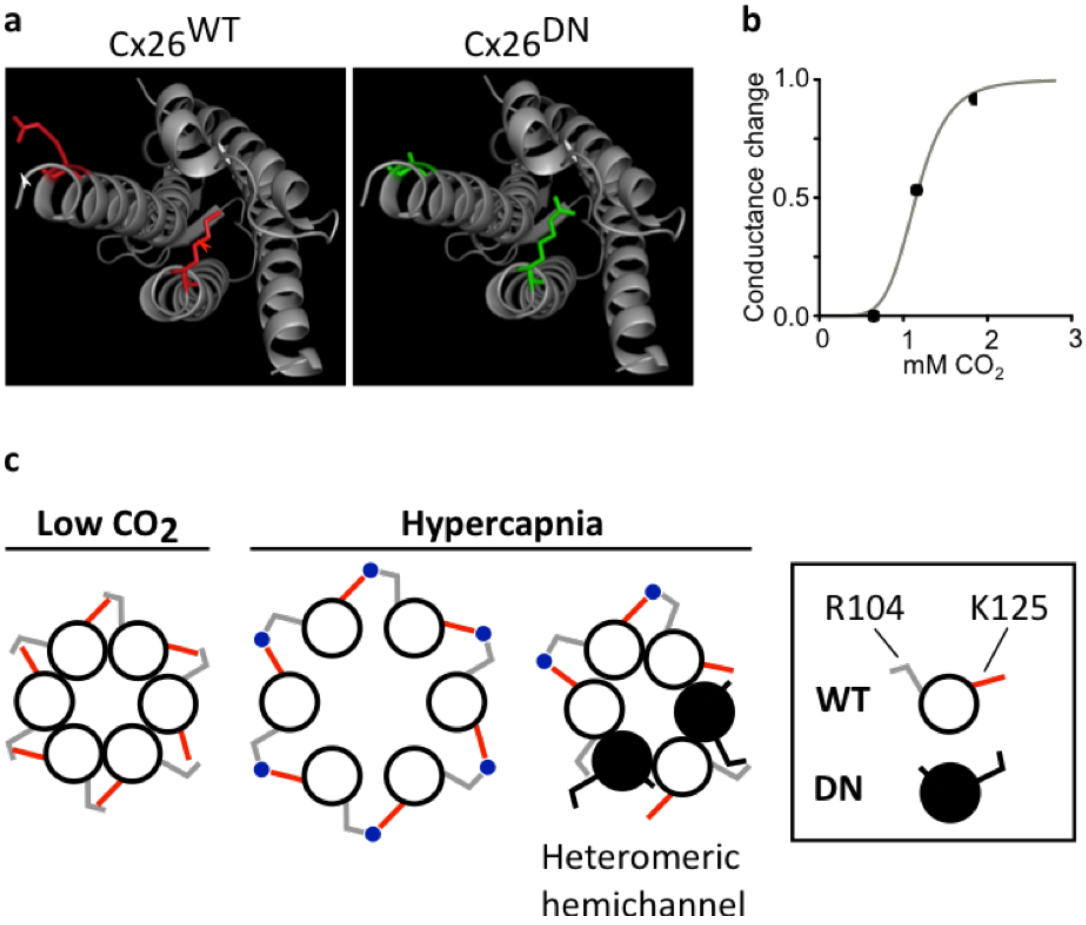

Figure 3.1 **Hypothesis for Removal of Hemichannel Opening by the Dominant Negative Connexin26 mutant**. **a)** Ribbon diagram, showing a single Connexin 26 subunit, highlighting the two amino acid residues vital for CO_2 sensing - R104 and K125 ($Cx26^{WT}$, left). In the $Cx26^{DN}$ mutant peptide, these two residues are mutated - R104→K and K125→R ($Cx26^{DN}$, right) - and will therefore be unable to undergo carbamylation and unable to form a salt bridge with adjacent connexin subunits. **b)** Whole-cell patch clamp conductance change from HeLa cells stably expressing $Cx26^{WT}$. The sigmoidal relationship between CO_2 concentration and conductance change suggests a strong level of cooperative binding between CO_2 molecules and Cx26 hemichannels. Therefore, it is likely that hemichannel opening requires most of the total six carbamate bridges to form in order to sufficiently stabilise the protein in an open state. **c)** We predict that $Cx26^{WT}$ and $Cx26^{DN}$ subunits will coassemble into heteromeric connexon hemichannels, and render the hemichannel insensitive to CO_2. The presence of DN subunits in the hemichannels will prevent the K125 carbamylation, and subsequent carbamate bridge formation, that usually occurs between neighbouring subunits under hypercapnic conditions (blue circles). A DN subunit would prevent the formation of a bridge with either neighbouring subunit. Without sufficient bridge formation it is expected that the characterised hypercapnia-induced conformational change will no longer occur, and thus the hemichannels will not open. *Figures a and b were produced by Nicholas Dale*

form bridges with either neighbouring connexin subunit. If this is the case, the resulting hemichannels should be insensitive to CO_2.

Considering that the K125R and R104A mutations do not disrupt the heteromeric specificity motif (Koval, Molina, and Burt 2014), which sits in TM3 (just after the CL) and dictates connexin coassembly compatibility, we expect that coassembly will occur between $Cx26^{WT}$ and $Cx26^{DN}$ subunits. If this happens, the presence of just one mutant subunit, in an otherwise WT connexon, would prevent two of the six intersubunit carbamate bridges from forming. If more $Cx26^{DN}$ subunits were present, then even more bridges would be disrupted (with the exact number depending on the number and stoichiometric positions of $Cx26^{DN}$ subunits). The sigmoidal relationship between CO_2 concentration and conductance change suggests a strong level of cooperative binding between CO_2 molecules and Cx26 hemichannel, **Figure 3.1b**. Because of this it is likely that hemichannel opening requires most (of the total six) carbamate bridges to form in order to sufficiently stabilise the protein in an open state; and therefore the presence of just one or two DN subunits may be sufficient to prevent such an open state being reached (**Figure 3.1c**). Based on this rationale, if $Cx26^{WT}$/$Cx26^{DN}$ coassembly occurs, we further hypothesise that the $Cx26^{DN}$ mutant will show a dominant negative effect and cause heteromeric hemichannels to be insensitive to CO_2 (like we expect from homomeric $Cx26^{DN}$ hemichannels).

If our hypotheses prove to be true, then the $Cx26^{DN}$ mutant could be introduced *in vivo* (e.g. through a Lentivirus) as a tool to remove CO_2 sensitivity from certain cell populations in animals of any age. The targeted cells would still express functional Cx26 (albeit a mix of endogenous WT and mutant subunits). In this way, this technique would provide the means to specifically investigate the CO_2 sensitivity property of Cx26 whilst limiting the confounding effects that that may come from KO of the Cx26 gene – namely compensation and disruption of other Cx26-related pathways. As system-wide Cx26 KO is lethal, owing to reduced nutrient and glucose uptake (Gabriel et al. 1998), such a tool would also provide an alternative to timely and costly cross-breeding KO studies.

Before the $Cx26^{DN}$ mutant is packaged into a viral vector and introduced into animals, it was important that proof of principle was provided so that we would understand the mechanism via which a potential phenotype arose. This chapter aims to characterise $Cx26^{DN}$/$Cx26^{WT}$ coassembly, through the use of Förster Resonance Energy Transfer (FRET), as well as the effect that the DN mutant has on Cx26 CO_2 sensitivity,

through the use of dye-loading techniques as described and discussed previously (see *2 Gating determinants of Connexin26 hemichannels: intracellular calcium and co2 sensitivity of a pathological mutation)*.

3.2 Materials and Methods

3.2.1 HeLa cell culture and sample preparation

HeLa DH and Cx26-HeLa cells for dye loading experiments were maintained and transfected as described previously (see *2.2.1 HeLa cell culture and sample preparation*). To ensure appropriate confluency for $Cx26^{DN}$ time course experiments, cells were plated at 3 different densities: $5x10^4$, $1x10^4$ and $5x10^3$ cells per well.

For FRET experiments, HeLa DH cells were maintained in Dulbecco's modified Eagle's medium (DMEM) supplemented with 10% fetal calf serum (FCS), 50 µg/mL Penicillin Streptomycin, and 3mM $CaCl_2$. Cells were grown at 37^0C in a 5% CO_2 humidified incubator. Cells were plated onto 35mm glass-bottomed dishes at $5x10^4$ cells per dish ($9cm^2$) 24hrs prior to transfection. HeLa cells were transiently transfected with 0.5µg of DNA of each pCAG-Connexin-fluorophore construct to be co-expressed (1µg total), using the GeneJuice transfection agent protocol (Merck Millipore). 72hrs post-transduction, cells were washed 3x with PBS, fixed with 4% PFA (paraformaldehyde) for 20-30 mins, washed a further 3x with PBS, and then stored in PBS at 4^0C. FRET studies were carried out within 2 weeks of fixation. PFA fixation is commonplace in FRET studies, and whilst it has been shown to significantly affect FRET efficiency when two flourophores are fused in the same protein (intramolecular FRET), it has no significant affect on FRET efficiency when fluorophores are in separate molecule (intermolecular FRET) (Anikovsky et al. 2008).

3.2.2 Construction of connexin gene constructs

All connexin-fluorophore constructs used in this chapter were constructed as described previously (see *2.2.5 Construction of connexin gene constructs*).

Connexin43 DNA sequence from *Rattus norvegicus* was purchased from Addgene (mCherry-Cx43-7, plasmid #55023, gifted by Michael Davidson) and subcloned into a PUC 19 vector such that the transcript would form a fusion protein with whichever fluorophore we engineered to be 3' (downstream) of Cx43 (as with Cx26 constructs).

Dominant Negative mutant Cx26 ($Cx26^{DN}$) DNA - with R104A K125R mutations was produced through two steps. First, Cx26 DNA with the K125R mutation and omitted STOP codon (to allow for fusion proteins) was synthesised by Genscript USA from the Cx26 sequence (accession number NM_001004099.1), and subsequently subcloned into a PUC 19 vector such that the transcript would form a fusion protein with mCherry at the C-terminus of Cx26. Second, the R104A mutation was introduced by Agilent Quikchange site directed mutagenesis, using PUC19-Cx26(K125R) DNA as the template. Primer sequences for the mutagenesis were as follows: Cx26(R104A) forward 5'GGC CTA CCG GAG ACA CGA AAA GAA AGC GAA GTT CAT GAA GG 3', Cx26(R104A) reverse 5'CCT TCA TGA ACT TCG CTT TCT TTT CGT GTC TCC GGT AGG CC 3'. PCR reactions were carried out as described previously (see *2.2.5 Construction of connexin gene constructs*).

Design and characterization of the Clover and mRuby2 protein fluorophores used in these experiments was published by (Lam et al. 2012). mRuby2 DNA was purchased from Addgene (mRuby2-C1, plasmid #54768, gifted by Michael Davidson) and subcloned into a PUC 19 vector so that it was 3' of whichever connexin we engineered to be 5' (upstream) of mRuby2. Clover DNA was a gift from Sergey Kasparov, Bristol, and was subcloned into a PUC 19 vector so that it was 3' of whichever connexin we engineered to be 5' (upstream) of Clover.

Amplification and subcloning were preformed as described previously (see *2.2.5 Construction of connexin gene constructs*).

3.2.3 Acceptor depletion FRET assay

Förster Resonance Energy Transfer (FRET) describes a specific type of energy transfer that occurs through nonradiative diploe-dipole coupling between two appropriate chromophores (Cheng 2006, Helms 2008, Förster 1948). This form of energy transfer is very sensitive to distance; with transfer efficiency being inversely proportional to the sixth power of the distance between the two chromophores (Harris 2010). In biology, this phenomenon can be exploited to determine if two molecules are within a certain distance of one another (typically 1-10nm) (Zheng 2006). If a given two flourophores have complementary characteristics (namely an overlap in the emission spectrum of one and the excitation spectrum of the other) they may be used as a FRET-pair. Within a FRET pair, electron excitation of the *donor* fluorophore (e.g. by light at a specific wavelength) may cause the transfer of energy to the *acceptor* fluorophore, rather than the emission

of photons, as the electrons drop back to their unexcited state. The transferred energy excites acceptor electrons, which do emit photons (within the acceptor's usual emission spectrum) as the electrons drop back to their unexcited state.

FRET can be detected by various approaches (Eidne, Kroeger, and Hanyaloglu 2002, Lippincott-Schwartz, Snapp, and Kenworthy 2001, Wouters et al. 1998), with FRET efficiency (%E) being the favoured measurement. %E is the percentage of excited photons that contribute to FRET. One common technique is acceptor depletion FRET (adFRET), which looks at the change in donor fluorescence intensity before and after photobleaching of the acceptor. If two fluorophores that constitute a FRET-pair are within 10nm of one another and the donor is excited, then some of the donor emission will be quenched by the acceptor as FRET occurs. This results in the donor emission intensity being lower than it would in the absence of acceptor. By photobleaching the acceptor the molecule is rendered permanently unable to fluoresce or undergo FRET (Diaspro et al. 2006). Subsequently, after photobleaching, there is no quenching of acceptor emission and the measured acceptor fluorescence intensity increases. If donor and acceptor molecules are not within FRET range (10 nm) then there will be no quenching and no change in acceptor intensity after photobleaching of the donor.

The adFRET assay used in experiments described in this chapter was based on the linear unmixing adFRET (u-adFRET) assay used by Gu *et al.* (Gu et al. 2004, Di et al. 2005, Yum et al. 2007), but was modified to remove the need of spectral unmixing. The FRET-pair used in the studies presented here were Clover (donor) and mRuby2 (acceptor). For adFRET studies, Clover/mRuby2 is the best FRET-pair yet characterised (Lam et al. 2012). It can be noted that, since the start of the studies presented here, the same group has developed mClover3 and mRuby3 variants, which are brighter and more photostable than Clover and mRuby2 (Bajar et al. 2016). However, these newer versions are no more spectrally advantageous than Clover/mRuby2, and the increased photostablity shown in mRuby3 would not be advantageous for the photobleaching required during adFRET. Unlike previous FRET-pairs (such as ECFP/EYFP), Clover/mRuby2 have very good separation in their emission spectra. In fact, it is possible to record channels with no spectral bleed-through, yielding separate measurements of pure Clover and pure mRuby2 emission (**Figure 3.2a**). Although adFRET only relies on donor intensity measurements in order to calculate FRET efficiency, and therefore a channel yielding pure clover emission is sufficient for this result, there is only so much that can be

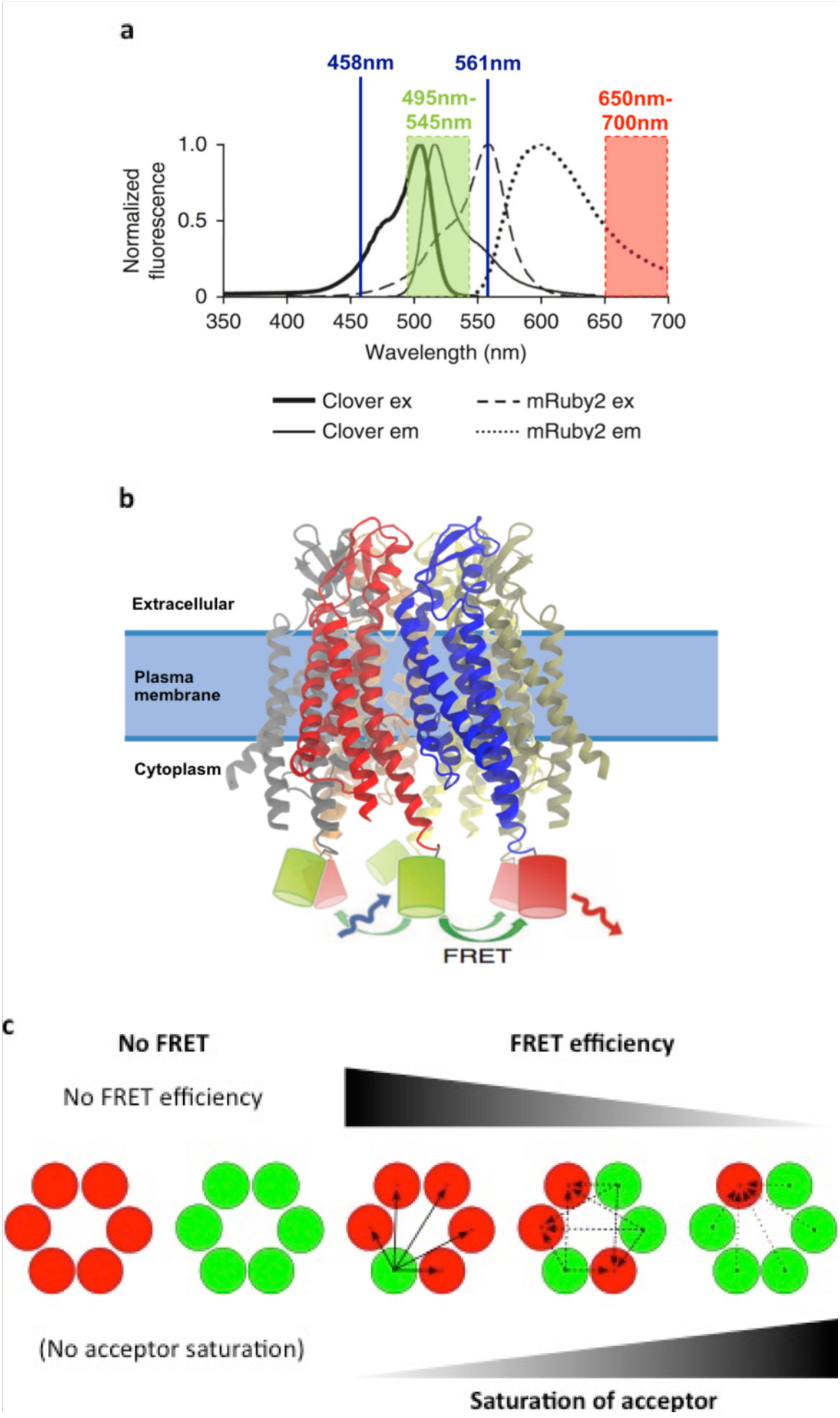
a
458nm
561nm
495nm-
545nm
650nm-
700nm
Normalized fluorescence
1.0
0.5
0
350
400
450
500
550
600
650
700
Wavelength (nm)
Clover ex
Clover em
mRuby2 ex
mRuby2 em
b
Extracellular
Plasma membrane
Cytoplasm
FRET
c
No FRET
FRET efficiency
No FRET efficiency
(No acceptor saturation)
Saturation of acceptor

Figure 3.2 Acceptor depletion Förster Resonance Energy Transfer rational. Connexin variants constructs were C-terminally tagged with ether Clover or mRuby2 and co-expressed for acceptor depletion Förster Resonance Energy Transfer (ad-FRET). **a)** Excitation and emission spectra of Clover and mRuby2. Two channels recording fluorescence between 495-545nm and 650-700nm are appropriate to yield pure fluorescence from Clover and mRuby2, respectively. By imaging sequentially with 458nm and 561nm lasers, these parameters ensure that there is no spectral bleed-through in the recorded images. Photobleaching during ad-FRET was carried out using the 561nm laser. *Image modified from Lam et al. 2012*. **b)** Diagrammatic representation showing a Connexin26 (Cx26) hexameric connexon made up of Cx26-Clover and Cx26-mRuby2 fusion proteins. The Clover and mRuby2 fluorophores attached to the C-terminus of the connexin subunits should be close enough for FRET to occur between Clover (donor) and mRuby2 (acceptor) fluorophores regardless of their assembled position. Blue squiggly arrow; excitation wavelength (458nm), red squiggly arrow, emission from mRuby2 due to FRET, green arrows; FRET after Clover excitation. Connexin43 fusion proteins are also C-terminal, with the fluorophore located on the cytoplasmic face. Diagram not to scale. *Molecular structure from Maeda 2009.* **c)** FRET will occur between subunits of heteromeric but not homomeric connexons. The measured FRET efficiency will be greatest when there is a low donor-acceptor ratio, however as the donor-acceptor ratio increases so does acceptor saturation. Increased acceptor saturation lowers the amount of energy that acceptor molecules sequester from any given donor molecule (represented by less solid lines) – thus yielding a lower FRET efficiency measurement.

interpreted from %E values. On the other hand, the collection of relative acceptor and donor intensity values allows for semi-quantitative analysis, and subsequent insight into the assembly of the two flourophores. Measuring mRuby2 fluorescence between 650-700nm was insufficient to observe FRET via sensitised emission (i.e. exciting clover and looking for mRuby2 emission) – presumably as insufficient signal could be detected within this range. However, measuring mRuby2 fluorescence between 650-700nm *was* sufficient to gather relative mRuby2 intensity values when exciting at 561nm argon, thus allowing for semi-quantitative analysis.

If two connexins coassemble into heteromeric hemichannels then by tagging one connexin variant with Clover and the other with mRuby2, cells will produce and express heteromeric hemichannels tagged with a mixture of Clover and mRuby2 (**Figure 3.2b**). In this case, the C-terminal Clover and mRuby2 fluorophores will be sufficiently close for FRET to occur (**Figure 3.2c**). In our adFRET studies a FRET signal can be seen as an increase in Clover emission intensity post mRuby2 photobleaching.

3.2.4 FRET data capture and analysis

PFA-fixed cells co-transfected with Cx-Clover (donor) and Cx-mRuby2 (acceptor) were examined with a Zeiss LSM 710 Confocal microscope; C-Apochromat 63x/1.20 W Korr

M27. Two channels were recorded: 495-545nm (clover) and 650-700nm (mRuby2), and images were acquired sequentially with 458nm and 561nm argon lasers (respectively) – **Figure 3.2a**. Imaging parameters for the Clover channel are as follows: power, 30.0; pinhole, 78.5; gain (master), 700; digital offset, 0; digital gain, 1.0. Imaging parameters for the mRuby2 channel are as follows: power, 30.0; pinhole, 78.5; gain (master), 750; digital offset, 0; digital gain, 1.0. Photobleaching was performed using the 561nm laser (as it only excites mRuby2) for 80 frames at 100% power, targeting ROI's. Image acquisition was as follows: ROIs were selected and drawn, including a background region and a ROI that was not to be bleached; pre-bleaching images were acquired for each channel; mRuby2 was photobleached; post-bleaching images were acquired for each channel. By keeping acquisition parameters identical across samples, it is possible to compare results.

Pixel intensities from each background-adjusted ROI were used to calculate FRET efficiency (E), bleaching efficiency (B), donor abundance relative to total fluorophore flourescence (D), acceptor abundance relative to total fluorophore flourescence (A), relative donor-acceptor ratio (DA ratio), relative acceptor quantity (A level), and donor-acceptor distance (R) as follows:

$$E = \frac{Clover_{post} - Clover_{pre}}{Clover_{post}}$$

$$\%E = E \times 100$$

$$B = \frac{mRuby2_{pre} - mRuby2_{post}}{mRuby2_{pre}}$$

$$D = \frac{Clover_{post}}{Clover_{post} + mRuby2_{pre}}$$

$$A = \frac{mRuby2_{pre}}{Clover_{post} + mRuby2_{pre}}$$

$$DA\ ratio = \frac{Clover_{post}}{mRuby2_{pre}}$$

$$A\ level\ =\ mRuby2_{pre}$$

$R = R_0(1-E)^{\frac{1}{6}}$ *where R_0 is the effective FRET distance for clover/mRuby2 (6.3nm) (Lam et al. 2012).*

Colocalisation threshold calculations were carried out in ImageJ using the Costes method (Costes et al. 2004); 100 iterations, omitting zero-zero pixels in threshold calculation. The Costes method takes into account the Numerical Aperture (NA) of the objective lens and the fluorescence emission wavelength in order to calculate how many pixels the point spread function covers in the image. Then it sets up a new random image by taking the image in one of the channels and moving point spread function sized sections of the image to random locations in the new (random) image. It then calculates the Pearson's correlation coefficient between the random image and the real image of the other channel; if they correlated as well as, or better than, the two real images, then the correlation that you have measured is no better then what you would have got by chance. This randomisation is iterated for as many times as is commanded (100 in these analyses). For the Costes colocalisation test a p-value = 1 indicates that none of the randomised images had a better correlation than the real image, thus the significance threshold is p = 0.95, with values < 0.95 being significant (i.e. no colocalisation). For box-whisker plots P-values were calculated using the Mann-Whitney U test in the statistical package R.

By obtaining relative Clover and mRuby2 abundances (through acquisition of pure Clover and mRuby2 signals) it is possible to perform semi-quantitative analysis in order to gain insight into the assembly of the co-expressed proteins. Using the FRET cluster model (Dewey and Hammes 1980), assessment of %E vs DA ratio and %E vs A-level plots can suggest whether a FRET signal has been brought about through the coassembly of the two fluorophores into clusters (which in this case would be heteromeric connexons), and whether the FRET signal has been brought about through random association of the two fluorophores (which in this case would be homomeric connexons clustering/packing tightly enough for FRET to occur between connexon hemichannels). For proteins that coassemble a negative correlation is expected between %E and DA ratio, with no correlation between %E and A-level. A positive correlation between %E and DA ratio suggests that random association was sufficient to yield FRET. It is possible for a FRET signal to be yielded by a combination of coassembly *and* random association. Here, this

analysis is referred to as “semi-quantitative” because only relative, not absolute, Clover and mRuby2 abundances are calculated; as such comparisons should only be made between experiments carried out with exactly the same parameters. Linear regression analysis was carried out in GraphPad Prism.

3.2.5 Experimental aCSF solutions

Experimental solutions used for experiments in this chapter have been described previously (see *2.2.6 – Experimental aCSF solutions*)

3.2.6 Dye loading assay

The dye loading assay used for experiments in this chapter have been described previously (see *2.2.7 – Dye loading assay*). For experiments involving co-expression of $Cx26^{DN}$ in Cx26-HeLa cells, dye loading was performed with control, hypercapnic, and zero Ca^{2+} conditions being tested over a 3 day period, beginning at 4 days post-transfection. These dye loading experiments were performed for Cx26-HeLa cells transiently transfected with $Cx26^{DN}$-mCherry and Cx26-HeLa cells that had not been transiently transfected.

3.2.7 Dye loading data capture and analysis

Time course $Cx26^{DN}$ dye loading experiments in this chapter were performed by Louise Meigh.

Data capture and analysis for the dye loading experiments in this chapter have been described previously (see *2.2.8 – Dye loading data capture and analysis*).

3.3 Results

3.3.1 Connexin26 WT colocalises with Connexin26 DN and Connexin43 WT when expressed *in vitro*

In order to study coassembly of $Cx26^{WT}$ and $Cx26^{DN}$ subunits, fusion protein constructs were developed to consist of a connexin variant ($Cx26^{WT}$, $Cx26^{DN}$, or $Cx43^{WT}$) with a C-terminal tag of Clover or mRuby2. Despite successful cloning of all six fusion protein combinations (confirmed by sequencing), only four of the resultant constructs showed

expression upon transfection of HeLa cells (confirmed by visible Clover/mRuby2 emission): $Cx26^{WT}$-Clover, $Cx26^{WT}$-mRuby2, $Cx26^{DN}$-mRuby2 and $Cx43^{WT}$-Clover.

HeLa cells were co-transfected with two of the connexin-fluorophore fusion constructs: $Cx26^{WT}$-Clover + $Cx26^{WT}$-mRuby2, $Cx26^{WT}$-Clover + $Cx26^{DN}$-mRuby2 or $Cx43^{WT}$-Clover + $Cx26^{WT}$-mRuby2. When coexpressed, all constructs showed some level of fluorescence in the plasma membrane (**Figure 3.3**), the most obvious of which is usually seen as gap junction plaques (observed as lines of fluorescence where two cells meet, **Figure 3.4**). This shows proteins are indeed being expressed in the membrane. Expression can also be seen throughout the stages of trafficking, including areas where it might be stored as vesicular reserves. In all co-expression combinations, very strong colocalisation (p-value = 1 for all images, with significance attributed to tests with p-value > 0.95) was found between both constructs – as determined by the Costes method for calculating colocalisation threshold (Costes et al. 2004). Such noticeable colocalisation shows that coexpressed protein subunits are within the same vicinity of one another (based on pixel limitations) and lays the foundation for FRET experiments to determine just how close the subunits are; and discern whether or not they are coassembling.

3.3.2 Connexin26 WT and Connexin26 DN subunits more closely interact than Connexin26 WT and Connexin 43 WT

In order the determine whether or not $Cx26^{WT}$ and $Cx26^{DN}$ subunits coassemble into heteromeric connexons, connexin variants tagged with either Clover or mRuby2 were coexpressed and the Förster Resonance Energy Transfer (FRET) between these two flourophores was measured. FRET is very sensitive to distance (decreasing at a rate of r^6, where r is the distance between donor and acceptor fluorophores), and does not occur beyond a separation of 10 nm (100 Å). As the largest cytoplasmic width of a connexon is ~9 nm (Maeda et al. 2009), if connexin subunits coassemble then the tagged fluorophores will be within FRET range of other subunits and a signal should be detected (**Figure 3.2b,c**). There are various techniques to assess FRET in biological systems, with measurements usually expressed as FRET efficiency (%E) – the percentage of excited photons that contribute to FRET. To remove issues of spectral bleed-through, acceptor depletion FRET (adFRET) was used to obtain the data reported here, with %E calculated as the % change in clover intensity. For a more detailed explanation of the adFRET assay see *3.2.3 acceptor depletion FRET assay*.

Following photobleaching of mRuby2 (acceptor), ROIs in $Cx26^{WT}$-Clover + $Cx26^{WT}$-mRuby2 and $Cx26^{WT}$-Clover + $Cx26^{DN}$-mRuby2 samples showed enhanced Clover (donor) fluorescence intensity, and reduced mRuby2 fluorescence intensity (**Figure 3.3, top four rows**). As Cx26 and Cx43 do not coassemble into heteromeric connexons (Gemel et al. 2004), we also investigated adFRET in cells that co-expressed Cx26 and Cx43. Following photobleaching of mRuby2 ROIs from samples coexpressing $Cx43^{WT}$-Clover + $Cx26^{WT}$-mRuby2 showed little change in the fluorescence intensity of Clover, despite reduced mRuby2 fluorescence intensity (**Figure 3.3, bottom two rows**).

The FRET efficiency of $Cx26^{WT}$ + $Cx26^{WT}$ (24±10%) and $Cx26^{WT}$ + $Cx26^{DN}$ (23±8%) were statistically greater than that of $Cx43^{WT}$ + $Cx26^{WT}$ (7±5%, $p < 0.001$), indicating the Cx26 variants have a higher degree of interaction compared to Cx26 + Cx43. The FRET efficiency between $Cx26^{WT}$ + $Cx26^{WT}$ and $Cx26^{WT}$ + $Cx26^{DN}$ was not statistically different.

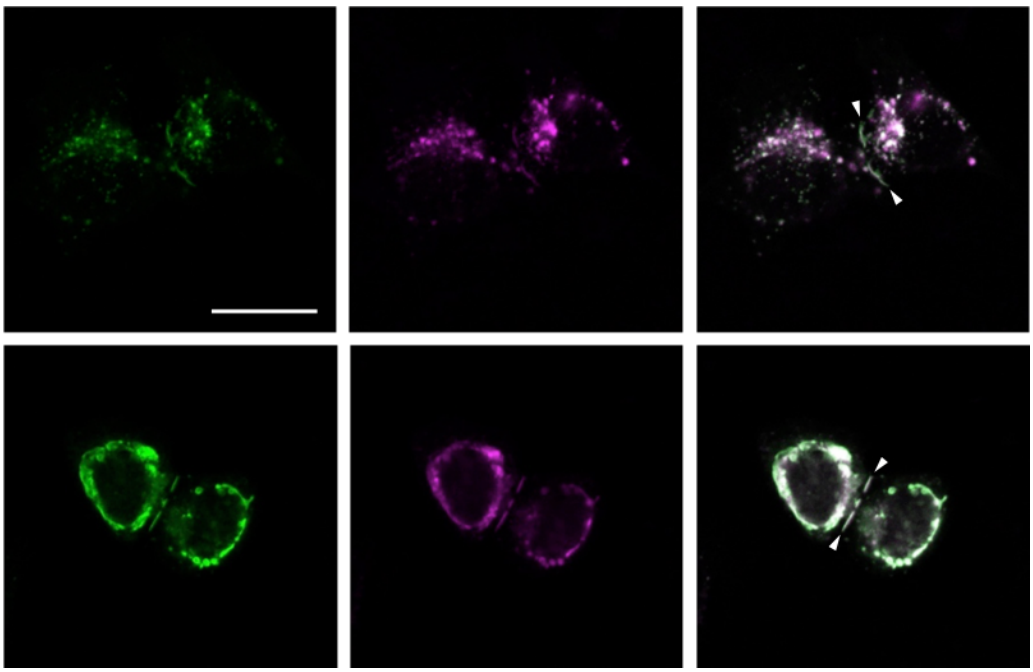

Figure 3.4 **Dominant Negative Connexin 26 localises to gap junction plaques**. HeLa cells were co-transfected with equal amounts of $Cx26^{WT}$-Clover and $Cx26^{DN}$-mRuby2. Cells were fixed after 48hrs and experiments were carried out on a Zeiss 710 Confocal microscope; C-Apochromat 63x/1.20 W Korr M27. Two channels were recorded: 495-545nm (Clover, green pseudocolour) and 650-700nm (mRuby2, magenta pseudocolour), and images were acquired sequentially with 458nm and 561nm argon lasers (respectively). Fluorescence of expressed fusion-proteins is shown before bleaching. Colocalisation is shown in white in the merged images (right channel). Two fields of view are shown as examples. Gap junction plaques is shown, white arrow. Scale bar, 20µm.

Table 3.1 Summary statistics for connexin co-expressions

Connexin Combination	Number of Cells	Number of ROIs	Mean FRET Efficiency ±s.d. (%)[a]	Mean Bleaching Efficiency ±s.d. (%)[b]	Mean D-A Distance ±s.d. (nm)[c]
$Cx26^{WT}$-Clover/ $Cx26^{WT}$-mRuby2	30	95	24±10	81±5	7.6±0.8
$Cx26^{WT}$-Clover/ $Cx26^{DN}$-mRuby2	26	74	23±8	79±5	7.8±0.6
$Cx43^{WT}$-Clover/ $Cx26^{WT}$-mRuby2	34	84	7±5	79±4	10.2±2.0[d]

[a] *FRET efficiency was calculated from background-adjusted ROIs as: $E = (clover_{post} - clover_{pre})/d_{post}$. $\%E = E \times 100$*

[b] *Bleaching efficiency was calculated from background-adjusted ROIs as: $Bleaching = (1 - (mRuby2_{post}/mRuby2_{pre}))$*

[c] *D-A distance was calculated as: $R = R_0((1-E)/E)^{1/6}$ where R_0 is the effective FRET distance for Clover/mRuby2 (6.3nm) and E is the measured FRET efficiency.*

[d] *5 ROIs with a FRET Efficiency < 0% (which only occurred during $Cx26^{WT}$ + $Cx43^{WT}$ experiments) were omitted from D-A distance calculations as a negative efficiency (representing clover intensity fluctuations in an area where no FRET occurred) would not be appropriate for such a calculation. Therefore, the reported value is calculated only from ROIs that contained $Cx43^{WT}$-Clover and $Cx26^{WT}$-mRuby2 subunits in close enough proximity for FRET to occur.*

As expected, unbleached regions showed FRET efficiency close to 0 (**Figure 3.5** and **Table 3.1**). Standard deviation values were no larger than those seen in similar studies (Di et al. 2005, Gu et al. 2004, Yum et al. 2007).

The contrast between the Cx26 coexpressions and the Cx26/Cx43 coexpression suggests that $Cx26^{WT}$-Clover and $Cx26^{DN}$-mRuby2 subunits assemble much closer than $Cx43^{WT}$-Clover + $Cx26^{WT}$-mRuby2 subunits – resulting in a greater FRET signal. It is highly likely that this greater FRET signal is a result of $Cx26^{WT}$ and $Cx26^{DN}$ subunit coassembly into heteromeric connexons.

3.3.3 Connexin26 WT and Connexin26 DN constructs show a negative correlation between FRET efficiency and donor-acceptor ratio

For each connexin pairing, fluorescence intensity values were used to calculate relative donor-acceptor (DA ratio) and relative acceptor intensity level (A-level). From these calculations, distribution plots of FRET efficiency (%E) vs. DA ratio and %E vs. A-level were produced (**Figure 3.6**). The distributions between ROIs from gap junctions and ROIs not from gap junctions appear to be equivalent for all comparisons (**Figure 3.7**), with the only observable difference seen when comparing gap junction and non gap junction ROIs in the $Cx26^{WT}/Cx43^{WT}$ %E vs. DA ratio plot, which shows that gap junction ROIs tended to have a greater DA ratio than non gap junction ROIs (however the variation/correlation is not different, just the shift in DA ratio).

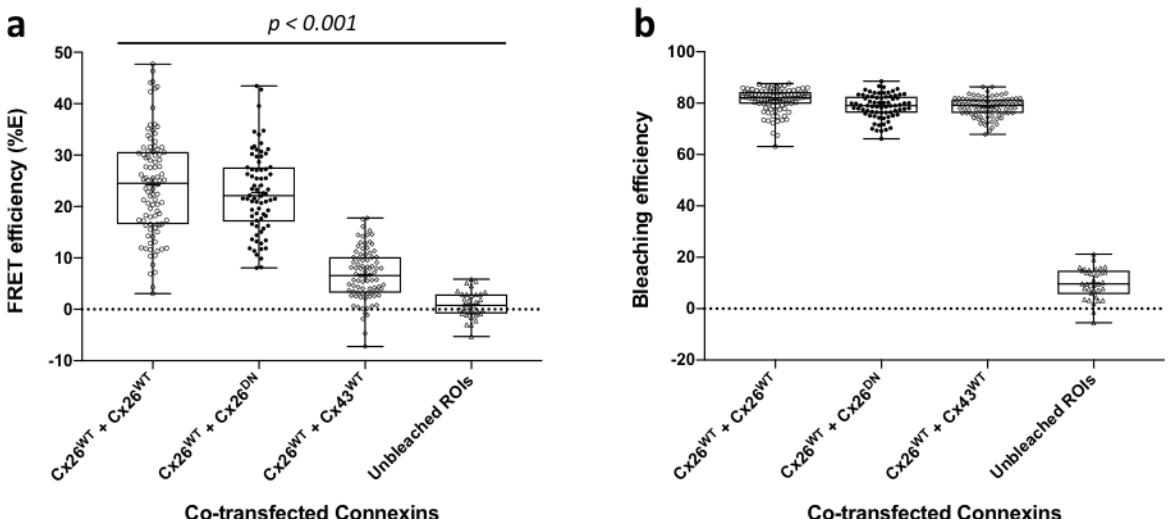

Figure 3.5 **FRET efficiency of coexpressed Connexin variants. a)** Box and whisker plot showing the difference in FRET efficiency (%E) across different connexin co-expression connexin samples. FRET efficiency was calculated from background-adjusted ROIs as: %E = 100 X ($clover_{post}$ - $clover_{pre}$)/$clover_{post}$. One-way ANOVA (represented by the top bar) was carried out in the statistical package SPSS. Post-hoc testing revealed all individual comparisons to be significant, at $p<0.001$, with the exception of the comparison between $Cx26^{WT}$ + $Cx26^{WT}$ and $Cx26^{WT}$ + $Cx26^{DN}$ datasets, which were not significantly different. **b)** Box and whisker plot showing mRuby2 bleaching efficiency during the acceptor depletion step. Whilst a small amount of bleaching occured in untargeted regions (presumably due to light scattering and/or reflection), targeted ROI's recieved drastically greater, but not complete, bleaching. Importantly all targeted regions showed highly similar bleaching efficiencies. Bleaching efficiency was calculated from background-adjusted ROIs as: Bleaching = (1 – ($mRuby2_{post}$/$mRuby2_{pre}$)). Boxes show the interquartile range. The median is indicated as a horizontal line within the box, and the mean is represented by a cross within the box. Range bars show minimum and maximum values. Cx, Connexin; ROI, region of interest.

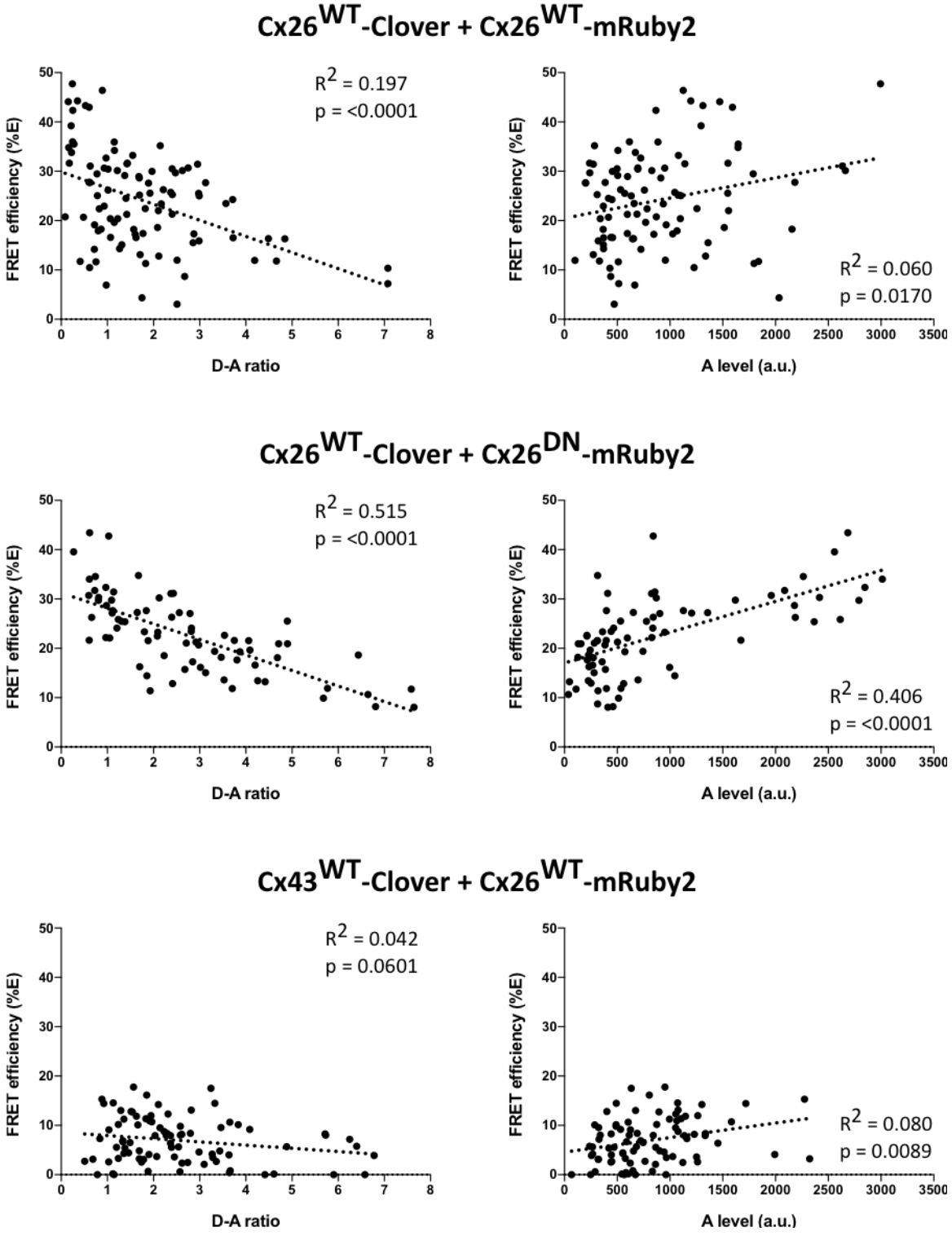

Figure 3.6 **Connexin26 variants coassemble into heteromeric connexons**. Acceptor depletion Förster Resonance Transfer (ad-FRET) was performed on HeLa cells coexpressing different combinations of connexins. Mean FRET efficiency (%E) is plotted as a function of relative donor-acceptor ratio (D-A ratio) or acceptor emission (A-Level). For proteins that coassemble a negative correlation is expected between %E and D-A ratio, with no correlation between %E and A-level. A positive correlation between %E and D-A ratio suggests that random association was sufficient to yield FRET. FRET measurements from cells co-expressing Cx26^{WT}-Clover + Cx26^{WT}-mRuby2 or Cx26^{WT}-Clover + Cx26^{DN}-mRuby2 show a negative correlation between %E and D-A ratio;

suggesting the two proteins interact in complexes – i.e. heteromeric connexons. However, these measurements also show a positive correlation between %E and A-level; suggesting that some of the interaction between the proteins was due to random association. FRET measurements from cells co-expressing $Cx43^{WT}$-Clover + $Cx26^{WT}$-mRuby2 showed no correlation between %E and D-A ratio, but a positive correlation between %E and A-level; suggesting that all of the FRET observed was a product of random association between homomeric connexon hemichannels. Each mark represents 1 ROI. As %E values < 0 do not make sense, they were plotted as 0. Linear regression analysis was carried out in GraphPad Prism.

FRET measurements from cells co-expressing $Cx26^{WT}$-Clover + $Cx26^{DN}$-mRuby2 show a clear negative correlation between %E and DA ratio, however also show a positive correlation between %E and A-level. FRET measurements from cells co-expressing $Cx26^{WT}$-Clover + $Cx26^{WT}$-mRuby2 show a weaker negative correlation between %E and DA ratio, and a very weak positive correlation between %E and A-level. FRET measurements from cells co-expressing $Cx43^{WT}$-Clover + $Cx26^{WT}$-mRuby2 showed no correlation between %E and DA ratio, and a very weak positive correlation between %E and A-level. Comparing these distributions, it is clear that the interactions between $Cx26^{WT}$/$Cx26^{WT}$ and $Cx26^{WT}$/$Cx26^{DN}$ are different to the interactions between $Cx26^{WT}$/$Cx43^{WT}$. The greater variation seen in $Cx26^{WT}$/$Cx26^{WT}$ indicates that there may be some bias in assembly/packing compared to $Cx26^{WT}$/$Cx26^{DN}$.

Based upon the membrane cluster model (Dewey and Hammes 1980), the negative correlation between %E and DA ratio indicates the presence of heteromeric connexons in $Cx26^{WT}$/$Cx26^{WT}$ and $Cx26^{WT}$/$Cx26^{DN}$ samples (i.e. coassembly), whilst any positive correlation between %E and A-level indicates that some level of random association (i.e. tight clustering of connexons) has taken place.

There is much variability in %E (represented by R^2 values), especially within the $Cx26^{WT}$/$Cx26^{WT}$ results. Other studies show similar variability (Di et al. 2005, Yum et al. 2007). This level of variability might be expected from these studies given the nature of the recordings taken; namely, the variability that can be expected from the transfection of different cells, and from the expression within different regions of different cells.

3.3.4 Connexin26 DN hemichannels do not open in response to CO_2

As with the $Cx26^{N14K}$ mutant (see *2.3.5 Connexin26 N14K hemichannels do not open in response to CO_2*), the hemichannel CO_2-sesntivity of the $Cx26^{DN}$ mutant (K125R, R104A) was also assessed using the same dye-loading technique. Parental HeLa cells expressing

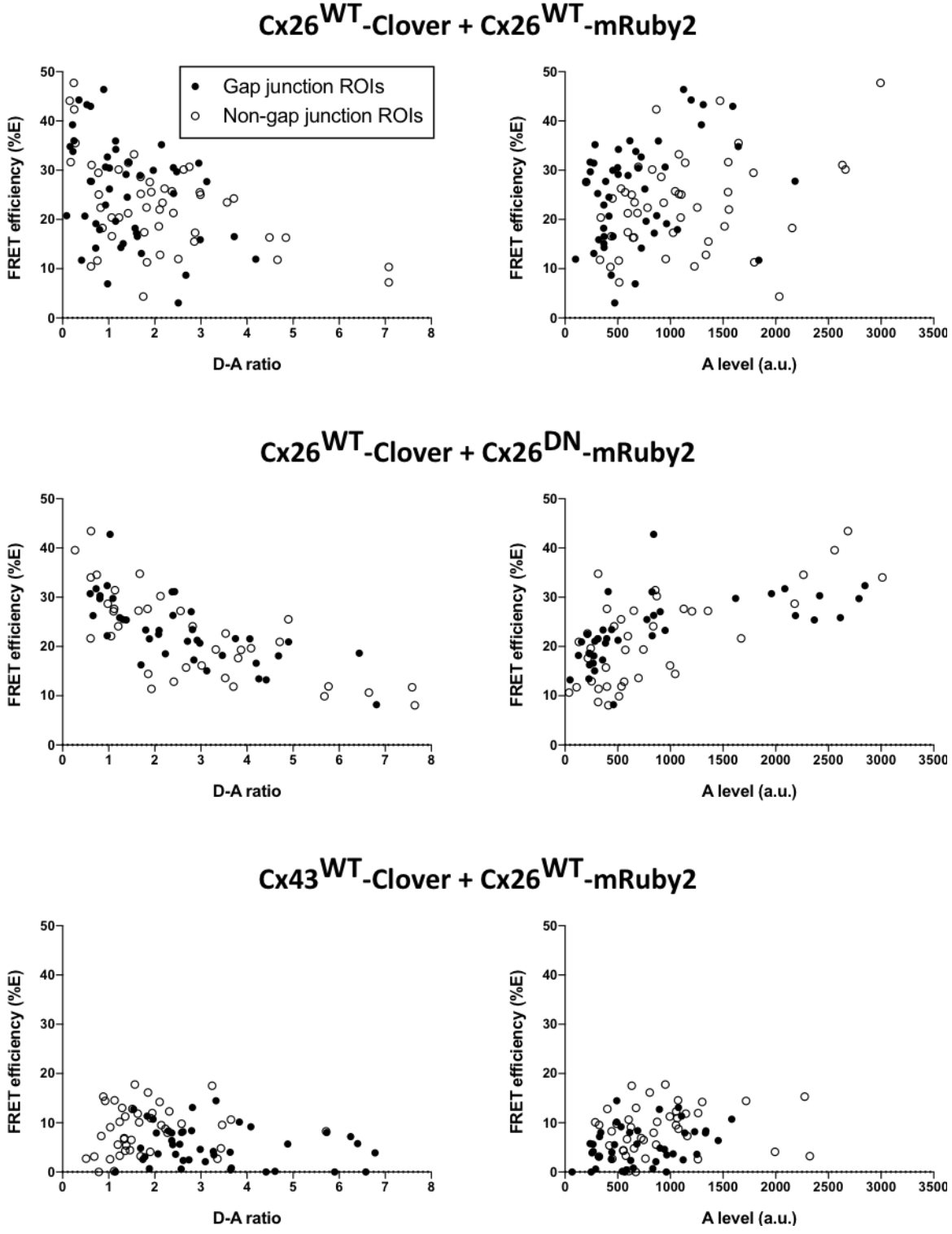

Figure 3.7 **Gap junction ROIs vs. non-gap junction ROIs**. Acceptor depletion Förster Resonance Transfer (ad-FRET) was carried out in HeLa cells coexpressing different combinations of connexins. Mean FRET efficiency (%E) is plotted as a function of relative donor-acceptor ratio (D-A ratio) or acceptor emission (A-Level). Distributions are split between ROIs recorded from regions clearly visible as gap junction plaques, black filled circles, and ROIs recorded from non-gap junction plaques (i.e. protein aggregates in plasma membrane hemichannel plaques or cytoplasmic vesicles), empty cirlces. All distributions can be seen to show no difference between

gap junction ROIs and non-gap junction ROIs, with the exception of cells co-expressing Cx43^{WT}-Clover + Cx26^{WT}-mRuby2; which showed gap junction ROIs shift, with respect to %E, towards higher D-A ratio (however there is no change in correlation of the two populations). Each mark represents 1 ROI. As %E values < 0 do not make sense, they were plotted as 0. Linear regression analysis was carried out in GraphPad Prism.

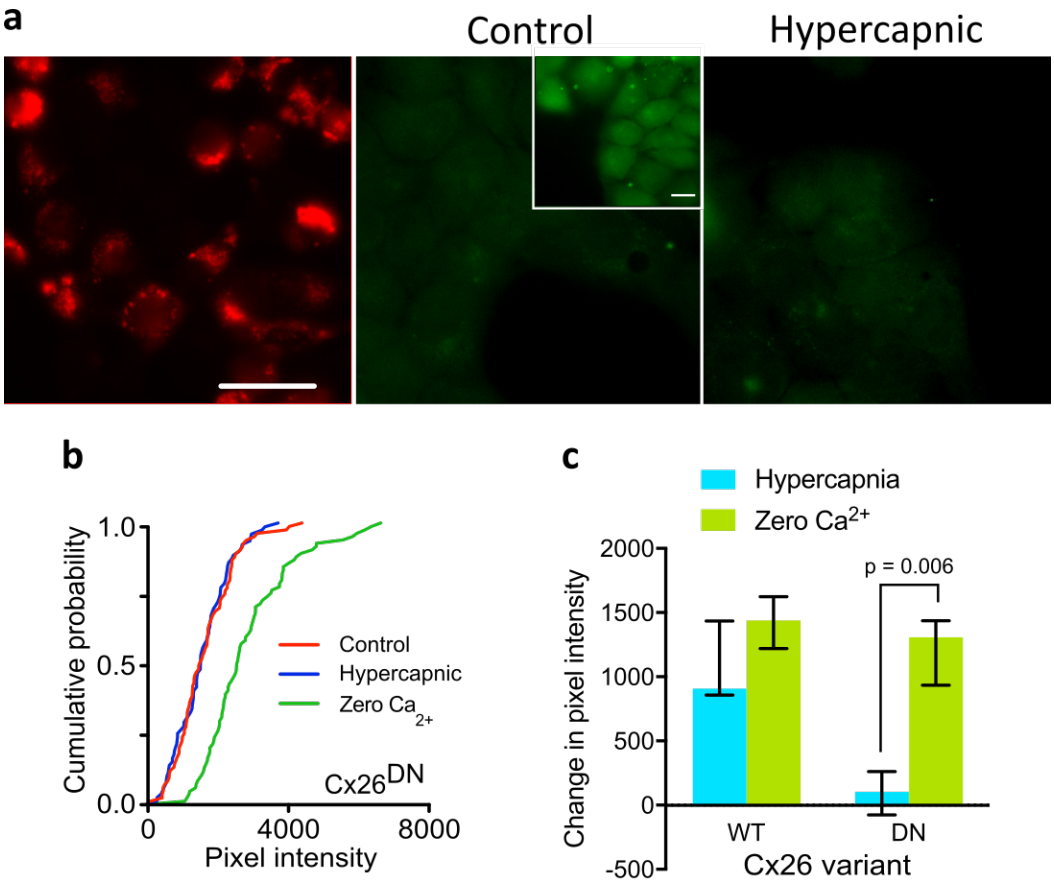

Figure 3.8 The Dominant Negative Connexin26 mutant (Cx26^{DN}) does not open in response to CO_2. HeLa cells were transfected with either Cx26^{DN}, and dye-loading experiments were carried out 3 days post-transfection. **a)** Representative images showing expression of mCherry tagged to Cx26^{DN} protein (left), and dye loading under 35mmHg PCO_2 (control, middle) and 55mmHg PCO_2 (hypercapnic, right) conditions – insert shows dye loading under zero Ca^{2+} conditions; a positive control showing functional Cx26 hemichannels. HeLa cells expressing Cx26^{DN} show no increase in dye loading under hypercapnic conditions. **b)** Cumulative probability distributions comparing mean pixel intensity for ROIS each condition. **c)** Median change in pixel intensity from baseline (35mmHg). Cells expressing Cx26^{DN} hemichannels are insensitive to CO_2 whilst cells expressing Cx26^{WT} hemichannels are sensitive to CO_2. Median pixel intensities (from independent repeats) were compared using the Mann-Whitney U test, n > 50 cells per treatment repeat, with 5 independent repeats for each treatment. Error bars show the first and third quartiles. Scale bars, 40µm.

$Cx26^{DN}$ showed no increase in dye loading in response to hypercapnic conditions (**Figure 3.8**), despite the expression of functional hemichannels in the plasma membrane (determined via extracellular zero Ca^{2+} control). These results suggest that, like $Cx26^{N14K}$, $Cx26^{DN}$ hemichannels do not open in response to CO_2.

3.3.5 Expression of Connexin26 DN removes CO_2-sensitive dye loading in cells stably expressing Connexin 26 WT

Similar to the $Cx26^{N14K}$ investigations (see *2.3.5 The Connexin26 N14K mutant acts to drastically reduce CO2 sensitivity from cells expressing wild-type Connexin26*) HeLa cells stably expressing $Cx26^{WT}$ (Cx26-HeLa cells) were transiently transfected with $Cx26^{DN}$-mCherry DNA. Cell CO_2 sensitivity was then monitored at 4, 5, and 6, days post-transfection by comparing dye loading under control and hypercapnic conditions. As transfections were made into cells stably expressing $Cx26^{WT}$ it was assumed that loss of CO_2-sensitivity would not be immediate, with time being needed for co-assembly with native Cx26, depletion of any native $Cx26^{WT}$ stores, and insertion into the membrane. As such, this time course was chosen in an attempt to document the onset of the dominant negative action. Un-transfected Cx26-HeLa cells were monitored over the same time period as a control.

Dye loading under hypercapnic conditions remains clear over the time course in untransfected Cx26-HeLa cells (**Figure 3.9a,b**). In contrast, Cx26-HeLa cells expressing $Cx26^{DN}$ show hypercapnia-induced dye loading at days 4 and 5, however by day 6 there is complete abolishment of dye-loading (**Figure 3.9c,d**). Dye loading above control conditions was significantly different when comparing hypercapnic conditions between non-transfected Cx26-HeLa cells and expressing $Cx26^{N14K}$ ($p = 0.001$), **Figure 3.9e**. Nevertheless, the continued presence of functional Cx26 hemichannels at day 6 is confirmed by a zero Ca^{2+} control – which exhibited increased dye loading compared to control conditions (**Figure 3.9c,d**). These results support our hypothesis, and suggest that $Cx26^{DN}$ acts in a dominant negative manner to completely remove CO_2 sensitivity from Cx26-HeLa cells.

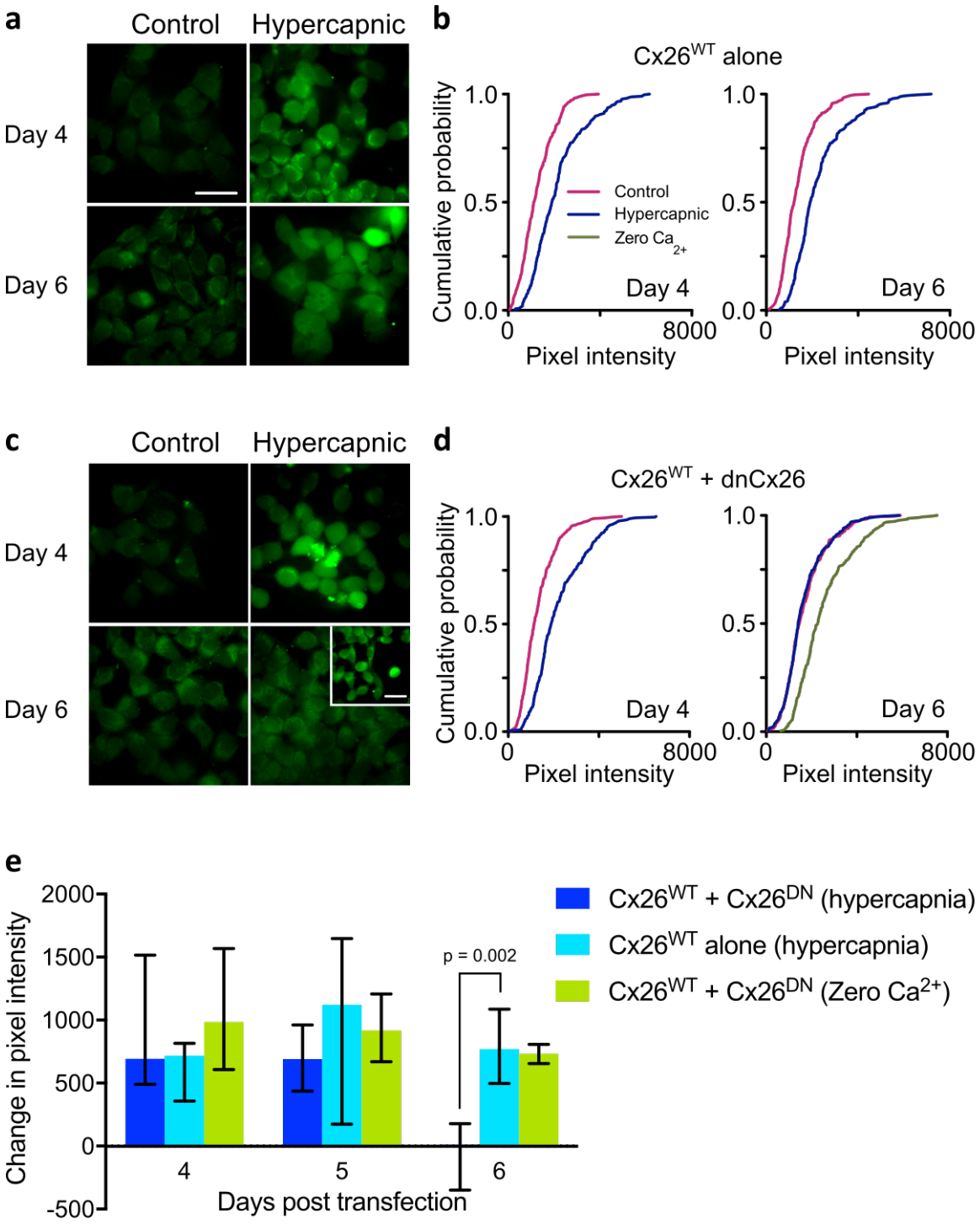

Figure 3.9 **The Dominant Negative Connexin26 mutant (Cx26^{DN}) removes CO2-sensitivity in HeLa cells stably expressing Cx26^{WT} (Cx26-HeLa cells).** Dye-loading under 35mmHg PCO_2 (control) or 55mmHg PCO_2 (hypercapnic) conditions revealed how the CO_2 sensitivity of Cx26-HeLa cells changes over time after transfection with Cx26^{DN}. **a, c)** Representative dye-loading images of Cx26-HeLa cells at day 4 and day 6 days after cells were either untreated (**a**) or transfection with Cx26$^{DN.}$ (**c**). At day 4 a significant increase in dye uptake can be seen in response to hypercapnic conditions, as compared to control conditions. In Cx26-HeLa cells transfected with Cx26^{DN} (**c**) very little difference in dye uptake can be seen between control and hypercapnic

conditions by day 6 – however an increase in dye uptake is visible in the zero ca^{2+} positive control (insert in bottom right panel), showing that functional Cx26 hemichannels are still present. **b, d)** Cumulative probability distributions comparing mean pixel intensity for each condition at day 4 and day 6 (untreated, **b**; transfected with $Cx26^{DN}$, **d**). n > 40 cells per treatment repeat, with 5 independent repeats for each treatment. **e)** Median change in pixel intensity from baseline (35mmHg) over days 4, 5, and 6 post-transfection. By 6 days post-transfection cells co-expressing $Cx26^{WT}$ and $Cx26^{DN}$ loose their ability to open in response to CO_2 but still open in response to Zero Ca^{2+}. In contrast, cells only expressing $Cx26^{WT}$ maintain CO2-sensitivity during the time course. Median pixel intensities (from 7 independent repeats) were compared using the Mann-Whitney U test. Scale bars, 40µm.

3.4 Discussion

3.4.1 Connexin26 DN is capable of trafficking to the membrane in the presence of wild-type Connexin26

When expressing fluorophore-tagged fusion proteins, such as the Connexin-fluorophore proteins expressed during our FRET studies, fluorophore fluorescence may be detected at the moment of peptide translation and throughout its assembly and trafficking. This includes possible storage as reserves in vesicles, and all the time it is present within the plasma membrane. Only once the protein is turned over and broken down will it definitely become undetectable. Because of this, it can be hard to discern which regions show expression in the membrane and which regions are showing some form of cytoplasmic residence, a problem that could be of consequence when choosing ROIs to measure during FRET experiments. As assembly of connexins into connexons is known to start in the ER, with significant assembly detectable within the ER-Golgi intermediate compartment ERGIC and Golgi (Martin et al. 2001, Zhang et al. 1996, George, Kendall, and Evans 1999), any intercellular regions of fluorescence that are recorded should yield results comparable to regions of fluorescence in the membrane – an assumption that has been confirmed in comparable adFRET studies (Di et al. 2005). That being said, Cx26 is also known to traffic by a non-golgi, microtuble-dependent, pathway (Martin et al. 2001, George, Kendall, and Evans 1999) and so added care should be taken when interpreting its expression within a cell.

In this study an equal number of ROIs were selected from regions of fluorescence within gap junctions and regions of fluorescence from non-gap junctions. Addressing the emphasis that this thesis has put on not treating hemichannels and gap junctions as the same entities, it must be noted that these FRET studies are an exception; the interest in

these studies lies in whether connexin variants coassemble into connexons, therefore measurements from gap junctions will still provide the same information as connexon docking (whilst affecting channel properties) does not alter the presence or properties of the fused fluorophores (the moiety being measured). Furthermore, because the fluorophores are cytoplasmic, the distance between the fluorophores in apposed cells is far too large for any FRET to occur.

As in the study by Di *et al.,* FRET efficiency (%E) distributions were compared between gap junction and non-gap junction regions (**Figure 3.7**), and it was also concluded that both have equivalent distributions. The only observable difference seen in our studies was a shift (with respect to %E) towards higher DA ratio values for gap junction ROIs in $Cx26^{WT}/Cx43^{WT}$ samples – however there is no change in correlation of the two populations. This difference might reflect a difference in how Cx26 and Cx43 connexons aggregate during trafficking and plasma membrane expression. As there was no difference in FRET efficiency distributions, and only fully assembled connexons are present in gap junctions (Martin et al. 2001, Zhang et al. 1996, George, Kendall, and Evans 1999), it can be inferred that the protein clusters recorded from non-gap junction ROIs are assembled connexons; be they midway through trafficking to the membrane, present in the membrane as *hemichannel* plaques, or potentially stored in vesicles as reserves.

Trafficking of connexins seems to vary greatly depending on the connexin variant and the system transfected into. For example, whilst wild-type connexins expressed *in vitro* show effective trafficking to the plasma membrane, some mutant connexins appear to show localisation primarily to the cytoplasm with limited trafficking to the plasma membrane (Di et al. 2002, Common et al. 2002, Marziano et al. 2003). Although we do not show data for *individual* expression of the $Cx26^{DN}$ mutant, our studies clearly show that *in vitro* coexpression of this mutant with $Cx26^{WT}$ results in its trafficking to the membrane, where it will be expressed in both gap-junctions and hemichannel.

3.4.2 Connexin26 WT and Connexin26 DN subunits coassemble into heteromeric connexon hemichannels

The membrane-clustering model (Dewey and Hammes 1980) has been used to explain molecular complex formations that are found in the plasma membrane and ER (Kenworthy, Petranova, and Edidin 2000, Lippincott-Schwartz, Snapp, and Kenworthy

2001, Silvius 2003, Wallrabe et al. 2003), and has since been functionally tested against connexin gap junction plaques with regular matrix structures (Unger et al. 1999, Yum et al. 2007, Di et al. 2005), where their FRET efficiency distributions provided the same interpretation of the cluster model. Applied to connexin studies, this model shows that an inverse correlation between %E and DA ratio reflects coassembly into clusters (heteromers). This is because with increasing amounts of donor relative to acceptor, the acceptor becomes saturated with energy from FRET and cannot accept more energy. The energy that would have been transferred, had there been additional acceptor molecules within its vicinity (10 nm), is emitted from the donor as photons pre-bleaching – thus reducing the calculated %E. The membrane cluster model also shows that a positive correlation between %E and A-level reflects randomly arranged molecules (homomeric connexons). This is because with increasing amounts of overall acceptor, more of the excitation energy is sequestered pre-bleaching – thus increasing %E.

Comparisons between mean %E strongly indicate coassembly of $Cx26^{WT}$ and $Cx26^{DN}$ subunits – there was no difference in mean FRET signal between $Cx26^{WT}/Cx26^{WT}$ and $Cx26^{WT}/Cx26^{DN}$ coexpressions, which were both significantly different to Cx26/Cx43 and unbleached regions (**Figure 3.5a**). By applying the membrane-clustering model this is confirmed. $Cx26^{WT}$-Clover/$Cx26^{DN}$-mRuby2 coexpressions showed a decrease in %E with DA ratio (**Figure 3.6**). This demonstrates the presence of FRET within clusters; i.e. that $Cx26^{WT}/Cx26^{DN}$ connexins coassemble into heteromeric connexons.

If we assume that there is no bias in the stoichiometric positioning of subunits within the heteromeric connexons formed then, at any given ROI, there will be a mix of stoichiometries within the population of connexons that is present – including homomeric $Cx26^{WT}$-Clover and $Cx26^{WT}$-mRuby2 connexons. If this is the case, it is interesting that our data shows less FRET efficiency (%E) variation in $Cx26^{WT}/Cx26^{DN}$ samples. This indicates that $Cx26^{DN}$ may favour an interaction with $Cx26^{WT}$, perhaps due to improved stability/trafficking, which would lead to a greater likelihood of heteromeric $Cx26^{WT}$-Clover/$Cx26^{DN}$-mRuby2 connexons being assembled (as opposed to homomeric connexons). Further to this, it could be speculated that the presence of homomeric connexons in $Cx26^{WT}/Cx26^{WT}$ samples, but not $Cx26^{WT}/Cx26^{DN}$ samples, is reflected by some low %E values at low DA ratios (**Figure 3.6**). In support of this, other studies, in HeLa cells and Keratinocytes, have also reported mutant connexins showing improved

plasma membrane trafficking when in the presence of wild type connexins (Di et al. 2005, Marziano et al. 2003, Thomas, Telford, and Laird 2004(de Wolf et al. 2016).

To try and get a sense of how accurate our results are let us assume the following conditions are true: i) all recorded FRET signal arises from coassembly (i.e. none is a result of homomeric connexon clustering), ii) all stoichiometric configurations within a heteromeric connexon have an equal probability of forming and ROIs contain sufficiently high numbers of connexons to reflect this non-bias, iii) connexin subunits are completely rigid and form equilateral hexagon structures, iv) the channel undergoes no conformational change, v) the chromophores responsible for FRET are positioned at the final amino acid residue of Connexin 26 (i.e. not somewhere within a fluorophore attached to the C-terminal end). In this scenario the mean DA ratio is equal to the mean distance between the corners of an equilateral hexagon, with lengths equal to those of Cx26, as determined by its crystal structure (Maeda et al. 2009). This is calculated to be 6.9 nm. The mean DA distances calculated from our data for $Cx26^{WT}/Cx26^{WT}$ (7.6±0.8 nm) and $Cx26^{WT}/Cx26^{DN}$ (7.8±0.6 nm). Although there are too many variables to make a direct comparison, it is not far-fetched to infer that, upon relaxing some of the assumptions made above, the experimental values plausibly reflect the mean distance as calculated from the crystal structure.

To conclude, by discerning FRET signals within connexons, we have shown that $Cx26^{WT}$ and $Cx26^{DN}$ subunits coassemble to form heteromeric connexons, which are subsequently expressed in the plasma membrane. This result meets the first criteria required for the creation of a well-understood dominantly negative CO_2-insensitive Cx26 mutant.

3.4.3 Connexin26 connexons can be found within 10nm of each other

A positive correlation between %E and A-level was also seen in $Cx26^{WT}/Cx26^{DN}$ coexpressions. Based on the membrane-clustering model this shows that some FRET occurred between clusters. FRET occurring between clusters indicates that connexons formed from $Cx26^{WT}/Cx26^{DN}$ also randomly cluster close enough for FRET to occur (this is in addition to inter-connexon FRET). Given that tight packing of Cx26 connexons into structured lattices has been observed in vertebrate gap junction plaques (Unger et al. 1997, 1999, Müller et al. 2002, Skerrett and Williams 2017, Makowski 1988, Leitch 1992),

some amount of inter-connexon FRET might be expected due to the close proximity of subunits in juxtaposed connexons.

Inter-connexon FRET was witnessed in all ROIs (not just gap junction ROIs), with no difference in the distributions obtained from gap junction and non-gap junction ROIs (**Figure 3.7**). This suggests that the structure of connexon packing in gap junction regions could be similar to that in non-gap junction regions (i.e. hemichannel aggregates and cytoplasmic vesicles).

Precisely how much FRET might be occurring between connexons is hard to gauge, as an estimate for the inter-connexon distance is difficult to predict. Despite X-ray diffraction and atomic force microscopy (AFM) studies that have viewed and calculated Cx26 centre-to-centre pore distance in vertebrate gap junction plaques (Müller et al. 2002, Oshima et al. 2013, Caspar et al. 1977, Revel and Karnovsky 1967, Robertson 1963, Makowski et al. 1984, Gogol and UNWIN 1986, Goodenough and Revel 1970, Hirokawa and Heuser 1982), resolution is still a limiting factor, and it is not known how the preparation of Cx26 plaques in these studies affects the *in vivo* structure (e.g. freeze-fracture preparations might cause membrane contraction). Furthermore, it has been acknowledged that: *"caution must be exercised in generalizing information related to size and spacing of channels from different preparations. Variations are evident within preparations, between preparations from the same organism, and between preparations from different organisms"* (Skerrett and Williams 2017). As such, although good structural measurements may be known for a single Cx26 connexon (Maeda et al. 2009), we do not know the true inter-connexon distance in our Cx26/Cx26 samples, neither are we able to predict it.

The mean DA distances calculated from our data for $Cx26^{WT}/Cx43^{WT}$ (10.2±2.0 nm) may provide insight into the average distance between the Cx26 and Cx43 plaque domains that have been observed in previous studies (Nagy et al. 2001, Rash et al. 2012, Gemel et al. 2004); however caution must be taken due to the different experimental conditions and sample preparations.

3.4.4 Connexin26 and Connexin43 connexons can be found within 10nm of each other

Cx26 and Cx43 do not coassemble into heteromeric connexons (Gemel et al. 2004) – which was confirmed in our study by the lack of correlation between %E and DA ratio

across the $Cx26^{WT}/Cx43^{WT}$ samples (**Figure 3.6**). *Ex vivo* studies have suggested that membrane expression of Cx26 and Cx43 connexons tend to aggregate into separate domains (within plaques or otherwise) based on the connexin/s subunits they are made from (Nagy et al. 2001, Rash et al. 2012, Gemel et al. 2004). However, these same studies show evidence that the domains juxtapose and overlap in places.

In our *in vitro* studies, at least some level of FRET signal is observed in all coexpressed connexin combinations. This included $Cx26^{WT}/Cx43^{WT}$ coexpression, although the values were significantly lower than Cx26/Cx26 coexpressions (**Figure 3.5**) and some ROIs yielded a %E ≤ 0. As FRET efficiency is not detectable at distances much greater than 10 nm (100 Å), the observation of a FRET signal in our $Cx26^{WT}/Cx43^{WT}$ samples shows that, *in vitro*, homomeric connexon packing in gap junction plaques, hemichannel plaques, and intracellular vesicles, can be within 10 nm of each other. In fact, only a few ROIs were calculated to have FRET efficiency ≤ 0, implying that ROIs in this study contained many regions in which Cx26 and Cx43 connexons were clustered amongst one another.

The lower FRET efficiency seen in $Cx26^{WT}/Cx43^{WT}$ samples (compared to $Cx26^{WT}/Cx26^{WT}$ and $Cx26^{WT}/Cx26^{DN}$ samples) shows either that packing of $Cx26^{WT}$ and $Cx43^{WT}$ connexons is less tight than Cx26/Cx26 connexon packing, or that the Cx26/Cx26 subunits coassembled into connexons (thus decreasing the distance between flourophores and increasing FRET efficiency), or both. The larger donor-acceptor distance calculated from $Cx26^{WT}/Cx43^{WT}$ samples (**Table 3.1**) reflects this difference in packing/coassembly.

3.4.5 Refinement of a previously published quantitative adFRET approach

The adFRET assay used in this chapter was based on the linear unmixing adFRET (u-adFRET) assay used by Gu *et al.* (Gu et al. 2004, Di et al. 2005, Yum et al. 2007). In these studies data is collected across the entire emission spectra of both fluorophore, and spectral unmixing is used to tackle spectral bleed-through and separate out donor and acceptor fluorophore signals. After unmixing, mean intensity values were measured from ROIs, and %E, DA ratio, and A-level were calculated based on relative acceptor and donor abundance values. The process of spectral unmixing can be tricky, and depend on algorithms that make certain assumptions. To unmix a population of flourophores, most approaches require tightly controlled preparation and acquisition of reference and test

samples; with all samples being prepared using the same technique (mounting medium, cell type, etc.), and recorded using identical parameters (gain, filters, objective, laser power, etc.). It is widely accepted that, because of this, acquisition of images is no trivial matter (McNamara et al. 2017, Zhang et al. 2015, Haraguchi et al. 2002, Lansford, Bearman, and Fraser 2001). The algorithms underlying spectral unmixing rely on binning the spectrum range and acquiring non-overlapping contiguous spectral channels, which are then used to fit the reference spectra to. With newer microscopes, allowing for multi-channel acquisition, this can be done fairly accurately however still introduces some level of error. Also, when spectrally unmixing flourophores capable of FRET the emission measured in unbleached regions will not include some donor signal that would be present in the absence of an acceptor. This is due to some of the signal being quenched by the interacting acceptor (i.e. FRET is occurring). Gu *et al.* recognised the presence of an invisible donor signal pre-photobleaching and corrected for it based on the assumption that this missed signal comes from a population of donors that are entirely non-radiative (Gu et al. 2004, Di et al. 2005). However, the invisible signal cannot be assumed to be the total quenching of a population of donors, and as such introduces error into the spectral unmixing calculations. Furthermore, it is known that FRET can alter the shape of a fluorophore's emission spectrum (McNamara et al. 2017, Thaler et al. 2005), something that is not addressed in the u-adFRET unmixing calculations. This has the potential to be a highly confounding factor, as reference spectra cannot be assumed to be suitable for a fluorophore that is undergoing FRET.

For FRET studies in this chapter, the u-adFRET assay was modified to remove the need to spectral unmixing. Rather than ECFP and EYFP, the FRET-pair Clover (donor) and mRuby2 (acceptor) was used. Unlike previous FRET-pairs (such as ECFP/EYFP), Clover/mRuby2 have very good separation in their emission spectra. In fact, it is possible to record channels with no spectral bleed-through, yielding separate measurements of pure Clover and pure mRuby2 emission (**Figure 3.2a**). These measurements provide relative abundance values that can then be used in calculations to determine DA ratio, and A-level.

The measurements obtained using the u-adFRET approach are reported as being quantitative (Gu et al. 2004, Di et al. 2005, Yum et al. 2007), however this method does not actually yield values for molecular abundancies of flourophores (just an abundance factor for each). As such, the DA and A-level values that are quantified in one experiment

cannot be compared to the values quantified in an experiment performed with different parameters. Without being able to calculate the actual values for proteins it may be fairer to call this approach semi-quantitative. This being said, quantitative analyses can still be performed on data yielded from this assay, and the %E *can* be compared across experiments. The mean %E reported from Cx26/Cx26 coexpressions in this chapter (24±10%) matches that reported in previous literature (24±13%) (Di et al. 2005). The distribution patterns for %E vs. DA ratio and %E vs. A-level can also be compared across results however, as explained, the values for DA ratio and A-level cannot. Therefore, these plots may see value shifts when comparing against different experimental parameters.

In the studies by Di, Gu, and Yum *et al.* only ROIs with a DA ratio of 0.33-3 are included to "*avoid calculation errors caused by low by low signal-to-noise ratio, and FRET efficiency saturation owing to high concentrations of donor/acceptor*" (Di et al. 2005). However, a low signal-to-noise ratio can be overcome through appropriate selection of ROIs; so that both fluorophore pixel intensities were sufficient for measurements, but not overexposed too the extent that they cap out at the maximum measureable intensity. Also, by restricting the ROIs by DA ratio there is the risk of cutting out data that contributes to the very relationships you are trying to discern; namely, the increase in DA ratio with decreasing FRET efficiency. This is because the DA ratio is only a relative ratio based on fluorescence intensities - it is not an actual value of the number of donor and acceptor molecules present within the ROI. As such, for each set of experimental parameters, you cannot be sure what DA ratio range will be relevant and should only omit this data after careful consideration.

By utilising Clover/mRuby2, and sacrificing the potential to collect light across the flourophores' entire spectra, it was possible to develop an approach that still maintains the (semi-)quantitative benefits of that developed by Gu, whilst removing the need for spectral unmixing calculations. This creates a more accessible assay that minimizes errors that may be introduced from experimental design/execution, as well as removing any errors that are inherent to the assumptions that are made during the spectral unmixing step.

3.4.6 Connexin 26 DN acts in a dominant negative fashion to eliminate CO_2-Sensitivity from connexon hemichannels

In an attempt to develop a tool that could be used to eradicate CO_2-mediated Cx26 hemichannel opening, a Cx26 mutant with K125R and R104A mutations was created, and it's effect on CO_2 sensing was tested. The design of this DN mutant was in such a way that any given $Cx26^{DN}$ subunit would be incapable of forming a carbamate bridge with either of its neighbours in a connexon.

In this chapter, dye-loading analysis has shown that homomeric $Cx26^{DN}$ hemichannels are insensitive to CO_2 (**Figure 3.8**). Furthermore, it was demonstrated that the CO_2 sensitivity of cells stably expressing $Cx26^{WT}$ is completely removed 6 days after the coexpression of this mutant (**Figure 3.9**). Therefore, $Cx26^{DN}$ acts in a dominant negative fashion, removing the cells ability to respond to CO_2 even when cells are stably expressing CO_2 sensitive Cx26. This result supports the carbamylation model of CO2-dependent opening of Cx26; i.e. that the K125 and R104 residues are involved in CO2 dependent channel opening of Cx26 (Meigh et al. 2013, Meigh et al. 2014, Meigh et al. 2015b).

Taken together with our FRET data, which shows that $Cx26^{WT}$ and $Cx26^{DN}$ connexin subunits readily coassemble into heteromeric connexons, we conclude that this dominant negative action occurs because $Cx26^{DN}$ and $Cx26^{WT}$ connexins form heteromeric hemichannels, which subsequent lose the ability to open in response to CO_2. Due to the deliberate design of this mutant we conclude that, in any given $Cx26^{WT}/Cx26^{DN}$ heteromeric hemichannel, this loss of CO_2 gating is due to the removal of a sufficient number of sites that are required for the carbamate bridge formation (i.e. K125 and R104 residues) that is responsible for channel opening. The incorporation of one $Cx26^{DN}$ subunit, into an otherwise $Cx26^{WT}$ connexon, would maintain four of the six bridges that are required for fully stabilising the hemichannel in its open state. Depending of the stoichiometric organisation of the connexins, the incorporation of two $Cx26^{DN}$ connexins could maintain a maximum of three interactions (if the $Cx26^{DN}$ subunits were adjacent to each other). The incorporation of three $Cx26^{DN}$ connexins could maintain a maximum of two interactions. The incorporation of four $Cx26^{DN}$ connexins could maintain a maximum of one interaction. The incorporation of five or six $Cx26^{DN}$ connexins would prevent any carbamylation-mediated interactions from occurring. The composition of the heteromeric connexons that are formed is unknown, however based

on our FRET distributions, we believe that there is no difference between assembly and packing of $Cx26^{WT}$ with either $Cx26^{WT}$ or $Cx26^{DN}$ – other than a potential bias away from the formation of homomeric $Cx26^{DN}$ connexons. Although we are not able to put a number on it, the level of cooperative binding between CO_2 molecules and Cx26 hemichannel (**Figure 3.1b**) suggests that the presence of just one or two DN subunits might be sufficient in preventing the open state being reached (**Figure 3.1c**). The number of intersubunit interactions required for channel opening could be further explored with elastic network modelling.

The loss of CO2-sensitivity observed upon $Cx26^{DN}$ transfection into Cx26-HeLa cells was not immediate, occurring approximately 6 days post transfection (**Figure 3.9**). Single expression of Cx26 variants into parental HeLa cells yields functional hemichannels in the plasma membrane by 72 hrs (Meigh et al. 2013, Meigh et al. 2014, Meigh 2015a, de Wolf et al. 2016, de Wolf, Cook, and Dale 2017). Cx26 turnover has a half-life of ~5 hours in mouse hepatocytes (Fallon and Goodenough 1981). Although the cellular dynamics in HeLa cells will differ somewhat, a turnover of 5 hours equates to ~99-100% turnover of plasma membrane connexins in a 48 hr period. As we did not see the action of $Cx26^{DN}$ until 6 days post-transfection, this suggests that turnover of Cx26 may occur from a pool or reservoir of connexons that reside within cytoplasmic vesicles. In this way, unlike transfections into parental cells, during which hemichannels would be transported to the plasma membrane and become functional more or less immediately, transfections into cells already expressing $Cx26^{WT}$ could require an additional 3 days for heteromeric assembly, sufficient replacement of reservoir connexons, and subsequent trafficking/turnover of non-functional connexons into the plasma membrane.

This chapter has shown that, as predicted, $Cx26^{WT}$ and $Cx26^{DN}$ subunits coassemble into heteromeric connexon hemichannels, and that the introduction of $Cx26^{DN}$ subunits into cells stably expressing $Cx26^{WT}$ completely removes the cells Cx26-mediated response to CO_2. As such, it is concluded that the formation of $Cx26^{DN}$/$Cx26^{WT}$ heteromeric hemichannels results in insufficient carbamate bridge formation under hypercapnic conditions (which would usually stabilise the channel in an open state), and that with enough time this effect will become widespread in cells natively expressing $Cx26^{WT}$ – thus resulting in cell-wide Cx26-mediated CO_2 insensitivity.

3.4.7 Dominant Negative Connexin 26 could be used for *in vivo* experiments to investigate the CO_2 sensitivity of connexin 26 expressing cells

The FRET experiments in this chapter have demonstrated that our engineered $Cx26^{DN}$ mutant readily coassembles with $Cx26^{WT}$ to form heteromeric connexons that are expressed in gap junction plaques, hemichannel plaques, and cytoplasmic vesicles. Our dye loading experiments in this chapter have demonstrated the ability of $Cx26^{DN}$ expression to remove native CO2-sensitivity from cells with stable $Cx26^{WT}$ expression. Furthermore, owing to the design of the mutant, we have a very clear understanding as to how this dominant negative effect is brought about. Consequently, introduction of $Cx26^{DN}$ into CO_2-sensitive cells *in vivo* could provide a method of manipulating certain cells in living animals in order to remove CO_2-dependent Cx26 channel opening, whilst leaving otherwise functional Cx26 protein.

By engineering the $Cx26^{DN}$ gene into a Lentivirus (LV) or Adeno-associated virus (AAV) construct, expressed on a tissue specific promoter, it would be possible to test the importance of Cx26 CO_2 sensitivity in any number of tissues. This has the benefit of testing a specific gating characteristic (CO_2), which limits any confounding effects that that may be brought about from the complete KO of the Cx26 gene (e.g. compensation, or disruption of other Cx26-related pathways). Also, as system-wide Cx26 KO is lethal (Gabriel et al. 1998), this would provide an alternative to timely and costly cross-breeding KO studies that targets.

One use of this technique would be to investigate the role and mechanism of Cx26 in respiratory chemoreception. Specifically, such a construct could be generated with a GFAP promoter, with targeted viral transduction at chemosensitive sites of the VMS. This would result in the expression of $Cx26^{DN}$ in glial cells of the VMS that are believed to be involved in a Cx26-mediated breathing response and would subsequently remove Cx26 CO_2 sensitivity. The manipulated system would lose the ATP release that usually occurs upon CO_2-dependent Cx26 hemichannel opening (Huckstepp et al. 2010a), allowing the role that glial Cx26 plays in the breathing response to be investigated. By using the $Cx26^{DN}$ tool in this manner, removal of Cx26 CO_2 sensitivity can take place post-natal, i.e. after the developmental stages during which compensation is likely to occur. Because the $Cx26^{DN}$ gene can be genetically introduced into cells it would enable *in vivo* breathing measurements to be taken from unanaesthetised animals, i.e physiological conditions.

4 PROGRESS TOWARDS TESTING THE ROLE OF CO_2-SENSING VIA CONNEXIN26 IN GLIAL CELLS AS A CHEMOSENSORY REGULATOR OF BREATHING

4.1 Introduction

Breathing enables the body to maintain blood pCO_2 and pO_2 levels: a vital function required to supply O_2 for cellular respiration and remove CO_2 to prevent respiratory acidosis. In order to adjust breathing, the body needs to be able to sense changes in these blood gases and respond in some way to bring about a change in breathing. Such modulation of breathing is known as respiratory chemoreception. This chapter focuses on central CO_2 chemoreception. CO_2 chemoreception takes precedence over O_2 chemoreception (Haldane and Priestley 1905, Phillipson, Duffin, and Cooper 1981, Spyer and Gourine 2009), with central CO_2 chemoreception responsible for around twice as much of the hypercapnic ventilatory response (HCVR) as peripheral CO_2 chemoreception (Forster et al. 2008).

It has been clearly demonstrated that the ventral medullary surface (VMS) contains sites important for central CO_2 chemoreception – in particular the rostral and caudal areas. These two areas were first identified based upon their acidification causing increased respiratory activity (Loeschcke 1982, Schlaefke, See, and Loeschcke 1970, Mitchell et al. 1963a, Mitchell et al. 1963b, Trouth et al. 1973, Schlaefke, Kille, and Loeschcke 1979). The general consensus is that the rostral chemosensitive area can be defined as the RTN/pFRG, however the caudal area is much less defined. In the search to understand which cells are responsible for chemoreception there has recently been much focus on the RTN, where a population of neurons have been found to respond to physiological changes in pH (Mulkey et al. 2004, Mulkey et al. 2006, Guyenet, Stornetta, and Bayliss 2008, Kumar et al. 2015). There has also been interest in the serotonergic raphé neurons, which run medial to the traditionally defined rostral and caudal sites (**Figure 1.1b-d**) and also play a role in detecting changes in pH (Richerson 2004, Ray et al. 2011, Brust et al. 2014). Alongside these players, and the focus of this chapter, there is also a chemoreceptive role for ATP signalling along the VMS (**Figure 1.1b**), which is released from sub-pial $GFAP^+$ cells in response to hypercapnia and mediates respiratory

activity by acting on respiratory neurons via P2X and P2Y receptors (Gourine et al. 2003, Gourine et al. 2005, Lorier et al. 2007, Gourine et al. 2010, Huckstepp et al. 2010a, Mulkey and Wenker 2011, Wenker et al. 2010, Wenker et al. 2012, Moreira et al. 2015).

In order for chemosensitive cells (like those reported in the RTN, raphé, and $GFAP^+$ cells) to be considered respiratory chemoreceptors, they must be capable of intrinsically detecting and responding to physiological changes in pCO_2. This requires a chemosensory transducer molecule that will sense a change in pCO_2 (be it via molecular CO_2, pH, or bicarbonate) and initiate a signalling pathway to adjust respiration. Potential chemosensory transducers have been suggested to play a role at certain VMS chemosensitive sites, with GPR4, TASK2, Kir4.1, NBCe1, and Cx26 all proposed to have an action in the RTN – some of which have accompanying KO studies showing decreased HCVR in conscious animals (see *1.3 Central respiratory chemosensory transducers for pCO_2*). Although some of these molecules may be relevant for responding to changes in pH only Cx26 has the ability to respond to CO_2 directly. Therefore, Cx26 is currently the strongest candidate to account for the pH-independent adaptive changes in breathing that have been reported (but are often overlooked) (Shams 1985, Harada, Kuno, and Wang 1985, Huckstepp et al. 2010a, Meigh et al. 2013). As such we chose to further investigate the role of Cx26 in chemoreception, by using a novel genetic tool.

As it stands KO of any protein from birth, as in the aforementioned studies of putative chemosensory transducers, introduces many unknow and unnatural variables into the development of an animal and its physiology (regardless of the cell specificity). In order to truly ascertain the physiological relevance that a protein plays in the HCVR of an intact, wild-type, animal it is important that we strive to develop and refine techniques that alter the animal system as little as possible. In order to achieve this goal, we require progressive experimental design such as the $Cx26^{DN}$ tool that has been characterised in the previous chapter (see *3 Characterisation of co-assembly and CO_2-Insensitivity of a Connexin26 dominant negative mutant*). Such an innovative technique brings with it benefits of temporal and spatial gene control similar to those provided by the Cre/lox recombination technique (Feil, Valtcheva, and Feil 2009), and thereby allow the natural development of mice before ablation of a protein's function. In this way, CO_2 chemoreception can be tested at any age and in a more realistic/physiological scenario than previous KO studies. Furthermore, by introducing $Cx26^{DN}$ via LV the system provides additional benefits of being able to target any part of the body without affecting other

tissues, and of specifically removing the Cx26 property of interest (i.e. CO_2-sensitivity) whilst maintaining expression of the protein within cells. Therefore, the LV-Cx26^{DN} system is applicable to rats (not just mice) and might be seen to allow for the investigation of CO_2-sensitivity in a scenario that is even more realistic/physiological than that produced by the cre/lox system.

As stimulation of the RTN (rostral chemosentive site) elicits a HCVR that consists of a large change in tidal volume (Li, Randall, and Nattie 1999) and there is unpublished evidence that Cx26 modulates tidal volume (but not frequency) in the caudal chemosensitive site of mice aged 3-7 months (personal communication from Nicholas Dale and Georgy Koentges – and discussed later in this chapter), we hypothesised that the same Cx26-mediated control of tidal volume is also important within the rostral chemosensitive site (**Figure 4.1**). If correct, removal of Cx26 CO_2 sensitivity in rostral glia, after adulthood, will result in a measurable reduction in adaptive changes in tidal volume. In this chapter this hypothesis is tested by utilising the Cx26^{DN} mutant that has previously been shown to remove CO_2 sensitivity from cells stably expressing Cx26^{WT} (see *3 Characterisation of co-assembly and CO2-Insensitivity of a Connexin26 dominant negative mutant*).

By using a LV harbouring the Cx26^{DN} gene, experiments in this chapter aimed to transduce glia at the rostral chemosensitive site (RTN) of the VMS, after mice reached adulthood. Cx26^{DN} expression will act to remove CO_2 sensitivity thereby preventing any Cx26-mediated ATP release that usually occurs within the RTN. Subsequently, the effect that Cx26 CO_2 gating has on the HCVR can be determined. Removing CO_2 sensitivity in this manner is much more elegant than the global KO studies of GPR4, TASK2, Kir4.1, and Cx26, and should provide a much more representative picture of chemoreception mechanics.

4.2 Materials and Methods

4.2.1 Lentivirus design and handling

Two lentivirus (LV) constructs were designed to introduce either the Cx26^{DN} or Cx26^{WT} gene into the host cell genome (**Figure 4.2a,b**). Constructs are ~4900bp in length. The sequence of interest consisted off the Cx26 gene variant (Cx26^{WT} or Cx26^{DN}) immediately followed by an internal ribosome entry site and Clover sequence (Cx26:IRES:Clover). In

this way, LV expression of Cx26 protein would be marked by the expression of the fluorescent protein Clover. As protein production via IRES translation results in an uncapped peptide, expression of Clover is likely to occur at approximately 1:10 translation rate compared to that of Cx26 (Mizuguchi et al. 2000, Martineau et al. 2004, HERNÁNDEZ et al. 2004, Hennecke et al. 2001, Dirks et al. 1994). To enhance translation of the Cx26:IRES:Clover transcripts, a woodchuck hepatitis virus posttranscriptional

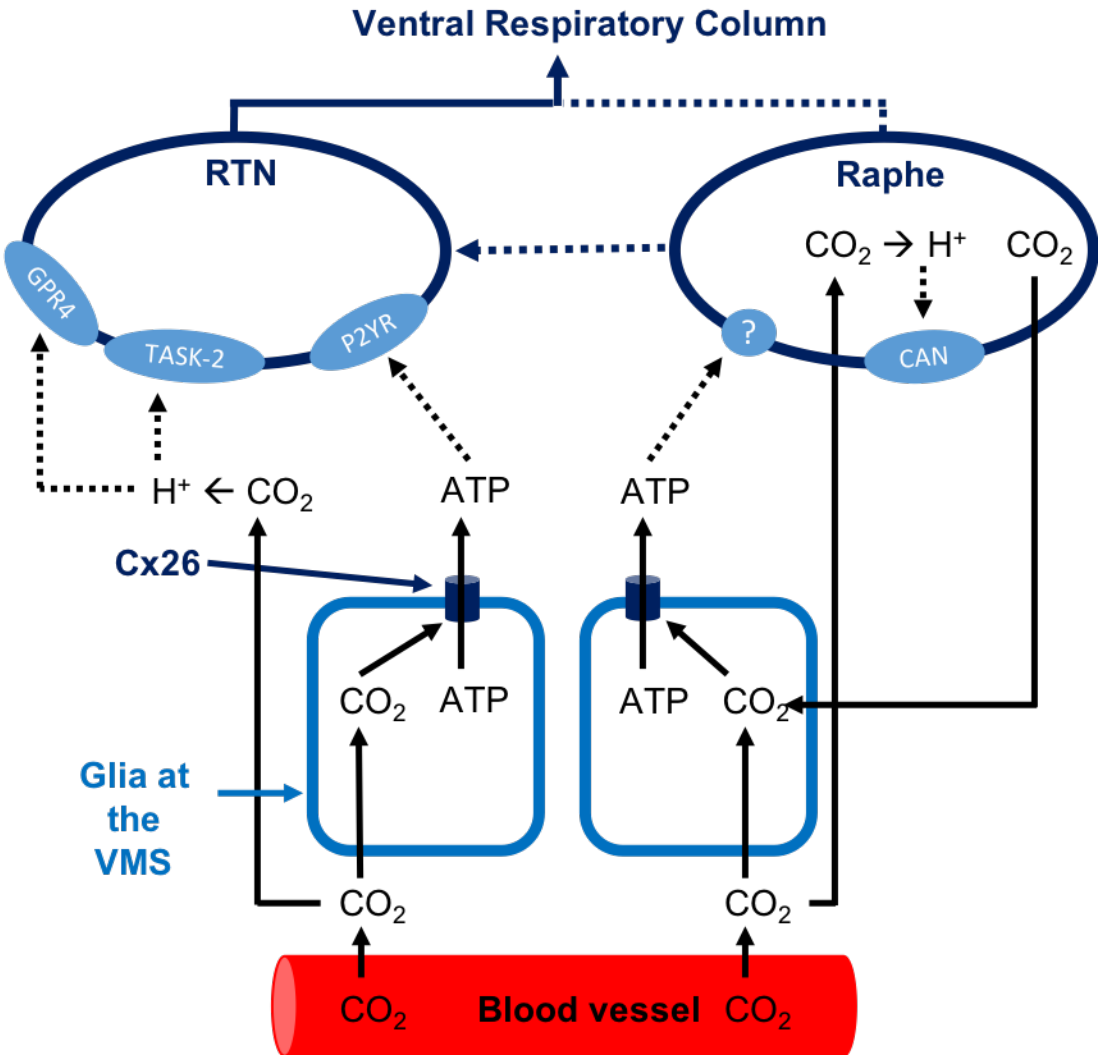

Figure 4.1 **Hypothetical contribution of Connexin26 to the hypercapnic respiratory response initiated in the rostral ventral medullary surface**. Schematic diagram showing how Connexin26 (Cx26)-mediated ATP release could augment the activation of chemosensitive neurons in the rostral part of the ventral medullary surface. Under hypercapnic conditions glia within the Retrotrapezoid nucleus (RTN) might be responsible for Cx26-mediated ATP release. ATP release would act on P2Y receptors of RTN neurons responsible for mediating a hypercapnic ventilatory response (HCVR). More medial to the RTN, similar ATP release could be responsible for acting on an unknown receptor of raphe magnus neurons responsible for mediating a HCVR. CO_2 produced by surrounding brain tissue would also feed into this pathway. CAN, channel responsible for a Calcium-activated non-selective cation current; TASK-2, two-pore-domain potassium channel type 2; GPR4, G protein-coupled receptor 4; P2YR, a GPCR purinergic receptor

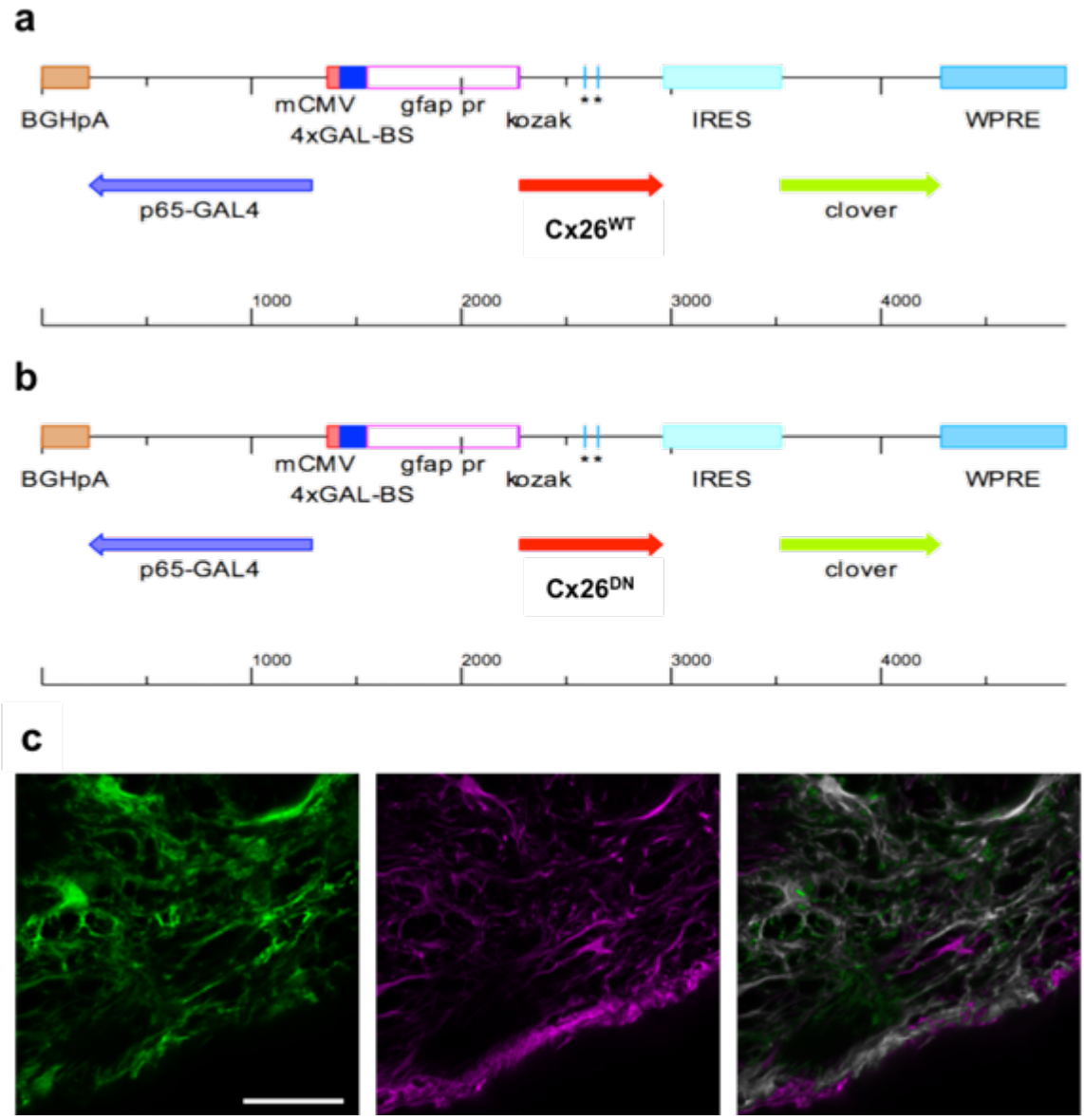

Figure 4.2 **Lentivirus design and *in vivo* expression**. **a,b)** Lentivirus construct sequences for the introduction of wild type Connexin 26 ($Cx26^{WT}$) (**a**) or Dominant Negative Cx26 ($Cx26^{DN}$) (**b**) into cells of the ventral medullary surface (VMS). Expression of Connexin 26 is under the control of a GFAP promoter, resulting in cell-specific expression only in those cells that express GFAP. An IRES:Clover sequence immediately after the Cx26 gene of interest provides a marker for which cells express the gene. Cx26 Constructs are ~4900bp in length. **c)** Maximum-intensity projection of cells at the VMS. GFP-amplification of Clover (green, left) shows expression of lentivirus constructs at the VMS expression. Glial cells are identified based on their morphology and positive immunostaining for the intermediate filament glial fibrillary acidic protein (GFAP) (magenta, middle). Co-localisation shows that construct expression occurs only within glial cells (grey, right). Scale; 40µm. Cx26, connexin; WT, wild type; DN, dominant negative; GFAP, glial fibrillary acidic protein; mCMV, mini cytomegalovirus; IRES, internal ribosome entry site; WPRE, woodchuck hepatitis virus posttranscriptional regulatory element; BGHpA, bovine growth hormone polyadenylation signal.

regulatory element (WPRE) was added after the Clover sequence. Expression of the Cx26:IRES:Clover constructs was under the control of a GFAP promoter, resulting in cell-specific expression only in cells that express GFAP (i.e. a subset of glia consisting predominantly of astrocytes). To increase expression of the virally-encoded Cx26:IRES:Clover sequence, the construct contained a mini-cytomegalovirus (mCMV) promoter to control for the expression of GAL4, which acts as an enhancer to the GFAP promoter, and subsequently Cx26:IRES:Clover transcription. The LV construct also contained a bovine growth hormone polyadenylation signal (BGHpA) for packaging purposes.

Lentivirus constructs were produced and packaged by Cyagen Biosciences (USA) using the third-generation packing system. This involves transfecting the lentiviral vectors (along with helper plasmids) into optimised packaging cells, which then package complete LV virons that are released into media. Released virons are then purified by PEG centrifugation. The third-generation system produces LV that is replication incompetent and thus very safe. Constructs had a titre > 10^8 TU/mL; as confirmed by qPCR on genomic DNA extracted from infected cells.

LV was aliquoted in a Category 2 Microbiological Safety Cabinet lab and stored at -80^{0}C. For injections, LV was removed and held at 4^{0}C until loaded into pipettes. All excess LV and contaminated surfaces were disinfected with 10% Chemgene.

4.2.2 Animals and brain surgery

All animal procedures were evaluated by the Animal Welfare and Ethical Review Board of the University of Warwick and carried out in strict accordance with the Animals (1986) Scientific Procedures Act of the UK under the authority of PIL JVW1, PPL 80/2555 and PC07DE9A3.

Male and female floxed Cx26 mice (Cohen-Salmon et al. 2002) (acquired from European Mouse Mutant Archive) between the ages of 12-18 weeks were used. As these mice were not cross bred, this genotype had no effect on Cx26 expression and should be considered wild type. This strain was chosen to remain consistent with Cx26-KO studies that were performed in the department (Nicholas Dale and Georgy Koentges, unpublished).

For LV injections, anaesthesia was induced in a gas chamber by isoflurane (4%), before being placed on a heating pad and fastened into a stereotaxic frame, with

facemask, where body temperature was maintained at 37^0C (feedback via a rectal probe) and anaesthesia was maintained by isoflurane (intranasal, 0.5-2.5%). Analgesia was provided in the form of Metacam (Meloxicam; sub-cutaneous, 2 mg/kg) at the point of securing the animal in the stereotaxic frame in order to minimise the time between the animal regaining consciousness and the therapeutic dose of Metacam being reached in the blood (~6 hours). At the same time atropine was administered (sub-cutaneous, 0.05 mg/kg) in order to counteract the effects of plural effusion caused by isoflurane. Eye ointment lubrication (Lacri-Lube) was applied directly after this pre-surgical medication to ease irritation that would arise due to the drying out of eyes and exposure to bright surgical lights during the procedure. To provide immediate analgesia, Subutex (Buprenorphine) was administered post-operatively (intraperitoneal, 0.05 mg/kg). When appropriate, additional analgesia was administered on days following surgery.

Attempts to approach the medulla, through the Dura and Arachnoid matter just beneath the Occipital bone resulted in severe brain herniation. Instead, the head was levelled and a craniotomy of the interparietal plate was performed to make two holes for bilateral injections. In this way, the pipette track for virus injections went down through the cerebellum and into the medulla (**Figure 4.3a**). To achieve as ventral expression as possible, the pipette was lowered until head or pipette movement indicated touching of the pipette at the ventral surface of the skull. At this point the pipette was retracted 0.100 mm and pressure was applied to inject the virus. If a small amount of pressure could not expel virus, the pipette was retracted in 0.050 increments (up to 0.200), testing virus injection each time. Virus injections were performed manually, using a 1 mL syringe, at a rate ~200 nL/min, and a total of 350-400 nL of undiluted virus was injected per side of the brain. Co-ordinates used in batch 1 were: 5.900 mm rostrocaudal, 1.100 mm mediolateral, and 5.300-5.900 mm dorsoventral. Co-ordinates used in batch 2 were: 5.750 and 6.050 mm rostrocaudal (two injections per side of the brain), 1.050 mm mediolateral, and 5.300-5.900 mm dorsoventral. Injections were made at a 9^0 angle. Co-ordinates were initially confirmed with fluorosphere injections.

4.2.3 Immunohistochemistry

Mice were culled by overdose of Isoflurane or intraperitoneal injection of Sodium Pentobarbital (>100 mg/kg), and transcardially perfused with paraformaldehyde (PFA; 4%). The brain was harvested and post-fixed in 4% PFA for 24hrs at 4^0C (to increase

a

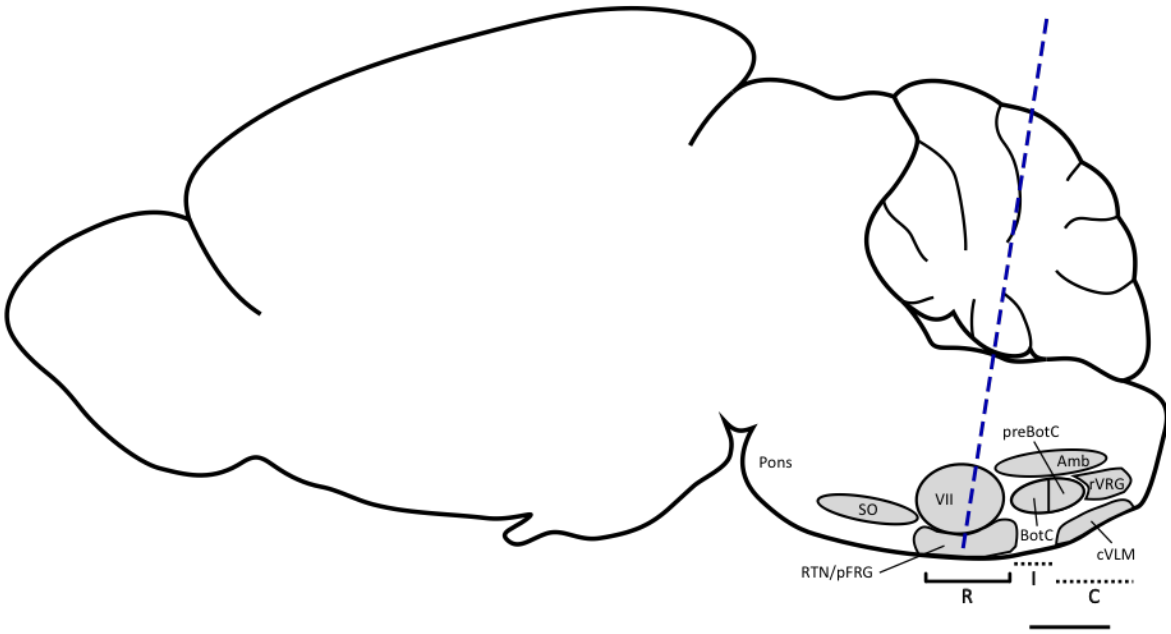
Pons
preBotC
Amb
rVRG
VII
SO
BotC
cVLM
RTN/pFRG
R
I
C

b

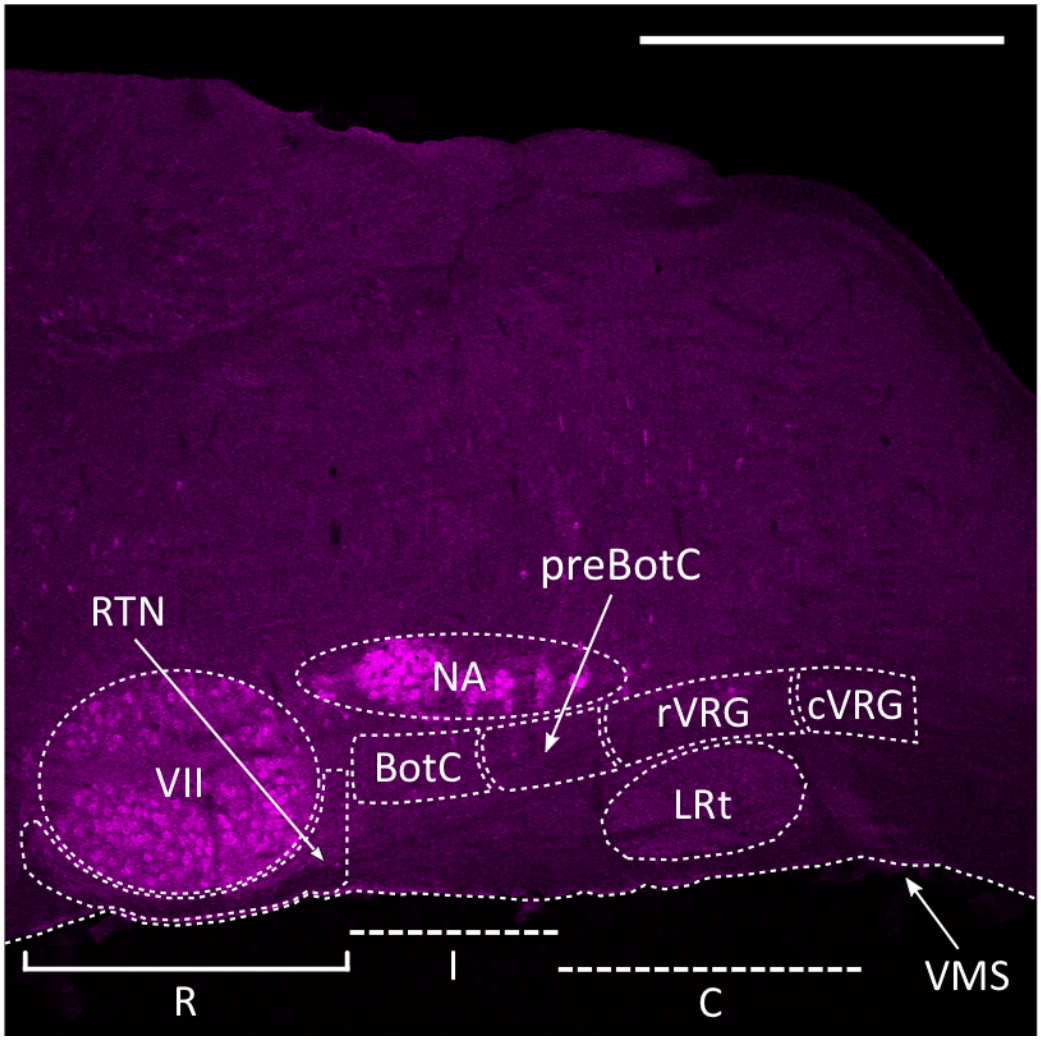
preBotC
RTN
NA
rVRG
cVRG
VII
BotC
LRt
VMS
R
I
C

Figure 4.3 **Virus injection target location**. **a)** Sagittal section of the mouse brain, showing pipette tract based on the coordinates 5.900 rostrocaudal, 1.100 mediolateral, with a 9^0 angle (blue dashed line). (image modified from Allen Brain Atlas Data Portal – http://atlas.brain-map.org/ - accessed on 12.08.2018). **b)** Mouse sagittal medullary section showing choline acetyltransferase immunostaining (magenta), with overlays showing key histological landmarks, and positioning of the ventrolateral respiratory column. In the diagrams up is dorsal, down in ventral, left is rostral, and right is caudal. R, rostral chemosensitive site; I, Intermediate chemosensitive site; C, caudal chemosensitive site; NA, nucleus ambiguous; VII, facial nucleus; preBot, pre-Bötzinger Complex; Bot, Bötzinger Complex; rVRG, rostral ventral respiratory group; RTN, retrotrapezoid nucleus; cVLM, caudal ventrolateral medulla; SO, superior olive; VMS, ventral medullary surface. Scale bars: 1 mm.

tissue fixing), before being transferred to 30% sucrose (for cryoprotection) until the brain sunk to the bottom of the sucrose – usually ~2-3 days. PFA and sucrose were made in PBS.

For sectioning, brainstems isolated, mounted with Tissue-Tek optimum cutting temperature compound (Sakura Finetek), and cut sagittally at 40 µm on a cryostat (Bright Instruments). Sections were arranged in order, in 24-well plates, and stored in PBS. For immunostaining, free-floating sections were incubated overnight in PBS containing 0.1% Triton X-100 (Sigma-Aldrich, UK) (0.1% PBS-T) and the appropriate primary antibodies from: goat anti-Choline Acetyltransferase (ChAT) (1:100) (Merck UK, ab144), chicken anti-GFP (1:500) (abcam, ab4674), rabbit anti-glial fibrillary acidic protein (GFAP) (1:500) (abcam, ab68428). Sections were then washed in PBS for 6 X 5 mins before incubation for 2.5-4 hrs in 0.1% PBS-T containing the appropriate secondary antibodies from: Donkey anti-goat Alexa Fluor 594 (1:250) (abcam, ab150132), goat anti-rabbit Alexa Fluor 594 (1:250) (abcam, ab150080), goat anti-chicken Alexa Fluor 488 (1:250) (abcam, ab150169). Immunohistochemistry experiments and set up were such that there was never a mix of antibodies that would result in undesired cross-reactivity. After secondary antibody incubation, sections were washed again in PBS for 6 X 5 mins before mounting onto polylysine-coated slides (Polysine, VWR). Mounted slices were left to dehydrate overnight before applying coverslips using either Aqua-Poly/Mount (Polysciences Inc., Germany) or Fluoroshield with DAPI (Sigma-Aldrich, UK). All steps were performed at 21^0C and during any period of incubation or washing sections were gently agitated on a shaker.

4.2.4 Immunohistochemistry imaging and virus expression scoring

Virus expression and immunostaining were imaged using a Zeiss-710 confocal laser microscope, and FIJI software was used for further analysis.

To gauge the expression level and location of LV constructs, the coverage of cell transduction (defined by un-amplified Clover expression) at either the rostral or caudal chemosensitive sites was inspected via confocal microscopy. A semi-quantitative score between 0-2 was given for each side of the brain, and scores were then pooled to give a mouse a score between 0-4. Scoring was as follows: 0, no expression; 1, visible expression (~1-50 cells); 2, high expression (>50 cells). The rostral chemosensitive region was considered to be the RTN, which was defined as the region ventral to the 7th nucleus (7N), plus regions that extend a little further rostral and caudal than the 7N. The caudal chemosensitive region is less well defined but was considered to be within 300 µm of the ventral surface, and span from the last quarter of the nucleus ambiguous, to the beginning of the caudal ventral respiratory group (cVRG). These definitions can be seen visually in **Figure 4.3b**. The mediolateral catchment area chosen for inclusion for expression scoring was any expression under the 7N (as defined by ChAT staining), plus an extra ~200 µm medial of the 7N.

4.2.5 Whole-body plethysmography

Hypercapnia-induced breathing responses in conscious mice were measured using whole-body plethysmography, as in previous studies (Trapp et al. 2008, Onodera et al. 1997). This involved placing animals in a plethysmograph (pressurised chamber) with an attached pressure transducer to measure the breathing of the mouse, and gas inlets and outlets to permit gas flow into and out of the chamber. Animal respiratory movements are detectable in this way as inhalation and exhalation consist of a minor delay between body cavity expansion/deflation and the flow of air into/out of the lungs (respectively). This delay occurs because airflow through the respiratory tract must overcome airway resistance, thus providing periods during which the chamber exhibits greater internal pressure (i.e. during inhalation when body cavity expansion reduces chamber volume) or reduced internal pressure (i.e. during exhalation when body cavity deflation increases chamber volume). The respiratory response to inspired CO_2 has been shown to match the response to intravenous CO_2 loads (Lamb 1966). Therefore, by altering the CO_2

composition of the gas passed into the chamber, this set up is capable of measuring the HCVR exhibited by subject animals.

A mixture of N2 (80%), O2 (~20%), and CO2 (0-9%) was passed through the chamber at a rate of 1 L/min; which was determined by a 1 L/min flow meter attached to the outlet and adjusted via a bleed valve situated before gas entered the chamber. Prior to its entry into the chamber, the gas was heated via a water bath, and its O2/CO2 composition was measured by a gas analyser (Hitech Instruments, GIR250 Dual Sensor Gas analyser). Every recording was calibrated, using a 1 mL syringe to injected 0.1, 0.2, and 0.5 mL volumes of air via a port for calibration. The pressure transducer output was amplified and recorded to a hard disk via a CED micro1401 interface and the Spike2 software (Cambridge Electronic Design, UK).

There were a couple of differences between the apparatus set up used to record breathing from animals in batch 1, and that used to record breathing from animals in batch 2. These are highlighted below.

<u>Batch 1 apparatus set up:</u>

The plethysmograph was constructed from an 850 mL plastic food storage container with a tight-fitting lid (Lock and Lock), which was filled to result in a chamber of volume ~500 mL (to providing better signal-to-noise) and covered in red plastic (to help the animal feel less exposed). The plethysmograph was placed on a heating mat, and gas was heated via a water bath before passing through the chamber. Because the chamber was filled from the bottom up (to reduce the volume) it was found that there was poor conductance of heat from the mat to the area of the chamber the animal was situated. As such, the chamber could not be heated much above 24^0C and animals remained very active in 0% CO_2 conditions. This made it difficult to acquire good traces of eupneic breathing. For the batch 1 setup the gas analyser was positioned immediately after $N_2/O_2/CO_2$ mixing and was responsible for pumping air into the chamber. Also, the pressure transducer output was hardware filtered, after amplification, in order to remove high and low frequency bands that marred the breathing waveform. Calibrations were performed after the animal was removed from the plethysmograph.

<u>Batch 2 apparatus set up:</u>

A new plethysmograph was made from an 850 mL plastic food storage container with a tight-fitting lid (Lock and Lock) but was cut down to a final volume ~400 ml and designed

to have very little distance between the surface that the animal sits on and heating mat. The chamber was covered in red plastic (to help the animal feel less exposed). With this new chamber, the temperature could be kept ~29^{0}C – the thermoneutral zone for mice (Speakman and Keijer 2013) – and animal activity notably decreased. Furthermore, for this batch of animals the gas analyser was set up to sample the gas before it entered the chamber, which prevented the need for any hardware filtering (i.e. the signal input to Spike2 was only amplified, but not filtered). Calibrations were performed whilst the animal was within the plethysmograph. The plethysmography chamber and set up (from batch 2) can be seen in **Figure 4.4**.

4.2.6 Plethysmography data capture and analysis

For plethysmography experiments, a mouse was placed in the plethysmograph at 0% CO_2 and allowed at least 20 minutes to acclimatise and settle. After adequate periods of eupneic breathing were acquired, animals were exposed to 3%, 6%, and 9% CO_2 successively for 5 minutes. A typical plethysmography trace can be seen in **Figure 4.5**.

Using the Spike2 software, plethysmography recordings were analysed by producing a cycle-by-cycle average for each breathing cycle from the recorded plethysmography trace/waveform (waveform averaging). For each condition (0%, 3%, 6%, and 9% CO_2), this required the selection of periods from the plethysmography trace during which the mouse was assessed to be quiescent and exhibiting eupneic breathing (as opposed to exploratory sniffing). To minimise any confounding effects from the fear response (that occurs with increasing CO_2), such periods were only selected from time points within 3-5 mins after onset of the condition (**Figure 4.5**). This selection window has been used in similar plethysmography studies (Davis et al. 2006). Waveform averaging yielded a measure for tidal volume and respiratory rate (mean time between waveform peaks). Tidal volume was calibrated and normalised to body weight.

All statistical analysis was performed in SPSS. For tidal volume and frequency, three-way mixed ANOVAs (which included repeated measures) were carried out, separately, with within-subject variables; week post-transduction and CO_2 level, and the between-subject variable; virus (as animals were either injected with the $Cx26^{WT}$ or the $Cx26^{DN}$ LV). For tidal volume at 6% (weeks 0-4) and week 3 (0%, 3%, 6%, and 9% CO_2) two-way mixed ANOVAs (which included repeated measures) were carried out, separately, with within-subject variables; week post-transduction *or* CO_2 level, and the

between-subject variable; virus. For tidal volume at week 3; 6%, a one-way ANOVA was carried out to compare the mean tidal volume across groups expressing the $Cx26^{WT}$ LV, $Cx26^{DN}$ LV, or no expression, at a particular chemosensitive site.

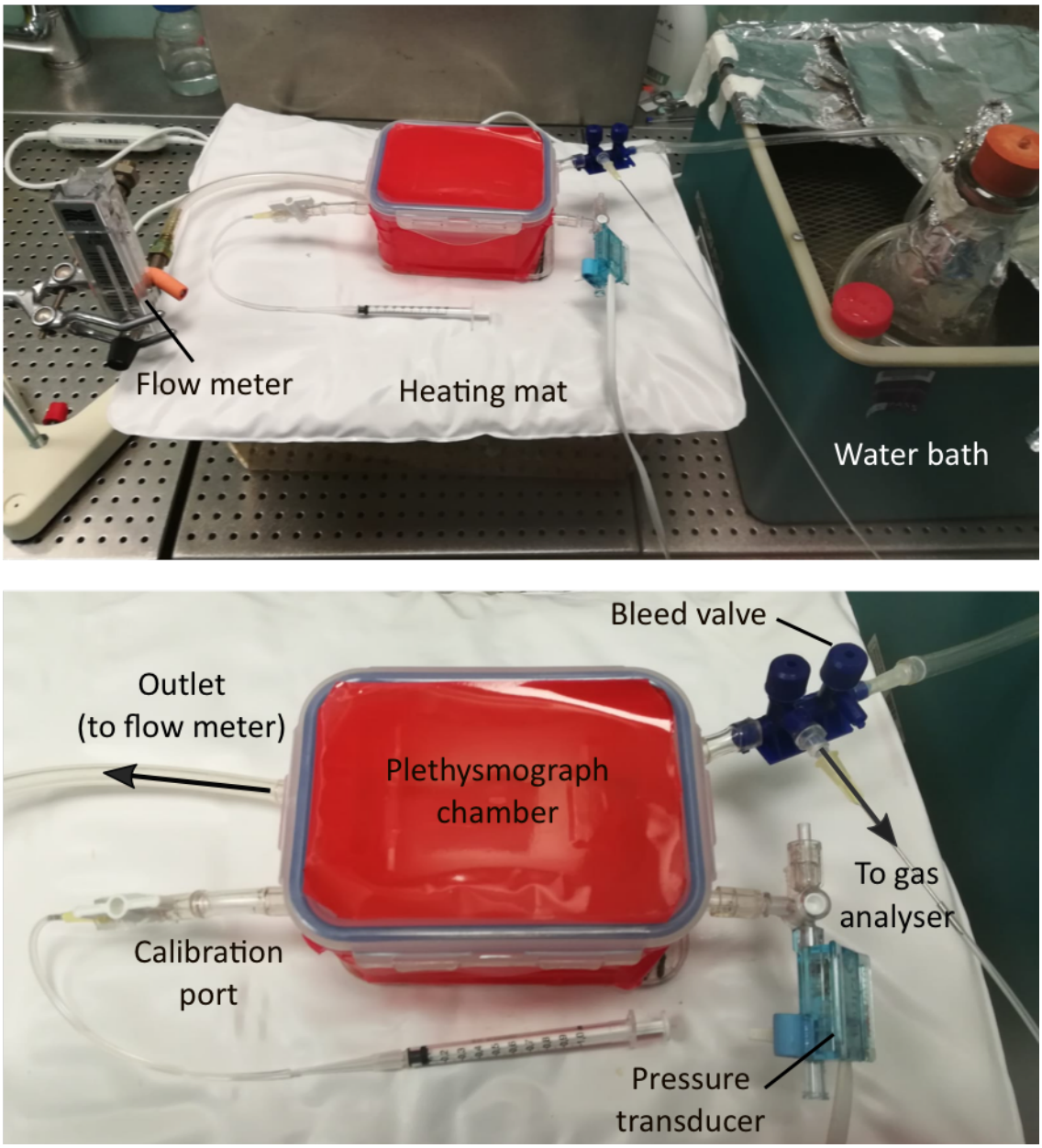

Figure 4.4 **Plethysmography apparatus and setup.** Plethysmographs were constructed from food storage containers, covered in red plastic (with one side transparent), and consisted of 4 ports for; i) gas inlet, ii) gas outlet, iii) pressure transduce, and iv) calibration syringe. The chamber shown in this figure is that used for batch 2 animals. Chambers were placed on a heating mat and gas was heated by passing tubing through a water bath before entering the chamber. The composition of CO_2 and O_2 was sampled and measured before entry to the chamber. By adjusting a bleed valve pre-entry, the flow rate of gas through the chamber was 1 L/min (measured by a fully open flow meter attached to the outlet port).

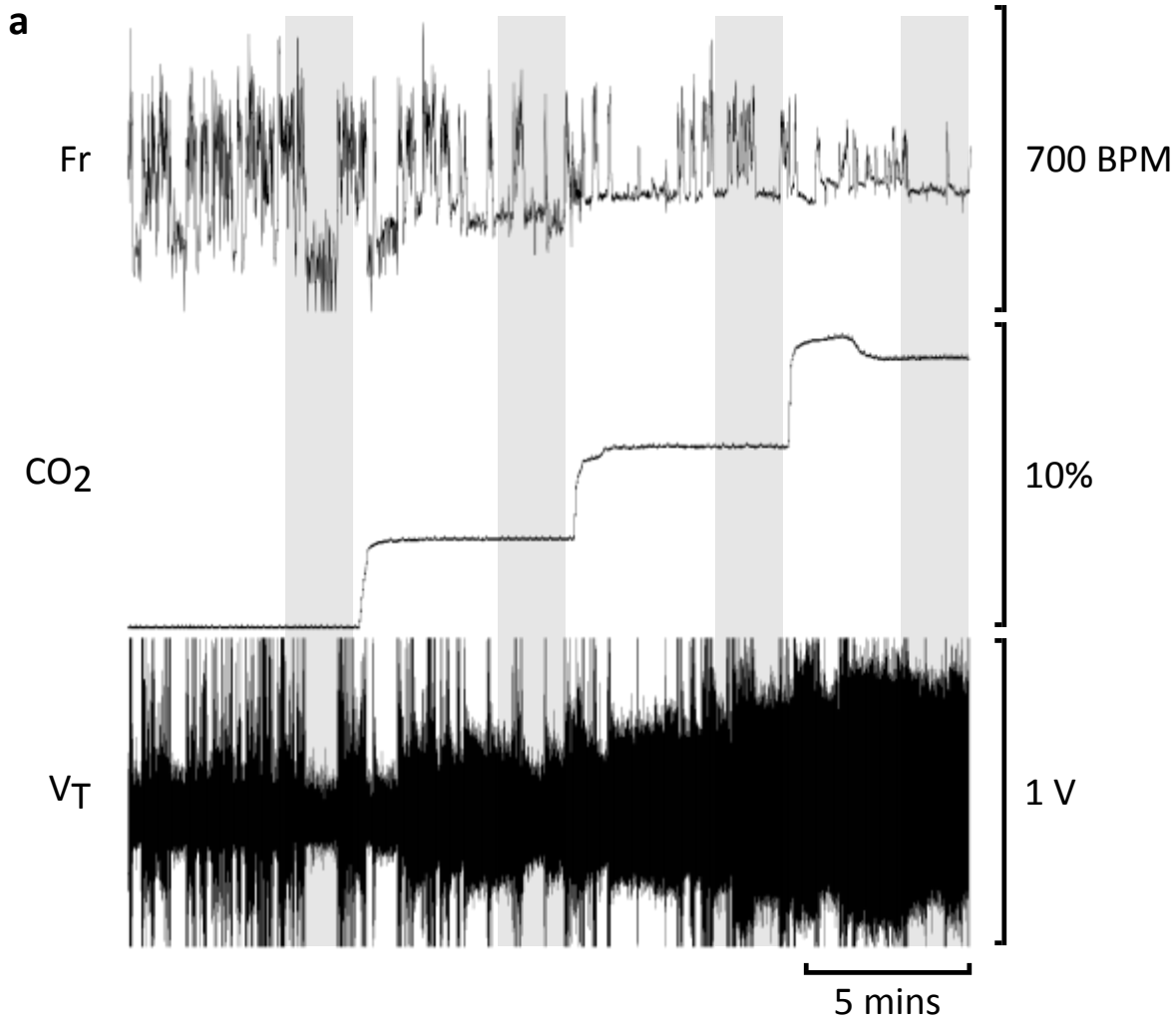
a
Fr
700 BPM
CO_2
10%
V_T
1 V
5 mins

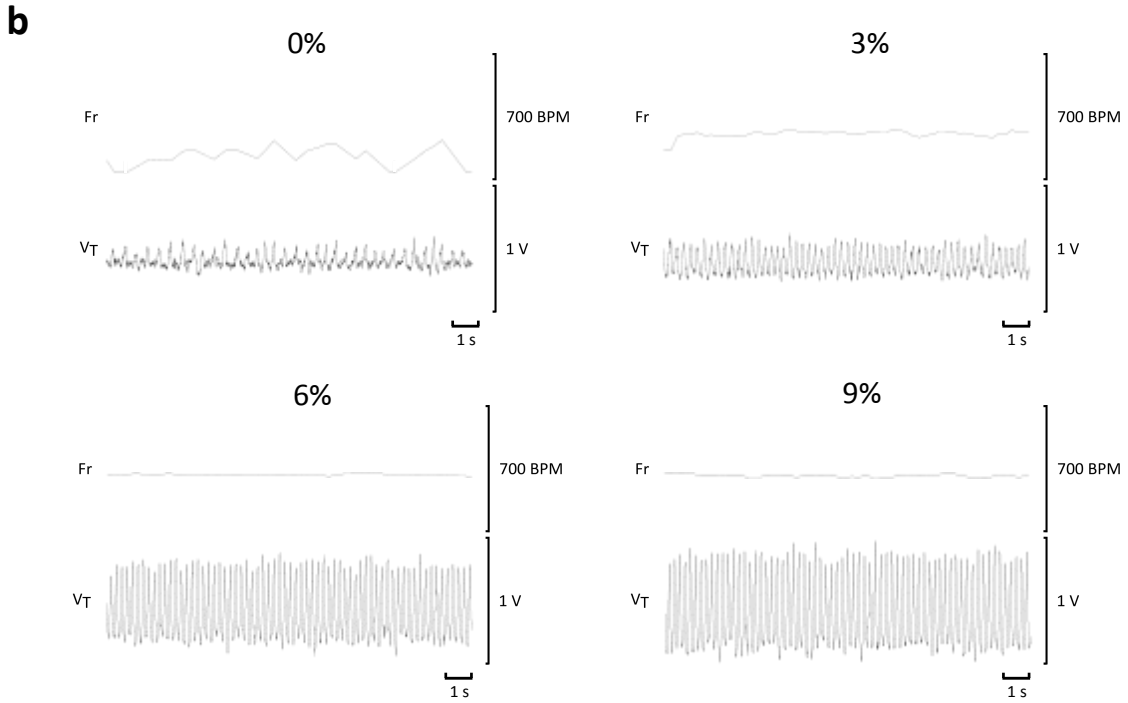
b
0%
3%
6%
9%
Fr
V_T
700 BPM
1 V
1 s

Figure 4.5 **Representative whole-body plethysmography trace from conscious wild-type mice showing typical breathing changes in response to hypercapnia**. Breathing frequency (Fr), CO_2 concentration (CO_2), and tidal volume (V_T) are plotted against a shared time axis. **a)** Experimental trace, taken before virus transduction, showing the end of the acclimatisation period at 0% CO_2, and the subsequent response to 3%, 6%, and then 9% CO_2. The plethysmograph was heated on a heating mat, keeping the chamber ~29^{0}C. Animals often experience a mild shock response from the change in environmental pCO_2, sometimes taking a couple of minutes of exposure in order to produce a steady trace when quiescent. Furthermore, as recordings were performed on unrestrained, unanaesthetised, animals much of a trace contains noise from movement, as well as exploratory-related breathing characteristics – such as sniffing. For these reasons, analysis was only preformed within the last two minutes of a given condition (grey bars), and only on sections, within the two minutes, during which the animal was quiescent, thus providing a steady and reproducible trace. **b)** Magnified traces from grey bars in (**a**), demonstrating quiescent breathing (and accompanying frequency) at 0%, 3%, 6% and 9% CO_2. V_T and Fr can be seen to increase (increased amplitude and frequency, respectively) as CO_2 concentration increases – with the most drastic changes seen between 0-3% and 3-6%. Some parts of the traces corresponding to very high noise due to animal movement were clipped in order to provide a better visual representation of the parts of the trace that were analysed.

4.2.7 Power calculation

To determine the number of animals (measurements) required to statistically discern if there is a difference in tidal volume between groups at 6% CO_2, a power calculation was performed in G*Power 3.1 (Faul et al. 2007, Faul et al. 2009). The calculation was based on the F-test "ANOVA: Repeated measures, within-between interaction", selecting "effect size specification as in SPSS" from the option window. Greenhouse-Geisser nonsphericity correction (ε) and partial eta squared values, calculated from the pilot study in the statistical package SPSS, were used for the power calculation. Other input parameters were set at 0.05 α-error probability, 0.8 power, and 3 groups ($Cx26^{WT}$, $Cx26^{DN}$, and sham injection).

4.3 Results

The data presented in this chapter chronologically documents the process and progression of viral injections, data analysis, and immunohistochemistry for two batches of animals. Data from the first batch is examined and discussed in its entirety before being re-evaluated in light of the immunohistochemistry; including an in-depth examination of the results at the most logical time point. The second batch is then

analysed in analogous manner (however there was no need for re-evaluation). Because such analysis does not fully conform to the structure and layout of previous chapters, this section (*4.3 Results*) comprises of results alongside less conventional discussion and is then succeeded by a more typical discussion section (*4.4 Discussion*).

Although KO of Cx26 in GFAP-expressing cells produces a reduction in tidal volume (personal communication from Nicholas Dale and Georgy Koentges), this KO occurred from birth and completely removed Cx26 expression in either all GFAP expressing cells, or almost all NCCs. Therefore, although informative, the Cx26-KO data was not appropriate for determining the study design of the $Cx26^{DN}$ Lentivirus (LV) experiments that are presented in this chapter. Instead, data in this chapter can be considered a pilot study for investigating the importance of Cx26 CO_2 sensitivity using this $Cx26^{DN}$ LV method.

4.3.1 Design and expression of lentivirus constructs

LV allows construct inserts of 2.5-5.0 kb and integrates into genomic DNA, allowing for prolonged construct expression that remains stable over at least two months *in vivo* (Osten, Dittgen, and Licznerski 2006, Feeley et al. 2006, Sugiyama et al. 2005). This contrasts Adenovirus, which can see a complete loss of expression by 4 weeks post transduction (Feeley et al. 2006), and Adeno-associated virus (AAV), which only has an insert capacity of 2.5 kb. Due to our construct lengths and planned time course experiments, LV was chosen over Adenovirus or AAV vectors.

In order to investigate the role of Cx26 CO_2 sensitivity *in vivo* LV constructs were designed to contain the $Cx26^{DN}$ gene, immediately followed by a downstream IRES:Clover sequence, all under control of the GFAP promoter (see *4.2.1 Lentivirus design and handling*), **Figure 4.2a**. In this way, targeted injections restrict the population of cells that are transduced, and the GFAP promoter ensures that the construct is only expressed in $GFAP^+$ cells. Owing to the downstream IRES:Clover sequence, visualisation of viral Cx26 expression was confirmed by soluble Clover fluorescence, and expression in $GFAP^+$ cells was confirmed by colocalisation with GFAP immunostaining. GFAP colocalisation and morphological examination showed Clover expression to be restricted to glia, with all cells expressing Clover also expressing GFAP (**Figure 4.2c**). The expression of the GFAP (an intermediate filament) is not necessarily ubiquitous in cells; therefore, it can be

expected that some regions of cells expressing soluble Clover will show no co-localisation with GFAP.

To control for the overexpression of Cx26, a second LV construct was designed to insert and express the $Cx26^{WT}$ gene in place of $Cx26^{DN}$ gene. As experiments involving $Cx26^{DN}$ and $Cx26^{WT}$ constructs were blinded, with identical experimental parameters, any breathing phenotype observed will be a result of the difference between $Cx26^{DN}$ and $Cx26^{WT}$ proteins. As the only difference between these two variants is the K125R and R104 mutations, any such phenotype can be concluded to be a consequence of altered CO_2 sensitivity.

4.3.2 Initial analysis of batch 1 animals showed no breathing phenotype

Mice aged 12-18 weeks were bilaterally injected with one of two LV constructs to introduce either the $Cx26^{DN}$ (n = 9) or $Cx26^{WT}$ (n = 9) gene into glia at the VMS. Injection co-ordinates aiming for the retrotrapezoid nucleus (RTN) were chosen and confirmed to match those areas studied in comparable respiratory studies and shown to be important in various respiratory responses (Guyenet et al. 2016, Huckstepp et al. 2015, Abbott et al. 2009). This area roughly corresponds to the medial half of the RTN, however the extent of virus spread seen in these experiments would cover the lateral part of the RTN as well.

Whole-body plethysmography was used to measure breathing frequency, tidal volume (V_T), and minute ventilation (V_E) at weeks 0-4 post-transduction (**Figure 4.6**). A visual examination of frequency (**Figure 4.6, middle panels**) shows high variation in the measurements, but no visible difference between mice injected with the $Cx26^{WT}$ or $Cx26^{DN}$ construct at any time point or CO_2 level. A Three-way mixed ANOVA (3WXA) calculated no statistical difference in frequency between virus groups at any CO_2 level, at any week.

A visual examination of tidal volume (V_T) data (**Figure 4.6, left panels**) shows higher variation at higher CO_2 levels, and a very subtle difference between WT and DN groups at week 3, 6% CO_2. Given that LV takes around a week to reach substantial levels of expression (Osten, Dittgen, and Licznerski 2006, Feeley et al. 2006) and that $Cx26^{DN}$ takes 6 days to take effect *in vitro* (**Figure 3.9**), we anticipated that an *in vivo* effect would take somewhere between 2-3 weeks, which would be consistent with this visual interpretation. However, 3WXA calculated no statistical difference, implying that any

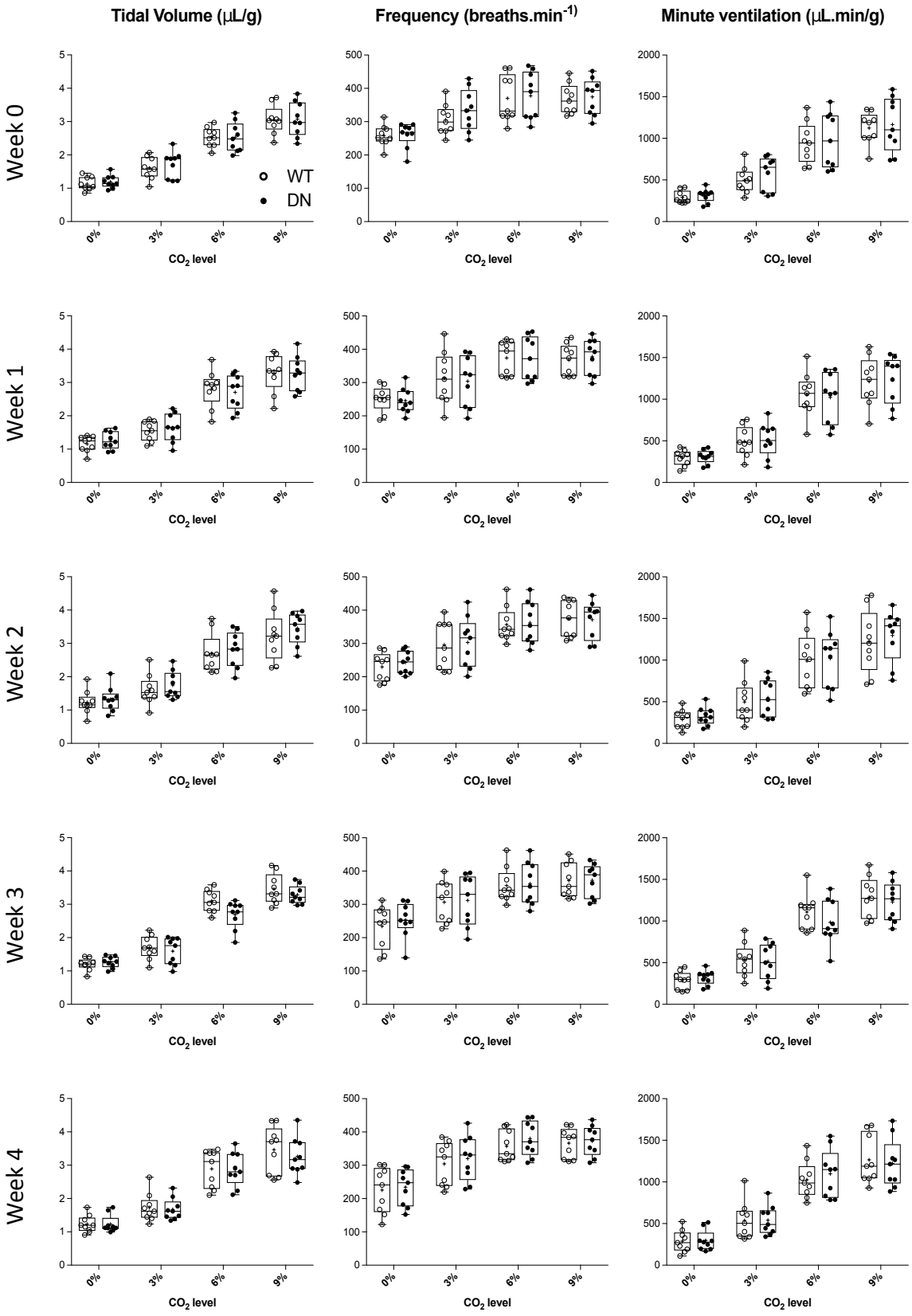

Figure 4.6 **Batch 1: Connexin26-mediated hypercapnic breathing response in conscious mice**. Mice aged 12-18 weeks were bi-laterally injected at the ventral medullary surface (VMS) to introduce either the Dominant Negative Connexin26 ($Cx26^{DN}$) or wild type Connexin26 ($Cx26^{WT}$) gene into genomic DNA. Whole-body plethysmography measurements of tidal volume (left), frequency (middle), and minute ventilation (right) were recorded for each mouse before

acetyltransferase immunostaining (magenta), with overlays showing key histological landmarks, and positioning of the ventrolateral respiratory column. **b-d)** Representative slices showing the locations of virus expression (Clover, green) within batch 1 animals. Due to decalibration of equipment, within batch 1 there were only some animals that had expression in the RTN (**b**), with the majority showing expression much more caudally - more caudal than the nucleus ambiguous (**c, d**). Bottom panels show magnification of the dashed rectangular overlays in the top panels. In the diagrams up is dorsal, down in ventral, left is rostral, and right is caudal. R, rostral chemosensitive site; I, Intermediate chemosensitive site; C, caudal chemosensitive site; NA, nucleus ambiguous; VII, facial nucleus; preBot, pre-Bötzinger Complex; Bot, Bötzinger Complex; rVRG, rostral ventral respiratory group; RTN, retrotrapezoid nucleus; VMS, ventral medullary surface. Scale bars: (**a**); 1mm, (**b-d** top panels); 1mm, (**b-d** bottom panels); 200µm (**b**), 100µm (**c**), 200µm (**d**).

In light of this expression-based subdivision in batch 1, animal data was reanalysed only including animals showing expression within the caudal chemosensitive area. Reanalysis of animals with expression in the RTN was not carried out due to insufficient numbers.

4.3.4 Batch 1 animals with expression at the caudal chemosensitive region show a blunted tidal volume response to 6% hypercapnia

Upon reanalysis of batch 1 frequency and tidal volume, including only those animals with expression in the caudal chemosensitive area, there was again no visual or statistical (3WXA) difference in frequency between WT and DN groups (**Figure 4.8, middle panels**). This suggests that expression of $Cx26^{DN}$ had no effect on adaptive changes in breathing frequency.

Interestingly, when comparing tidal volume (**Figure 4.8, left panels**) the subtle difference that was seen between WT and DN groups at week 3, 6% CO_2 (**Figure 4.6, week 3 left panel**), becomes more apparent when only animals with caudal expression are compared (**Figure 4.8, week 3 left panel**). Nevertheless, 3WXA still found no statistical difference in tidal volume between WT and DN groups.

Given that any effect resulting from LV-introduction of $Cx26^{DN}$ was anticipated to take between 2-3 weeks to manifest, and the recent data suggesting Cx26 expression in caudal $GFAP^{+}$ cells control adaptive changes in tidal volume, it seems too coincidental that this difference at week 3, 6% CO_2, gets more pronounced upon selecting for caudal expression. As such, despite the lack of statistical support from the 3WXA, this difference at week 3, 6% CO_2, was investigated further (**Figure 4.9**).

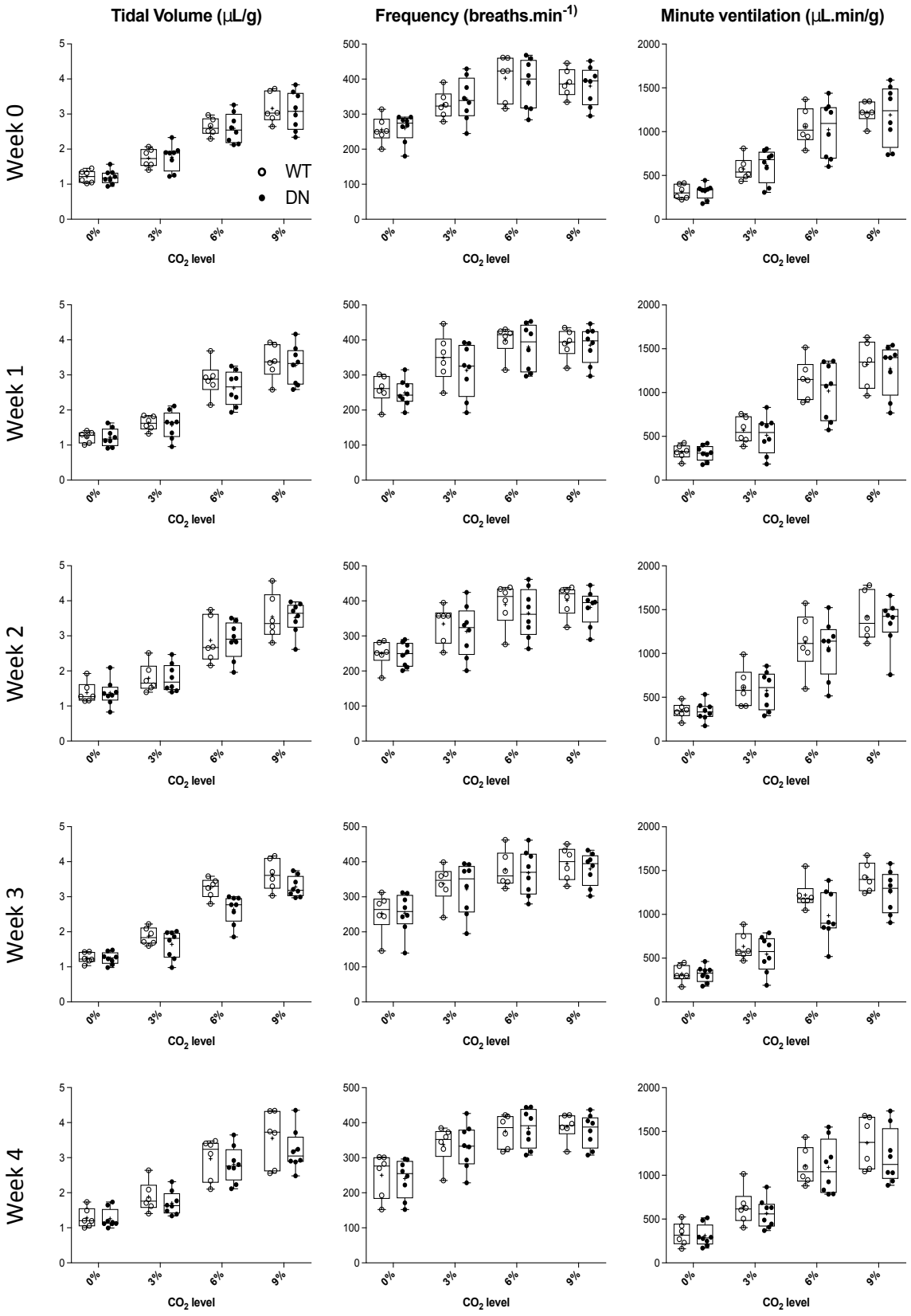

Figure 4.8 **Batch 1 caudal virus expression only: Connexin26-mediated hypercapnic breathing response in conscious mice**. This data ONLY INCLUDES mice from Batch 1 that were found to have expression at the caudal chemosensitive site of the ventral medullary surface, as opposed to those that only had expression more rostrally. Mice aged 12-18 weeks were bi-laterally injected at the ventral medullary surface (VMS) to introduce either the Dominant Negative

Connexin26 ($Cx26^{DN}$) or wild type Connexin26 ($Cx26^{WT}$) gene into genomic DNA. Whole-body plethysmography measurements of tidal volume (left), frequency (middle), and minute ventilation (right) were recorded for each mouse before transduction (week 0) and each week, for four weeks, post-transduction (weeks 1-4). At each time point, recordings were taken at 0%, 3%, 6%, and 9% CO_2. Data is plotted by week, grouping animals based on whether they are expressing $Cx26^{DN}$ (black circles, n = 8) or $Cx26^{WT}$ (empty circle, n = 6). At week 3 a difference in adaptive changes in tidal volume, between mice expressing $Cx26^{WT}$ and $Cx26^{DN}$, could be inferred - especially at 6% CO_2. A three-way mixed ANOVA was carried out separately for tidal volume, frequency, and minute ventilation in the statistical package SPSS, testing across the variables: week, CO_2 level, and the type of virus transduced with ($Cx26^{WT}$ or $Cx26^{DN}$), as well as the interactions between them. In all three tests, a significant difference was calculated only for CO_2 level – i.e statistical comparisons across the entire dataset did not support the visual indication of a tidal volume phenotype. Recordings were taken in the CED software Spike2, with tidal volume calculated as the difference between peak and trough values after waveform averaging (with respect to each breath), frequency calculated as the number of breaths per minute, and minute ventilation calculated as the product of the two. All recordings were calibrated using values obtained by puffing 0.1mL, 0.2mL, and 0.5mL volumes of air into the chamber (using a 1mL syringe). Boxes show the interquartile range. The median is indicated as a horizontal line within the box, and the mean is represented by a cross within the box. Range bars show minimum and maximum values.

When considering week 3 recordings as an isolated experiment (i.e. omitting repeated measurements from other weeks) a two-way mixed ANOVA (2WXA) does reveal a statistical difference ($p = 0.019$), with post-hoc testing calculating significant differences between WT and DN groups at both 6% (0.005, one-tailed) and 9% (0.049, one-tailed) CO_2. It is probable that no statistical significance is found when testing across all weeks in the 3WXA due to the high variation across weeks (**Figure 4.9b**) – WT, 2.9±0.5 µL/g; DN, 2.7±0.5 µL/g. High V_T variation has been observed in other plethysmography studies (Stunden et al. 2001, Davis et al. 2006).

In an attempt to deduce what caused the difference seen at week 3, 6% CO_2, the few animals with no expression in the caudal area (2.9±0.2 µL/g, n = 4) were compared to animals in the WT (3.3±0.5 µL/g, n = 6) and DN (2.6±0.5 µL/g, n = 8) groups that did show expression caudally (**Figure 4.9c**). There was no significant difference between animals with no caudal expression and either group, which raises the question of whether animals expressing $Cx26^{DN}$ caudally exhibited a reduced HCVR or whether animals expressing $Cx26^{WT}$ caudally exhibited a heightened HCVR.

By semi-quantitatively scoring expression at the caudal chemosensitive site, we may glean insight into the effect of each variant. Plotting relative virus expression scores

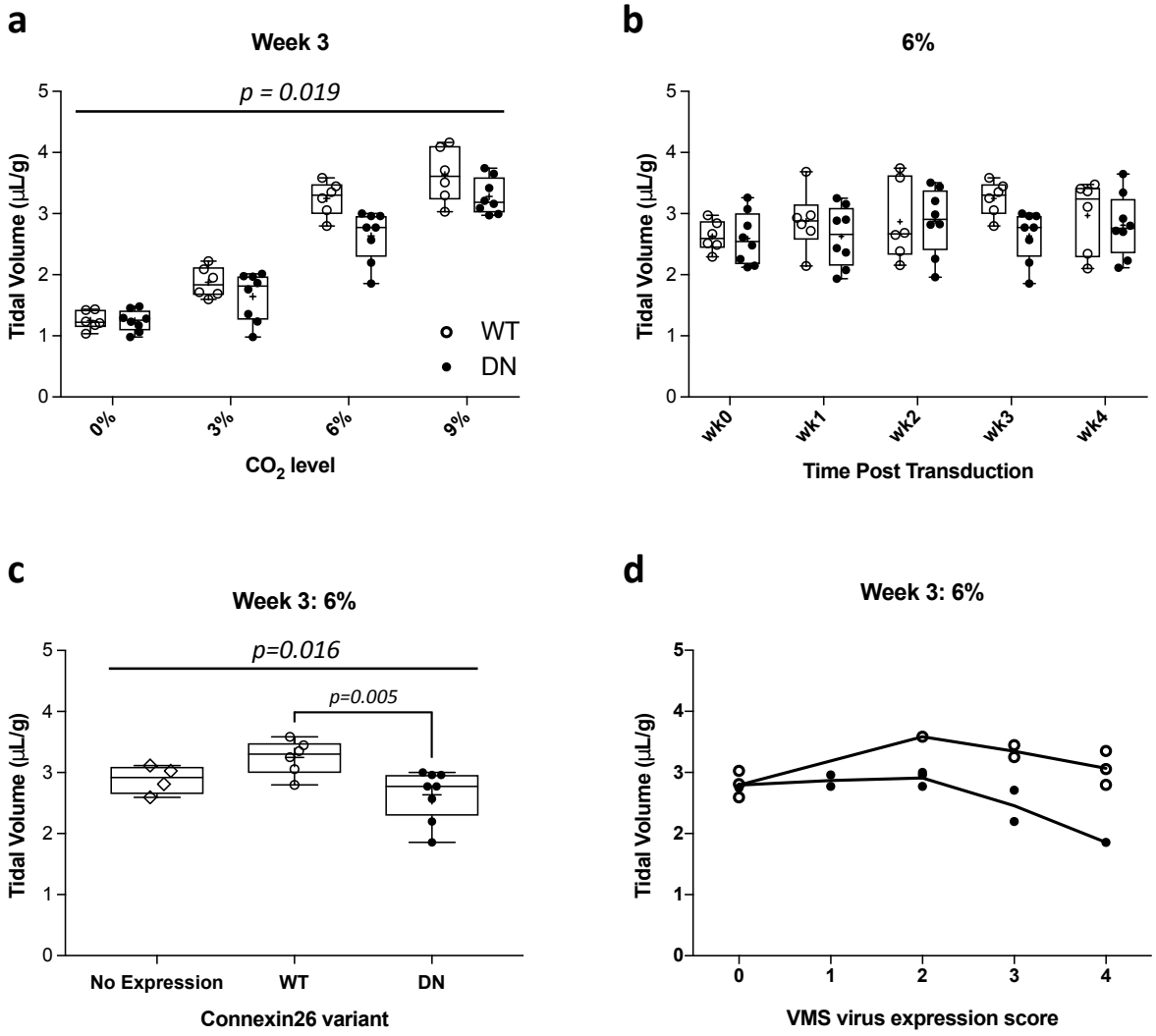

Figure 4.9 **Batch 1: possible tidal volume phenotype in response to 6% CO_2 at 3 weeks post-transduction**. This data compares tidal volume (V_T), from mice in batch 1, based on the scored virus expression at the caudal chemosensitive site of the ventral medullary surface (VMS). **a)** Whole-body plethysmography measurements of V_T in response to hypercapnic conditions, recorded at 3 weeks post-transduction. Taken as an isolated experiment (i.e. not including repeated measurements from weeks 0, 1, 2, or 4), a two-way mixed ANOVA reveals that a significant difference in V_T is evident for the interaction between virus expressed and CO_2 level ($p = 0.019$). Post hoc testing revealed a significant difference in V_T at 6% between animals expressing the $Cx26^{DN}$ virus construct in the caudal area (black circles, n = 8) and those animals expressing the $Cx26^{WT}$ virus construct in the caudal area (empty circle, n = 6). **b)** Change in V_T, at 6% CO_2, across weeks 0-4. Despite a difference at weeks 3, no significant interaction is calculated between virus expressed and week, presumably due to the high variation in V_T measurements that can be seen across the time course. **c)** V_T recorded at week 3, 6% CO_2. One-way ANOVA shows a significant difference in V_T depending on group, with post hoc tests revealing a difference between animals expressing $Cx26^{WT}$ and $Cx26^{DN}$ at the caudal chemosensitive region ($p = 0.005$, one-tailed). Mice with no expression in the caudal region are shown (empty triangles) as a comparison. **d)** V_T with respect to the level of expression in the caudal chemosensitive area of

the VMS. Using the Clover fluorescence as an indicator of viral-Cx26 expression, a semi-quantitative score was assigned to each animal based on the Clover expression (apparent under confocal microscopy) that was seen at the caudal chemosensitive site of the VMS. The difference between $Cx26^{WT}$ and $Cx26^{DN}$ groups increases with the level of virus expression. All statistical tests were carried out in the statistical package SPSS. Boxes show the interquartile range. The median is indicated as a horizontal line within the box, and the mean is represented by a cross within the box. Range bars show minimum and maximum values.

against V_T (**Figure 4.9d**) indicated that there is no correlation between V_T and the level of $Cx26^{WT}$ expression at the caudal site. However, there does appear to be a negative correlation between V_T and the level of $Cx26^{DN}$ expression at the caudal site. This indicates that increasing the number of glia expressing $Cx26^{DN}$ in the caudal area has a negative effect on adaptive changes in tidal volume.

Examination of these results suggests that expression of $Cx26^{DN}$ in glia within the caudal chemosensitive area might reduce adaptive changes in tidal volume at 3 weeks post-transduction. However, proper statistical analysis including all repeated measures across weeks 0-4 does not support any such difference. Furthermore, if a phenotype is observed 3 weeks post transduction, there is question as to why this phenotype cannot be perceived 4 weeks post transduction.

When comparing V_E of caudal-expressing batch 1 animals (**Figure 4.8, right panels**), the visual difference in V_T at week3, 6%, appears to be replicated in 5 of the 8 animals from the DN group, with the remaining three showing values similar to those from the WT group – perhaps as these 3 were able to compensate for lower V_T by increasing their breathing frequency. Other than at weeks 3, there is no visual or statistical difference between WT and DN at any timepoint or CO_2 level.

4.3.5 Batch 2 animals showed no breathing phenotype and accurate injection sites

LV injections into animals from batch 1 were inaccurate, due to faulty apparatus, and shed no light on the chemoreceptive role of Cx26 in RTN glia. Therefore, after fixing the apparatus and reconfirming injection coordinates (with fluorosphere beads), a second blinded study was carried out in the same manner as batch 1 (WT, n = 9; DN, n = 8). For the second batch some refinements were made to the plethysmography apparatus and recording (see *4.2.5 Whole-body plethysmography*). Also, two smaller LV injections were given per side of the brain (0.250 µm apart in the rostrocaudal axis) in an attempt for better virus coverage along the rostrocaudal axis of the RTN.

A visual examination of frequency data (**Figure 4.10, middle panels**) shows significantly lower variation than that seen in batch 1, and no visible difference between mice injected with the $Cx26^{WT}$ or $Cx26^{DN}$ construct at any time point or CO_2 level. A 3WXA calculated no statistical difference in frequency between virus groups at any CO_2 level, at any week. A visual examination of tidal volume (V_T) data (**Figure 4.10, left panels**) shows higher variation at higher CO_2 levels, but no visible difference between WT and DN groups. A 3WXA calculated no statistical significance for tidal volume between virus groups was found. Appropriately, V_E (**Figure 4.10, right panels**) also shows no visual or statistical difference between WT and DN at any timepoint or CO_2 level.

Unlike batch 1, the immunohistochemistry on batch 2 animals showed consistent virus expression in the RTN (**Figure 4.11**), thus there was no need for group sub-division or reanalysis. In light of this, data from batch 2 animals suggests that expression of $Cx26^{DN}$ in glia within the RTN has no affect on the HCVR exhibit by these animals, as there was no difference in either breathing frequency or tidal volume measurements between DN and control (WT) groups.

For comparison with data from batch 1 animals, a more detailed analysis of batch 2 tidal volume data was carried out at the conditions most expected to show a phenotype, i.e. week 3, 6% (**Figure 4.12**). No statistical difference was found when treating week 3 measurements as an isolated experiment (**Figure 4.12a**), despite removal of the high variation that was again seen across weeks 0-4 (**Figure 4.12b**). There was no difference between WT and DN groups even when considering only data from 6% CO_2 at week 3 (**Figure 4.12c**), and no correlation, for either virus group, between LV construct expression in the RTN and tidal volume.

4.3.6 Different $GFAP^+$ cell morphologies at the ventral medullary surface

For LV experiments in this chapter transcription was driven by a GFAP promoter and therefore a range of glial cells were transduced along the VMS. Although different glia morphologies have been reported throughout the brain (Matyash and Kettenmann 2010, Kettenmann and Verkhratsky 2016) there has been little characterisation specifically in the VMS – with the exception of some more dorsal astrocytes within the preBötzinger complex (Sheikhbahaei et al. 2018). In our LV-GFAP:$Cx26^{DN}$ we observed many different morphologies in the rostral and caudal chemosensitive areas, which suggests a range of $GFAP^+$ cell subtypes (**Figure 4.13** and **Figure 4.14**).

Figure 4.14 Glia morphologies in the caudal chemosensitive region of the ventral medullary surface. **a)** Histological landmarks shown by choline acetyltransferase immunostaining (magenta), identifying the rostrocaudal region (thick dashed rectangle) of cells shown in **b-f**. **b-f)** Maximum-intensity projections of glia at the ventral medullary surface (VMS) expressing Cx26-IRES:Clover**.** Some glia at the ventral surface (glia limitans) have their cell bodies pushed flat along the surface, again with processes extending dorsally (white arrows). This cell morphology closely matches that of a sub-population of neural-crest cells that have been shown to play a role in Connexin26-mediated CO_2 chemoreception. The yellow arrow in **d** points to a possible artery or vein bifurcation, as seen by the Y-shaped glial cell arrangement. In the diagrams up is dorsal, down in ventral, left is rostral, and right is caudal. Blue; DAPI, magenta; choline acetyltransferase immunostaining. Scale bars: (**a**), 1mm; (**b-f**), 50µm. In the sections shown in this figure, the leptomeninges have mostly fallen away leaving the glia limitans as the outermost layer.

4.4 Discussion

In this section the role that Cx26 plays in adaptive changes in breathing frequency and adaptive changes in tidal volume is considered in turn, at both the RTN and the caudal chemosensitive areas.

Also, in this section selected data from Cx26-KO studies performed by Xintao Zhang (which have been alluded to previously as "personal communication from Nicholas Dale and Georgy Koentges") is included (**Supplement figure 4.1** and **Supplement figure 4.2**) due to its importance in interpreting the results of this chapter.

4.4.1 The role that Connexin26 CO_2 sensitivity plays in adaptive changes in breathing frequency at the rostral chemosensitive site

Cx26 is not expressed in neurons along the VMS, however it is within the leptomeninges and in $GFAP^+$ cells of the glial limitans, including tracts of cells alongside penetrating blood vessels (Huckstepp et al. 2010a, Nagy et al. 2001, Solomon et al. 2001, Mercier and Hatton 2001), **Supplement figure 4.1b**. Recent analysis has calculated Cx26 expression to extend 87±10 µm into the rostral chemosensitive area (**Supplement figure 4.1b, top right panel**) and has shown that, despite its ubiquitous expression, specific removal of Cx26 from in the leptomeninges has no effect on breathing (personal communication from Nicholas Dale and Georgy Koentges). As brains from our experiments showed clear transduction in cells of the glial limitans (**Figure 4.7** and **Figure 4.11**) we have assumed that $Cx26^{DN}$ expression successfully removed CO_2-mediated Cx26 hemichannel opening, and the subsequent Cx26-mediated ATP release, from glia in these transduced areas. This

expectation is based on our *in vitro* dye loading results, which showed $Cx26^{DN}$ removes Cx26 opening under hypercapnic conditions *in vitro* (see *3 Characterisation of co-assembly and CO2-Insensitivity of a Connexin 26 dominant negative mutant*). It must be noted however that ATP release from transduced glia was not recorded, and therefore our interpretations should only be considered putative until more data is provided.

When LV-GFAP:Cx26 variants were expressed at the rostral chemosensitive site (RTN), there was no difference in breathing frequency between WT and DN groups during hypercapnia (at any CO_2 level, at any week) (**Figure 4.10**). This suggests that Cx26 CO_2 sensitivity plays no role in modulating breathing frequency at the rostral chemosensitive site – as its removal has no effect on adaptive changes in frequency. Indeed, given that peripheral chemoreceptors are responsible for a very large amount of frequency control (Berkenbosch et al. 1979), and that GPR4 appears to have filled the role for frequency control via central chemoreceptors (Kumar et al. 2015), such a result is perhaps unsurprising.

This result is consistent with our hypothesis that Cx26-mediated ATP release influences adaptive changes in tidal volume, working in parallel with mechanisms that influence the frequency side of the HCVR (such as those associated with GPR4). This result is also consistent with data from GFAP:Cx26-KO mice, which showed no difference in adaptive changes in breathing frequency between wild-type mice and mice with conditional deletion of Cx26 from $GFAP^+$ cells (**Supplement figure 4.1c**).

An alternative explanation as to why there was no change in breathing frequency, when $Cx26^{DN}$ is expressed, is that under hypercapnic conditions Cx26 hemichannels are opened by more than just CO_2 and therefore we see no phenotype as ATP is still released. However this is unlikely as other logical candidates for a hypercapnia-evoked Cx26 response (pH, HCO_3^-, $[Ca^{2+}]_i$) have been shown to have no effect on Cx26 hemichannel gating (Huckstepp et al. 2010b) (see *2 Gating determinants of Connexin26 hemichannels: intracellular calcium and CO2 sensitivity of a pathological mutation*).

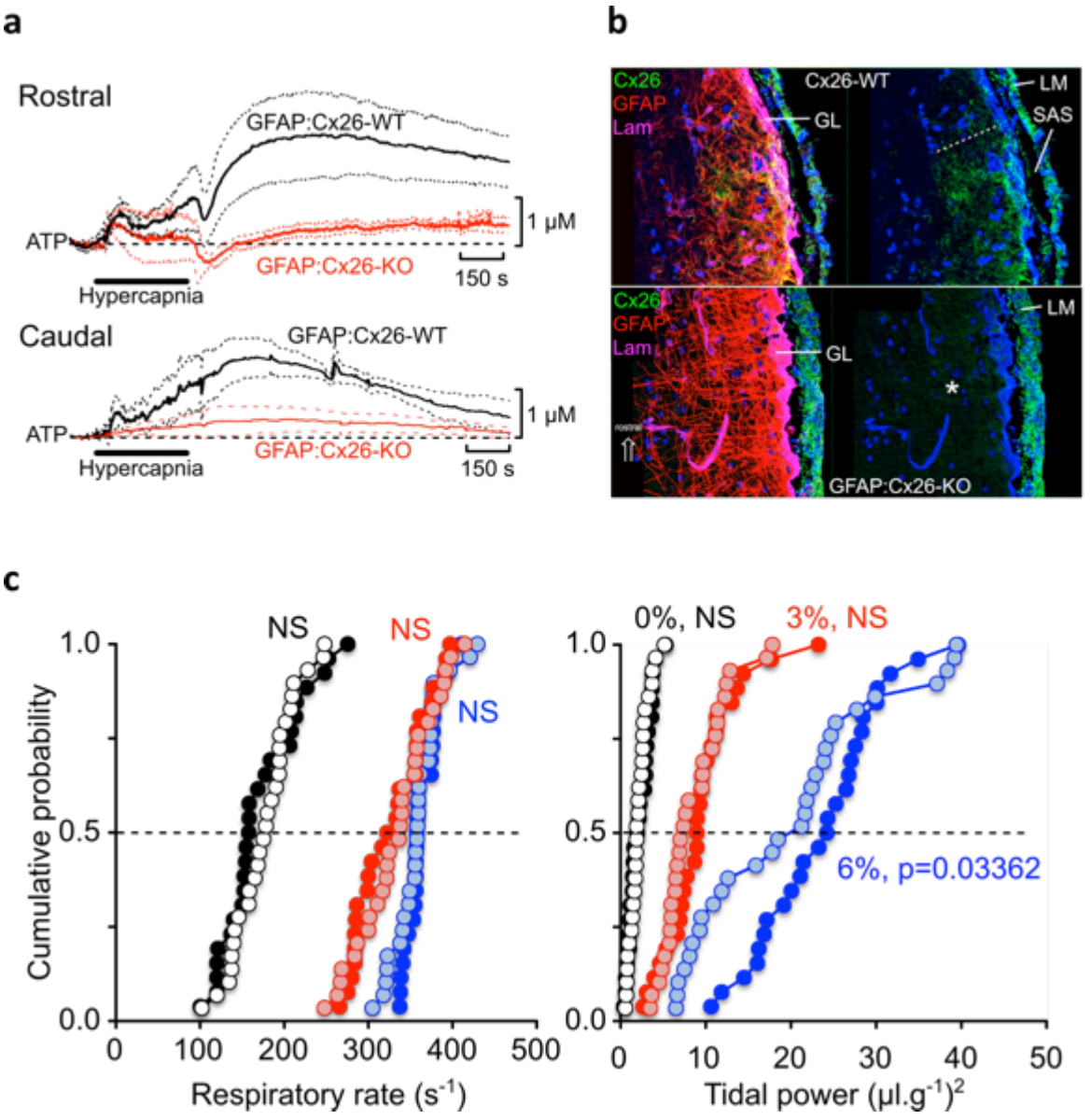

Supplement figure 4.1 **Connexin26 expression in GFAP$^+$ cells contributes to respiratory chemoreception**. **a)** Biosensor recordings of CO_2-evoked ATP release from horizontal slices of the ventral medullary surface (VMS), recorded from GFAP:Cx26-WT and GFAP:Cx26-KO mice. Deletion of Cx26 from GFAP$^+$ cells drastically reduces CO2-evoked ATP release from the rostral (top) and caudal (bottom) chemosensory areas. Each trace is an average of 5 experiments, dashed line indicates the standard error. **b)** *Top panels:* VMS parasagittal section of the rostral chemosensitive area from a WT mouse showing immunostaining for GFAP (red), laminin (magenta), and Cx26 (green), with Hoechst staining (blue). Cx26 expressing extends 87 ± 10 µm into the rostral WT chemosensitive area (dotted line). *Bottom pannels:* Equivalent section from a GFAP:Cx26-KO mouse. Cx26 staining remains in the leptomeninges, but is completely absent from parenchyma (asterisk), thus demonstrating that it is normally expressed in GFAP$^+$ cells. *Right panels* show Hoechst and Cx26 staining only. GL, glia limitans; LM, leptomeninges; SAS, subarachnoid space. Scale bars, 20 µm. **c)** Cumulative probability plots of respiratory rate (left) and tidal power (right) for mice at 0% (black circles), 3% (red circles), and 6% (blue circles) inspired CO_2. The lighter filled circles represent data from GFAP:Cx26-KO mice whilst the fully filled circles represent data from GFAP:Cx26-WT. Tidal power is obtained from a power spectrum

created by FFT analysis (Spike2 software) and is intrinsically related to tidal volume – it corresponds to the integral of the breathing trace. There is no difference in respiratory rate between wild type and knockout mice at any CO_2 level. The tidal power of breathing for GFAP:Cx26-KO mice is significantly less than WT mice at 6% inspired CO2, but no different at any other CO_2 level. *Data and figures were produced by Xintao Zhang.*

4.4.2 The role that Connexin26 CO_2 sensitivity plays in adaptive changes in tidal volume at the rostral chemosensitive site

When LV-GFAP:Cx26 variants were expressed at the rostral chemosensitive site (RTN), there was no difference in tidal volume between WT and DN groups during hypercapnia (at any CO_2 level, at any week) (**Figure 4.10**). Expression of $Cx26^{DN}$ was in the correct location, and the transduction coverage with the RTN was good. Based on our assumption that $Cx26^{DN}$ successfully removes glial Cx26 CO_2 sensitivity, and subsequent ATP release, this result suggest that Cx26 CO_2 sensitivity plays no role in modulating tidal volume at the rostral chemosensitive site – as its removal has no effect on adaptive changes in tidal volume. This does not support our hypothesis that Cx26-mediated ATP release influences adaptive changes in tidal volume, and therefore the hypothesis is rejected.

These results are consistent with the conclusion made from Cx26-KO studies. In these investigations floxed Cx26 mice (the same used for experiments in this thesis) were crossed with GFAP-Cre mice or Wnt1-Cre mice, resulting in tissue-wide KO of the Cx26 gene in either all $GFAP^+$ cells or (almost all) neural crest cells (NCCs), respectively. The Wnt1-Cre transgene is not expressed in astrocytes (or their progenitors), and so astrocytes in Wnt1:Cx26-KO mice still expressed Cx26. On the other hand, all NCCs cells expressing Cx26 also expressed GFAP. Furthermore, NCCs were only found in the caudal (not rostral) chemosensitive area. Whole-body plethysmography showed a reduction in adaptive changes in tidal volume (but not frequency) in both GFAP:Cx26-KO (**Supplement figure 4.1c**) and Wnt1:Cx26-KO mice (**Supplement figure 4.2c**). This phenotype was observed in mice aged 3-7 months. The phenotype for both sets of mice were similar (if anything larger in Wnt1:Cx26-KO mice), which suggests that only Cx26 expression in the caudally-located NCCs contributes to adaptive changes in tidal volume – and that Cx26 in all other $GFAP^+$ cells provides no additional respiratory drive (compare **Supplement figure 4.1c** and **Supplement figure 4.2c**). This suggests that Cx26 expression in the RTN is not necessary for chemoreception.

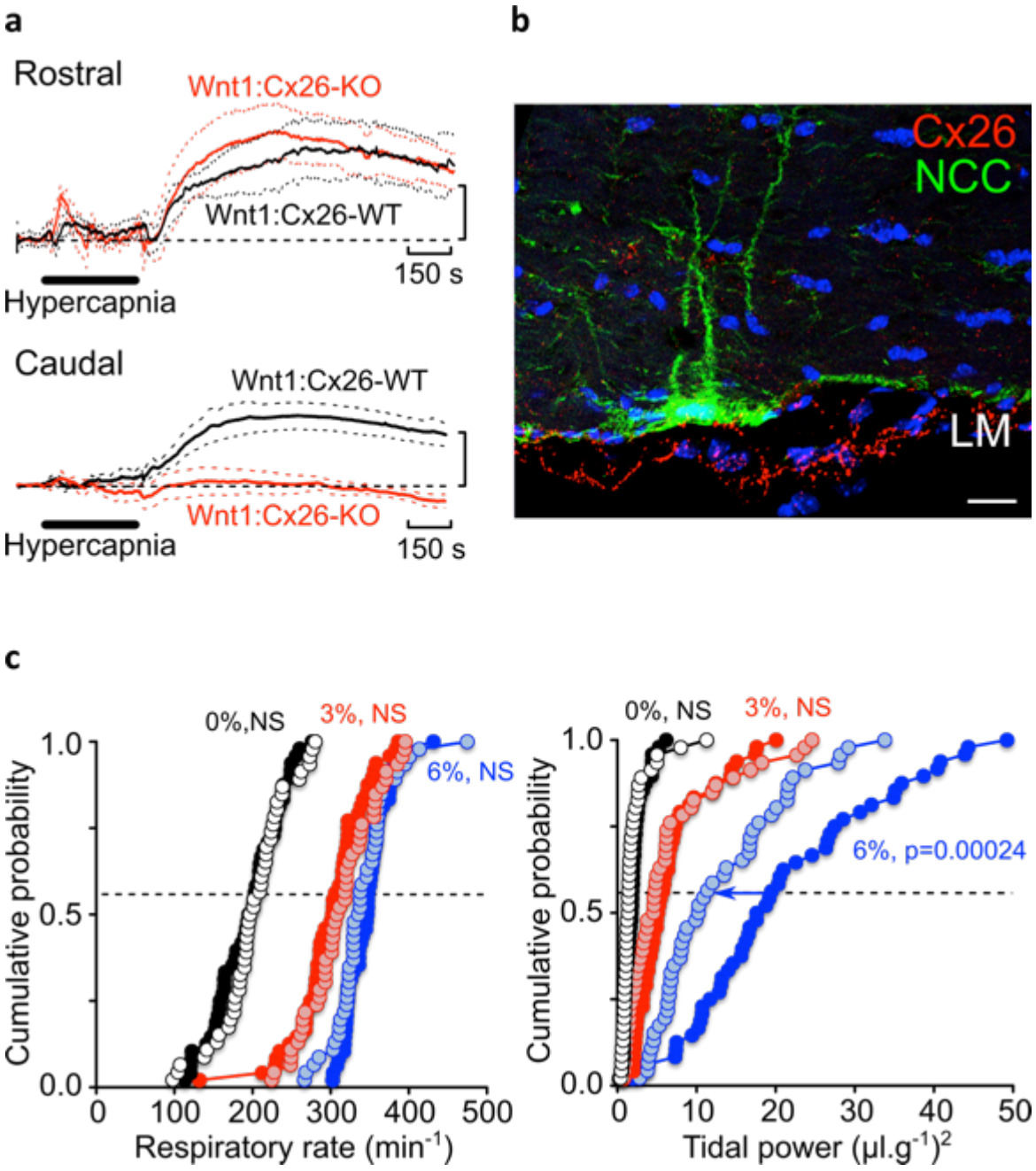

Supplement figure 4.2 **Connexin26 expression in neural crest cells of the caudal medulla contributes to respiratory chemoreception**. **a)** Biosensor recordings of CO_2-evoked ATP release from horizontal slices of the ventral medullary surface (VMS), recorded from Wnt1:Cx26-WT and Wnt1:Cx26-KO mice. Deletion of Cx26 from $Wnt1^+$ cells has no effect on CO2-evoked ATP release from the rostral chemosensory area (top), but drastically reduces it in the caudal chemosensitive area (bottom). Each trace is an average of 5 experiments, dashed line indicates the standard error. **b)** Anatomical characterization of the $GFAP^+$ neural crest cells in caudal medulla. Genetically marked neural crest cells (vGFP, green) can be seen to express Cx26 (red) and GFAP (magenta) and reach deep into the brain parenchyma. Image from a confocal z-stack, maximum intensity. Scale bar, 20 µm. **c)** Cumulative probability plots of respiratory rate (left) and tidal power (right) for mice at 0% (black circles), 3% (red circles), and 6% (blue circles) inspired CO_2. The lighter filled circles represent data from Wnt1:Cx26-KO mice whilst the fully filled circles represent data from Wnt1:Cx26-WT. Tidal power is obtained from a power spectrum created by

FFT analysis (Spike2 software) and is intrinsically related to tidal volume – it corresponds to the integral of the breathing trace. There is no difference in respiratory rate between wild type and knockout mice at any CO_2 level. The tidal power of breathing for Wnt1:Cx26-KO mice is significantly less than WT mice at 6% inspired CO_2, but no different at any other CO_2 level. *Data and figures were produced by Xintao Zhang.*

It is unknown what effect ablating Cx26 from all $GFAP^+$ or $Wnt1^+$ cells from birth has on the development of the respiratory networks. For example, connexin dependent signalling is important in neural progenitor cell proliferation and the maturation of neuronal networks (Malmersjö et al. 2013, Jäderstad et al. 2010), and, of particular importance for these studies, the e-pF (which later becomes the pF_L that adjoins the RTN) requires connexins for embryonic synchronisation of its oscillator (Fortin and Thoby-Brisson 2009). How much of this development is reliant on Cx26 is unknown, however it is feasible for some form of compensation to occur in response to the absence of Cx26 in supporting glial cells. Such compensation could mask the contribution that Cx26 normally plays in $GFAP^+$ cells of wild-type mice. However, data in this chapter would also suggest that Cx26 in $GFAP^+$ cells of the RTN are not necessary for chemoreception.

Recently it has been suggested that during hypercapnia astrocytic release of PGE_2 occurs in a connexin-mediated manner and acts alongside ATP to increase respiratory drive (see *1.2.7 Glia and ATP release*). It was suggested that hypercapnic release of PGE_2 might occur through Cx26 hemichannels (Forsberg et al. 2016, Forsberg, Ringstedt, and Herlenius 2017). In this chapter we assume that CO_2-evoked Cx26 hemichannel opening was removed from RTN glia, however there was no effect (decrease or increase) on the HCVR. This suggests that, under physiological conditions in conscious mice, either PGE_2 release does not occur through Cx26 hemichannels or (as PGE_2 data was obtained from neonatal mice) that the release of PGE_2 from the RTN ceases to be important in central chemoreception some time before 3 months.

4.4.3 Connexin26-mediated ATP release in the RTN

Non-Cx26 mediated mechanisms of ATP release, which are pH-dependent, have been reported in astrocytes within the RTN (Gourine et al. 2010, Wenker et al. 2010). However, at the VMS only very small changes in pH occur in response to physiological changes in pCO_2 (Shams 1985), with pH maintained between 7.4 and 7.25 (Fencl 1971, 1986) and a pCO_2 >100mmHg required for pH to drop below pH 7.1 (Katsura et al. 1992b,

Katsura, Ekholm, and Siesjö 1992a). Therefore, it is unknown to what extent these pH-dependent mechanisms will exert their effect under mild-moderate hypercapnia conditions. Nevertheless, these mechanisms should be taken into consideration when evaluating ATP-mediated hypercapnic responses as certain sources of data do show that they occur within realistic physiological conditions (see *1.2.7 Glia and ATP*).

Regardless of the roles of pH-mediated ATP release, biosensor recordings show clear CO_2-mediated ATP release in the RTN, which is completely abolished when Cx26 is ablated from $GFAP^+$ cells (**Supplement figure 4.1a, top panel**). Given this, if Cx26-mediated ATP release in the RTN was necessary for chemoreception, experiments in this chapter would have been expected to yield at least a hint of a phenotype (**Figure 4.10** and **Figure 4.12**). Therefore, although we do not confirm the status of ATP release in these experiments it is inferred that, in the RTN of mice aged 3-5 months, CO_2-evoked ATP release via Cx26 hemichannels is not necessary for central CO_2 chemoreception. Whether Cx26-mediated ATP release in the RTN has a more pivotal role during other stages of rodent life is yet to be answered.

Results from this chapter suggest that such Cx26-mediated ATP release does not contribute to the HCVR (frequency or tidal volume) in the RTN. This raises the question as to whether there is a role for Cx26-mediated ATP release in the RTN of adult mice, other than a redundant chemoreception system. Perhaps the most likely alternative role is to cause vasoconstriction on local blood vessels. Usually blood vessels dilate during hypercapnia in order to increase O_2 supply to, and CO_2 removal from, tissue. However, it has recently been discovered that vascular tone in the RTN is maintained during hypercapnia via puringergic signalling (Hawkins et al. 2017). This would help ensure that CRC receive accurate and consistent chemosensory information during hypercapnia. Given that ATP induces vasoconstriction in other areas of the brain (Kur and Newman 2014, Peppiatt et al. 2006), astrocytic ATP release in the RTN is a likely candidate to mediate this effect. Alternative roles for Cx26-mediated ATP release in the RTN are put forward in the next chapter (see *5.2 Connexin26 mediated ATP release in RTN - what does it do if it does not regulate breathing?*).

It should be noted that, despite the spread of the virus, there was very little transduction of cells in the area medial to the RTN, where serotonergic raphé neurons reside. These raphé neurons do not fall within the traditionally defined rostral chemosensitive area however have been found to be chemosensitive (Richerson 2004,

Teran, Massey, and Richerson 2014, Li, Zhou, and Nattie 2006, Messier, Li, and Nattie 2004), and might benefit from glial ATP release in their role of generating a chemoreceptive signal. As has been mentioned, GFAP:Cx26-KO mice might have undergone compensation that masked the contribution of rostral $GFAP^+$ cells and therefore we cannot rule out the possibility that Cx26-mediated ATP release is important in regulating the HCVR at these more medial sites.

4.4.4 The role that Connexin26 CO_2 sensitivity plays in adaptive changes in breathing frequency at the caudal chemosensitive site

When LV-GFAP:Cx26 variants were expressed at the caudal chemosensitive site, there was no difference in breathing frequency between WT and DN groups during hypercapnia (at any CO_2 level, at any week) (**Figure 4.8**). Based on our assumption that $Cx26^{DN}$ successfully removes glial Cx26 CO_2 sensitivity, and subsequent ATP release, this result suggest that Cx26 CO_2 sensitivity plays no role in modulating breathing frequency at the caudal chemosensitive site – as its removal has no effect on adaptive changes in frequency.

This result supports the unpublished Cx26-KO data showing that the removal of Cx26 from a sup-population of $GFAP^+$ cells in the caudal chemosensitive area reduces adaptive changes in tidal volume but has no effect on adaptive changes in breathing frequency (**Supplement figure 4.2c**). As with the RTN, this is perhaps unsurprising given the major contribution to frequency control that has already been attributed to peripheral chemoreceptors and GPR4.

4.4.5 The role that Connexin26 CO_2 sensitivity plays in adaptive changes in tidal volume at the caudal chemosensitive site

When LV-GFAP:Cx26 variants were accidently expressed at the caudal chemosensitive site (RTN), a 3WXA revealed no statistical difference in tidal volume between WT and DN groups during hypercapnia (at any CO_2 level, at any week) (**Figure 4.8**). However, at week 3 a lower tidal volume can visually be seen at 6% in mice expressing $Cx26^{DN}$, with a 21% reduction in mean tidal volume compared to animals expressing $Cx26^{WT}$. This difference is supported by statistical analysis when week 3 is taken as an isolated dataset (**Figure 4.9a,c**) and suggests that removal of Cx26 CO_2 sensitivity from glia in the caudal

chemosensitive area reduces adaptive changes in tidal volume. This possibility is further supported as tidal volume decreased with increasing $Cx26^{DN}$ virus expression (**Figure 4.9d**).

Isolated analysis of week 3 data also reveals a decrease in the DN group at 9% CO_2 ($p = 0.049$, one tailed). This is barely significant however supports the difference seen at 6% CO_2. In contrast, at 3% CO_2 (week 3) no difference is seen, presumably as this level of hypercapnia was insufficient to see an effect of $Cx26^{DN}$ expression. Exposure of animals to 9% CO_2 is really pushing physiological conditions, and so this data might not accurately reflect systems that are usually responsible for coordinating a HCVR. At this level of CO_2 pH is likely driven down to levels at which pH-mediated ATP release readily occurs (Gourine et al. 2010, Wenker et al. 2010), which would result in compensation for the ATP not being released via Cx26, and subsequently increase respiratory drive. Nevertheless, if there is Cx26-mediated control of tidal volume at 6% CO_2 it stands to reason that the response occurring at 9% is also, at least in part, mediated by Cx26.

The tidal volume phenotype at 6% is consistent with GFAP:Cx26-KO studies, which identified a small population of $GFAP^{+}$ neural crest cells that were responsible for Cx26-mediated control of tidal volume, at 6% but not 3% CO_2, in this same caudal area (**Supplement figure 4.2c**). Although not definitive, this consistency further supports the tidal volume phenotype seen at week 3, 6% CO_2, in mice expressing $Cx26^{DN}$ in the caudal medulla.

One inconsistency of this conclusion is that the phenotype observed 3 weeks post transduction is not discernible in recordings taken a week later. We anticipated $Cx26^{DN}$ would require 2-3 weeks, from LV-GFAP:$Cx26^{DN}$ transduction, to take effect; needing time to be expressed in sufficient quantities, and then for heteromeric connexons to replace potential connexon turnover stores, and finally for the expression of heteromeric hemichannels in the plasma membrane to overcome the function of any remaining $Cx26^{WT}$ homomeric hemichannels. This explains why a phenotype was not observed until week 3. It is possible that the phenotype disappears at week 4 due to compensation from other chemoreception mechanisms. Although this may seem fast for compensation to occur, owing to the importance of breathing the respiratory system is known to be capable of such adjustments. For example, in goats carotid sinus nerve denervation led to a 60% loss of the HCVR and an inability to regulate blood gases during room air breathing; however this was rectified after just 2 weeks (Pan et al. 1998).

The data from mice with LV expression in the caudal chemosensitive data, alongside that from Cx26-KO studies, indicates that Cx26 CO_2 sensitivity in the caudal chemosensitive area is highly likely to be important in modulating tidal volume. If this result proves to be valid it would demonstrate the role of Cx26 in the respiratory response of conscious animals. Furthermore, it would evidence the progression from identification and mutation of the CO_2-binding motif in Cx26, through to confirmation of the very breathing phenotype that was predicted to result from such a mutant.

We expect that the tidal volume phenotype was only subtle as a consequence of accidentally targeting the caudal chemosensitive area. Therefore, expression in the caudal area has not been optimised to transduce these caudal cells reliably. Sub-optimal expression of $Cx26^{DN}$ is likely to have reduced the effect size in these studies. As such, even an indication that $Cx26^{DN}$ expression in the caudal medulla affected tidal volume warrants the need to purposely target this area to confirm whether or not $Cx26^{DN}$ expression reduces adaptive changes in tidal volume. To this end, the data that has been collected from mice with expression in the caudal chemosensitive area should be considered a (unintentional) pilot study for a full study, which will use the LV-GFAP:Cx26 constructs to comprehensively investigate the role of Cx26 CO_2 sensitivity in glia within this caudal chemosensitive area. (see *4.4.8 Future work: design of a full study to investigate the role of Connexin26 CO2 sensitivity in glia within the caudal chemosensitive site*).

As with transduction in the rostral medulla, caudal transduction did not appear to spread too far medially into the vicinity of the chemosensitive raphé nuclei, and so we cannot comment on the role of Cx26-mediated ATP in this caudomedial region of the VMS. This being said, immunohistochemistry was less clear in the caudal area and so it is possible that, given their long processes, some of the transduced cells made connections as far as these raphé neurons.

4.4.6 Summary of the role Connexin26 CO_2 sensitivity plays in chemoreception at the ventral medullary surface

Based on our assumption that $Cx26^{DN}$ successfully removes glial Cx26 CO_2 sensitivity, and subsequent ATP release, from our data we deduce that Cx26 CO_2 sensitivity plays no role in modulating breathing frequency or tidal volume in the RTN. We also conclude that Cx26 CO_2 sensitivity plays no role in modulating breathing frequency in the caudal

chemosensitive area. However, our data suggests that Cx26 CO_2 sensitivity could play an important role in modulating tidal volume in the caudal chemosensitive areas (**Table 4.1**).

A given chemosensory signalling pathway might be reasoned to influence only one of breathing tidal volume or frequency due to the pathway affecting either the amplitude or the number of the signals it produces. For example, Cx26-mediated ATP release at the caudal site might affect only tidal volume because glial efferents send signals to the cVLM which then send larger signals to the preBotC (resulting in deeper breaths). On the other hand, chemoreceptive pathways responsible for modulating breathing frequency can be imagined to act by increasing the number of signals that are received by the integrating nuclei (thereby increasing the number of breaths produced).

Table 4.1 Summary of the role that Cx26 hemichannels play in chemoreception at different chemosensitive sites at the ventral medullary surface

	Breathing Frequency (Fr)	Tidal Volume (V_T)
Retrotrapezoid nucleus	No role	No role
Caudal chemosensitive area	No role	Prospective role[a]

[a] *experiments are to be repeated to confirm/reject observations made in this study*

4.4.7 Glia morphologies could prove important for function

Differences between glial populations are proving to be as varied and important as different neuronal populations (Jäkel and Dimou 2017). Recently, chemosensitive glia in the VMS have started to be characterised (Sheikhbahaei et al. 2018, Forsberg, Ringstedt, and Herlenius 2017), which will help begin to build up a picture as to how we should categorise these glial populations and what their functions are. It has been noted that central chemosensitive cells in the VMS, including astrocytic glial cells, are often close to the surface of the glial limitans and/or have cell bodies or processes in juxtaposition to penetrating blood vessels (Richerson 2004, Gourine et al. 2010, Wenker et al. 2010, Huckstepp et al. 2010a). This stands to reason as the VMS is affluently supplied with blood vessels and so these locations would allow for a more accurate measurement of

blood pCO2, thereby making these cells highly suitable for directing a HCVR or other hypercapnic responses.

Expression of GFAP-driven Clover (from LV-GFAP:Cx26:IRES:Clover constructs) within the rostral and caudal chemosensitive areas of the VMS highlighted a range of glia morphologies (**Figure 4.13** and **Figure 4.14**). Many of these cells have processes that are much thicker and less branched than traditional star-shaped astrocytes and reach deep into the parenchyma to make connections with cells. Although Cx26 expression is found throughout the glia limitans in these areas, it might be that such expression is only a property of a sub-population of $GFAP^+$ cells, which would be specifically responsible for Cx26-mediated ATP release. Such a sub-population might be identifiable by its morphology, with their processes expected to make connections with nearby respiratory nuclei. Alternatively, Cx26 expression could be fairly homogenous throughout all $GFAP^+$ cells in the chemosensitive areas, and perhaps the morphology of a glial population tailors the function of this chemosensory transducer.

Other groups have reported that astrocytes in the RTN are involved in chemoreception via non-Cx26 mediated, pH sensitive, mechanisms (Gourine et al. 2010, Wenker et al. 2010). Based on morphology alone we cannot confidently confirm the presence of these pH sensitive astrocytes in our sections, although it likely that many were transduced. The flat-bodied glia (with few processes and limited branching) that were transduced in the caudal chemosensory area (**Figure 4.14, white arrows**) seem to conform to a unique morphology and may be differentiated from the round-bodied glia seen in our studies. In fact, the morphology of these flat-bodied cells closely matches those of the $GFAP^+$ NCC population that is responsible for Cx26-mediated adaptive changes in tidal volume (**Supplement figure 4.2b**). If these flat-bodied cells are indeed from the same NCC population then the reduced tidal volume seen in batch 1 DN mice (at week 3, 6% CO_2) becomes even more convincing as it links this phenotype to the same protein (Cx26) and cells (NCCs) that have been shown to be responsible for adaptive changes in tidal volume (Wnt1:Cx26-KO studies, **Supplement figure 4.2**).

The morphology of different glial cell types could reflect the niche role for the chemosensory transducer/s expressed within them. The long, dorsal-reaching, processes seen in many of the transduced cells are highly likely to convey signals from the ventral surface to dorsal neurons (e.g. respiratory nuclei of the VLRC). If both CO_2- and pH-mediated chemoreception in glia are important, then perhaps chemoreceptors

responsible for each mechanism are expressed in distinct glial populations that have morphologies appropriate for sampling from, and signalling to, different locations. If glia are receiving different CO_2 input signals (e.g. CO_2 or pH), or receiving them from different locations, glial networks might be set up, connected by gap junction and hemichannel signalling. This would act to amplify and summate chemosensory signals in order to ensure an effective and efficient HCVR.

4.4.8 Future work: design of a full study to investigate the role of Connexin26 CO_2 sensitivity in glia within the caudal chemosensitive site

Data presented in this chapter suggest that Cx26-mediated ATP release in the RTN is not necessary for central chemoreception in mice aged 3-5months. In contrast, when animals expressed $Cx26^{DN}$ in the caudal chemosensitive region there was a decrease in tidal volume 3 weeks post-transduction at higher CO_2 levels (**Figure 4.9**), and at no other time point (**Figure 4.8**). However, this difference was only statistically supported when testing across CO_2 level at week 3 (**Figure 4.9a**), and not when testing across the entire dataset (3WXA), or across week at 6% CO_2 (**Figure 4.9b**). Taken together these statistics suggest that the differences observed in week 3 are a coincidence. However, considering this result was from accidental targeting of the caudal chemosensitive area and so closely matches the phenotype from Cx26:KO studies, such a coincidence should not be overlooked.

A positive result in the caudal area would provide proof-of-principle for the use of $Cx26^{DN}$ as a genetic tool to investigate CO_2-dependent signalling via Cx26 *in vivo*, thereby validating the conclusions made previously in this chapter. As the data looks so promising, the tidal volume analysis from batch 1 animals has been considered as a pilot study, and the results have been used for a power analysis in order to plan a full study into the effect of expressing $Cx26^{DN}$ in glia at the caudal chemosensitive area.

During these experiments it is likely that some glial cells that do not natively express Cx26 are transduced, resulting in the expression of Cx26 (WT or DN) in glia that do not usually expresses Cx26. As such, it might be suggested that this could result in hyper-chemosensitivity in areas injected with LV-GFAP:$Cx26^{WT}$. Although analysis suggests that $Cx26^{DN}$ is reducing adaptive changes in tidal volume rather than $Cx26^{WT}$ increasing adaptive changes (**Figure 4.9d**), this data is from accidental targeting, has a low number of repeats, and has no statistical support. Therefore, this must be

considered preliminary and does not rule out the possibility that the difference between WT and DN groups at week 3, 6% CO_2, might be (at least in part) due to increased chemosensitivity brought about through $Cx26^{WT}$ expression in glia not normally express Cx26 – thus increasing the amount of ATP released during hypercapnic conditions. An argument could also be made for increased ATP release in response to overexpression of $Cx26^{WT}$ in transduced cells that are natively expressing Cx26. For these reasons the full study has been designed to include a third group of animals that are not transduced with a Cx26 gene, but instead receive a sham injection. This will provide a comparison for animals expressing $Cx26^{WT}$, to control for any abnormal expression of $Cx26^{WT}$.

A suitable power calculator could not be found for determining sample size based around a 3WXA (i.e. analysing data across all weeks and all CO_2 levels). It is assumed that the difference in tidal volume at week 3, 6% CO_2, is not validated by a 3WXA because of the variation across weeks 0-4 (**Figure 4.9b**). Therefore the power calculation was instead carried out in G*power 3.1 (see *4.2.7 Power calculation*), based around a 2WXA looking at tidal volume at 6% CO_2, across all weeks. As a statistical significance has already been shown by a 2WXA looking at week 3, across all CO_2 levels (**Figure 4.9a**), this power calculation should convey a sample size that will also provide acceptable power from a 3WXA to analyse the entire dataset (as was performed in this chapter). For the power calculation, nonsphericity correction and partial eta squared values (0.674 and 0.148, respectively) were calculated from batch 1 animals (pilot study); treating the 4 animals with no caudal virus expression as the third group (representing the sham injections).

The total sample size for a full study, with power 0.8, was calculated to be 36 (i.e. 12 in each group). This contrasts the sample size of 18 (with groups of n = 8, 6, and 4) that was used for the pilot study. With intentional targeting in the caudal chemosensitive area and improved plethysmography techniques it is likely that this sample size will result in greater power than 0.8, and will also help increase the power of analysis by 3WXA.

In addition to this study, similar targeting of glial cells underneath the raphé neurons might be carried out. These serotonergic nuclei have been shown to be chemosensitive but reside more medial than the traditional rostral and caudal chemosensitive areas. Therefore, it is possible Cx26 may play a chemoreceptive role at these sites by augmenting raphé stimulation (**Figure 4.1**).

5 DISCUSSION

In this chapter we discuss experiments and interpretations from Chapter 4 (see *4 Progress towards testing the role of CO_2-sensitivity via Connexin26 in glial cells as a chemosensory regulator of breathing*) in a broader context; discussing the limitations of the LV-GFAP:Cx26 experiments used, speculating on the importance of Cx26-mediated ATP release in the RTN, and commenting on our current understanding of respiratory chemoreception.

5.1 Caveats of the LV-GFAP:Cx26 experiments

This thesis has reported on the use of lentivirus to introduce the Dominant Negative Cx26 mutant ($Cx26^{DN}$) in $GFAP^+$ cells as a means of investigating the effect of Cx26 CO_2-sensitivity in specific regions of the VMS, in mice aged 3-4 months. Unlike non-inducible KO studies, the LV-GFAP:Cx26 technique prevents any compensation that may drastically change the respiratory system during early development, thereby ensuring that $Cx26^{DN}$ is introduced to a wild-type system. As $Cx26^{DN}$ expression is dependent on LV transduction, it also allows for manipulation of specific populations of $GFAP^+$ cells (rather than global KO in all $GFAP^+$ cells).

Despite its advantages there are still a couple of unknown variables associated with this technique. Virus injections involve lowering a capillary through the brain in order to access the region of interest. It is possible that the trauma caused by this might damage tissue that is important to the behaviour under investigation, thereby confounding the data. Such trauma might also cause inflammation. This would be of particular relevance to our studies given the recent data implicating PGE_2 to central chemoreception (Forsberg et al. 2016, Forsberg, Ringstedt, and Herlenius 2017). Although this might influence plethysmography measurements up to a week after surgery, it is unlikely to affect measurements taken after two weeks post-transduction.

In this thesis the data obtained from our LV-GFAP:Cx26 experiments does not fully exclude some alternative interpretations of the results – thereby identifying aspects

that could be amended in order to better optimise the study design for future experimentation. These are discussed below.

5.1.1 Experimental controls

In this thesis two groups of animals were studied, those transduced with LV-GFAP:$Cx26^{DN}$ and those transduced with LV-GFAP:$Cx26^{WT}$. These groups were chosen to control for the overexpression of Cx26 and therefore be able to attribute any difference between the two groups specifically to the mutations in the Dominant Negative, i.e. lack of CO_2-sensitivity. Some may suggest that expression of either $Cx26^{WT}$ or $Cx26^{DN}$ could affect the system in some way that alters the HCVR other than influencing CO_2 sensitivity. Our data would argue against this possibility as no visual or statistical difference in V_T or frequency was found (grouping DN and WT measurements) between week 0 (pre-transduction) and the following 4 weeks (**Figure 4.6**, **Figure 4.8**, and **Figure 4.10**).

It is plausible however that overexpression of $Cx26^{WT}$, especially in glia that do not normally express Cx26, might create a system that is hypersensitive to CO_2 as a result of extra Cx26 causing extra CO_2-evoked ATP release. It would be expected that this would produce animals that are hypersensitive to hypercapnia, resulting in an increased HCVR. Although our virus expression data would argue against these possibilities (**Figure 4.9d**), we are aware that repeats were low and there is no statistical support for this interpretation.

In the full study, that has been planned to target the caudal chemosensitive site, a second control has been included in the form of a group of animals that will be subjected to sham injections (see *4.4.8 Future work: design of a full study to investigate the role of Connexin26 CO2 sensitivity in glia within the caudal chemosensitive site*). This should provide evidence to concretely support any similar interpretations that are made from this study.

Another criticism of the results reported in this thesis may be that there is no true positive control – the reduced tidal volume seen with caudal $Cx26^{DN}$ expression at week 3, 6%, was not supported by a 3-way mixed ANOVA including all data across all weeks. Without a clear positive control the study is open to certain criticism regarding the functionality of the LV-GFAP:$Cx26^{DN}$ technique. To address this concern, the follow up study should include biosensor recordings to confirm that Cx26-mediates ATP release is indeed removed from chemosentive regions expressing $Cx26^{DN}$; thereby validating our

results in the context of our current understanding of glia-mediated chemoreception (see *1.2.7 Glia and ATP release*).

5.1.2 Undetermined roles of Cx26

Connexins have been shown to play an important role within the central respiratory networks (Wenker et al. 2012, Moreira et al. 2015, Forsberg et al. 2016, Huckstepp et al. 2010a). Although this includes Cx26 hemichannels (Huckstepp et al. 2010a), a role for Cx26 gap junctions has not been ruled out. Unpublished data suggests that Cx26 gap junctions are also gated by CO_2 via the same mechanism that is dependent on K125 and R104 residues, but that Cx26 gap junctions close under hypercapnic conditions (personal communication from Nicholas Dale). Therefore, the same K125R R104A mutations are likely to disrupt $Cx26^{DN}$ gap junction closure during hypercapnia (in the same way they disrupt Cx26 hemichannel opening). If this is the case, and Cx26 gap junctions play a role in the respiratory network, then the expression of $Cx26^{DN}$ could affect chemoreception in ways other than preventing hemichannel mediated ATP release. This introduces an unknow variable when interpreting our results.

It is known that Cx26 is capable of forming heteromeric connexons and heterotypic gap junctions with a variety of other members from the connexin family (Koval, Molina, and Burt 2014). Included amongst these Cx26 is compatible with Cx32, which is also CO_2-sensitive (although much less sensitive than Cx26) and is known to be expressed in certain glia in the brain, and in the VMS (although precisely which cells in the VMS is unknown) (Huckstepp et al. 2010a, Nagy et al. 2003). The function of heteromeric Cx26/Cx32 connexon hemichannels or heterotypic Cx26/Cx32 gap junctions is unknown. It is also unconfirmed whether $Cx26^{DN}$ coassembles with Cx32 in the same way as $Cx26^{WT}$ – although coassembly is likely considering the K125R and R104A mutations do not affect the compatibility motifs that have been identified for heteromeric (or heterotypic) oligomerisation (Koval, Molina, and Burt 2014) – however if $Cx26^{DN}$ and Cx32 were to coassembly the resultant heteromeric connexon would be expected to be CO_2 insensitive given the dominant negative nature of $Cx26^{DN}$. Again, these unknown variables bring additional complexity when interpreting our results, and would do the same were this tool used to investigate Cx26 functions in other tissues (that express connexins able to coassemble with Cx26).

5.2 Connexin26 mediated ATP release in RTN - what does it do if it does not regulate breathing?

Cx26-mediated ATP release in both the RTN and caudal chemosensitive region has been shown to occur *in vitro*, in adult mice brain slices, at a pCO_2 that is within the bodies physiological range (**Supplement figure 4.1a** and **Supplement figure 4.2b**). However, it has also been shown *in vitro*, in neonatal mice, that adenosine in the preBötC is capable of inhibiting inspiratory drive (Zwicker et al. 2011). If this were the case in the RTN in our mice then this would explain why introduction of the $Cx26^{DN}$ mutant had no effect (i.e. the action of Cx26-mediated ATP release is usually inhibited by adenosine).

Alternatively, it could be argued that Cx26 hemichannels do not open in the RTN *in vivo*, in intact animals. This could be due to some yet unknown mechanism that is capable of controlling the microenvironment of the RTN such that, in intact animals, the pCO_2 never rises high enough for Cx26 carbamylation – and therefore ATP release does not actually occur under true physiological conditions. Another reason Cx26 might not open in the RTN is due to Cx26 modulators that are acting to close the hemichannels. *In vivo*, negative modulators may be present in higher concentrations in the RTN compared to other regions expressing Cx26 (e.g. the caudal area), thus preventing CO_2-mediated opening. If this is the case, one candidate for such modulation would be taurine. Taurine (as well as other aminosulfonates) close Cx26 hemichannels upon acidification (Locke et al. 2011, Yu et al. 2007) and is present in higher levels in the rostral ventrolateral medulla compared to the caudal ventrolateral medulla (Kubo, Kihara, and Misu 1989). Such modulators of Cx26 opening could contribute to a complex concoction within the cerebrospinal fluid, which is tightly regulated in order to mediate appropriate hypercapnic responses at different chemosensitive sites.

It should be noted that, although possible, the mechanisms suggested above are unlikely to be completely absent in brain slices. Therefore, assuming that Cx26-mediated ATP release does occurs in the RTN of adult mice *in vivo*, our results raise the question as to the purpose of this ATP release. We have already discussed a role that it might play in maintaining vascular tone in the RTN – thereby ensuring accurate and consistent chemosensory signals are received during hypercapnia (see *4.4.3 Connexin26-mediated ATP release in the RTN*). However, it is possible that in the RTN such ATP release has alternative, or additional, functional roles.

Given the number of projections, from RTN glia, that terminate on the facial nucleus (VII) (**Figure 4.13**), below we speculate on some alternative pathways, linked to VII functions, that Cx26-mediated ATP release might be involved in.

5.2.1 Control of airway resistance

If glial projections to the VII were able to influence facial muscle movements during a hypercapnic response, they could potentially aid efficient ventilation through control of airway resistance.

Central facial palsy arises through defects in the VII, and damage to the mid face complex results in the loss of flattening of the nasolabial fold, and subsequent collapse of the nostril – this results in difficulty breathing (Gausas 2006). It could be that ATP release via Cx26 hemichannels act on the VII neurons of the mid face complex in order to help open nasal passages during hypercapnia, thereby reducing resistance and allowing easier airflow. Alternatively, the ATP release could act to stimulate the stylohyoid and/or digastric laryngeal muscles, which are innervated by the VII (Facialis 1918). During inspiration the larynx is stimulated (Green and Neil 1955) and is required to be moved in order to not obstruct the trachea (e.g. the vocal cords need to be pulled apart). In this way, the larynx also affects airway resistance.

Under these theories, expression of $Cx26^{DN}$ in the RTN, as in our studies, would have resulted in increased resistance in the airways. This would have resulted in difficulty breathing but not necessarily a difference in either tidal volume or frequency, as animals could exert extra effort to maintain a normal V_T and frequency. Testing for a change in airway resistance would require a mouse measurement similar to the FEV1 (forced expiratory volume in the first second of exhalation), which is measured during human spirometry, or better still a measure of specific airway resistance (sR_{aw}, cmH20.s). To obtain this recording dual-chamber plethysmography should be implemented. In dual-chamber plethysmography animals are restrained by means of a rubber neck collar that separates a thoracic and a nasal chamber. A plethysmograph is capable of producing a trace due to the changes in pressure that only arise due to air flow needing to overcome airway resistance (see *4.2.5 Whole-body plethysmography*). By recording air flow in the two chambers resistance is able to be recorded by means of the time delay between a change in pressure in the thoracic chamber and a change in pressure in the nasal chamber.

5.2.2 Species-specific role

Given that our studies were performed in mice, species-specific roles should be considered when interpreting the results. Species-specific glia have been reported, e.g. interlaminar glia present in the cerebral cortex of primate brains is not present in the cerebral cortex of rodent brain (Colombo et al. 1995, Colombo 1996, Colombo and Reisin 2004). Therefore, it could be speculated that many of the surface glia seen at the VMS in our study project to the VII to play a role specific to rodents. As rodents are obligate nasal breathers this role might be a specialised mechanisms for controlling airway resistance, as discussed above (see *5.2.1 Control of airway resistance*).

Alternatively, given that the VMS is the key site for many respiratory-related behaviors, such species-specific glia could be involved in a behavior such as sniffing - which is drastically more important for rodents and used during exploration. If these cells release ATP in response to hypercapnia, then the connections they make with the VII might be proposed to control muscles that are involved in increasing/decreasing sniffing under hypercapnic conditions.

Even between rodents there might be differences in the respiratory network. Of note to the work presented here, there is *in vitro* data (from neonatal brain slices) suggesting that in the preBötC of mice, but not rats, there is high ectonucleotidase activity that degrades ATP to adenosine, which subsequently acts antagonistically to ATP in order to inhibit respiratory drive. If such activity exists elsewhere in the brainstem of mice, e.g. the RTN, then the drive to breathe that is caused by ATP in mice might not be as clear-cut.

5.2.3 Hypercapnia-induced auditory hypervigilance

The VII innervates the stapedius, which attaches to, and controls dampening/amplifying vibrations of, the staples in the ear. This is turn dampens/amplifies the sound waves that are perceived by the brain (Drake, Vogl, and Mitchell 2009). Cx26-mediated ATP release could be responsible for either causing contraction or relaxation of the stapedius, thereby dampening or amplifying sounds (respectively). If Cx26-mediated ATP release were to relax the stapedius this would amplify sounds during periods of high CO_2. Also, the Superior Olive (SO) sits just rostral and dorsal of the RTN (**Figure 1.1**). The medial SO

(MSO) and lateral SO (LSO) are initial relay stations for incoming auditory information from the cochlear nucleus. ATP release from the glia in question might diffuse towards these networks and act on them to improve their performance.

It could be rationalised that sound enhancement during periods of high CO_2 could be beneficial. When animals become very active during the 'fight or flight' response (e.g escaping or fighting predators) they will produce excess CO_2. Under these circumstances it might be advantageous to amplify sounds in order to become more aware of threatening stimuli. Also, when rodents sleep in burrows the CO_2 levels rise due to there being many bodies in a confined space. At night it might be advantageous for pray animals to heighten their sense of hearing in order to be more aware of roaming predators. This would be consistent with Cx26 evolutionary studies which have shown alligator Cx26 is not sensitive to CO2. This predator does not sleep in burrows or have any need to increase its hearing at night.

It is well established that defects in Cx26 are a major contributor to hearing loss (Petersen and Willems 2006), however much of this pathology has been attributed to properties of Cx26 other than CO_2 sensitivity. Given the infancy of Cx26 CO_2 sensitivity research, it is feasible that additional and/or alternative mechanisms underlying Cx26-related hearing loss are yet to be linked to this property. If such a connection existed between Cx26 CO_2 sensitivity in the RTN and innervation of the stapedius, it would identify a novel Cx26-related mechanism that might be defective in certain patients and contribute to their hearing-loss pathology. Such a connection would also provide a link between the loss of CO_2 sensitivity seen in KID syndrome mutants and the deafness symptoms that present in KID syndrome patents. This link would be in addition to that made between Cx26 CO2 sensitivity and reduced respiratory drive (Meigh et al. 2014).

5.3 Better understanding central respiratory chemoreception: experimental considerations

The *in vitro* and *in vivo* research that has been undertaken into understanding respiration has granted us some invaluable insight and understanding that has been, and will continue to be, of benefit for biomedical research and healthcare implications. However, when studying respiration there are a couple of considerations that cannot be

overlooked, for fear of producing conflicting interpretations and conclusions that are not fully relevant.

5.3.1 Age dependent hypercapnic respiratory response

Whilst there is debate over the changes in rodent HCVR from P0-P12 there is a general consensus that it increases from ~P12-P30 (Darnall 2010). At least one further change in chemoreception occurs over the lifetime of the animal, as older mice (32-44 weeks) show a lower HCVR than those in early adulthood (10-16 weeks) (Onodera et al. 1997). The precise reasons (mechanical and evolutionary) for these changes are unknown. Nonetheless, because the system witnesses these changes, age is an important factor for both experimental design and data interpretation. Many studies acquire data from neonates or report mixed data from neonatal *in vitro* slice recordings and *in vivo* plethysmography from animals at a much older age (sometimes adulthood). Conclusions made from these experiments should be accepted with caution (in the same way as data from anaesthetised animal should be).

In this thesis it has been suggested that Cx26 CO_2-sensitivity is not important for chemoreception in the RTN in mice aged 3-4 months (which falls within the "adult period), however we cannot comment on the importance of Cx26 during other phases of development. We also provide evidence suggesting that Cx26 CO_2-sensitivity is important in chemoreception in the caudal area of mice at this same age. This may seem contradictory to GPR4/TASK-2 double-KO mice that show complete abolishment of a HCVR, however this conclusion was made from a sample size of only 4 and so is not reliable (Kumar et al. 2015). Nevertheless, if this double-KO data were to be accepted then one explanation of our data is that glial chemosensitivity (including Cx26-mediated ATP release in the caudal region) only becomes important at later stages of development, when it takes over part of the role that GPR4/TASK-2 plays earlier in development.

If glia were to only take on a chemoreceptive role later in development it might be speculated that respiratory nuclei start off as vital components for chemoreception early in the lifespan of an animal, as the brain is smaller and chemosensory signals can easily penetrate to these neurons. However, as the brain grows throughout the animal's life these nuclei end up residing further from the ventral surface than they once did; thereby relying on the emergence of new chemosensitive cell types that are more

suitably positioned (closer to blood vessels and the aCSF) and can take over some of the chemoreceptive responsibilities, sending signals via long processes. In the medulla, proliferation of glia ventral to respiratory nuclei might also provide extra protection and support for these nuclei – especially given that they are located in a part of the brain that is significantly more mobile and exposed than other parts. If glia were to mature into chemoreceptive roles throughout development there might be potential for future therapies to accelerate their development in young patients with central respiratory problems, thereby compensating for defects in CRCs responsible for neonatal chemoreception.

5.3.2 Relevant experimental techniques

The LV-GFAP:Cx26^{DN} technique presented in this thesis aims to maintain the animal system in a state that is as physiological as possible. As has been discussed throughout this thesis, this method is more precise than KO genetic studies – both temporally and spatially refining the targeting of a specific component. It is also more physiological than optogenetic stimulation, which overstimulates the system and might stimulate a pathway that would not usually be activated in the animal - thus providing a false positive. In this way the LV-GFAP:Cx26^{DN} method allows for accurate interpretations as to the relevance that Cx26 CO_2-sensitivity, in distinct areas, has on modulating breathing. However even this technique can be criticised for disturbances it might cause within a system (see *5.1 Caveats of the LV-GFAP:Cx26 experiments*).

Perhaps the only truly physiological experiments would be those capable of imaging cellular activity live in conscious animals. Recording neuronal and glial firing in chemosensitive areas would provide us with definitive answers as to which cell populations are active under relevant hypercapnia conditions. From there, relevant CRCs (and their chemosensory transducers) can become the focus of research, with the aim of further understanding respiratory pathways and providing targets for therapeutic purposes.

Other members of the Dale group have been able to record such activity from RTN neurons and glia using the latest *in vivo* Ca^{2+} imaging techniques. However, the results are highly unexpected. Using the head-mounted nVista microscope (Inscopix, USA) live Ca^{2+} imaging from neurons and glia in the VMS have been recorded. Very recent, unpublished, data shows that in the RTN of conscious adult mice there is no

neuronal or glial activation in response to hypercapnia (personal communication from Nicholas Dale). Interestingly the data also show that cells in the raphé magnus do respond to hypercapnia. This shows the importance for *in vivo* experiments to be performed under true physiological conditions and also reveals a revelationary discovery – that the RTN is not involved in responding to chemoreception in conscious adult animals but the raphé magnus is. Such a result supports the findings in this thesis – that removal of Cx26-mediated ATP release in the RTN has no effect on adaptive changes in breathing and must presumably have some other physiological role. Since the raphé magnus and RTN are close together, future experimenters need to be careful in targeting their manipulations precisely to these areas.

6 CONCLUSION

This thesis has detailed the progress made towards using a mutant version of the Connexin26 (Cx26) – dubbed 'Dominant Negative' Cx26 ($Cx26^{DN}$) – to remove CO_2-sensitivty from cells natively expressing wild-type Cx26 protein ($Cx26^{WT}$). This thesis has demonstrated that $Cx26^{DN}$ subunits remove CO_2-induced hemichannel opening in a dominant negative manner by coassembling with $Cx26^{WT}$ to form heteromeric connexon hemichannels. *In vivo* expression of $Cx26^{DN}$, to remove Cx26-mediated ATP release from glia at the ventral medullary surface (VMS), suggests that Cx26 plays no role in central respiratory chemoreception within the RTN but is likely to play a role in mediating tidal volume at the caudal chemosensitive site. Expression of $Cx26^{DN}$ in the caudal chemosensitive site was accidental and these experiments must be repeated in order confirm whether or not Cx26 expression is indeed important in this area.

If $Cx26^{DN}$ expression is confirmed to reduce adaptive changes in tidal volume, these findings will not only shed light on our understanding of central respiratory chemoreception but will also validate the use of $Cx26^{DN}$ as a novel genetic tool that can elegantly remove Cx26 CO_2 sensitivity from specific cells. By allowing us to selectively probe discrete populations of cells, at any stage of development, such a tool could spearhead research into the virtually unexplored role that Cx26 CO_2 gating has in the body.

REFERENCES

Abbott, Stephen BG, Ruth L Stornetta, Michal G Fortuna, Seth D Depuy, Gavin H West, Thurl E Harris, and Patrice G %J Journal of Neuroscience Guyenet. 2009. "Photostimulation of retrotrapezoid nucleus phox2b-expressing neurons in vivo produces long-lasting activation of breathing in rats." 29 (18):5806-5819.

Abudara, Verónica, John Bechberger, Moises Freitas-Andrade, Marijke De Bock, Nan Wang, Geert Bultynck, Christian C Naus, Luc Leybaert, and Christian Giaume. 2014. "The connexin43 mimetic peptide Gap19 inhibits hemichannels without altering gap junctional communication in astrocytes." *Frontiers in cellular neuroscience* 8:306.

Acker, H. 1989. "PO2 chemoreception in arterial chemoreceptors." *Annual review of physiology* 51 (1):835-844.

Anderson, Tatiana M, Alfredo J Garcia, Nathan A Baertsch, Julia Pollak, Jacob C Bloom, Aguan D Wei, Karan G Rai, and Jan-Marino Ramirez. 2016. "A novel excitatory network for the control of breathing." *Nature* 536 (7614):76.

Anderson, Tatiana M, and Jan-Marino Ramirez. 2017. "Respiratory rhythm generation: triple oscillator hypothesis." *F1000Research* 6.

Anikovsky, Max, Lianne Dale, Stephen Ferguson, and Nils %J Biophysical journal Petersen. 2008. "Resonance energy transfer in cells: a new look at fixation effect and receptor aggregation on cell membrane." 95 (3):1349-1359.

Anselmi, Fabio, Victor H Hernandez, Giulia Crispino, Anke Seydel, Saida Ortolano, Stephen D Roper, Nicoletta Kessaris, William Richardson, Gesa Rickheit, and Mikhail A Filippov. 2008. "ATP release through connexin hemichannels and gap junction transfer of second messengers propagate Ca2+ signals across the inner ear." *Proceedings of the National Academy of Sciences* 105 (48):18770-18775.

Aristotle. approx. 350 BC. *On Youth and Old Age, On Life and Death, On Breathing*. Edited by Translated by G. R. T. Ross. http://classics.mit.edu/Aristotle/youth_old.1.1.html: Alex Catalogue.

Arita, H., K. Ichikawa, S. Kuwana, and N. Kogo. 1989. "Possible locations of pH-dependent central chemoreceptors: intramedullary regions with acidic shift of extracellular fluid pH during hypercapnia." *Brain Res* 485 (2):285-93.

Arita, Ken, Masashi Akiyama, Tomoyasu Aizawa, Yoshitaka Umetsu, Ikuo Segawa, Maki Goto, Daisuke Sawamura, Makoto Demura, Keiichi Kawano, and Hiroshi Shimizu. 2006. "A novel N14Y mutation in Connexin26 in keratitis-ichthyosis-deafness syndrome: analyses of altered gap junctional communication and molecular structure of N terminus of mutated Connexin26." *The American journal of pathology* 169 (2):416-423.

Bajar, Bryce T, Emily S Wang, Amy J Lam, Bongjae B Kim, Conor L Jacobs, Elizabeth S Howe, Michael W Davidson, Michael Z Lin, and Jun Chu. 2016. "Improving brightness and photostability of green and red fluorescent proteins for live cell imaging and FRET reporting." *Scientific Reports* 6:20889.

Bao, Li, Silviu Locovei, and Gerhard Dahl. 2004. "Pannexin membrane channels are mechanosensitive conduits for ATP." *FEBS letters* 572 (1-3):65-68.

Bao, Li, Frederick Sachs, and Gerhard Dahl. 2004. "Connexins are mechanosensitive." *American Journal of Physiology-Cell Physiology* 287 (5):C1389-C1395.

Bao, Xiaoyong, Guillermo A Altenberg, and Luis Reuss. 2004. "Mechanism of regulation of the gap junction protein connexin 43 by protein kinase C-mediated phosphorylation." *American Journal of Physiology-Cell Physiology* 286 (3):C647-C654.

Bargiello, Thaddeus A, Qingxiu Tang, Seunghoon Oh, and Taekyung Kwon. 2012. "Voltage-dependent conformational changes in connexin channels." *Biochimica et Biophysica Acta (BBA)-Biomembranes* 1818 (8):1807-1822.

Beltramello, Martina, Valeria Piazza, Feliksas F Bukauskas, Tullio Pozzan, and Fabio Mammano. 2005. "Impaired permeability to Ins (1, 4, 5) P 3 in a mutant connexin underlies recessive hereditary deafness." *Nature cell biology* 7 (1):63.

Bennett, Brad C, Michael D Purdy, Kent A Baker, Chayan Acharya, William E McIntire, Raymond C Stevens, Qinghai Zhang, Andrew L Harris, Ruben Abagyan, and Mark Yeager. 2016. "An electrostatic mechanism for Ca 2+-mediated regulation of gap junction channels." *Nature communications* 7:8770.

Berg, Jeremy M, John L Tymoczko, and GJ Gatto Jr. 2002. "Stryer: Biochemistry." *WH Freeman and Company* 5:306-307.

Berkenbosch, A, J Van Dissel, CN Olievier, J De Goede, and J Heeringa. 1979. "The contribution of the peripheral chemoreceptors to the ventilatory response to CO2 in anaesthetized cats during hyperoxia." *Respiration physiology* 37 (3):381-390.

Bernard, D. G., A. Li, and E. E. Nattie. 1996. "Evidence for central chemoreception in the midline raphé." *J Appl Physiol (1985)* 80 (1):108-15. doi: 10.1152/jappl.1996.80.1.108.

Berquin, P, L Bodineau, F Gros, and N Larnicol. 2000. "Brainstem and hypothalamic areas involved in respiratory chemoreflexes: a Fos study in adult rats." *Brain research* 857 (1-2):30-40.

Bond, CT, M Pessia, XM Xia, A Lagrutta, MP Kavanaugh, and JP Adelman. 1994. "Cloning and expression of a family of inward rectifier potassium channels." *Receptors & channels* 2 (3):183-191.

Bootman, Martin D, and Michael J Berridge. 1995. "The elemental principles of calcium signaling." *Cell* 83 (5):675-678.

Bootman, Martin D, Tony J Collins, Claire M Peppiatt, Larissa S Prothero, Lauren MacKenzie, Patrick De Smet, Marianne Travers, Stephen C Tovey, Jeong T Seo, and Michael J Berridge. 2001. "Calcium signalling—an overview." Seminars in cell & developmental biology.

Boscan, Pedro, Anthony E Pickering, and Julian FR Paton. 2002. "The nucleus of the solitary tract: an integrating station for nociceptive and cardiorespiratory afferents." *Experimental physiology* 87 (2):259-266.

Bradley, S. R., V. A. Pieribone, W. Wang, C. A. Severson, R. A. Jacobs, and G. B. Richerson. 2002. "Chemosensitive serotonergic neurons are closely associated with large medullary arteries." *Nat Neurosci* 5 (5):401-2. doi: 10.1038/nn848.

Brust, Rachael D, Andrea E Corcoran, George B Richerson, Eugene Nattie, and Susan M Dymecki. 2014. "Functional and developmental identification of a molecular subtype of brain serotonergic neuron specialized to regulate breathing dynamics." *Cell reports* 9 (6):2152-2165.

Bruzzone, Roberto, Michael T Barbe, Nurith J Jakob, and Hannah Monyer. 2005. "Pharmacological properties of homomeric and heteromeric pannexin hemichannels expressed in Xenopus oocytes." *Journal of neurochemistry* 92 (5):1033-1043.

Bruzzone, Santina, Lucrezia Guida, Elena Zocchi, Luisa Franco, and Antonio De Flora. 2001. "Connexin 43 hemi channels mediate Ca2+-regulated transmembrane NAD+ fluxes in intact cells." *The FASEB Journal* 15 (1):10-12.

Bukauskas, Feliksas F, and Vytas K Verselis. 2004. "Gap junction channel gating." *Biochimica et Biophysica Acta (BBA)-Biomembranes* 1662 (1):42-60.

Burra, Sirisha, and Jean X Jiang. 2011. "Regulation of cellular function by connexin hemichannels." *International journal of biochemistry and molecular biology* 2 (2):119.

Caceres‐Rios, Hector, Lourdes Tamayo‐Sanchez, Carola Duran‐Mckinster, MA Orozco, and Ramon Ruiz‐Maldonado. 1996. "Keratitis, ichthyosis, and deafness (KID syndrome): review of the literature and proposal of a new terminology." *Pediatric dermatology* 13 (2):105-113.

Carandini, Matteo. 2012. "From circuits to behavior: a bridge too far?" *Nature neuroscience* 15 (4):507.

Carpenter, E, CJ Hatton, and C Peers. 2000. "Effects of hypoxia and dithionite on catecholamine release from isolated type I cells of the rat carotid body." *The Journal of physiology* 523 (3):719-729.

Caspar, DL, DA Goodenough, Lee Makowski, and WC Phillips. 1977. "Gap junction structures. I. Correlated electron microscopy and x-ray diffraction." *The Journal of Cell Biology* 74 (2):605-628.

Ceriani, Federico, Tullio Pozzan, and Fabio Mammano. 2016. "Critical role of ATP-induced ATP release for Ca2+ signaling in nonsensory cell networks of the developing cochlea." *Proceedings of the National Academy of Sciences* 113 (46):E7194-E7201.

Chamberlin, Nancy L, Matthias Eikermann, Philipp Fassbender, David P White, and Atul Malhotra. 2007. "Genioglossus premotoneurons and the negative pressure reflex in rats." *The Journal of physiology* 579 (2):515-526.

Chen, Yongyue, Yanqin Deng, Xiaoyong Bao, Luis Reuss, and Guillermo A Altenberg. 2005. "Mechanism of the defect in gap-junctional communication by expression of a connexin 26 mutant associated with dominant deafness." *The FASEB journal* 19 (11):1516-1518.

Cheng, Ping-Chin. 2006. "The contrast formation in optical microscopy." In *Handbook of biological confocal microscopy*, 162-206. Springer.

Clapham, David E. 2007. "Calcium signaling." *Cell* 131 (6):1047-1058.

Cohen, Morton I, and Jack L Feldman. 1977. "Models of respiratory phase switching." Fed. Proc.

Cohen-Salmon, Martine, Thomas Ott, Vincent Michel, Jean-Pierre Hardelin, Isabelle Perfettini, Michel Eybalin, Tao Wu, Daniel C Marcus, Philine Wangemann, and Klaus %J Current Biology Willecke. 2002. "Targeted ablation of connexin26 in the inner ear epithelial gap junction network causes hearing impairment and cell death." 12 (13):1106-1111.

Colombo, J. A. 1996. "Interlaminar astroglial processes in the cerebral cortex of adult monkeys but not of adult rats." *Acta Anat (Basel)* 155 (1):57-62.

Colombo, J. A., and H. D. Reisin. 2004. "Interlaminar astroglia of the cerebral cortex: a marker of the primate brain." *Brain Res* 1006 (1):126-31. doi: 10.1016/j.brainres.2004.02.003.

Colombo, J. A., A. Yáñez, V. Puissant, and S. Lipina. 1995. "Long, interlaminar astroglial cell processes in the cortex of adult monkeys." *J Neurosci Res* 40 (4):551-6. doi: 10.1002/jnr.490400414.

Common, John EA, David Becker, Wei-Li Di, Irene M Leigh, Edel A O'Toole, and David P Kelsell. 2002. "Functional studies of human skin disease-and deafness-associated connexin 30 mutations." *Biochemical and biophysical research communications* 298 (5):651-656.

Costes, Sylvain V, Dirk Daelemans, Edward H Cho, Zachary Dobbin, George Pavlakis, and Stephen Lockett. 2004. "Automatic and quantitative measurement of protein-protein colocalization in live cells." *Biophysical journal* 86 (6):3993-4003.

Cotrina, Maria Luisa, Jane H-C Lin, Alexandra Alves-Rodrigues, Shujun Liu, Jiang Li, Hooman Azmi-Ghadimi, Jian Kang, Christian CG Naus, and Maiken Nedergaard. 1998. "Connexins regulate calcium signaling by controlling ATP release." *Proceedings of the National Academy of Sciences* 95 (26):15735-15740.

Cotrina, Maria Luisa, Jane H-C Lin, and Maiken Nedergaard. 1998. "Cytoskeletal assembly and ATP release regulate astrocytic calcium signaling." *Journal of Neuroscience* 18 (21):8794-8804.

Cui, Yan, Kaiwen Kam, David Sherman, Wiktor A Janczewski, Yu Zheng, and Jack L Feldman. 2016. "Defining preBötzinger complex rhythm-and pattern-generating neural microcircuits in vivo." *Neuron* 91 (3):602-614.

da Silva, G. S., A. Li, and E. Nattie. 2010. "High CO2/H+ dialysis in the caudal ventrolateral medulla (Loeschcke's area) increases ventilation in wakefulness." *Respir Physiol Neurobiol* 171 (1):46-53. doi: 10.1016/j.resp.2010.01.014.

Dalamón, Viviana Karina, Paula Buonfiglio, Margarita Larralde, Patricio Craig, Vanesa Lotersztein, Keith Choate, Norma Pallares, Vicente Diamante, and Ana Belén Elgoyhen. 2016. "Connexin 26 (GJB2) mutation in an Argentinean patient with keratitis-ichthyosis-deafness (KID) syndrome: a case report." *BMC medical genetics* 17 (1):37.

Darnall, Robert A. 2010. "The role of CO2 and central chemoreception in the control of breathing in the fetus and the neonate." *Respiratory physiology & neurobiology* 173 (3):201-212.

Dauger, S., A. Pattyn, F. Lofaso, C. Gaultier, C. Goridis, J. Gallego, and J. F. Brunet. 2003. "Phox2b controls the development of peripheral chemoreceptors and afferent visceral pathways." *Development* 130 (26):6635-42. doi: 10.1242/dev.00866.

Davis, Suzanne E, Greg Solhied, Mary Castillo, M Dwinell, Dan Brozoski, and Hubert V Forster. 2006. "Postnatal developmental changes in CO2 sensitivity in rats." *Journal of Applied Physiology* 101 (4):1097-1103.

De Vuyst, Elke, Elke Decrock, Liesbet Cabooter, George R Dubyak, Christian C Naus, W Howard Evans, and Luc Leybaert. 2006. "Intracellular calcium changes trigger connexin 32 hemichannel opening." *The EMBO journal* 25 (1):34-44.

de Wolf, Elizabeth, Jonathan Cook, and Nicholas Dale. 2017. "Evolutionary adaptation of the sensitivity of connexin26 hemichannels to CO2." *Proc. R. Soc. B* 284 (1848):20162723.

de Wolf, Elizabeth, Joseph van de Wiel, Jonathan Cook, and Nicholas Dale. 2016. "Altered CO2 sensitivity of connexin26 mutant hemichannels in vitro." *Physiological reports* 4 (22).

de Zwart‐Storm, Eugene A, Rafael FM Rosa, Patricia E Martin, Regina Foelster‐Holst, Jorge Frank, Ana EK Bau, Paulo RG Zen, Carla Graziadio, Giorgio A Paskulin, and Miriam A Kamps. 2011. "Molecular analysis of connexin26 asparagine14 mutations associated with syndromic skin phenotypes." *Experimental dermatology* 20 (5):408-412.

Dev, N. B., and H. H. Loeschcke. 1979. "Topography of the respiratory and circulatory responses to acetylcholine and nicotine on the ventral surface of the medulla oblongata." *Pflugers Arch* 379 (1):19-27.

Dewey, TG, and GG Hammes. 1980. "Calculation on fluorescence resonance energy transfer on surfaces." *Biophysical journal* 32 (3):1023-1035.

Di, Wei-Li, Yan Gu, John EA Common, Trond Aasen, Edel A O'Toole, David P Kelsell, and Daniel Zicha. 2005. "Connexin interaction patterns in keratinocytes revealed morphologically and by FRET analysis." *Journal of cell science* 118 (7):1505-1514.

Di, Wei-Li, James Monypenny, John EA Common, Cameron TC Kennedy, Katalin A Holland, Irene M Leigh, Elizabeth L Rugg, Daniel Zicha, and David P Kelsell. 2002. "Defective trafficking and cell death is characteristic of skin disease-associated connexin 31 mutations." *Human molecular genetics* 11 (17):2005-2014.

Diaspro, Alberto, Giuseppe Chirico, Cesare Usai, Paola Ramoino, and Jurek Dobrucki. 2006. "Photobleaching." In *Handbook of biological confocal microscopy*, 690-702. Springer.

Dirks, W, C Mielke, S Karreman, B Haase, M Wirth, W Lindenmaier, and H Hauser. 1994. "Applications of expression vectors containing bicistronic transcription units in mammalian cells." In *Cell Culture in Pharmaceutical Research*, 239-265. Springer.

Dobbins, Elizabeth G, and Jack L Feldman. 1994. "Brainstem network controlling descending drive to phrenic motoneurons in rat." *Journal of Comparative Neurology* 347 (1):64-86.

Drake, Richard, A Wayne Vogl, and Adam WM Mitchell. 2009. *Gray's Anatomy for Students E-Book*: Elsevier Health Sciences.

Dubreuil, V., M. Thoby-Brisson, M. Rallu, K. Persson, A. Pattyn, C. Birchmeier, J. F. Brunet, G. Fortin, and C. Goridis. 2009. "Defective respiratory rhythmogenesis and loss of central chemosensitivity in Phox2b mutants targeting retrotrapezoid nucleus neurons." *J Neurosci* 29 (47):14836-46. doi: 10.1523/JNEUROSCI.2623-09.2009.

Eidne, Karin A, Karen M Kroeger, and Aylin C Hanyaloglu. 2002. "Applications of novel resonance energy transfer techniques to study dynamic hormone receptor interactions in living cells." *Trends in Endocrinology & Metabolism* 13 (10):415-421.

Ellis-Davies, GC, and Jack H Kaplan. 1994. "Nitrophenyl-EGTA, a photolabile chelator that selectively binds Ca2+ with high affinity and releases it rapidly upon photolysis." *Proceedings of the National Academy of Sciences* 91 (1):187-191.

Engelking, Larry R. 2015. "Respiratory Acidosis." In *Textbook of Veterinary Physiological Chemistry*, 584-589. Academic Press.

Evans, Charles Lovatt, Hamilton Hartridge, and EH Starling. 1956. *Principles of human physiology*. Vol. 553: Churchill London.

Fabris, Gisele, Alexandre A Steiner, Janete A Anselmo-Franci, and Luiz GS Branco. 2000. "Role of nitric oxide in rat locus coeruleus in hypoxia-induced hyperventilation and hypothermia." *Neuroreport* 11 (13):2991-2995.

Facialis, N. 1918. "The Facial Nerve." In *Gray's Anatomy of the Human Body*, 905. HILADELPHIA: LEA & FEBIGER, 1918 NEW YORK: BARTLEBY.COM, 2000.

Fairchild, Karen, Mary Mohr, Alix Paget-Brown, Christa Tabacaru, Douglas Lake, John Delos, Joseph Randall Moorman, and John Kattwinkel. 2016. "Clinical associations of immature breathing in preterm infants: part 1—central apnea." *Pediatric research* 80 (1):21.

Fallon, Regis F, and Daniel A Goodenough. 1981. "Five-hour half-life of mouse liver gap-junction protein." *The Journal of cell biology* 90 (2):521-526.

Falquetto, B., L. M. Oliveira, A. C. Takakura, D. K. Mulkey, and T. S. Moreira. 2018. "Inhibition of the hypercapnic ventilatory response by adenosine in the retrotrapezoid nucleus in awake rats." *Neuropharmacology* 138:47-56. doi: 10.1016/j.neuropharm.2018.05.029.

Faul, Franz, Edgar Erdfelder, Axel Buchner, and Albert-Georg %J Behavior research methods Lang. 2009. "Statistical power analyses using G* Power 3.1: Tests for correlation and regression analyses." 41 (4):1149-1160.

Faul, Franz, Edgar Erdfelder, Albert-Georg Lang, and Axel %J Behavior research methods Buchner. 2007. "G* Power 3: A flexible statistical power analysis program for the social, behavioral, and biomedical sciences." 39 (2):175-191.

Feeley, Brian T, Augustine H Conduah, Osamu Sugiyama, Lucie Krenek, Irvin SY Chen, and Jay R Lieberman. 2006. "In vivo molecular imaging of adenoviral versus lentiviral gene therapy in two bone formation models." *Journal of orthopaedic research* 24 (8):1709-1721.

Feil, S., N. Valtcheva, and R. Feil. 2009. "Inducible Cre mice." *Methods Mol Biol* 530:343-63. doi: 10.1007/978-1-59745-471-1_18.

Feldman, Jack L, Morton I Cohen, and Paul Wolotsky. 1976b. "Powerful inhibition of pontine respiratory neurons by pulmonary afferent activity." *Brain research* 104 (2):341-346.

Feldman, Jack L, and Christopher A Del Negro. 2006. "Looking for inspiration: new perspectives on respiratory rhythm." *Nature Reviews Neuroscience* 7 (3):232-241.

Feldman, Jack L, Christopher A Del Negro, and Paul A Gray. 2013. "Understanding the rhythm of breathing: so near, yet so far." *Annual review of physiology* 75:423-452.

Feldman, Jack L, and H Gautier. 1976a. "Interaction of pulmonary afferents and pneumotaxic center in control of respiratory pattern in cats." *Journal of neurophysiology* 39 (1):31-44.

Feldman, Jack L, and Sten Grillner. 1983. "Control of vertebrate respiration and locomotion: a brief account." *Physiologist* 26 (5):310.

Feldman, Jack L, and Kaiwen Kam. 2015. "Facing the challenge of mammalian neural microcircuits: taking a few breaths may help." *The Journal of physiology* 593 (1):3-23.

Feldman, JL, CA Connelly, HH Ellenberger, and JC Smith. 1990. "The cardiorespiratory system within the brainstem." *Eur J Neurosci* 3 (suppl):171.

Fencl, V. 1971. "Distribution of H+ and HCO3− in cerebral fluids, Ion Homeostasis of the Brain. TheRegulation of Hydrogen and Potassium Ion Concentrations in Cerebral Intra- and Extracellular Fluids."175–185.

Fencl, V. 1986. "Acid‐Base Balance in Cerebral Fluids." *Handbook of Physiology, The Respiratory System, Control of Breathing*.

Ferreira, Caroline M, Patrícia M de Paula, and Luiz GS Branco. 2004. "Role of L-glutamate in the locus coeruleus of rats in hypoxia-induced hyperventilation and anapyrexia." *Respiratory physiology & neurobiology* 139 (2):157-166.

Filosa, Jessica A, Jay B Dean, and Robert W Putnam. 2002. "Role of intracellular and extracellular pH in the chemosensitive response of rat locus coeruleus neurones." *The Journal of physiology* 541 (2):493-509.

Fiori, Mariana C, Vania Figueroa, Maria E Zoghbi, Juan C Saéz, Luis Reuss, and Guillermo A %J Journal of Biological Chemistry Altenberg. 2012. "Permeation of calcium through purified connexin 26 hemichannels." 287 (48):40826-40834.

Forsberg, David, Zachi Horn, Evangelia Tserga, Erik Smedler, Gilad Silberberg, Yuri Shvarev, Kai Kaila, Per Uhlén, and Eric Herlenius. 2016. "CO2-evoked release of PGE2 modulates sighs and inspiration as demonstrated in brainstem organotypic culture." *Elife* 5:e14170.

Forsberg, David, Thomas Ringstedt, and Eric Herlenius. 2017. "Astrocytes release prostaglandin E2 to modify respiratory network activity." *Elife* 6:e29566.

Forster, H. V., P. Martino, M. Hodges, K. Krause, J. Bonis, S. Davis, and L. Pan. 2008. "The carotid chemoreceptors are a major determinant of ventilatory CO2 sensitivity and of PaCO2

during eupneic breathing." *Adv Exp Med Biol* 605:322-6. doi: 10.1007/978-0-387-73693-8_56.

Fortin, Gilles, and Muriel Thoby-Brisson. 2009. "Embryonic emergence of the respiratory rhythm generator." *Respiratory physiology & neurobiology* 168 (1-2):86-91.

Fukuda, Y., and H. H. Loeschcke. 1979. "A cholinergic mechanism involved in the neuronal excitation by H+ in the respiratory chemosensitive structures of the ventral medulla oblongata of rats in vitro." *Pflugers Arch* 379 (2):125-35.

Förster, Th. 1948. "Zwischenmolekulare energiewanderung und fluoreszenz." *Annalen der physik* 437 (1 – 2):55-75.

Gabriel, Heinz-Dieter, Dirk Jung, Christoph Bützler, Achim Temme, Otto Traub, Elke Winterhager, and Klaus %J The Journal of cell biology Willecke. 1998. "Transplacental uptake of glucose is decreased in embryonic lethal connexin26-deficient mice." 140 (6):1453-1461.

Garg, S. K., D. T. Lioy, S. J. Knopp, and J. M. Bissonnette. 2015. "Conditional depletion of methyl-CpG-binding protein 2 in astrocytes depresses the hypercapnic ventilatory response in mice." *J Appl Physiol (1985)* 119 (6):670-6. doi: 10.1152/japplphysiol.00411.2015.

Gargaglioni, Luciane H, Lynn K Hartzler, and Robert W Putnam. 2010. "The locus coeruleus and central chemosensitivity." *Respiratory physiology & neurobiology* 173 (3):264-273.

Gausas, Roberta E. 2006. "Facial Paralysis: A Comprehensive Approach to Current Management." In *Oculoplastics and Orbit*, 191-204. Springer.

Gemel, Joanna, Virginijus Valiunas, Peter R Brink, and Eric C Beyer. 2004. "Connexin43 and connexin26 form gap junctions, but not heteromeric channels in co-expressing cells." *Journal of cell science* 117 (12):2469-2480.

George, Christopher H, Jonathan M Kendall, and W Howard Evans. 1999. "Intracellular trafficking pathways in the assembly of connexins into gap junctions." *Journal of Biological Chemistry* 274 (13):8678-8685.

Gerido, Dwan A, Adam M DeRosa, Gabriele Richard, and Thomas W White. 2007. "Aberrant hemichannel properties of Cx26 mutations causing skin disease and deafness." *American Journal of Physiology-Cell Physiology* 293 (1):C337-C345.

Gerrits, Peter O, and Gert Holstege. 1996. "Pontine and medullary projections to the nucleus retroambiguus: A wheat germ agglutinin – horseradish peroxidase and autoradiographic tracing study in the cat." *Journal of Comparative Neurology* 373 (2):173-185.

Gestreau, C., D. Heitzmann, J. Thomas, V. Dubreuil, S. Bandulik, M. Reichold, S. Bendahhou, P. Pierson, C. Sterner, J. Peyronnet-Roux, C. Benfriha, I. Tegtmeier, H. Ehnes, M. Georgieff, F. Lesage, J. F. Brunet, C. Goridis, R. Warth, and J. Barhanin. 2010. "Task2 potassium channels set central respiratory CO2 and O2 sensitivity." *Proc Natl Acad Sci U S A* 107 (5):2325-30. doi: 10.1073/pnas.0910059107.

Gogol, E, and N UNWIN. 1986. "GAP JUNCTION STRUCTURE-THE EFFECTS OF DETERGENT TREATMENT AND LATTICE VARIATION." BIOPHYSICAL JOURNAL.

Gomes, Priya, Sangly P Srinivas, Willy Van Driessche, Johan Vereecke, and Bernard Himpens. 2005. "ATP release through connexin hemichannels in corneal endothelial cells." *Investigative Ophthalmology & Visual Science* 46 (4):1208-1218.

González, Daniel, Juan M Gómez-Hernández, and Luis C Barrio. 2006. "Species specificity of mammalian connexin-26 to form open voltage-gated hemichannels." *The FASEB journal* 20 (13):2329-2338.

Goodenough, Daniel A, Jeffrey A Goliger, and David L Paul. 1996. "Connexins, connexons, and intercellular communication." *Annual review of biochemistry* 65 (1):475-502.

Goodenough, Daniel A, and Jean Paul Revel. 1970. "A fine structural analysis of intercellular junctions in the mouse liver." *The Journal of cell biology* 45 (2):272-290.

Gourine, Alexander V, Lucy Atkinson, Jim Deuchars, and K Michael Spyer. 2003. "Purinergic signalling in the medullary mechanisms of respiratory control in the rat: respiratory neurones express the P2X2 receptor subunit." *The Journal of physiology* 552 (1):197-211.

Gourine, Alexander V, Vitaliy Kasymov, Nephtali Marina, Feige Tang, Melina F Figueiredo, Samantha Lane, Anja G Teschemacher, K Michael Spyer, Karl Deisseroth, and Sergey

Kasparov. 2010. "Astrocytes control breathing through pH-dependent release of ATP." *Science* 329 (5991):571-575.

Gourine, Alexander V, Enrique Llaudet, Nicholas Dale, and K Michael Spyer. 2005. "ATP is a mediator of chemosensory transduction in the central nervous system." *Nature* 436 (7047):108-111.

Green, JH, and E Neil. 1955. "The respiratory function of the laryngeal muscles." *The Journal of physiology* 129 (1):134-141.

Gu, Y, WL Di, DP Kelsell, and D Zicha. 2004. "Quantitative fluorescence resonance energy transfer (FRET) measurement with acceptor photobleaching and spectral unmixing." *Journal of microscopy* 215 (2):162-173.

Guyenet, Patrice G, Douglas A Bayliss, Ruth L Stornetta, Marie‐Gabrielle Ludwig, Natasha N Kumar, Yingtang Shi, Peter GR Burke, Roy Kanbar, Tyler M Basting, and Benjamin B %J The Journal of physiology Holloway. 2016. "Proton detection and breathing regulation by the retrotrapezoid nucleus." 594 (6):1529-1551.

Guyenet, Patrice G, Ruth L Stornetta, and Douglas A Bayliss. 2008. "Retrotrapezoid nucleus and central chemoreception." *The Journal of physiology* 586 (8):2043-2048.

Gómez-Hernández, Juan M, Marta de Miguel, Belen Larrosa, Daniel González, and Luis C Barrio. 2003. "Molecular basis of calcium regulation in connexin-32 hemichannels." *Proceedings of the National Academy of Sciences* 100 (26):16030-16035.

Hajnóczky, György, György Csordás, Sudipto Das, Cecilia Garcia-Perez, Masao Saotome, Soumya Sinha Roy, and Muqing %J Cell calcium Yi. 2006. "Mitochondrial calcium signalling and cell death: approaches for assessing the role of mitochondrial Ca2+ uptake in apoptosis." 40 (5-6):553-560.

Haldane, John Scott, and John Gillies Priestley. 1905. "The regulation of the lung-ventilation." *The Journal of physiology* 32 (3-4):225.

Harada, YOSHIO, MOTOY Kuno, and YONG ZHENG Wang. 1985. "Differential effects of carbon dioxide and pH on central chemoreceptors in the rat in vitro." *The Journal of physiology* 368 (1):679-693.

Haraguchi, Tokuko, Takeshi Shimi, Takako Koujin, Noriyo Hashiguchi, and Yasushi Hiraoka. 2002. "Spectral imaging fluorescence microscopy." *Genes to Cells* 7 (9):881-887.

Harper, Ronald M, Hannah C Kinney, Peter J Fleming, and Bradley T Thach. 2000. "Sleep influences on homeostatic functions: implications for sudden infant death syndrome." *Respiration physiology* 119 (2-3):123-132.

Harris, Daniel C. 2010. "Applications of Spectrophotometry." In *Quantitative chemical analysis*, 419-444. WH Freeman New York.

Haruna, Kunitaka, Yasushi Suga, Ami Oizumi, Yuki Mizuno, Hideharu Endo, Toshiaki Shimizu, Toshio Hasegawa, and Shigaku Ikeda. 2010. "Severe form of keratitis–ichthyosis–deafness (KID) syndrome associated with septic complications." *The Journal of dermatology* 37 (7):680-682.

Hassinger, TD, PB Guthrie, PB Atkinson, MVL Bennett, and SB Kater. 1996. "An extracellular signaling component in propagation of astrocytic calcium waves." *Proceedings of the National Academy of Sciences* 93 (23):13268-13273.

Hawkins, Virginia E, Fred W Kolling 4th, Craig E Nelson, and Daniel K Mulkey. 2016. "Conditional knockout of astrocytic Kir4. 1 channels impairs central respiratory drive despite maintaining a subset of Cx26+ astrocytes within the RTN." *The FASEB Journal* 30 (1_supplement):772.13-772.13.

Hawkins, Virginia E, Ana C Takakura, Ashley Trinh, Milene R Malheiros-Lima, Colin M Cleary, Ian C Wenker, Todd Dubreuil, Elliot M Rodriguez, Mark T Nelson, Thiago S Moreira, and Daniel K Mulkey. 2017. "Purinergic regulation of vascular tone in the retrotrapezoid nucleus is specialized to support the drive to breathe." *Elife* 6:e25232.

Hawkins, Virginia, Fushan Kuo, Laura Bellemare, Diana Perez, Todd Dubreuil, and Daniel Mulkey. 2014. "Conditional knockdown of Kir4. 1 in astrocytes blunts the hypercapnic respiratory response in awake mice (872.7)." *The FASEB Journal* 28 (1_supplement):872.7.

Hawkins, Virginia, and Daniel Mulkey. 2015. "Astrocyte Kir4. 1 Channels Contribute to Central Respiratory Drive." *The FASEB Journal* 29 (1_supplement):860.12.

Helms, Volkhard. 2008. ". "Fluorescence Resonance Energy Transfer." In *Principles of computational cell biology*, 202. John Wiley & Sons.

Hennecke, Meike, Marcin Kwissa, Karin Metzger, André Oumard, Andrea Kröger, Reinhold Schirmbeck, Jörg Reimann, and Hansjörg %J Nucleic acids research Hauser. 2001. "Composition and arrangement of genes define the strength of IRES-driven translation in bicistronic mRNAs." 29 (16):3327-3334.

Hernandez, Greco Paula Vazquez-Pianzola, Jose M Sierra, and Rolando J. RNA Rivera-Pomar. 2004. "Internal ribosome entry site drives cap-independent translation of reaper and heat shock protein 70 mRNAs in Drosophila embryos." 10 (11):1783-1797.

Hewitt, Amy, Rachel Barrie, Michael Graham, Kara Bogus, JC Leiter, and Joseph S Erlichman. 2004. "Ventilatory effects of gap junction blockade in the RTN in awake rats." *American Journal of Physiology-Regulatory, Integrative and Comparative Physiology* 287 (6):R1407-R1418.

Heywood, P, K Murphy, DR Corfield, MJ Morrell, RS Howard, and A Guz. 1996. "Control of breathing in man; insights from the 'locked-in'syndrome." *Respiration physiology* 106 (1):13-20.

Hirokawa, Nobutaka, and John Heuser. 1982. "The inside and outside of gap-junction membranes visualized by deep etching." *Cell* 30 (2):395-406.

Hodges, M. R., G. J. Tattersall, M. B. Harris, S. D. McEvoy, D. N. Richerson, E. S. Deneris, R. L. Johnson, Z. F. Chen, and G. B. Richerson. 2008. "Defects in breathing and thermoregulation in mice with near-complete absence of central serotonin neurons." *J Neurosci* 28 (10):2495-505. doi: 10.1523/JNEUROSCI.4729-07.2008.

Hodges, Matthew R, and George B Richerson. 2010. "Medullary serotonin neurons and their roles in central respiratory chemoreception." *Respiratory physiology & neurobiology* 173 (3):256-263.

Holloway, Benjamin B, Kenneth E Viar, Ruth L Stornetta, and Patrice G Guyenet. 2015. "The retrotrapezoid nucleus stimulates breathing by releasing glutamate in adult conscious mice." *European Journal of Neuroscience* 42 (6):2271-2282.

Hooper, Scott L. 2000. "Central pattern generators." *Current Biology* 10 (5):R176-R179.

Hosford, PS, V Mosienko, K Kishi, G Jurisic, K Seuwen, B Kinzel, MG Ludwig, JA Wells, IN Christie, and L Koolen. 2018. "CNS distribution, signalling properties and central effects of G-protein coupled receptor 4." *Neuropharmacology*.

Huang, Yi-Jen, Yutaka Maruyama, Gennady Dvoryanchikov, Elizabeth Pereira, Nirupa Chaudhari, and Stephen D Roper. 2007. "The role of pannexin 1 hemichannels in ATP release and cell–cell communication in mouse taste buds." *Proceedings of the National Academy of Sciences* 104 (15):6436-6441.

Huckstepp, R. T., E. Llaudet, and A. V. Gourine. 2016. "CO2-Induced ATP-Dependent Release of Acetylcholine on the Ventral Surface of the Medulla Oblongata." *PLoS One* 11 (12):e0167861. doi: 10.1371/journal.pone.0167861.

Huckstepp, Robert TR, Kathryn P Cardoza, Lauren E Henderson, and Jack L Feldman. 2015. "Role of parafacial nuclei in control of breathing in adult rats." *The Journal of Neuroscience* 35 (3):1052-1067.

Huckstepp, Robert TR, and Nicholas Dale. 2011. "Redefining the components of central CO2 chemosensitivity–towards a better understanding of mechanism." *The Journal of physiology* 589 (23):5561-5579.

Huckstepp, Robert TR, Robert Eason, Anshu Sachdev, and Nicholas Dale. 2010b. "CO2‐dependent opening of connexin 26 and related β connexins." *The Journal of physiology* 588 (20):3921-3931.

Huckstepp, Robert TR, Lauren E Henderson, Kathryn P Cardoza, and Jack L Feldman. 2016. "Interactions between respiratory oscillators in adult rats." *Elife* 5:e14203.

Huckstepp, Robert TR, Rachid Id Bihi, Robert Eason, K Michael Spyer, Nikolai Dicke, Klaus Willecke, Nephtali Marina, Alexander V Gourine, and Nicholas Dale. 2010a. "Connexin

hemichannel‐mediated CO2‐dependent release of ATP in the medulla oblongata contributes to central respiratory chemosensitivity." *The Journal of physiology* 588 (20):3901-3920.

Huda, R., S. L. Pollema-Mays, Z. Chang, G. F. Alheid, D. R. McCrimmon, and M. Martina. 2012. "Acid-sensing ion channels contribute to chemosensitivity of breathing-related neurons of the nucleus of the solitary tract." *J Physiol* 590 (19):4761-75. doi: 10.1113/jphysiol.2012.232470.

Iyyathurai, Jegan, Catheleyne D'hondt, Nan Wang, Marijke De Bock, Bernard Himpens, Mauricio A Retamal, Jimmy Stehberg, Luc Leybaert, and Geert Bultynck. 2013. "Peptides and peptide-derived molecules targeting the intracellular domains of Cx43: gap junctions versus hemichannels." *Neuropharmacology* 75:491-505.

Janczewski, Wiktor A, and Jack L Feldman. 2006. "Distinct rhythm generators for inspiration and expiration in the juvenile rat." *The Journal of physiology* 570 (2):407-420.

Janecke, Andreas R, Hans Christian Hennies, Barbara Günther, Gabriele Gansl, Josef Smolle, Elisabeth M Messmer, Gerd Utermann, and Olaf Rittinger. 2005. "GJB2 mutations in keratitis‐ichthyosis‐deafness syndrome including its fatal form." *American Journal of Medical Genetics Part A* 133 (2):128-131.

Johnson, Shereé M, Naohiro Koshiya, and Jeffrey C Smith. 2001. "Isolation of the kernel for respiratory rhythm generation in a novel preparation: the pre-Botzinger complex “island”." *Journal of neurophysiology* 85 (4):1772-1776.

Jäderstad, Johan, Linda M Jäderstad, Jianxue Li, Satyan Chintawar, Carmen Salto, Massimo Pandolfo, Vaclav Ourednik, Yang D Teng, Richard L Sidman, and Ernest Arenas. 2010. "Communication via gap junctions underlies early functional and beneficial interactions between grafted neural stem cells and the host." *Proceedings of the National Academy of Sciences* 107 (11):5184-5189.

Jäkel, Sarah, and Leda Dimou. 2017. "Glial cells and their function in the adult brain: a journey through the history of their ablation." *Frontiers in cellular neuroscience* 11:24.

Kam, Kaiwen, Jason W Worrell, Wiktor A Janczewski, Yan Cui, and Jack L Feldman. 2013. "Distinct inspiratory rhythm and pattern generating mechanisms in the preBötzinger complex." *Journal of Neuroscience* 33 (22):9235-9245.

Kamermans, Maarten, Iris Fahrenfort, Konrad Schultz, Ulrike Janssen-Bienhold, Trijntje Sjoerdsma, and Reto Weiler. 2001. "Hemichannel-mediated inhibition in the outer retina." *Science* 292 (5519):1178-1180.

Kanamaru, M, and I Homma. 2007. "Effects of CO2 inhalation on 5-HT release in the dorso-medial medulla oblongata in infant." *Neuroscience Research* 58:S162–S162

Kanaporis, Giedrius, Peter R Brink, and Virginijus Valiunas. 2010. "Gap junction permeability: selectivity for anionic and cationic probes." *American Journal of Physiology-Cell Physiology* 300 (3):C600-C609.

Kasymov, V., O. Larina, C. Castaldo, N. Marina, M. Patrushev, S. Kasparov, and A. V. Gourine. 2013. "Differential sensitivity of brainstem versus cortical astrocytes to changes in pH reveals functional regional specialization of astroglia." *J Neurosci* 33 (2):435-41. doi: 10.1523/JNEUROSCI.2813-12.2013.

Katsura, K., B. Asplund, A. Ekholm, and B. K. Siesjö. 1992b. "Extra- and Intracellular pH in the Brain During Ischaemia, Related to Tissue Lactate Content in Normo- and Hypercapnic rats." *Eur J Neurosci* 4 (2):166-176.

Katsura, K., A. Ekholm, and B. K. Siesjö. 1992a. "Tissue PCO2 in brain ischemia related to lactate content in normo- and hypercapnic rats." *J Cereb Blood Flow Metab* 12 (2):270-80. doi: 10.1038/jcbfm.1992.37.

Kawai, A, D Ballantyne, K Mückenhoff, and P Scheid. 1996. "Chemosensitive medullary neurones in the brainstem‐‐spinal cord preparation of the neonatal rat." *The Journal of Physiology* 492 (1):277-292.

Kawai, Akira, Hiroshi Onimaru, and Ikuo Homma. 2006. "Mechanisms of CO2/H+ chemoreception by respiratory rhythm generator neurons in the medulla from newborn rats in vitro." *The Journal of physiology* 572 (2):525-537.

Kelly, Brent, Annabelle Lozano, Guillermo Altenberg, and Tomoko Makishima. 2008. "Connexin 26 mutation in keratitis–ichthyosis–deafness (KID) syndrome in mother and daughter with combined conductive and sensorineural hearing loss." *International journal of dermatology* 47 (5):443-447.

Kelsell, David P, John Dunlop, Howard P Stevens, Nicholas J Lench, JN Liang, Gareth Parry, Robert F Mueller, and Irene M Leigh. 1997. "Connexin 26 mutations in hereditary non-syndromic sensorineural deafness." *Nature* 387 (6628):80.

Kenworthy, Anne K, Nadezda Petranova, and Michael Edidin. 2000. "High-resolution FRET microscopy of cholera toxin B-subunit and GPI-anchored proteins in cell plasma membranes." *Molecular biology of the cell* 11 (5):1645-1655.

Kettenmann, H, and A Verkhratsky. 2016. "Glial cells: neuroglia." In *Neuroscience in the 21st Century: From Basic to Clinical*, 547-578.

Kinney, Hannah C, and Bradley T Thach. 2009. "The sudden infant death syndrome." *New England Journal of Medicine* 361 (8):795-805.

Kniggendorf, Ann-Kathrin, Merve Meinhardt-Wollweber, Xiaogang Yuan, Bernhard Roth, Astrid Seifert, Niels Fertig, and Carsten Zeilinger. 2014. "Temperature-sensitive gating of hCx26: high-resolution Raman spectroscopy sheds light on conformational changes." *Biomedical optics express* 5 (7):2054-2065.

Koizumi, Hidehiko, Stanley E Smerin, Tadashi Yamanishi, Bindiya R Moorjani, Ruli Zhang, and Jeffrey C Smith. 2010. "TASK channels contribute to the K+-dominated leak current regulating respiratory rhythm generation in vitro." *Journal of Neuroscience* 30 (12):4273-4284.

Koizumi, Hidehiko, Christopher G Wilson, Stephen Wong, Tadashi Yamanishi, Naohiro Koshiya, and Jeffrey C Smith. 2008. "Functional imaging, spatial reconstruction, and biophysical analysis of a respiratory motor circuit isolated in vitro." *Journal of Neuroscience* 28 (10):2353-2365.

Kojima, Takashi, Miduturu Srinivas, Alfredo Fort, Mathew Hopperstad, Marcia Urban, Elliot L Hertzberg, Yohichi Mochizuki, and David C Spray. 2001. "TPA induced expression and function of human connexin 26 by post-translational mechanisms in stably transfected neuroblastoma cells." *Cell structure and function* 24 (6):435-441.

Koppelhus, Uffe, L Tranebjaerg, Gitte Esberg, M Ramsing, Marianne Lodahl, Nanna Dahl Rendtorff, Hanne Vebert Olesen, and M Sommerlund. 2011. "A novel mutation in the connexin 26 gene (GJB2) in a child with clinical and histological features of keratitis–ichthyosis–deafness (KID) syndrome." *Clinical and experimental dermatology* 36 (2):142-148.

Korsak, Alla, Shahriar Sheikhbahaei, Asif Machhada, Alexander V Gourine, and Robert TR %J Scientific reports Huckstepp. 2018. "the Role of parafacial Neurons In the Control of Breathing During exercise." 8 (1):400.

Koval, Michael, Samuel A Molina, and Janis M Burt. 2014. "Mix and match: investigating heteromeric and heterotypic gap junction channels in model systems and native tissues." *FEBS letters* 588 (8):1193-1204.

Krause, Katie Lynn, Hubert V Forster, Suzanne E Davis, Thomas Kiner, Joshua M Bonis, Lawrence G Pan, and Baogang Qian. 2009. "Focal acidosis in the pre-Botzinger complex area of awake goats induces a mild tachypnea." *Journal of Applied Physiology* 106 (1):241-250.

Kubin, L. 1994. "Central pathways of pulmonary and airway vagal afferents." *Regulation of breathing*:219-284.

Kubo, T, M Kihara, and Y Misu. 1989. "Altered amino acid levels in brainstem regions of spontaneously hypertensive rats." *Clinical and Experimental Hypertension. Part A: Theory and Practice* 11 (2):233-241.

Kumar, Nalin M, and Norton B Gilula. 1996. "The gap junction communication channel." *Cell* 84 (3):381-388.

Kumar, Natasha N, Ana Velic, Jorge Soliz, Yingtang Shi, Keyong Li, Sheng Wang, Janelle L Weaver, Josh Sen, Stephen BG Abbott, and Roman M Lazarenko. 2015. "Regulation of breathing

by CO2 requires the proton-activated receptor GPR4 in retrotrapezoid nucleus neurons." *Science* 348 (6240):1255-1260.

Kur, Joanna, and Eric A Newman. 2014. "Purinergic control of vascular tone in the retina." *The Journal of physiology* 592 (3):491-504.

Lam, Amy J, François St-Pierre, Yiyang Gong, Jesse D Marshall, Paula J Cranfill, Michelle A Baird, Michael R McKeown, Jörg Wiedenmann, Michael W Davidson, and Mark J Schnitzer. 2012. "Improving FRET dynamic range with bright green and red fluorescent proteins." *Nature methods* 9 (10):1005-1012.

Lamb, Thomas W. 1966. "Ventilatory responses to intravenous and inspired carbon dioxide in anesthetized cats." *Respiration physiology* 2 (1):99-104.

Lansford, Rusty, Gregory H Bearman, and Scott E Fraser. 2001. "Resolution of multiple GFP color variants and dyes using two-photon microscopy and imaging spectroscopy." *Journal of biomedical optics* 6 (3):311-319.

Larnicol, N., F. Wallois, P. Berquin, F. Gros, and D. Rose. 1994. "c-fos-like immunoreactivity in the cat's neuraxis following moderate hypoxia or hypercapnia." *J Physiol Paris* 88 (1):81-8.

Lazic, Tamara, Kimberly A Horii, Gabriele Richard, Daniel I Wasserman, and Richard J Antaya. 2008. "A report of GJB2 (N14K) Connexin 26 mutation in two patients—a new subtype of KID syndrome?" *Pediatric dermatology* 25 (5):535-540.

Lee, Jack R, Adam M DeRosa, and Thomas W White. 2009. "Connexin mutations causing skin disease and deafness increase hemichannel activity and cell death when expressed in Xenopus oocytes." *Journal of Investigative Dermatology* 129 (4):870-878.

Leinonen, Pekka, Vesa Aaltonen, Sanna Koskela, Petri Lehenkari, Timo Korkiamäki, and Juha Peltonen. 2007. "Impaired gap junction formation and intercellular calcium signaling in urinary bladder cancer cells can be improved by Gö6976." *Cell communication & adhesion* 14 (4):125-136.

Leitch, Beulah. 1992. "Ultrastructure of electrical synapses." *Electron microscopy reviews* 5 (2):311-339.

Leusen, IR. 1953a. "Chemosensitivity of the respiratory center: Influence of CO2 in the cerebral ventricles on respiration." *American Journal of Physiology-Legacy Content* 176 (1):39-44.

Leusen, IR. 1953b. "Chemosensitivity of the respiratory center: Influence of changes in the H+ and total buffer concentrations in the cerebral ventricles on respiration." *American Journal of Physiology-Legacy Content* 176 (1):45-51.

Levit, Noah A, Caterina Sellitto, Hong-Zhan Wang, Leping Li, Miduturu Srinivas, Peter R Brink, and Thomas W White. 2015. "Aberrant Connexin26 Hemichannels Underlying Keratitis–Ichthyosis–Deafness Syndrome Are Potently Inhibited by Mefloquine." *Journal of Investigative Dermatology* 135 (4):1033-1042.

Levit, Noah A, and Thomas W White. 2015. "Connexin hemichannels influence genetically determined inflammatory and hyperproliferative skin diseases." *Pharmacological research* 99:337-343.

Li, A., and E. Nattie. 2008. "Serotonin transporter knockout mice have a reduced ventilatory response to hypercapnia (predominantly in males) but not to hypoxia." *J Physiol* 586 (9):2321-9. doi: 10.1113/jphysiol.2008.152231.

Li, Aihua, Margaret Randall, and Eugene E Nattie. 1999. "CO2 microdialysis in retrotrapezoid nucleus of the rat increases breathing in wakefulness but not in sleep." *Journal of Applied Physiology* 87 (3):910-919.

Li, Aihua, Shawn Zhou, and Eugene Nattie. 2006. "Simultaneous inhibition of caudal medullary raphe and retrotrapezoid nucleus decreases breathing and the CO2 response in conscious rats." *The Journal of physiology* 577 (1):307-318.

Li, Haiying, Tai-Feng Liu, Ahmed Lazrak, Camillo Peracchia, Gary S Goldberg, Paul D Lampe, and Ross G Johnson. 1996. "Properties and regulation of gap junctional hemichannels in the plasma membranes of cultured cells." *The Journal of cell biology* 134 (4):1019-1030.

Lilly, Evelyn, Caterina Sellitto, Leonard M Milstone, and Thomas W White. 2016. "Connexin channels in congenital skin disorders." Seminars in cell & developmental biology.

Lippincott-Schwartz, Jennifer, Erik Snapp, and Anne Kenworthy. 2001. "Studying protein dynamics in living cells." *Nature reviews Molecular cell biology* 2 (6):444.

Locke, Darren, Fabien Kieken, Liang Tao, Paul L Sorgen, and Andrew L Harris. 2011. "Mechanism for modulation of gating of connexin26-containing channels by taurine." *The Journal of general physiology* 138 (3):321-339.

Lodish, Harvey, Arnold Berk, James E Darnell, Chris A Kaiser, Monty Krieger, Matthew P Scott, Anthony Bretscher, Hidde Ploegh, and Paul Matsudaira. 2008. *Molecular cell biology*: Macmillan.

Loeschcke, Hans H. 1982. "Central chemosensitivity and the reaction theory." *The Journal of Physiology* 332 (1):1-24.

Loeschcke, HH, J De Lattre, ME Schläfke, and CO Trouth. 1970. "Effects on respiration and circulation of electrically stimulating the ventral surface of the medulla oblongata." *Respiration physiology* 10 (2):184-197.

Lopez, William, Jayalakshmi Ramachandran, Abdelaziz Alsamarah, Yun Luo, Andrew L Harris, and Jorge E Contreras. 2016. "Mechanism of gating by calcium in connexin hemichannels." *Proceedings of the National Academy of Sciences* 113 (49):E7986-E7995.

Lorier, Amanda R, Adrianne G Huxtable, Dean M Robinson, Janusz Lipski, Gary D Housley, and Gregory D Funk. 2007. "P2Y1 receptor modulation of the pre-Bötzinger complex inspiratory rhythm generating network in vitro." *Journal of Neuroscience* 27 (5):993-1005.

Ludwig, M. G., M. Vanek, D. Guerini, J. A. Gasser, C. E. Jones, U. Junker, H. Hofstetter, R. M. Wolf, and K. Seuwen. 2003. "Proton-sensing G-protein-coupled receptors." *Nature* 425 (6953):93-8. doi: 10.1038/nature01905.

Maeda, Shoji, So Nakagawa, Michihiro Suga, Eiki Yamashita, Atsunori Oshima, Yoshinori Fujiyoshi, and Tomitake Tsukihara. 2009. "Structure of the connexin 26 gap junction channel at 3.5 Å resolution." *Nature* 458 (7238):597-602.

Makowski, Lee. 1988. "X-ray diffraction studies of gap junction structure." In *Advances in Molecular and Cell Biology*, 119-158. Elsevier.

Makowski, Lee, DLD Caspar, WC Phillips, and DA Goodenough. 1984. "Gap junction structures: V. Structural chemistry inferred from X-ray diffraction measurements on sucrose accessibility and trypsin susceptibility." *Journal of molecular biology* 174 (3):449-481.

Malmersjö, Seth, Paola Rebellato, Erik Smedler, Henrike Planert, Shigeaki Kanatani, Isabel Liste, Evanthia Nanou, Hampus Sunner, Shaimaa Abdelhady, and Songbai Zhang. 2013. "Neural progenitors organize in small-world networks to promote cell proliferation." *Proceedings of the National Academy of Sciences*:201220179.

Marina, Nephtali, Ana P Abdala, Stefan Trapp, Aihua Li, Eugene E Nattie, James Hewinson, Jeffrey C Smith, Julian FR Paton, and Alexander V Gourine. 2010. "Essential role of Phox2b-expressing ventrolateral brainstem neurons in the chemosensory control of inspiration and expiration." *Journal of Neuroscience* 30 (37):12466-12473.

Martin, Patricia EM, Geraldine Blundell, Shoeb Ahmad, Rachel J Errington, and W Howard Evans. 2001. "Multiple pathways in the trafficking and assembly of connexin 26, 32 and 43 into gap junction intercellular communication channels." *Journal of cell science* 114 (21):3845-3855.

Martineau, Yvan, Christine Le Bec, Laurent Monbrun, Valérie Allo, Ming Chiu, Olivier Danos, Hervé Moine, Hervé Prats, and Anne-Catherine %J Molecular and cellular biology Prats. 2004. "Internal ribosome entry site structural motifs conserved among mammalian fibroblast growth factor 1 alternatively spliced mRNAs." 24 (17):7622-7635.

Marziano, Nerissa K, Stefano O Casalotti, Anne E Portelli, David L Becker, and Andrew Forge. 2003. "Mutations in the gene for connexin 26 (GJB2) that cause hearing loss have a dominant negative effect on connexin 30." *Human molecular genetics* 12 (8):805-812.

Massey, C. A., K. E. Iceman, S. L. Johansen, Y. Wu, M. B. Harris, and G. B. Richerson. 2015. "Isoflurane abolishes spontaneous firing of serotonin neurons and masks their pH/CO_2 chemosensitivity." *J Neurophysiol* 113 (7):2879-88. doi: 10.1152/jn.01073.2014.

Matyash, V., and H. Kettenmann. 2010. "Heterogeneity in astrocyte morphology and physiology." *Brain Res Rev* 63 (1-2):2-10. doi: 10.1016/j.brainresrev.2009.12.001.

Mazereeuw‐Hautier, J, E Bitoun, J Chevrant‐Breton, SYK Man, C Bodemer, C Prins, C Antille, J‐H Saurat, D Atherton, and JI Harper. 2007. "Keratitis‐ichthyosis‐deafness syndrome: disease expression and spectrum of connexin 26 (GJB2) mutations in 14 patients." *British Journal of Dermatology* 156 (5):1015-1019.

McNamara, George, Jeffrey Larson, Stanley Schwartz, and Micheal Davidson. 2017. "Spectral Imaging and Linear Unmixing." 2017 Nikon Instruments Inc., accessed 9th April.

Meigh, Louise. 2015a. "CO2 carbamylation of proteins as a mechanism in physiology." *Biochemical Society Transactions* 43 (3):460-464.

Meigh, Louise, Daniel Cook, Jie Zhang, and Nicholas Dale. 2015b. "Rational design of new NO and redox sensitivity into connexin26 hemichannels." *Open biology* 5 (2):140208.

Meigh, Louise, Sophie A Greenhalgh, Thomas L Rodgers, Martin J Cann, David I Roper, and Nicholas Dale. 2013. "CO2 directly modulates connexin 26 by formation of carbamate bridges between subunits." *Elife* 2:e01213.

Meigh, Louise, Naveed Hussain, Daniel K Mulkey, and Nicholas Dale. 2014. "Connexin26 hemichannels with a mutation that causes KID syndrome in humans lack sensitivity to CO2." *Elife* 3:e04249.

Mellen, Nicholas M, Wiktor A Janczewski, Christopher M Bocchiaro, and Jack L Feldman. 2003. "Opioid-induced quantal slowing reveals dual networks for respiratory rhythm generation." *Neuron* 37 (5):821-826.

Mercier, Frederic, and Glenn I Hatton. 2001. "Connexin 26 and basic fibroblast growth factor are expressed primarily in the subpial and subependymal layers in adult brain parenchyma: roles in stem cell proliferation and morphological plasticity?" *Journal of Comparative Neurology* 431 (1):88-104.

Messier, Michelle L, Aihua Li, and Eugene E Nattie. 2004. "Inhibition of medullary raphe serotonergic neurons has age-dependent effects on the CO2 response in newborn piglets." *Journal of Applied Physiology* 96 (5):1909-1919.

Mhaske, Pallavi V, Noah A Levit, Leping Li, Hong-Zhan Wang, Jack R Lee, Zunaira Shuja, Peter R Brink, and Thomas W White. 2013. "The human Cx26-D50A and Cx26-A88V mutations causing keratitis-ichthyosis-deafness syndrome display increased hemichannel activity." *American Journal of Physiology-Cell Physiology* 304 (12):C1150-C1158.

Minta, Akwasi, JP Kao, and Roger Y Tsien. 1989. "Fluorescent indicators for cytosolic calcium based on rhodamine and fluorescein chromophores." *Journal of Biological Chemistry* 264 (14):8171-8178.

Mishra, Shivani, Himani Pandey, Priyanka Srivastava, Kausik Mandal, and Shubha R Phadke. 2018. "Connexin 26 (GJB2) Mutations Associated with Non-Syndromic Hearing Loss (NSHL)." *The Indian Journal of Pediatrics*:1-6.

Mitchell, RA, HH Loeschcke, WH Massion, and JW Severinghaus. 1963b. "Respiratory responses mediated through superficial chemosensitive areas on the medulla." *Journal of Applied Physiology* 18 (3):523-533.

Mitchell, RA, HH Loeschcke, JW Severinghaus, BW Richardson, and WH Massion. 1963a. "Regions of respiratory chemosensitivity on the surface of the medulla." *Annals of the New York Academy of Sciences* 109 (2):661-681.

Mizuguchi, Hiroyuki, Zhili Xu, Akiko Ishii-Watabe, Eriko Uchida, and Takao %J Molecular Therapy Hayakawa. 2000. "IRES-dependent second gene expression is significantly lower than cap-dependent first gene expression in a bicistronic vector." 1 (4):376-382.

Montgomery, Jay R, Thomas W White, Bryan L Martin, Maria L Turner, and Steven M Holland. 2004. "A novel connexin 26 gene mutation associated with features of the keratitis-ichthyosis-deafness syndrome and the follicular occlusion triad." *Journal of the American Academy of Dermatology* 51 (3):377-382.

Moore, Jeffrey D, Martin Deschênes, Takahiro Furuta, Daniel Huber, Matthew C Smear, Maxime Demers, and David Kleinfeld. 2013. "Hierarchy of orofacial rhythms revealed through whisking and breathing." *Nature* 497 (7448):205.

Moore, Jeffrey D, David Kleinfeld, and Fan Wang. 2014. "How the brainstem controls orofacial behaviors comprised of rhythmic actions." *Trends in neurosciences* 37 (7):370-380.

Moreira, Thiago S, Cleyton R Sobrinho, Ian C Wenker, Daniel K Mulkey, and Ana C Takakura. 2013. Purinergic signaling in the retrotrapezoid nucleus (RTN) contributes to central and peripheral chemoreflexes by divergent mechansims. Federation of American Societies for Experimental Biology.

Moreira, Thiago S, Ian C Wenker, Cleyton R Sobrinho, Barbara F Barna, Ana C Takakura, and Daniel K Mulkey. 2015. "Independent purinergic mechanisms of central and peripheral chemoreception in the rostral ventrolateral medulla." *The Journal of physiology* 593 (5):1067-1074.

Mulkey, D. K., E. M. Talley, R. L. Stornetta, A. R. Siegel, G. H. West, X. Chen, N. Sen, A. M. Mistry, P. G. Guyenet, and D. A. Bayliss. 2007. "TASK channels determine pH sensitivity in select respiratory neurons but do not contribute to central respiratory chemosensitivity." *J Neurosci* 27 (51):14049-58. doi: 10.1523/JNEUROSCI.4254-07.2007.

Mulkey, Daniel K, Akshitkumar M Mistry, Patrice G Guyenet, and Douglas A Bayliss. 2006. "Purinergic P2 receptors modulate excitability but do not mediate pH sensitivity of RTN respiratory chemoreceptors." *Journal of Neuroscience* 26 (27):7230-7233.

Mulkey, Daniel K, Ruth L Stornetta, Matthew C Weston, Johnny R Simmons, Anson Parker, Douglas A Bayliss, and Patrice G Guyenet. 2004. "Respiratory control by ventral surface chemoreceptor neurons in rats." *Nature neuroscience* 7 (12):1360-1369.

Mulkey, Daniel K, and Ian C Wenker. 2011. "Astrocyte chemoreceptors: mechanisms of H+ sensing by astrocytes in the retrotrapezoid nucleus and their possible contribution to respiratory drive." *Experimental physiology* 96 (4):400-406.

Mörschel, Michael, and Mathias Dutschmann. 2009. "Pontine respiratory activity involved in inspiratory/expiratory phase transition." *Philosophical Transactions of the Royal Society of London B: Biological Sciences* 364 (1529):2517-2526.

Müller, Daniel J, Galen M Hand, Andreas Engel, and Gina E Sosinsky. 2002. "Conformational changes in surface structures of isolated connexin 26 gap junctions." *The EMBO journal* 21 (14):3598-3607.

Nagy, James I, Andrei V Ionescu, Bruce D Lynn, and John E Rash. 2003. "Connexin29 and connexin32 at oligodendrocyte and astrocyte gap junctions and in myelin of the mouse central nervous system." *Journal of Comparative Neurology* 464 (3):356-370.

Nagy, James I, Xinbo Li, Jeremy Rempel, Gerald Stelmack, Daywin Patel, William A Staines, Thomas Yasumura, and John E Rash. 2001. "Connexin26 in adult rodent central nervous system: demonstration at astrocytic gap junctions and colocalization with connexin30 and connexin43." *Journal of Comparative Neurology* 441 (4):302-323.

Nagy, JI, BD Lynn, O Tress, K Willecke, and JE Rash. 2011. "Connexin26 expression in brain parenchymal cells demonstrated by targeted connexin ablation in transgenic mice." *European Journal of Neuroscience* 34 (2):263-271.

Nattie, E. 1999. "CO2, brainstem chemoreceptors and breathing." *Progress in neurobiology* 59 (4):299-331.

Nattie, Eugene E, and Aihua Li. 2002. "CO2 dialysis in nucleus tractus solitarius region of rat increases ventilation in sleep and wakefulness." *Journal of applied physiology* 92 (5):2119-2130.

Nattie, Eugene, and Aihua Li. 2012. "Central chemoreceptors: locations and functions." *Comprehensive Physiology*.

Neher, Erwin, and Takeshi %J Neuron Sakaba. 2008. "Multiple roles of calcium ions in the regulation of neurotransmitter release." 59 (6):861-872.

Neubauer, Judith A, and Jagadeeshan Sunderram. 2004. "Oxygen-sensing neurons in the central nervous system." *Journal of Applied Physiology* 96 (1):367-374.

Neul, JL, WE Kaufmann, DG Glaze, J Christodoulou, AJ Clarke, N Bahi-Buisson, H Leonard, ME Bailey, NC Schanen, M Zappella, A Renieri, P Huppke, and AK Percy. 2010. "Rett syndrome: revised diagnostic criteria and nomenclature." *Ann Neurol* (68(6)):944-50

Nichols, Nicole L, Lynn K Hartzler, Susan C Conrad, Jay B Dean, and Robert W Putnam. 2008. "Intrinsic chemosensitivity of individual nucleus tractus solitarius (NTS) and locus coeruleus (LC) neurons from neonatal rats." In *Integration in Respiratory Control*, 348-352. Springer.

Nicholson, B, R Dermietzel, D Teplow, O Traub, K Willecke, and J-P Revel. 1987. "Two homologous protein components of hepatic gap junctions." *Nature* 329 (6141):732.

Núñez-Abades, Pedro A, Ana M Morillo, and Rosario Pásaro. 1993. "Brainstem connections of the rat ventral respiratory subgroups: afferent projections." *Journal of the autonomic nervous system* 42 (2):99-118.

Ohtake, P. J., H. V. Forster, L. G. Pan, T. F. Lowry, M. J. Korducki, and A. A. Whaley. 1996. "Effects of cooling the ventrolateral medulla on diaphragm activity during NREM sleep." *Respir Physiol* 104 (2-3):127-35.

Okada, Yasumasa, Zibin Chen, Wuhan Jiang, Shun-Ichi Kuwana, and Frederic L Eldridge. 2002. "Anatomical arrangement of hypercapnia-activated cells in the superficial ventral medulla of rats." *Journal of Applied Physiology* 93 (2):427-439.

Okada, Yasumasa, Zibin Chen, and Shun-ichi Kuwana. 2001. "Cytoarchitecture of central chemoreceptors in the mammalian ventral medulla." *Respiration physiology* 129 (1-2):13-23.

Oku, Yoshitaka, Haruko Masumiya, and Yasumasa Okada. 2007. "Postnatal developmental changes in activation profiles of the respiratory neuronal network in the rat ventral medulla." *The Journal of physiology* 585 (1):175-186.

Olsen, Michelle L, and Harald Sontheimer. 2008. "Functional implications for Kir4. 1 channels in glial biology: from K+ buffering to cell differentiation." *Journal of neurochemistry* 107 (3):589-601.

Onodera, Makoto, Tomoyuki Kuwaki, Mamoru Kumada, and Yoshiaki %J The Japanese journal of physiology Masuda. 1997. "Determination of ventilatory volume in mice by whole body plethysmography." 47 (4):317-326.

Orellana, Juan A, Rommy von Bernhardi, Christian Giaume, and Juan C Sáez. 2012. "Glial hemichannels and their involvement in aging and neurodegenerative diseases." *Reviews in the neurosciences* 23 (2):163-177.

Oshima, Atsunori, Tomohiro Matsuzawa, Kouki Nishikawa, and Yoshinori Fujiyoshi. 2013. "Oligomeric structure and functional characterization of Caenorhabditis elegans Innexin-6 gap junction protein." *Journal of Biological Chemistry* 288 (15):10513-10521.

Osten, Pavel, Tanjew Dittgen, and Pawel Licznerski. 2006. "The dynamic synapse: molecular methods in ionotropic receptor biology." In.: CRC Press.

Pace, R. W., D. D. Mackay, J. L. Feldman, and C. A. Del Negro. 2007. "Role of persistent sodium current in mouse preBötzinger Complex neurons and respiratory rhythm generation." *J Physiol* 580 (Pt. 2):485-96. doi: 10.1113/jphysiol.2006.124602.

Pagliardini, Silvia, Wiktor A Janczewski, Wenbin Tan, Clayton T Dickson, Karl Deisseroth, and Jack L Feldman. 2011. "Active expiration induced by excitation of ventral medulla in adult anesthetized rats." *The Journal of Neuroscience* 31 (8):2895-2905.

Pan, LG, HV Forster, P Martino, PJ Strecker, J Beales, A Serra, TF Lowry, MM Forster, and AL Forster. 1998. "Important role of carotid afferents in control of breathing." *Journal of Applied Physiology* 85 (4):1299-1306.

Paterson, David S, Gerard Hilaire, and Debra E Weese-Mayer. 2009. "Medullary serotonin defects and respiratory dysfunction in sudden infant death syndrome." *Respiratory physiology & neurobiology* 168 (1-2):133-143.

Pearson, Rachael A, Nicholas Dale, Enrique Llaudet, and Peter Mobbs. 2005. "ATP released via gap junction hemichannels from the pigment epithelium regulates neural retinal progenitor proliferation." *Neuron* 46 (5):731-744.

Peppiatt, Claire M, Clare Howarth, Peter Mobbs, and David Attwell. 2006. "Bidirectional control of CNS capillary diameter by pericytes." *Nature* 443 (7112):700.

Pessia, Mauro, Stephen J Tucker, Kevin Lee, Chris T Bond, and John P Adelman. 1996. "Subunit positional effects revealed by novel heteromeric inwardly rectifying K+ channels." *The EMBO journal* 15 (12):2980-2987.

Petersen, MB, and PJ Willems. 2006. "Non‐syndromic, autosomal‐recessive deafness." *Clinical genetics* 69 (5):371-392.

Phillipson, ELIOT A, JAMES Duffin, and JOEL D Cooper. 1981. "Critical dependence of respiratory rhythmicity on metabolic CO2 load." *Journal of Applied Physiology* 50 (1):45-54.

Pocock, Gillian, Christopher D Richards, David Richards, and David A Richards. 2013. *Human physiology*: Oxford university press.

Poon, Chi-Sang, and Gang Song. 2017. "The Norepinephrine-dependent 'Postinspiratory Complex'is NOT an Autonomous Generator of the Postinspiratory Rhythm." *The FASEB Journal* 31 (1_supplement):729.2-729.2.

Powell, Frank L, B Cindy Kim, S Randall Johnson, and Zhenxing Fu. 2009. "Oxygen sensing in the brain–invited article." In *Arterial Chemoreceptors*, 369-376. Springer.

Prabhakar, Nanduri R. 2006. "O2 sensing at the mammalian carotid body: why multiple O2 sensors and multiple transmitters?" *Experimental physiology* 91 (1):17-23.

Ptak, K., T. Yamanishi, J. Aungst, L. S. Milescu, R. Zhang, G. B. Richerson, and J. C. Smith. 2009. "Raphé neurons stimulate respiratory circuit activity by multiple mechanisms via endogenously released serotonin and substance P." *J Neurosci* 29 (12):3720-37. doi: 10.1523/JNEUROSCI.5271-08.2009.

Punjabi, Naresh M. 2008. "The epidemiology of adult obstructive sleep apnea." *Proceedings of the American Thoracic Society* 5 (2):136-143.

Ramanantsoa, Nelina, Marie-Rose Hirsch, Muriel Thoby-Brisson, Véronique Dubreuil, Julien Bouvier, Pierre-Louis Ruffault, Boris Matrot, Gilles Fortin, Jean-François Brunet, and Jorge Gallego. 2011. "Breathing without CO2 chemosensitivity in conditional Phox2b mutants." *Journal of Neuroscience* 31 (36):12880-12888.

Ramirez, J. M., C. S. Ward, and J. L. Neul. 2013. "Breathing challenges in Rett syndrome: lessons learned from humans and animal models." *Respir Physiol Neurobiol* 189 (2):280-7. doi: 10.1016/j.resp.2013.06.022.

Rash, John E, Naomi Kamasawa, Kimberly GV Davidson, Thomas Yasumura, Alberto E Pereda, and James I Nagy. 2012. "Connexin composition in apposed gap junction hemiplaques revealed by matched double-replica freeze-fracture replica immunogold labeling." *The Journal of membrane biology* 245 (5-6):333-344.

Ray, Russell S, Andrea E Corcoran, Rachael D Brust, Jun Chul Kim, George B Richerson, Eugene Nattie, and Susan M Dymecki. 2011. "Impaired respiratory and body temperature control upon acute serotonergic neuron inhibition." *Science* 333 (6042):637-642.

Revel, JP, and M_J Karnovsky. 1967. "Hexagonal array of subunits in intercellular junctions of the mouse heart and liver." *The Journal of cell biology* 33 (3):C7.

Richerson, G. B., W. Wang, M. R. Hodges, C. I. Dohle, and A. Diez-Sampedro. 2005. "Homing in on the specific phenotype(s) of central respiratory chemoreceptors." *Exp Physiol* 90 (3):259-66; discussion 266-9. doi: 10.1113/expphysiol.2005.029843.

Richerson, George B. 2004. "Serotonergic neurons as carbon dioxide sensors that maintain pH homeostasis." *Nature Reviews Neuroscience* 5 (6):449.

Richter, DW. 1996. "Neural regulation of respiration: rhythmogenesis and afferent control." In *Comprehensive human physiology*, 2079-2095. Springer.

Robertson, J David. 1963. "The occurrence of a subunit pattern in the unit membranes of club endings in Mauthner cell synapses in goldfish brains." *The Journal of cell biology* 19 (1):201-221.

Rosin, Diane L, Darryl A Chang, and Patrice G Guyenet. 2006. "Afferent and efferent connections of the rat retrotrapezoid nucleus." *Journal of Comparative Neurology* 499 (1):64-89.

Sanchez, Helmuth A, Rick Bienkowski, Nefeli Slavi, Miduturu Srinivas, and Vytas K Verselis. 2014. "Altered inhibition of Cx26 hemichannels by pH and Zn2+ in the A40V mutation associated with keratitis-ichthyosis-deafness syndrome." *Journal of Biological Chemistry*:jbc. M114. 578757.

Sanchez, Helmuth A, Nefeli Slavi, Miduturu Srinivas, and Vytas K Verselis. 2016. "Syndromic deafness mutations at Asn 14 differentially alter the open stability of Cx26 hemichannels." *The Journal of general physiology* 148 (1):25-42.

Sanchez, Helmuth A, and Vytas K Verselis. 2014. "Aberrant Cx26 hemichannels and keratitis-ichthyosis-deafness syndrome: insights into syndromic hearing loss." *Frontiers in cellular neuroscience* 8:354.

Sato, M, JOHN W Severinghaus, and ALLAN I Basbaum. 1992. "Medullary CO2 chemoreceptor neuron identification by c-fos immunocytochemistry." *Journal of Applied Physiology* 73 (1):96-100.

Sbidian, E, D Feldmann, J Bengoa, S Fraitag, V Abadie, Y de Prost, C Bodemer, and S Hadj‐Rabia. 2010. "Germline mosaicism in keratitis‐ichthyosis‐deafness syndrome: pre‐natal diagnosis in a familial lethal form." *Clinical genetics* 77 (6):587-592.

Schalper, Kurt A, Helmuth A Sánchez, Sung C Lee, Guillermo A Altenberg, Michael H Nathanson, and Juan C Sáez. 2010. "Connexin 43 hemichannels mediate the Ca2+ influx induced by extracellular alkalinization." *American Journal of Physiology-Cell Physiology* 299 (6):C1504-C1515.

Scheckenbach, KE Ludwig, Sophie Crespin, Brenda R Kwak, and Marc Chanson. 2011. "Connexin channel-dependent signaling pathways in inflammation." *Journal of vascular research* 48 (2):91-103.

Schlaefke, Marianne E, JF Kille, and HH Loeschcke. 1979. "Elimination of central chemosensitivity by coagulation of a bilateral area on the ventral medullary surface in awake cats." *Pflügers Archiv* 378 (3):231-241.

Schlaefke, ME, WR See, and HH Loeschcke. 1970. "Ventilatory response to alterations of H+ ion concentration in small areas of the ventral medullary surface." *Respiration physiology* 10 (2):198-212.

Schwarzacher, Stephan W, Udo Rüb, and Thomas Deller. 2010. "Neuroanatomical characteristics of the human pre-Bötzinger complex and its involvement in neurodegenerative brainstem diseases." *Brain* 134 (1):24-35.

Shams, H. 1985. "Differential effects of CO2 and H+ as central stimuli of respiration in the cat." *Journal of Applied Physiology* 58 (2):357-364.

Sheikhbahaei, Shahriar, Brian Morris, Jared Collina, Sommer Anjum, Sami Znati, Julio Gamarra, Ruli Zhang, Alexander V Gourine, and Jeffrey C Smith. 2018. "Morphometric analysis of astrocytes in brainstem respiratory regions." *Journal of Comparative Neurology*.

Silvius, John R. 2003. "Fluorescence energy transfer reveals microdomain formation at physiological temperatures in lipid mixtures modeling the outer leaflet of the plasma membrane." *Biophysical journal* 85 (2):1034-1045.

Sinclair, JD, Walter St John, and D Battlett. 1985. "Enhancement of respiratory response to carbon dioxide produced by lesioning caudal regions of the nucleus of the tractus solitarius." *Brain research* 336 (2):318-320.

Skerrett, I Martha, and Jamal B Williams. 2017. "A structural and functional comparison of gap junction channels composed of connexins and innexins." *Developmental neurobiology* 77 (5):522-547.

Smith, Jeffrey C, Howard H Ellenberger, Klaus Ballanyi, Diethelm W Richter, and Jack L Feldman. 1991. "Pre-Botzinger complex: a brainstem region that may generate respiratory rhythm in mammals." *Science* 254 (5032):726-729.

Solomon, Irene C, Ki H Chon, and Melissa N Rodriguez. 2003. "Blockade of brain stem gap junctions increases phrenic burst frequency and reduces phrenic burst synchronization in adult rat." *Journal of Neurophysiology* 89 (1):135-149.

Solomon, Irene C, Norman H Edelman, and Marvin H O'Neal III. 2000. "CO2/H+ chemoreception in the cat pre-Botzinger complex in vivo." *Journal of Applied Physiology* 88 (6):1996-2007.

Solomon, Irene C, Tami J Halat, M Raafat El-Maghrabi, and Marvin H O'Neal III. 2001. "Localization of connexin26 and connexin32 in putative CO2-chemosensitive brainstem regions in rat." *Respiration physiology* 129 (1-2):101-121.

Somjen, G. G. 1988. "Nervenkitt: notes on the history of the concept of neuroglia." *Glia* 1 (1):2-9. doi: 10.1002/glia.440010103.

Song, N., R. Guan, Q. Jiang, C. J. Hassanzadeh, Y. Chu, X. Zhao, X. Wang, D. Yang, Q. Du, X. P. Chu, and L. Shen. 2016. "Acid-sensing ion channels are expressed in the ventrolateral medulla and contribute to central chemoreception." *Sci Rep* 6:38777. doi: 10.1038/srep38777.

Sonoda, Shozo, Eisuke Uchino, Koh-Hei Sonoda, Shinichi Yotsumoto, Eiichi Uchio, Yasushi Isashiki, and Taiji Sakamoto. 2004. "Two patients with severe corneal disease in KID syndrome." *American journal of ophthalmology* 137 (1):181-183.

Speakman, John R, and Jaap %J Molecular metabolism Keijer. 2013. "Not so hot: optimal housing temperatures for mice to mimic the thermal environment of humans." 2 (1):5-9.

Spyer, K Michael, and Alexander V Gourine. 2009. "Chemosensory pathways in the brainstem controlling cardiorespiratory activity." *Philosophical Transactions of the Royal Society of London B: Biological Sciences* 364 (1529):2603-2610.

St John, Walter M. 1998. "Neurogenesis of patterns of automatic ventilatory activity." *Progress in neurobiology* 56 (1):97-117.

St John, WM, and Thomas A Bledsoe. 1985. "Genesis of rhythmic respiratory activity in pons independent of medulla." *Journal of Applied Physiology* 59 (3):684-690.

Steffens, Melanie, Friederike Göpel, Anaclet Ngezahayo, Carsten Zeilinger, Arne Ernst, and Hans-Albert Kolb. 2008. "Regulation of connexons composed of human connexin26 (hCx26) by temperature." *Biochimica et Biophysica Acta (BBA)-Biomembranes* 1778 (5):1206-1212.

Steijlen, PM, RS Bladergroen, and EH Hoefsloot. 2004. "A phenotype resembling the Clouston syndrome with deafness is associated with a novel missense GJB2 mutation." *The Journal of investigative dermatology* 123 (2):291-293.

Stergiopoulos, Kathleen, José Luis Alvarado, Marta Mastroianni, José F Ek-Vitorin, Steven M Taffet, and Mario Delmar. 1999. "Hetero-domain interactions as a mechanism for the regulation of connexin channels." *Circulation Research* 84 (10):1144-1155.

Stong, Benjamin C, Qing Chang, Shoeb Ahmad, and Xi Lin. 2006. "A novel mechanism for connexin 26 mutation linked deafness: cell death caused by leaky gap junction hemichannels." *The Laryngoscope* 116 (12):2205-2210.

Stornetta, Ruth L, Thiago S Moreira, Ana C Takakura, Bong Jin Kang, Darryl A Chang, Gavin H West, Jean François Brunet, Daniel K Mulkey, Douglas A Bayliss, and Patrice G Guyenet. 2006. "Expression of Phox2b by brainstem neurons involved in chemosensory integration in the adult rat." *Journal of Neuroscience* 26 (40):10305-10314.

Stout, Charles, Daniel A Goodenough, and David L Paul. 2004. "Connexins: functions without junctions." *Current opinion in cell biology* 16 (5):507-512.

Stunden, CE, Jessica A Filosa, AJ Garcia, Jay B Dean, and Robert W Putnam. 2001. "Development of in vivo ventilatory and single chemosensitive neuron responses to hypercapnia in rats." *Respiration physiology* 127 (2-3):135-155.

Stuth, EA, Astrid G Stucke, and Edward J Zuperku. 2012. "Effects of anesthetics, sedatives, and opioids on ventilatory control." *Compr Physiol* 2 (4):2281-367.

Sugiyama, Osamu, Dong Sung An, Sam PK Kung, Brian T Feeley, Seth Gamradt, Nancy Q Liu, Irvin SY Chen, and Jay R Lieberman. 2005. "Lentivirus-mediated gene transfer induces long-term transgene expression of BMP-2 in vitro and new bone formation in vivo." *Molecular Therapy* 11 (3):390-398.

Sáez, Juan C, Viviana M Berthoud, Maria C Branes, Agustin D Martinez, and Eric C Beyer. 2003. "Plasma membrane channels formed by connexins: their regulation and functions." *Physiological reviews* 83 (4):1359-1400.

Sáez, Juan C, and Luc Leybaert. 2014. "Hunting for connexin hemichannels." *FEBS letters* 588 (8):1205-1211.

Sánchez, Helmuth A, Gülistan Meşe, Miduturu Srinivas, Thomas W White, and Vytas K Verselis. 2010. "Differentially altered Ca2+ regulation and Ca2+ permeability in Cx26 hemichannels formed by the A40V and G45E mutations that cause keratitis ichthyosis deafness syndrome." *The Journal of general physiology* 136 (1):47-62.

Takakura, Ana C, and Thiago S Moreira. 2016. "The retrotrapezoid nucleus as a central brainstem area for central and peripheral chemoreceptor interactions." *Experimental physiology* 101 (4):455-456.

Takakura, Ana Carolina Thomaz, Thiago Santos Moreira, Eduardo Colombari, Gavin H West, Ruth L Stornetta, and Patrice G Guyenet. 2006. "Peripheral chemoreceptor inputs to retrotrapezoid nucleus (RTN) CO2‐sensitive neurons in rats." *The Journal of physiology* 572 (2):503-523.

Tan, Wenbin, Wiktor A Janczewski, Paul Yang, Xuesi M Shao, Edward M Callaway, and Jack L Feldman. 2008. "Silencing preBötzinger complex somatostatin-expressing neurons induces persistent apnea in awake rat." *Nature neuroscience* 11 (5):538.

Teran, Frida A, Cory A Massey, and George B Richerson. 2014. "Serotonin neurons and central respiratory chemoreception: where are we now?" In *Progress in brain research*, 207-233. Elsevier.

Terrinoni, Alessandro, Andrea Codispoti, Valeria Serra, Ernesto Bruno, Biagio Didona, Mauro Paradisi, Steven Nisticò, Elena Campione, Bianca Napolitano, and Laura Diluvio. 2010a. "Connexin 26 (GJB2) mutations as a cause of the KID syndrome with hearing loss." *Biochemical and biophysical research communications* 395 (1):25-30.

Terrinoni, Alessandro, Andrea Codispoti, Valeria Serra, Biagio Didona, Ernesto Bruno, Robert Nisticò, Michela Giustizieri, Marco Alessandrini, Elena Campione, and Gerry Melino. 2010. "Connexin 26 (GJB2) mutations, causing KID Syndrome, are associated with cell death due to calcium gating deregulation." *Biochemical and biophysical research communications* 394 (4):909-914.

Terrinoni, Alessandro, Andrea Codispoti, Valeria Serra, Biagio Didona, Ernesto Bruno, Robert Nisticò, Michela Giustizieri, Marco Alessandrini, Elena Campione, and Gerry Melino. 2010b. "Connexin 26 (GJB2) mutations, causing KID Syndrome, are associated with cell death due to calcium gating deregulation." *Biochemical and biophysical research communications* 394 (4):909-914.

Thaler, Christopher, Srinagesh V Koushik, Paul S Blank, and Steven S Vogel. 2005. "Quantitative multiphoton spectral imaging and its use for measuring resonance energy transfer." *Biophysical journal* 89 (4):2736-2749.

Theparambil, S. M., I. Ruminot, H. P. Schneider, G. E. Shull, and J. W. Deitmer. 2014. "The electrogenic sodium bicarbonate cotransporter NBCe1 is a high-affinity bicarbonate carrier in cortical astrocytes." *J Neurosci* 34 (4):1148-57. doi: 10.1523/JNEUROSCI.2377-13.2014.

Thomas, T., and K. M. Spyer. 2000. "ATP as a mediator of mammalian central CO2 chemoreception." *J Physiol* 523 Pt 2:441-7.

Trapp, S, S. J. Tucker, and A. V. Gourine. 2011. "Respiratory responses to hypercapnia and hypoxia in mice with genetic ablation of Kir5.1." *Experimental physiology* (*96* (4)):451-459.

Trapp, Stefan, M Isabel Aller, William Wisden, and Alexander V %J Journal of Neuroscience Gourine. 2008. "A role for TASK-1 (KCNK3) channels in the chemosensory control of breathing." 28 (35):8844-8850.

Trouth, CO, HH Loeschcke, J Berndt, and E-M Betzinger. 1973. "A superficial substrate on the ventral surface of the medulla oblongata influencing respiration." *Pflügers Archiv* 339 (2):135-152.

Turovsky, E., A. Karagiannis, A. P. Abdala, and A. V. Gourine. 2015. "Impaired CO2 sensitivity of astrocytes in a mouse model of Rett syndrome." *J Physiol* 593 (14):3159-68. doi: 10.1113/JP270369.

Turovsky, E., S. M. Theparambil, V. Kasymov, J. W. Deitmer, A. G. Del Arroyo, G. L. Ackland, J. J. Corneveaux, A. N. Allen, M. J. Huentelman, S. Kasparov, N. Marina, and A. V. Gourine. 2016. "Mechanisms of CO2/H+ Sensitivity of Astrocytes." *J Neurosci* 36 (42):10750-10758. doi: 10.1523/JNEUROSCI.1281-16.2016.

Turovsky, Egor, Shefeeq M Theparambil, Vitaliy Kasymov, Joachim W Deitmer, Ana Gutierrez del Arroyo, Gareth L Ackland, Jason J Corneveaux, April N Allen, Matthew J Huentelman, and

Sergey Kasparov. 2016. "Mechanisms of CO2/H+ sensitivity of astrocytes." *Journal of Neuroscience* 36 (42):10750-10758.

Unger, Vinzenz M, Nalin M Kumar, Norton B Gilula, and Mark Yeager. 1997. "Projection structure of a gap junction membrane channel at 7 A resolution." *Nature structural biology* 4 (1):39-43.

Unger, Vinzenz M, Nalin M Kumar, Norton B Gilula, and Mark Yeager. 1999. "Three-dimensional structure of a recombinant gap junction membrane channel." *Science* 283 (5405):1176-1180.

Unwin, PNT, and PD Ennis. 1984. "Two configurations of a channel-forming membrane protein." *Nature* 307 (5952):609.

Unwin, PNT, and G Zampighi. 1980. "Structure of the junction between communicating cells." *Nature* 283 (5747):545.

Van Geel, M, MAM Van Steensel, W Küster, HC Hennies, R Happle, PM Steijlen, and A König. 2002. "HID and KID syndromes are associated with the same connexin 26 mutation." *British Journal of Dermatology* 146 (6):938-942.

Van Nhieu, Guy Tran, Caroline Clair, Roberto Bruzzone, Marc Mesnil, Philippe Sansonetti, and Laurent Combettes. 2003. "Connexin-dependent inter-cellular communication increases invasion and dissemination of Shigella in epithelial cells." *Nature cell biology* 5 (8):720.

Veasey, S. C., C. A. Fornal, C. W. Metzler, and B. L. Jacobs. 1995. "Response of serotonergic caudal raphe neurons in relation to specific motor activities in freely moving cats." *J Neurosci* 15 (7 Pt 2):5346-59.

Veasey, S. C., C. A. Fornal, C. W. Metzler, and B. L. Jacobs. 1997. "Single-unit responses of serotonergic dorsal raphe neurons to specific motor challenges in freely moving cats." *Neuroscience* 79 (1):161-9.

Vincent, Anne, and Fabien Tell. 1997. "Postnatal changes in electrophysiological properties of rat nucleus tractus solitarii neurons." *European Journal of Neuroscience* 9 (8):1612-1624.

Vinken, Mathieu. 2015. "Connexin hemichannels: novel mediators of toxicity." *Archives of toxicology* 89 (1):143-145.

Virchow, R. 1858. "Die Cellularpathologie in ihrer Begründung auf physiologische und pathologische Gewebelehre ".

Wallrabe, Horst, Masilamani Elangovan, Almut Burchard, Ammasi Periasamy, and Margarida Barroso. 2003. "Confocal FRET microscopy to measure clustering of ligand-receptor complexes in endocytic membranes." *Biophysical journal* 85 (1):559-571.

Wang, Nan, Marijke De Bock, Elke Decrock, Mélissa Bol, Ashish Gadicherla, Mathieu Vinken, Vera Rogiers, Feliksas F Bukauskas, Geert Bultynck, and Luc Leybaert. 2013. "Paracrine signaling through plasma membrane hemichannels." *Biochimica et Biophysica Acta (BBA)-Biomembranes* 1828 (1):35-50.

Wang, Nan, Elke De Vuyst, Raf Ponsaerts, Kerstin Boengler, Nicolás Palacios-Prado, Joris Wauman, Charles P Lai, Marijke De Bock, Elke Decrock, and Mélissa Bol. 2013. "Selective inhibition of Cx43 hemichannels by Gap19 and its impact on myocardial ischemia/reperfusion injury." *Basic research in cardiology* 108 (1):309.

Wang, Sheng, Najate Benamer, Sebastian Zanella, Natasha Kumar, Yingtang Shi, Michelle Bevengut, David Penton, Patrice Guyenet, Florian Lesage, and Christian Gestreau. 2014. "TASK-2 channels contribute to pH sensitivity of retrotrapezoid nucleus chemoreceptor neurons (872.4)." *The FASEB Journal* 28 (1 Supplement):872.4.

Wang, W., J. H. Pizzonia, and G. B. Richerson. 1998. "Chemosensitivity of rat medullary raphe neurones in primary tissue culture." *J Physiol* 511 (Pt 2):433-50.

Wang, W., and G. B. Richerson. 1999. "Development of chemosensitivity of rat medullary raphe neurons." *Neuroscience* 90 (3):1001-11.

Wenker, Ian C, Orsolya Kréneisz, Akiko Nishiyama, and Daniel K Mulkey. 2010. "Astrocytes in the retrotrapezoid nucleus sense H+ by inhibition of a Kir4. 1–Kir5. 1-like current and may contribute to chemoreception by a purinergic mechanism." *Journal of neurophysiology* 104 (6):3042-3052.

Wenker, Ian Christopher, Ana Takakura, Thiago Moreira, and Daniel Kent Mulkey. 2012. "Regulation of ventral surface chemoreceptors by purinergic signaling." *The FASEB Journal* 26 (1 Supplement):894.1-894.1.

West, J. B. 2012. *Respiratory physiology: the essentials*: Lippincott Williams & Wilkins.

Willecke, Klaus, Jürgen Eiberger, Joachim Degen, Dominik Eckardt, Alessandro Romualdi, Martin Güldenagel, Urban Deutsch, and Goran Söhl. 2002. "Structural and functional diversity of connexin genes in the mouse and human genome." *Biological chemistry* 383 (5):725-737.

Winterstein, Hans. 1911. "Die Regulierung der Atmung durch das Blut." *Pflüger's Archiv für die gesamte Physiologie des Menschen und der Tiere* 138 (4-6):167-184.

Winterstein, Hans. 1949. "The "Reaction Theory" of respiratory regulation." *Cellular and Molecular Life Sciences* 5 (6):221-226.

Wouters, Fred S, Philippe IH Bastiaens, Karel WA Wirtz, and Thomas M Jovin. 1998. "FRET microscopy demonstrates molecular association of non‐specific lipid transfer protein (nsL‐TP) with fatty acid oxidation enzymes in peroxisomes." *The EMBO journal* 17 (24):7179-7189.

Wu, J, H Xu, W Shen, and C Jiang. 2004. "Expression and coexpression of CO 2-sensitive Kir channels in brainstem neurons of rats." *The Journal of membrane biology* 197 (3):179-191.

Xu, H., N. Cui, Z. Yang, Z. Qu, and C. Jiang. 2000. "Modulation of kir4.1 and kir5.1 by hypercapnia and intracellular acidosis." *J Physiol* 524 Pt 3:725-35.

Xu, Ji, and Bruce J Nicholson. 2013. "The role of connexins in ear and skin physiology—functional insights from disease-associated mutations." *Biochimica et Biophysica Acta (BBA)-Biomembranes* 1828 (1):167-178.

Yotsumoto, S, T Hashiguchi, X Chen, N Ohtake, A Tomitaka, H Akamatsu, K Matsunaga, S Shiraishi, H Miura, and J Adachi. 2003. "Novel mutations in GJB2 encoding connexin‐26 in Japanese patients with keratitis‐ichthyosis‐deafness syndrome." *British Journal of Dermatology* 148 (4):649-653.

Yu, Jinshu, Christian A Bippes, Galen M Hand, Daniel J Muller, and Gina E Sosinsky. 2007. "Aminosulfonate modulated pH induced conformational changes in connexin26 hemichannels." *Journal of Biological Chemistry*.

Yum, Sabrina W, Junxian Zhang, Virginijus Valiunas, Giedrius Kanaporis, Peter R Brink, Thomas W White, and Steven S Scherer. 2007. "Human connexin26 and connexin30 form functional heteromeric and heterotypic channels." *American Journal of Physiology-Cell Physiology* 293 (3):C1032-C1048.

Zhang, J, H Li, L Chai, L Zhang, J Qu, and T Chen. 2015. "Quantitative FRET measurement using emission‐spectral unmixing with independent excitation crosstalk correction." *Journal of microscopy* 257 (2):104-116.

Zhang, Jian-Ting, Mingang Chen, Cynthia I Foote, and Bruce J Nicholson. 1996. "Membrane integration of in vitro-translated gap junctional proteins: co-and post-translational mechanisms." *Molecular biology of the cell* 7 (3):471-482.

Zheng, Jie. 2006. "Spectroscopy-based quantitative fluorescence resonance energy transfer analysis." In *Ion Channels*, 65-77. Springer.

Ziemann, A. E., J. E. Allen, N. S. Dahdaleh, I. I. Drebot, M. W. Coryell, A. M. Wunsch, C. M. Lynch, F. M. Faraci, M. A. Howard, M. J. Welsh, and J. A. Wemmie. 2009. "The amygdala is a chemosensor that detects carbon dioxide and acidosis to elicit fear behavior." *Cell* 139 (5):1012-21. doi: 10.1016/j.cell.2009.10.029.

Zwicker, JD, V Rajani, LB Hahn, and GD Funk. 2011. "Purinergic modulation of preBötzinger complex inspiratory rhythm in rodents: the interaction between ATP and adenosine." *The Journal of physiology* 589 (18):4583-4600.